An Investigation into Improving the Repeatability of Steady-State Measurements from Nonlinear Systems

Methods for measuring repeatable data from steady-state engine tests were evaluated. A comprehensive and novel approach to acquiring high quality steady-state emissions data was developed.

Thomas Patrick DWYER

Thesis submitted for the Doctor of Philosophy in Automotive Engineering

School of Engineering

Faculty of Engineering and Informatics

University of Bradford

2014

Acknowledgements

I would like to thank my family for their encouragement throughout my studies. In particular I would like to thank my parents, Prof. Timothy Dwyer and Kathryn Rundell, and sister, Harriet Evans, for their constant advice and support.

I would also like to thank both my supervisors, Prof. Kambiz Ebrahimi and Dr. Byron Mason, for their guidance and words of wisdom.

Finally I'd like to thank my friends and colleagues at the University of Bradford, specifically the team in HyPER-C for keeping my research on track.

I dedicate this work and research to my Grandfather, John Rundell, who will always be an inspiration. He was a source of wondrous and intellectual conversations until the moment he passed.

Abstract

Thomas Patrick DWYER

An Investigation into Improving the Repeatability of Steady-State Measurements from Nonlinear Systems

Key words: Test repeatability, data quality, engine calibration, system characterisation

The calibration of modern internal combustion engines requires ever improving measurement data quality such that they comply with increasingly stringent emissions legislation. This study establishes methodology and a software tool to improve the quality of steady-state emissions measurements from engine dynamometer tests.

Literature shows state of the art instrumentation are necessary to monitor the cycle-by-cycle variations that significantly alter emissions measurements. Test methodologies that consider emissions formation mechanisms invariably focus on thermal transients and preconditioning of internal surfaces.

This work sought data quality improvements using three principle approaches. An adapted steady-state identifier to more reliably indicate when the test conditions reached steady-state; engine preconditioning to reduce the influence of the prior day's operating conditions on the measurements; and test point ordering to reduce measurement deviation.

Selection of an improved steady-state indicator was identified using correlations in test data. It was shown by repeating forty steady-state test points that a more robust steady-state indicator has the potential to reduce the measurement deviation of particulate number by 6%, unburned hydrocarbons by 24%, carbon monoxide by 10% and oxides of nitrogen by 29%. The variation of emissions measurements from those normally observed at a repeat baseline test point were significantly influenced by varying the preconditioning power. Preconditioning at the baseline operating condition converged emissions measurements with the mean of those typically observed. Changing the sequence of steady-state test points caused significant differences in the measured engine performance. Examining the causes of measurement deviation allowed an optimised test point sequencing method to be developed.

A 30% reduction in measurement deviation of a targeted engine response (particulate number emissions) was obtained using the developed test methodology. This was achieved by selecting an appropriate steady-state indicator and sequencing test points. The benefits of preconditioning were deemed short-lived and impractical to apply in every-day engine testing although the principles were considered when developing the sequencing methodology.

Contents

Nomenclature

Acronym	Description
aTDC	Crank angle degrees after Top Dead Centre
bTDC	Crank angle degrees before Top Dead Centre
CA	Crank angle degrees
CCV	Cycle-to-Cycle Variability
CI	Compression Ignition
CO	Carbon monoxide
CO_2	Carbon dioxide
CoV	Coefficient of Variation
CPC	Condensation Particle Counter
CVS	Constant Volume Sampling
DFMEA	Design Failure Mode Effects Analysis
DFSS	Design For Six-Sigma
DoE	Design of Experiments
D_P	Particulate diameter
ECU	Electronic Control Unit
EGR	Exhaust Gas Recirculation
EMC	Engine Mapping and Calibration
EOI	End of Injection
EPA	Environmental Protection Agency
ESC	European Stationary Cycle
ETC	European Transient Cycle
EVC	Exhaust Valve Closing
FB	Fuel consumption
FID	Flame Ionisation Detector
FMEA	Failure Modes and Effects Analysis

FRP	Fuel Rail Pressure
GDI	Gasoline Direct Injection
GTDI	Gasoline Turbocharged Direct Injection
GUI	Graphical User Interface
HC	Hydrocarbons
hp	Horsepower
IC	Internal Combustion
IVO	Intake Valve Opening
kph	Kilometre per hour
kW	Kilowatt
MAF	Manifold Air Flow
MAP	Manifold Air Pressure
MB	Model Building
MFB	Mass Fraction Burned
MPa	Mega Pascal
ms	Millisecond
MV	Model Validation
NDIR	Non Dispersive Infra-Red
NEDC	New European Driving Cycle
NA	Naturally Aspirated
Nm	Newton metres
NMHC	Non-methane hydrocarbons
NOx	Oxides of nitrogen
OBD	On-board diagnostics
OEM	Original Equipment Manufacturer
PD	Product Development
PFMEA	Process Failure Mode Effects Analysis

PID	Proportional Integral Derivative
PIV	Particle Image Velocimetry
PM	Particulate Mass
PMP	Particle Measurement Program
PN	Particulate Number
RI	Repeatability Index
rpm	Revolutions per minute
RSM	Response Surface Model
SA	Spark timing (Spark Advance)
SI	Spark Ignition
SID	System Identification
SOF	Soluble Organic Fraction
SOI	Start of Injection
Std	Standard deviation
TLRT	Transfer Line Residence Time
TWC	Three Way Catalyst
UDC	Urban Drive Cycle
ULSD	Ultra low sulphur diesel
UUT	Unit Under Test
WHTC	World Harmonized Transient Cycle
WOT	Wide Open Throttle

Greek Letters	Description
φ	Equivalence ratio
ω	Angular velocity

Chapter 1

Introduction

Internal combustion engines have been improving since Otto first developed the spark-ignition engine in 1876. The past 138 years have witnessed a transformation of both compression ignition (CI) and spark ignition (SI) varieties and four-stroke engines are now exceeding 95% conversion efficiency of fuel [1].

Automotive original equipment manufacturers (OEMs) must continue improving their analytical techniques to maintain engine development. With the help of forced induction the power produced per swept volume continues to improve but dependably reducing emissions is the prime focus of development. Forthcoming Euro 6 legislation stipulates emissions must conform to the set levels for a driving life of 160,000 km following the sale of a vehicle [2].

Automotive engineers expend a large effort into furthering development by learning about the combustion process through practical research and, more recently, computer simulations. The level of refinement is becoming increasingly difficult to be measured using traditional methods and innovative solutions such as in-cylinder pressure transducers and engines with specific visual access must be developed. Figure 1.1 [3] shows an image taken of an optical access engine immediately following ignition. Flame propagation can

be determined over time using image processing software to improve simulations of emissions [4], [5] and phenomena such as knock [6]. Similar analysis can be carried out on other events that were otherwise hidden from view such as the fuel-spray pattern and penetration [7]. Massive volumes of test data are produced developing an engine up to the standards required by legislation and expected by the customer.

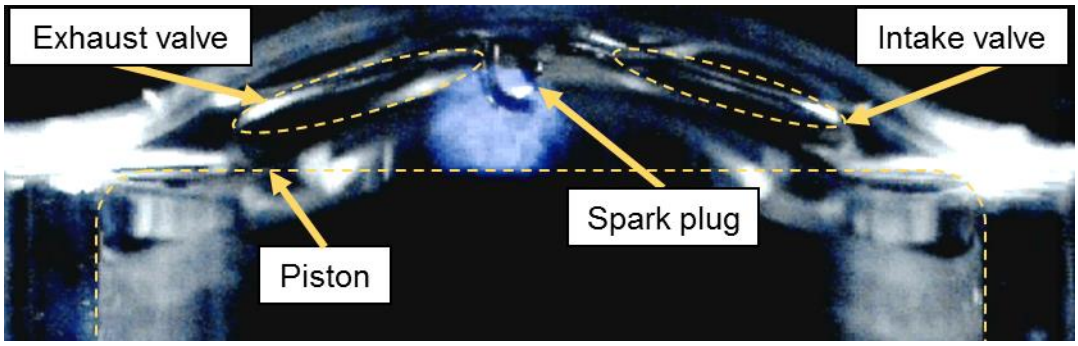

Figure 1.1 Cropped side-view of an optical access engine (adapted from [3])

Significant work has been done by several authors [8]–[11] to increase the usefulness of test data by adopting statistical techniques from other fields of research. Refinements in instrumentation also aids engine development as the test data are more precise. The full potential of innovative statistical techniques and more capable instrumentation may not be reached unless traditional engine testing techniques are improved.

1.1 Engine mapping and calibration – Outline and challenges

Engine mapping and calibration (EMC) is the process by which optimal engine actuator settings are determined and then incorporated within the control strategy as look-up tables on the electronic control unit (ECU). The definition of optimality depends on whether the engine being developed is intended for racing or production. For the context of this thesis gasoline production engines

will be discussed. There are numerous sub-processes at each EMC step although Table 1.1 provides a brief overview of the main stages.

Table 1.1 EMC processes

Process	Description
Testing	Data are recorded at many thousands of predetermined test points
Modelling	Mathematical-based computer models are generated to represent the physical system
Calibration	Models are used to determine the optimal engine settings over the operating regime and these are used to populate the ECU look-up tables

Testing may be viewed as the foundations of EMC and improvements made at this stage will directly impact the subsequent calibration stages. Anomalous test data may be impossible to rectify at a later date because checking large volumes of test data in sufficient detail is often impractical. The test points for a modern EMC are selected to achieve maximum usefulness from the data in order to reduce the testing required [12]. This is generally achieved by evenly distributing the test points within the operating region. This maximises the potential difference in operating conditions between test points and increases the importance, or “weight”, of data from each test point.

Challenges faced in a modern EMC are different to those in the past although the goal, which is to achieve all deliverables in an efficient way. The goal has remained the same. The current generation of automotive engines are designed to generate more power whilst emitting fewer pollutants. This trend has continued from the first emissions legislation that was introduced circa

1960 in the USA [13]. As more types of harmful exhaust emissions are identified the legislation adapts to control the environmental and health impact caused by the vehicles on the road [2], [14], [15].

A modern EMC has stringent legislation to adhere by. Emissions limits are the most important factor when a new vehicle is designed to be sold and the primary calibration effort will be to optimise engine performance for minimised tail pipe emissions. Failing to meet the limits is unacceptable as this will mean financial penalties for the OEM [16].

Reducing emissions via calibration is inherently challenging as minimising one inevitably causes another to increase. Figure 1.2 [17] shows how air/fuel causes opposing trends for several tail-pipe emissions. A three-way catalyst (TWC), which chemically reduces oxides of nitrogen (NOx), carbon monoxide (CO) and hydrocarbon (HC) emissions, is depended upon to conform to current legislation. Particulate mass (PM) filters and urea injection are examples of forthcoming technologies as limits reduce further.

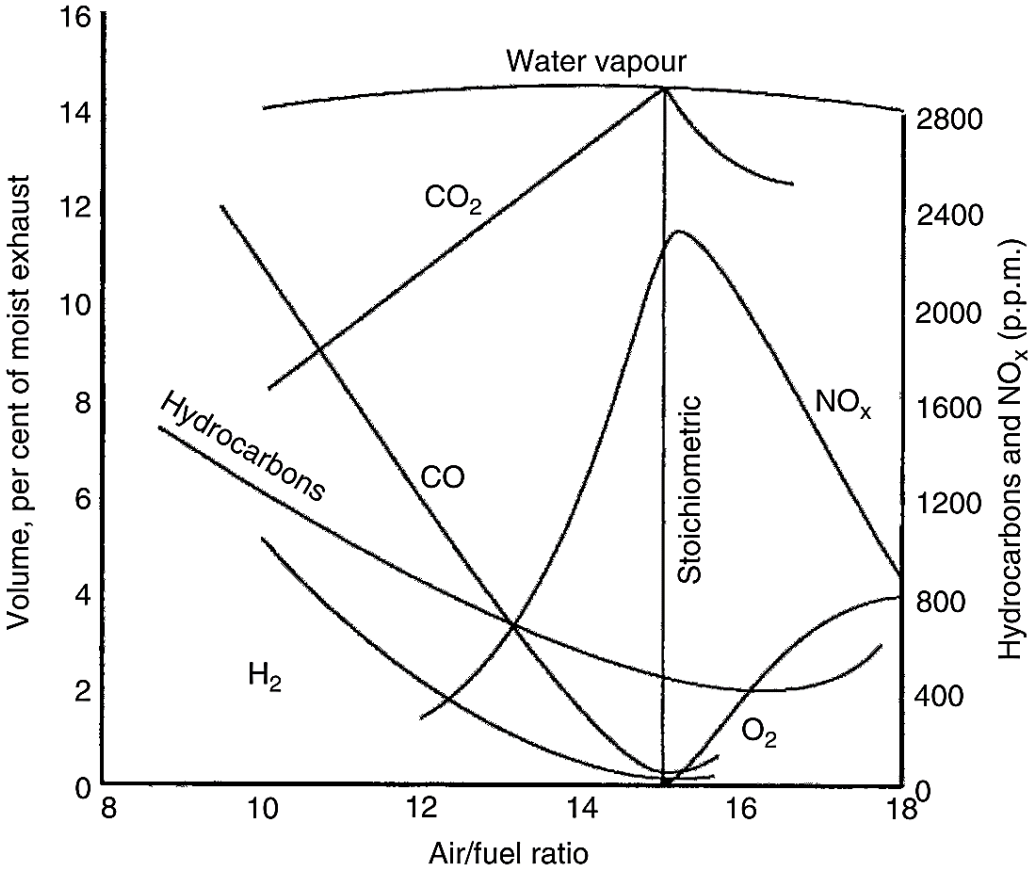

Figure 1.2 Relation between exhaust emissions and air/fuel ratio for gasoline engines [17]

Initial emissions legislation required minimal technological advances when positive crank case ventilation was mandated [13]. When carbon monoxide (CO) and hydrocarbon (HC) emissions standards were adopted in 1966 further developments were essential. Catalytic converters were developed that allowed conversion of harmful emissions species to relatively harmless compounds. This style of exhaust after-treatment requires specific oxygen levels to operate effectively [1], which in turn meant improved control over the air-fuel mixture was needed. Engine calibration can only provide limited performance benefits before developments in engine design are required. Technologies such as fuel injection, variable valve-timing and electronic

control systems were ultimately developed. Table 1.2 provides a brief explanation of the benefits of these technologies.

Table 1.2 Outline of several commonplace engine technologies

Technology	Key operating point	Specific benefits
Fuel injection	Variable timed fuelling events	Increased fuel vaporisation from high pressure fuel spray, more accurate control of air-fuel ratio, faster transient response
Variable valve-timing	Adjustable timings of intake and exhaust valve opening and closing events	Optimising start and end of gas transfer processes depending on specific operating conditions
Electronic control systems	Programmable engine control	Flexible and intelligent on-the-fly alterations of combustion events

A vehicle will have to conform to the legislation native to the country when being sold and meet the customer expectations in terms of driveability. The limits for NOx emissions in China have been lower than in the US since 2008, whereas particulate mass emissions in the US are lower [14], [18]. These contrasting requirements will require different calibration techniques.

It should be noted that differences in regulations make a simple comparison between countries misleading. Figure 1.3 [19] is a graphic showing the different emissions standards for various countries and regions that follow the same guidelines.

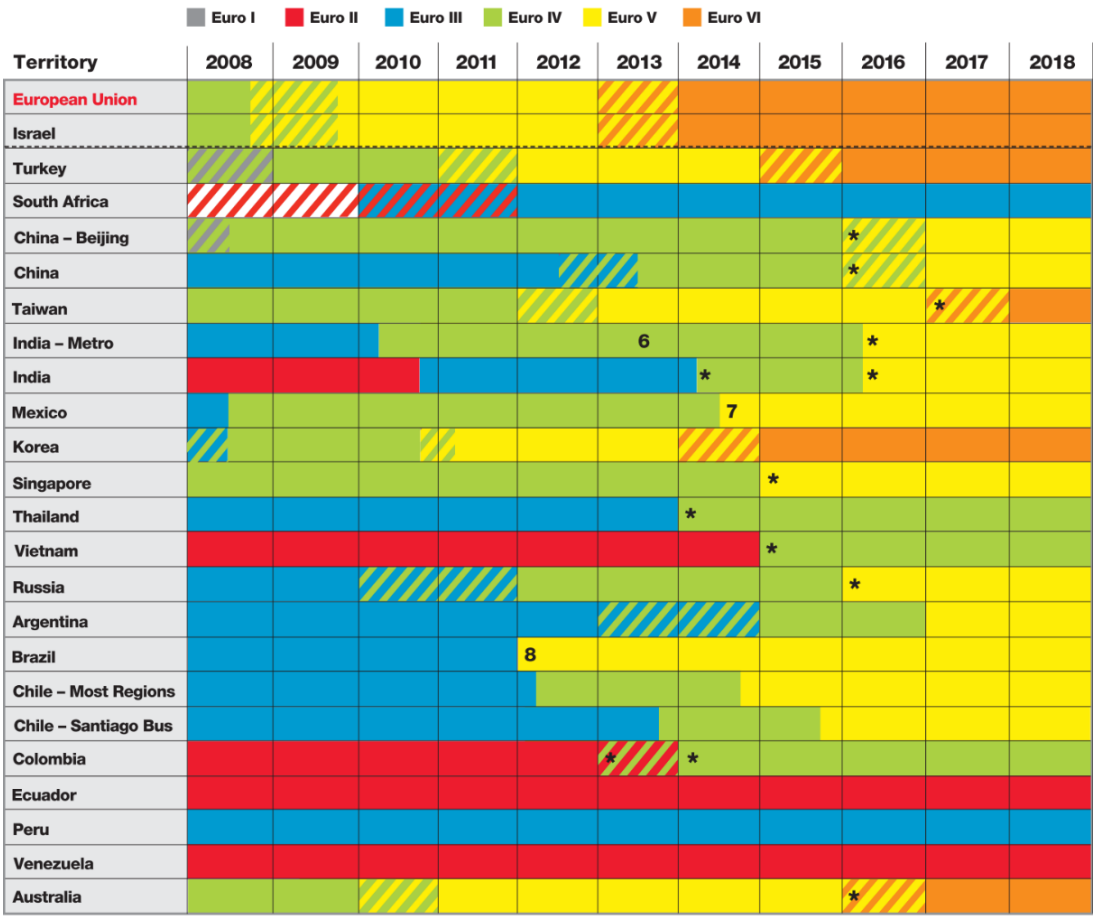

Figure 1.3 Timeline of countries which are abiding by the European emissions standards. Striped cells represent a cross-over period [19]

Table 1.3 below is a key for the numbers that appear on the figure above.

Table 1.3 Key for the figure above

Item	Description
*	Projected or proposed
6.	For India metro, Euro IV in 2010 without on-board diagnostics (OBD), Q2 2013 with OBD
7.	For Mexico, Q4 2014 Euro V is contingent upon ultra-low sulphur diesel (ULSD); Euro VI also possible
8.	For Brazil, PROCONVE P7, Motor Vehicles Air Pollution Control Program

For reference, Table 1.4 [20] below shows the progression from Euro I to VI.

Table 1.4 Euro emissions standards [20]

	THC	NMHC	NOx	CO	PM	PN
			mg/km			#/km
Euro I	-	-	-	2720	-	-
Euro II	-	-	-	2200	-	-
Euro III	200	-	150	2300	-	-
Euro IV	100	-	80	1000	-	-
Euro V	100	68	60	1000	4.5	-
Euro VI	100	68	60	1000	4.5	$6.0x10^{11}$

Challenges such as these place a high demand on the procedures used within EMC to perform correctly and ensure targets are met.

1.2 Nonlinear system identification and measurement

Engine testing is the practise of measuring the response of a nonlinear system. A nonlinear system is one where the output(s) respond indirectly proportionally

to the input(s). Examples of nonlinear systems include turbulent fluid flows, climate and weather prediction, systems biology, social and behavioural modelling, cognitive measurement, bio-sensing and applications involving large numbers of sensors and actuators [21].

Measuring data from nonlinear systems poses challenges that are not present with linear systems due to a complex system response. A predefined test sequence can be used to excite the system in a controlled manner, providing data to generate mathematical models that describe the underlying processes properly.

A simplistic approach is to view the system as a nonlinear regression problem and apply standard methods of solving. The relationship between the system outputs and a known regression vector can then be described by a simple function described by:

$$y(t) = g\big(\varphi(t)\big) + e(t)$$ **Equation 1.1 [22]**

where y are the system outputs, t is time, g is a coefficient, $\varphi(t)$ is the regression vector and e is the error term. The regression vector, Equation 1.2, is a function of all inputs $(u(s))$ and outputs (y) prior to time (t):

$$\varphi(t) = f(y(t-1), u(t-1), y(t-2), u(t-2), \dots)$$ **Equation 1.2 [23]**

where f is some nonlinear function. When Equation 1.1 and Equation 1.2 are parameterised it is possible to forecast the system response at time (t) under

conditions based on known inputs. Parameterisation can be done using test data or information gleaned from previous models. Intuitively, test data should generate a more accurate model but the test data must be precise. Physics models based on first principles, otherwise known as white box models, may be accurate under some circumstances and will provide less noisy data since the data are derived from equations instead of measurements.

All models are wrong [24] and the resulting data should be applied with caution because incorrect conclusions may be drawn. The model responses are mathematical representations and may not perform well over the full range of inputs unless fully characterised. In other words a combination of inputs will not necessarily generate the correct outputs unless the system has been validated at that point.

It is possible to use a model with many terms to exactly fit the data but this “over-fitting” can be problematic. Such dangers can be the extended processing time required to solve the equations and a model that doesn’t accurately represent the physical system. To prevent over-fitting a 5^{th} order equation is generally accepted as the maximum for engine responses [25]. It is desirable to have the lowest order model that accurately represents the physical system to help in more accurate analysis, prediction and control whilst requiring a reduced computational load.

To generate a mathematical model of a system using test data the responses of the physical system must be recorded. This data will be used to characterise the system by describing models.

Characterising a nonlinear system can be achieved using a variety of input functions, or test signals. Some common types of test signals are shown in Table 1.5.

Table 1.5 Examples of some basic input functions [26]

Name	Input function
Impulse function	$u(t) = c \cdot \delta t$
Step function	$u(t) = c$
Ramp function	$u(t) = c \cdot t$
Sinusoidal function	$u(t) = c \cdot sin(\omega t)$

where $u(t)$ is the function of time, c is a constant, δt is the change in time, t is the current time and ω is angular velocity.

The test signals in Table 1.5 are very simple functions that would allow the control system to be identified with relative ease. The type of test signal used should match the form of input most frequently experienced by the system under normal operation. Step-changes are typically used during steady-state mapping of automotive engines [27], [28] and so it seems logical that the step-change input function be used for characterising the system response.

For example, Cook and Powell [29] used models to predict the intake manifold pressure and engine speed response following small step-changes in throttle angle of an IC engine, Figure 1.4. The authors estimated the system by employing analytical curve-fitting techniques to dynamometer-obtained experimental data.

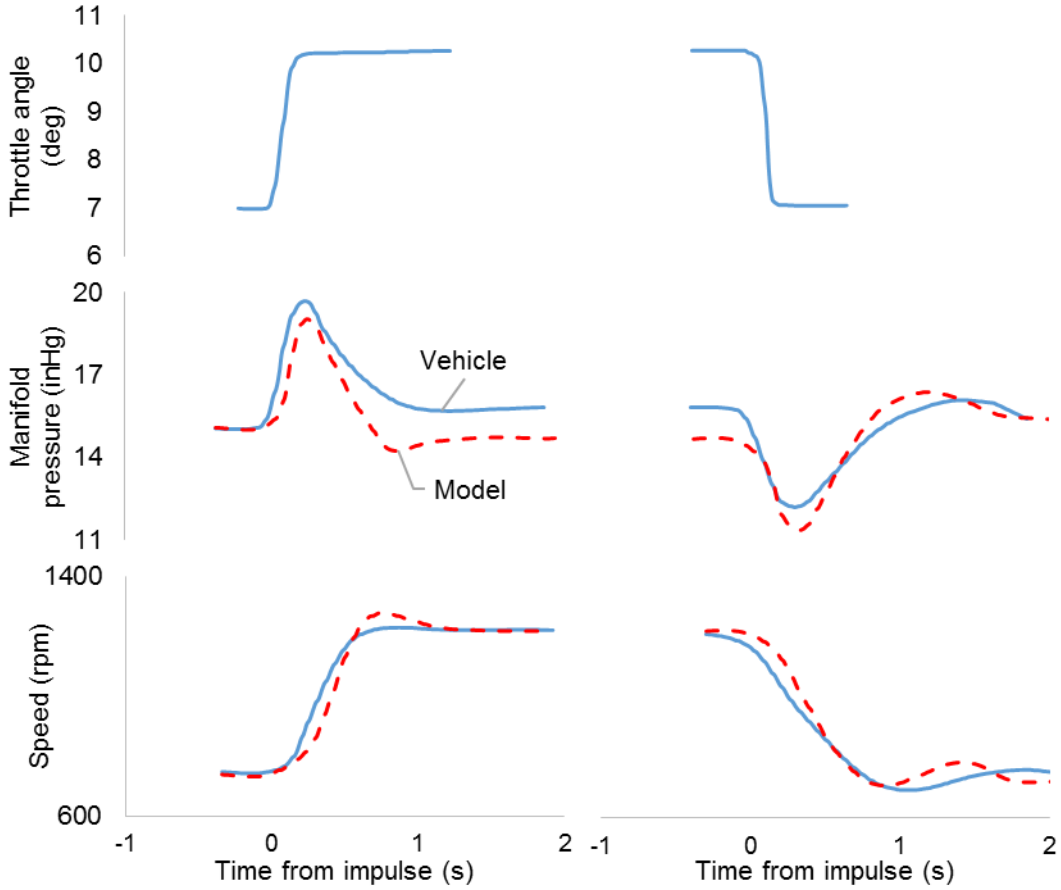

Figure 1.4 Sample transient response for validation of a four-cylinder carburetted engine (adapted from [29])

Many successful attempts have since been made to accurately model the performance characteristics of IC engines [30], [31] and the knowledge has been applied to data driven model-based engine calibration [32], [33]. There are software packages available such as AVL BOOST [34] and GT-POWER [35]that are capable of simulating various engine performance metrics. The software packages require extensive parameterisation using some fundamental engine features such as the number of cylinders, swept volume and valve-train dynamics. A relatively quick model of the engine is then created and preliminary performance characteristics such as fuel consumption can be obtained at a range of simulated operating conditions. Improving the

model accuracy can be achieved by increasing the parameterisation or validating the model with test data from the physical system.

1.3 Experiment design and test point ordering

Increasing numbers of engine actuators and responses that need optimisation have required improved experiment design. To prevent an impractical volume of test data being needed for an EMC the test points are now selected using computer software. A modern experiment will use intelligent design tables, commonly known as Design of Experiments (DoE), to design the experiment. Applications of DoE are now used in calibrating hybrid power systems for simultaneously optimising traditional powertrain and managing battery temperature [36], [37].

In many cases Latin-Hypercube Sampling is chosen by the DoE to achieve a complete and equally distributed covering of the design space [38]. This is a space-filling method whereby a pre-determined n-dimensional space is populated with equally distributed test points. A 2D example of how the approach works is shown in Figure 1.5. The method consists of separating the range of each variable in *N* intervals and drawing a probe in each interval. Each interval has only one node in it, allowing the test points to be distributed more evenly than if randomly placed.

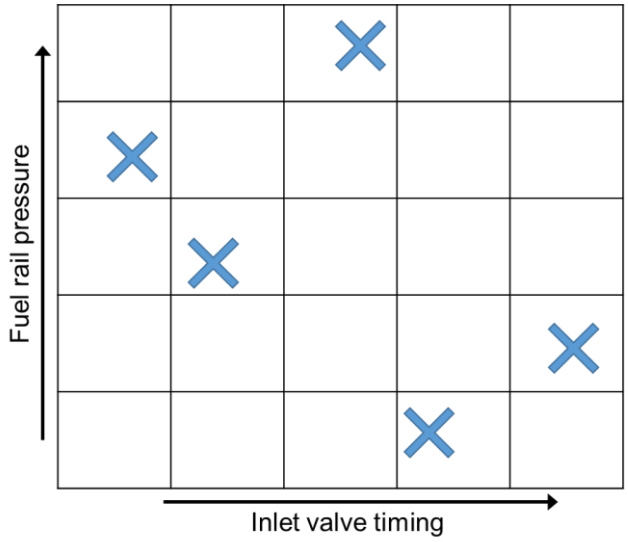

Figure 1.5 2D Latin-Hypercube Sampling technique

DoE works best with an iterative procedure as this allows model evolution and permits additional testing in areas of low confidence. However this approach is time consuming, computationally expensive, and there is no guarantee that more data will improve the model.

Measurements of particulate number (PN), hydrocarbons (HC), carbon monoxide (CO) and particulate mass (PM) emissions are affected for several minutes by prior operating conditions [39]–[41]. This means emissions data being recorded during steady-state tests may not be representative of the set operating conditions. Giechaskiel *et al.* [39] found that PN emissions from a light-duty diesel engine were significantly affected by approaching the same steady-speed set point from different conditions. A change in speed from 90 kph to 100 kph caused PN emissions to increase by a factor of eight compared to a change from 110 kph to 100 kph. Vojtisek-Lom *et al.* [40] observed HC, CO and PM emissions from a CI engine running on rapeseed oil were affected for tens of minutes depending on the prior operating conditions. The

magnitude of non-volatile emissions levels were affected by different types of preconditioning [41]. Preconditioning describes the operational history that may be immediately prior to or several hours before the current test point. Evidence in literature indicates that emissions may be correlated to the preconditioning operating conditions.

It is the conditions other than the controlled test variables that change between test points that cause variations in measurements. Exhaust conditions such as dilution ratio, temperature, humidity and aerosol chemistry may all change particle formation [42]. Engine temperatures will not change instantaneously, causing parameters such as mixture preparation, the mass of inducted air and parasitic losses to settle gradually. The goal of a DoE is to maximise the usefulness from each data sample by ensuring each test point is unique [43] but this reduces the likelihood of anomalous measurements being detected since the trends observed in data will be undefined.

1.4 Steady-state

A test is ‘steady-state’ when the unit under test (UUT) is subjected to constant conditions whilst data are recorded. However as noted in Section 1.3 it may not be evident when the conditions are suitably stable and some engine responses will be more sensitive. For less sensitive parameters such as fuel consumption the relative rate of change is quick following a change in operating condition. The exhaust emissions may take longer to stabilise since the influencing factors cause a greater degree of change. Humidity, for example, will influence particulate emission formation within the cylinder due

to changes in combustion chemistry and in the exhaust due to the rate of nucleation [42].

Steady-state test points can last several minutes and the average value used to mitigate transients in the system response. Non-regulated steady-state testing will likely vary between test facilities and may also differ between operators. Different length tests will inevitably generate a different mean value for the same test point.

When performing an EMC which contains 1000's of steady-state test points there is potential for a significant proportion of data to be anomalous. Ensuring the UUT is operating under the conditions defined will help improve the representativeness of data. This can be achieved with a methodology that accounts for the factors relevant to measuring repeatable data.

1.5 Aims and objectives

Aim

To develop a rigorous methodology for obtaining high quality steady-state test data from dynamic systems.

Objectives

i. Identify optimum indicators of steady-state engine operation
ii. Address parameters that influence the repeatability of emissions measurements
iii. Establish robust and sustainable methodology for efficient engine testing

iv. Implement the methodology using an established engine mapping and calibration test foundation
v. Bring together the methodology in a software tool

1.6 Contribution

An improved approach to steady-state testing has been established and a software tool has been developed to facilitate the application of this methodology.

The improved approach includes a methodology that indicates optimum variable(s) to monitor for reliable steady-state indication when changing operating condition. In addition, any long-term instabilities of measured responses to the control actuators are matched. The software tool analyses this data for correlations that are used to sequence test points. One or more responses can be chosen and the test point order optimised accordingly to reduce instability of the elected response(s) during testing.

Using this methodology it was possible to reduce the deviation of particulate number emissions measurements by 31.9% when compared to a typical DoE-style test methodology. The coefficient of variation of PN data was also improved by approximately 19.4%.

1.7 Structure of thesis

This thesis starts with details of the typical exhaust emissions measured during a modern engine mapping and calibration. Specific focus is given to particulate emissions with details of particulate emissions formation mechanisms, measurement variation and measurement techniques.

The literature review continues with a discussion about measuring data from steady-state engine tests. The focus is on testing for calibration and how the data are used in a modern engine mapping and calibration scenario. The design of experiment processes used within the experimentation of this thesis are also described.

Approaches found in literature for ensuring high quality steady-state measurement data are then discussed and a review of improving test data repeatability through methodology presented.

Following the literature review Section 3 explains the statistical techniques used in the data analysis.

The empirical section is in two parts. The first commences by explaining the equipment, facility and experimental methods used in this thesis. Data from experiments that aimed to improve steady-state repeatability are then presented. The first experiment observed the temperature response of key system fluids following a number of step-changes in speed and load. The second compared key engine responses when a different steady-state indicator was used at a repeat test point. The third compared data quality from a set of steady-state test points when different steady-state indicators were used. The fourth related preconditioning at different power outputs to the engine performance measured during a baseline operating condition. A fifth experiment in this section describes a method to quickly determine the optimal variable to indicate steady-state operation.

The second empirical section commences with an investigative analysis of test data that were collected during steady-state testing. The analysis aimed to determine whether correlations could be detected between the movement of the engine actuators and the data quality of the measured engine responses. Following the positive results of this analysis the test points were then re-run in different sequences and the variation in engine responses reviewed. An optimal test point sequence for the same test points was developed for reducing the variability of an elected engine response, particulate number emissions.

The function of a software tool that was developed to combine the findings of this thesis is explained in the penultimate section. This section also goes into depth to describe the processing steps that were developed using a worked example. The thesis is concluded with final remarks and a discussion.

Chapter 2

Literature Review

2.1 Introduction

This chapter begins with a background of the measured engine responses that are targeted in calibration. This background provides the relevant information to understand the results that will be discussed in this thesis.

An overview of the current understanding of engine testing for calibration is then presented. Some novel methodologies used in engine mapping and calibration are discussed.

A description of the model based engine mapping and calibration technique used in the research is presented with a worked example. The major influential factors on data quality from literature are then discussed.

2.2 Exhaust emissions and fuel consumption

First and foremost an engine calibration must be capable of making the engine conform to emissions legislation. It is only once the calibration engineers are confident that the vehicle will pass the necessary homologation that effort can be made to improve other aspects of performance. The emissions species that are controlled by legislation, thus requiring some attention during calibration, are carbon dioxide (CO_2), carbon monoxide (CO), oxides of nitrogen (NOx), hydrocarbons (HC) and particulates.

The performance and exhaust emissions profile of an internal combustion engine relies heavily on the processes occurring in the combustion chamber. Many factors influence the in-cylinder processes and a list by Martyr [44] highlights some important factors.

Table 2.1 Factors that significantly alter emissions during homogeneous combustion (adapted from [44])

Factor	Description
Flow pattern (swirl and turbulence)	Efficient combustion depends on complete oxidation of the fuel within a limited time. Increasing in-cylinder motion will increase the interaction between fuel and oxygen
Fuel injection	Better atomised fuel presents a higher surface area for greater fuel-oxygen contact area
Degree of cooling of chamber walls, piston and bore	Higher temperatures will enhance fuel vaporisation and thus combustion efficiency

All variations of the above list will vary the in-cylinder processes, resulting in a slightly different burn profile. The combustion efficiency, and therefore engine performance and emissions, will increase or decrease depending on the particular characteristics of the burn profile.

2.2.1 Emissions formation

There are several gas exchange processes, illustrated in Figure 2.1 [1], involved in the formation of exhaust emissions. Firstly air and fuel are mixed together during induction, Figure 2.1 (2) to (4). All processes from the moment

air enters the intake manifold until ignition occurs affect charge composition [45]–[48].

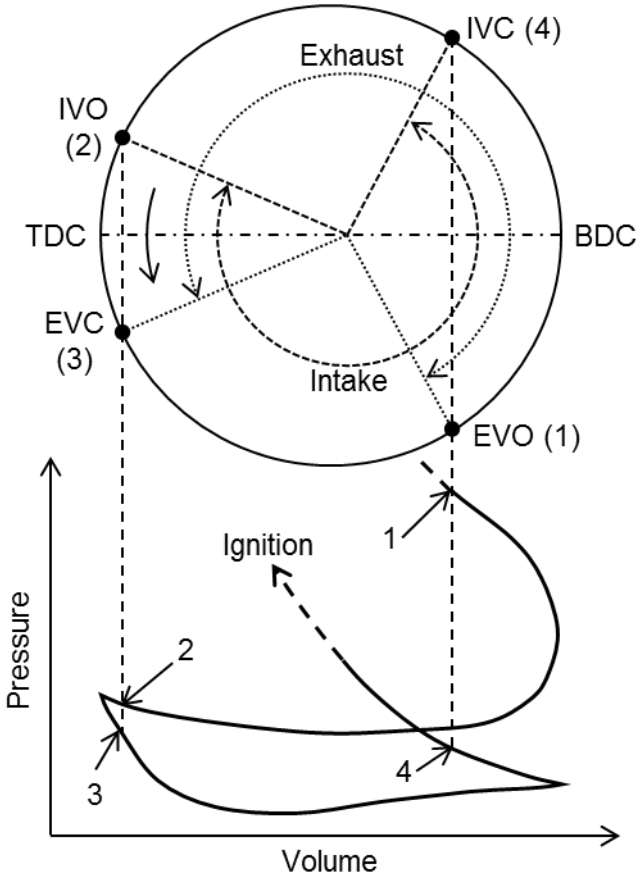

Figure 2.1 Valve timing and pressure-volume diagram at wide open throttle (adapted from [1])

Air temperature plays a role in the level of mixture preparation. Cooler air is denser, which improves volumetric efficiency by increasing the mass of air inducted per cycle, Equation 2.1, but warmer charge air can help with fuel vaporisation. Humidity will alter the characteristics of the charge air by reducing the charge temperature. This is caused by more energy being required by water compared to air to increase in temperature by the same amount. More water vapour will displace oxygen in the cylinder thus reducing the moles of oxygen available for combustion as shown using:

$$\eta_v = \frac{\dot{m}_a \cdot 120}{\rho_{a.i} \cdot V_d \cdot N_{eng}}$$ **Equation 2.1**

where η_v is volumetric efficiency, $\dot{m}_a$ is mass air flow, $\rho_{a.i}$ is inlet air density, V_d is displacement and N_{eng} is the number of strokes taken per cycle.

The humidity can also affect particle growth post-combustion, as described by

$$\frac{\mathrm{d}D_p}{\mathrm{d}t} = 2k\frac{\left(\rho_{vapour} - \rho_{sat}\right)}{\rho_{droplet}}\left(\frac{RT}{2M\pi}\right)^{0.5}$$ **Equation 2.2 [42]**

where M is the molecular mass, R is the universal gas constant, T is temperature, ρ is the droplet density, the vapour density or the saturation vapour density (according to the suffix) and k is the concurrent take-up of water.

Upon ignition the flame kernel will develop at a rate dependent on the mixture strength at the spark location [49]. The flame will then propagate according to a number of factors but mainly mixture strength, homogeneity, and turbulence. The charge will continue to burn until the fuel or oxygen is depleted, which is when temperatures and pressures should peak. CO oxidises to CO_2 and NO formation mechanisms commence following this, the rates depending on the chemical composition of the mixture [1].

As the exhaust gases leave the combustion chamber, position (1) on Figure 2.1, temperatures reduce and the chemistry of NO then CO freezes. Some residuals drawn up from the crevices under vacuum may now begin oxidation,

prompting additional HC emissions. Precursors to particulates that have been formed are now present in the exhaust system, where further cooling allows nucleation of solid carbonaceous particles [42].

2.3 Carbon dioxide (CO_2) emissions

Cars are responsible for around 12% of total CO_2 emissions in Europe [16]. CO_2 is formed during combustion when a carbon-based fuel is oxidised. The example for Octane is given by

$$2C_8H_{18} + 25O_2 \rightarrow 16CO_2 + 18H_2O$$ **Equation 2.3**

The processes by which CO_2 forms during combustion using gasoline or diesel is much more complex than the ideal equation presented above but the chemistry is sufficient to describe stoichiometric (balanced) operation. The actual path by which this process takes place is understood only for simple fuels, such as hydrogen, methane and propane, whereas for fuels with more complicated structures the details are not well defined [1].

2.4 Carbon monoxide (CO) emissions

CO is a toxic, greenhouse gas that is formed during the principle reaction steps in the hydrocarbon combustion mechanism. The steps are shown, Equation 2.4 with *R* representing the hydrocarbon radical

$$RH \rightarrow R \rightarrow RO_2 \rightarrow RCHO \rightarrow RCO \rightarrow CO$$ **Equation 2.4 [1]**

When operating at stoichiometry or slightly lean CO oxidises into CO_2 as per the equation shown by

$$CO + OH = CO_2 + H$$ **Equation 2.5 [1]**

The oxidation reaction above requires temperatures in excess of 700°C. As Figure 2.2 [1] shows oxidation increases rapidly with hotter exhaust gas temperatures.

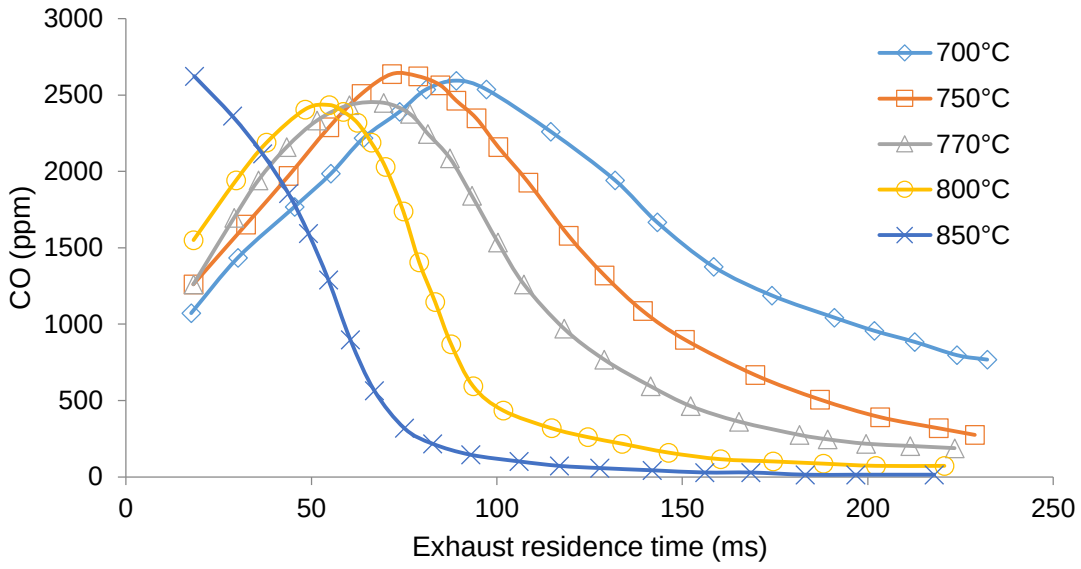

Figure 2.2 Exhaust CO concentrations (adapted from [1])

Reductions in CO emissions may be achieved by improved combustion efficiency as this allows more time for CO to oxidise to CO_2. The United States Environmental Protection Agency have released data of ambient CO concentrations in several U.S. districts for between 1980 and 2009 [50]. The data shows a significant decrease in ambient carbon monoxide, with an 80% reduction nationwide, from a national average of 8.95ppm to 1.76ppm.

2.5 Hydrocarbon (HC) emissions

Unburned hydrocarbons are a remnant of the combustion process when fuel is not completely oxidised, such as during rich operation or when a misfire occurs. A reasonable 3-way catalyst can convert almost all of the HC which may remain in the exhaust when operating at the correct temperature. The first few moments after a cold-start will mean a low conversion efficiency until the desired temperature is reached.

HC emissions from a 1.6 litre gasoline engine were recorded for the first 100s of the New European Drive Cycle (NEDC), Figure 2.3 [51], showing a clear difference in engine out (pre-cat) and tailpipe (post-cat) HC emissions. From about 30 seconds the catalyst has warmed up and there are almost no detectable tailpipe HC emissions, indicated by the cumulative tailpipe emissions trace.

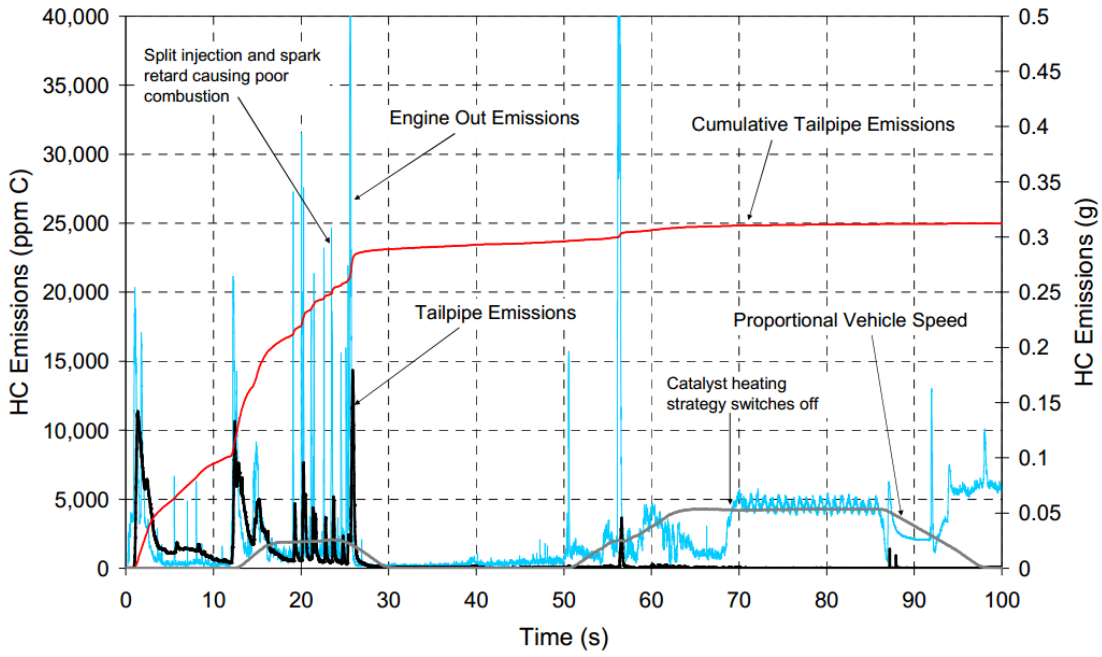

Figure 2.3 Engine out and tailpipe HC emissions from a cold-start NEDC [51]

It has been observed that hydrocarbon emissions are strongly linked with PN. Nuclei-mode particle emissions, the smallest classification of particulates, can be avoided by reducing the concentrations of volatile particle precursors like sulphuric acid and heavy hydrocarbons in the exhaust [52].

2.6 Oxides of nitrogen (NOx) emissions

Combustion with air forms nitrogen monoxide (NO), nitrogen dioxide (NO_2) and very small amounts of nitrous oxide (N_2O). These are collectively referred to as oxides of nitrogen (NOx). The main component that is formed within the high temperatures of combustion is NO.

The specifics of NOx generation have been outlined [1] but the principle reactions are shown in the following equations:

$$O + N_2 = NO + N$$ **Equation 2.6**

$$N + O_2 = NO + O$$ **Equation 2.7**

$$N + OH = NO + H$$ **Equation 2.8**

NO emissions form in both the flame front and post flame gases, and when the flame reaction zone is extremely thin due to the high pressures of combustion the amount tends to increase when there is a larger diffusion flame [1]. Such a flame will be present when the reactants are not premixed but mixing will occur when the reaction begins.

The rate of NOx formation depends on conditions during combustion. The rates of Equation 2.6 to Equation 2.8 at their specific conditions are shown in Figure 2.4 [1]. Bifurcations are also occurring in form of reverse reactions, which are also outlined in Figure 2.4 [1]. This highlights the difficulty of modelling NO formation.

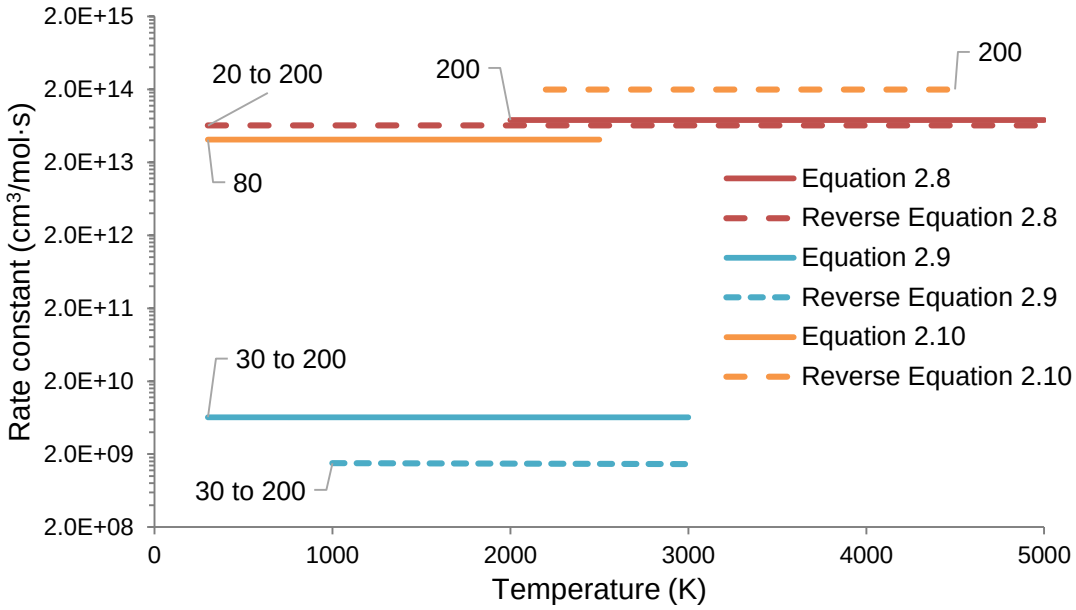

Figure 2.4 NO rate reactions across relevant tempeartures for various mechanisms labelled with percentage uncertainty, in form "## *to* ##" if uncertainty varies across temperature range (adapted from [1])

2.7 Particulate number (PN) emissions

A by-product of incomplete combustion is particulate matter (PM) that is formed when combustion occurs in fuel-rich (λ > 1) regions. This occurs when hydrocarbon molecules decompose in the presence of high temperatures and insufficient oxygen, i.e. pyrolysis [42]. This forms radicals and smaller molecules that are the precursors to the formation of soot nuclei. A variety of processes including agglomeration and surface growth increase the mass of the particulates which then become the larger carbonaceous particles (soot) [53].

Particulate matter can sometimes be visible as smoke from the tail pipe of diesel vehicles. When combustion is more efficient less visible smoke is produced however there are still small components that are known as particulates. These particulates are optically invisible and cannot be measured

via the opacity of the emissions. Instead methods of measurement involving counting the number have been developed and so the measure is referred to as particulate number (PN). Factors that influence PN formation and measurement will be discussed.

2.7.1 Legislation

Particulate emissions legislation is being continually revised as the health implications are realised [54]. The USA was the first to bring forward legislation in 1980 to limit the particle mass emissions from diesel passenger cars and light-duty trucks. Legislation is informed from epidemiological investigations that strongly indicate harmful effects of particles on health [55]–[57]. European legislation now includes particulate number emissions from all types of road-going vehicles and PN is coming under increased scrutiny as the dangers of the smaller particles are realised [57]–[59]. Particulates are primarily harmful due to their ability to embed themselves deep within the respiratory tract where the body cannot easily remove them.

Current legislation in Europe stipulates gasoline direct injection (GDI) engines must emit no more than $6x10^{11}$/km of particles larger than 23 nm in diameter when measured using the particle measurement program (PMP) protocol for solid particle number measurement [60]. Specifically this dictates the particle diameter must be between 23nm - 4µm and of sufficiently low volatility to survive evaporation after a residence time of 0.2 seconds at 300°C. Understanding of the factors that influence mixture preparation can help reduce PN emissions and research is increasingly focussing on this topic [53], [61]–[63].

2.7.2 Composition

The knowledge surrounding particulate matter and its composition is incomplete but continuing to improve. The latest understanding is that they formed from elemental carbon and very low volatility hydrocarbons (HC's) [60]. The source of low volatility HC's may be derived from lubricant that is temporarily stored on internal surfaces, such as in the catalyst, silencer or muffler. This process occurs through adsorption with carbon and then via evaporation during regeneration. This can also occur when volatile components slip through when exhaust temperatures are low and condense in the exhaust system [64]. These components are then released in response to high temperatures in the exhaust.

2.7.3 Formation mechanisms

A full description of PN formation is not yet known but it is agreed that diffusion burning from insufficient mixture preparation causes high particulate emissions [65]. Literature has identified a number of key mechanisms that are involved in the formation of particulate matter and one model considers 99 chemical species and 527 reactions [66]. An abbreviated description has generally been accepted to provide a fundamental understanding of the formation process, such as with the oxidation of petrol when a surrogate hydrocarbon is used. This description of particulate formation is depicted in Figure 2.5 [42] with the stages outlined below the figure.

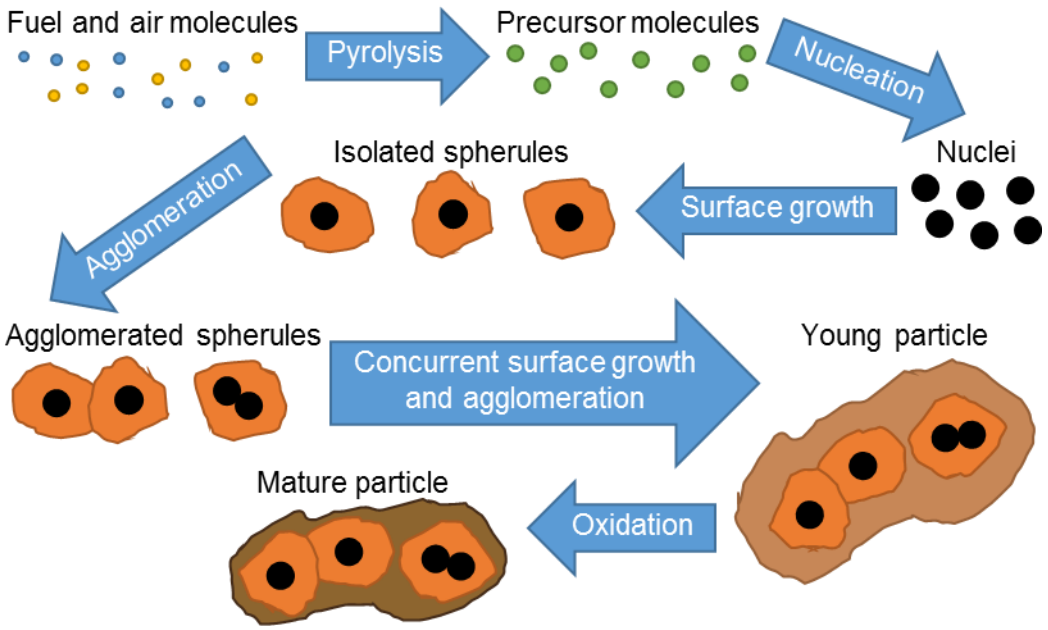

Figure 2.5 Conceptual scheme for the formation of soot-born particulate (adapted from [42])

The following list describes the steps illustrated in Figure 2.5 [42]. It should be noted that the number of steps involved from the conception of the precursors to the mature particle extend across a longer time period compared to the other emissions. This extended formation period is a reason why particulate emissions observations are often the least repeatable measurement on the test bed [67], [68]. The list is compiled from work by Eastwood [42] with additional sources provided where examples in literature were found.

i. Pyrolysis (of fuel)
    a. Hydrocarbons are the main material for pyrolysis, which occurs when the fuel is present in high temperatures and limited oxygen [42]
    b. One theory from Zhao *et al.* is that particulates also form within the exhaust system from the diffusion burning of partly volatised liquid fuel droplets [69]

ii. Nucleation

    a. Soot from incomplete combustion of fuel and/or oil, ash from fuel/oil additives and engine wear can contribute to nucleation [70]

iii. Surface growth
    a. Volatile components such as the sulphates, organics and nitrates adhere to the nuclei upon contact to form isolated spherules

iv. Agglomeration
    a. Particle size increases as contact is made between the spherules

v. Concurrent surface growth and agglomeration
    a. Simultaneous agglomeration and adsorption of volatile components further increases particle size

vi. Oxidation
    a. Residual heat energy in the exhaust gas removes the more volatile species on the particle surface to form a more stable structure

Once the particles are formed they will continue to evolve until they are captured by the measuring instrument. The types of particles that are detected are ranked, in order of increasing size, as nucleation-mode, accumulation-mode and course-mode. The PMP only stipulates PN is detected however there are instruments available that provide particle size distribution. Accumulation-mode particles are formed by a similar mechanism to agglomeration, by which the surfaces of particles bond and the structure increases in mass.

A GDI engine was run lean, i.e. with less fuel available, and was found to emit 90% fewer particles than when operating with a rich mixture [71]. During lean operation the nucleation-mode particles contributed more than 85% of the total

number of particles. Since the initial step in the formation of particles is pyrolysis of fuel there should be lower or no particulate emissions when there is no excess fuel present.

A reduction in PN can be achieved during homogeneous combustion by improving mixture preparation as this will increase the interaction of fuel and air, reducing the fuel available for pyrolysis. Raising the temperature of engine coolant should improve mixture preparation as fuel will be vaporised quicker upon contact with internal surfaces. This was observed to have a strong influence on the PN emissions of a wall-guided GDI vehicle [72]. Fuel evaporation rises exponentially with temperature and reduce pooling of fuel on the piston was observed with increased temperatures [73].

2.7.4 PN variation

Particle formation continues within the exhaust, allowing a significantly longer time for variation compared to the other exhaust emissions species [42].

Particulate formation is a similar process for gasoline and diesel engines [74]. A typical size distribution for a GDI vehicle is shown in Figure 2.6 [75]. The number of ultrafine particles (D_p < 100nm) is generally greater than the larger particles but the mass of these particles is significantly smaller. This creates difficulty when measuring PM since there could be a far higher number of smaller particles that are not adequately represented. Using a counting technique, or even better a size spectrometry as in Figure 2.6 [75], ensures full understanding of the measurement being undertaken.

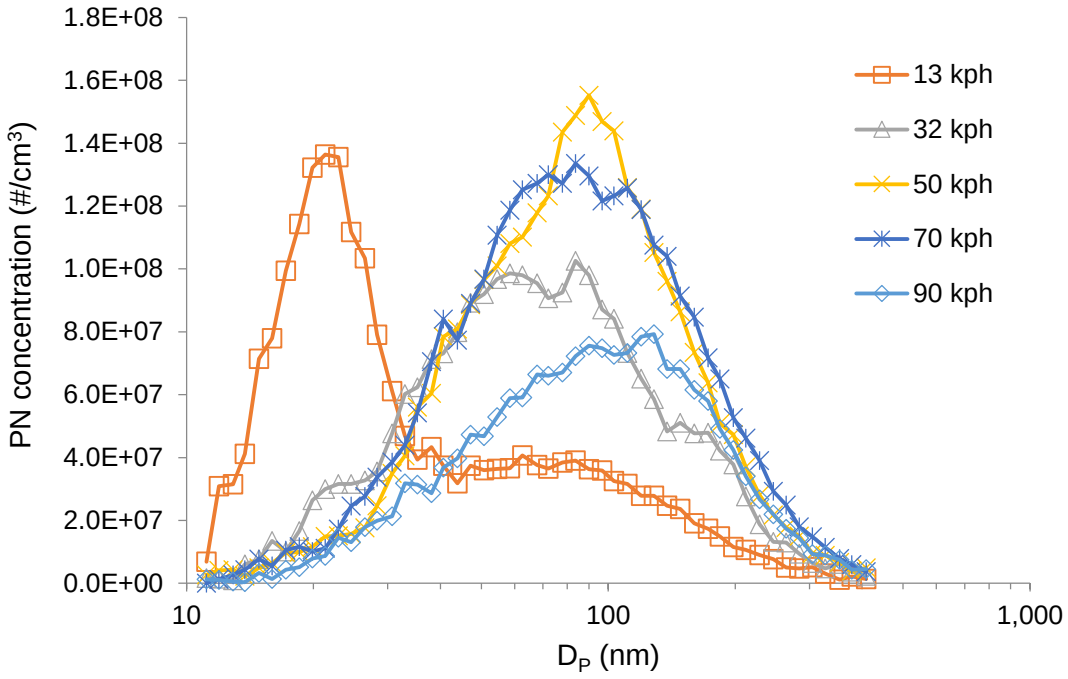

Figure 2.6 Number-weighted exhaust particle size distributions from a GDI vehicle at a range of speeds (adapted from [75])

Particles interacting in the exhaust stream may combine in a process known as agglomeration. Gasoline PN concentrations of approximately 10^5 p/cm^3 are thought to be too low for agglomeration to have a significant effect, but when the concentration rises above 10^7 p/cm^3 it is thought to play an increasingly important role in the number of observed particulates [76].

A number of factors which are thought to be sources of variation in particulate number are discussed by Yokoi *et al.* [77]. Some mechanisms that reduce PN are interception, thermophoresis, diffusion, sedimentation, electrostatic attraction and inertial deposition [42]. A detailed description of the most influential factors is provided below.

Within the exhaust pipework there are mechanisms in play that vary PN by ultimately causing deposition onto the internal surfaces. The main types of

particle-wall interactions are shown, Figure 2.7. The effectiveness of the mechanisms depends on the particle size as this primarily determines other physical attributes. The dominant mechanism which affects accumulation-mode particles is thermophoretic deposition [78], in which observed mass losses were estimated at more than 5%. Another study found gravitational forces to significantly attribute to particle deposition in parallel with thermophoresis [79].

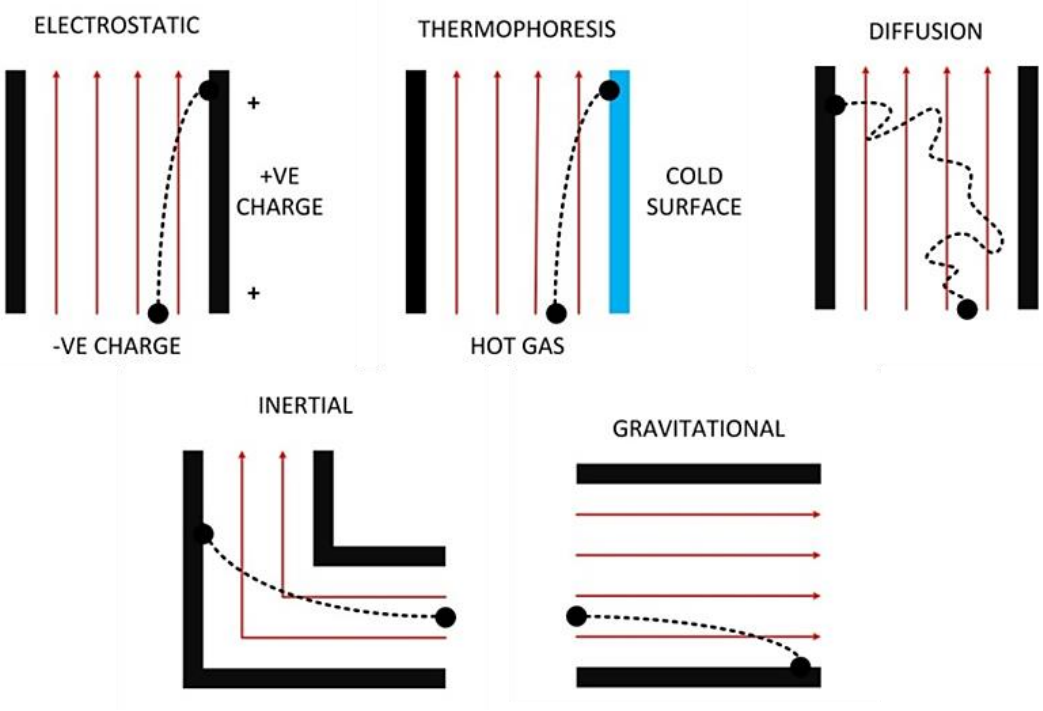

Figure 2.7 Deposition mechanisms for particle-wall interactions

Losses of particulate emissions have also been attributed to the auxiliary systems. Deposits in the catalyst and EGR system are known to contribute to PN variation [64], [67], [79]. A reduction in PN of 78% was seen across the catalytic converter when operating at low power conditions [67]. This was attributed to both inertial impaction within the catalyst and the loss of volatile particulate matter. Graskow *et al.* [67] observed the organic compounds were

the main fraction that was lost within the catalyst, which then later becomes part of nuclei mode particulates.

Silencers can also act as physical barriers to particulate emissions, especially since they include complex internal components in their design such as thin baffles with eccentric holes, internal connecting tubes, perforated baffles and sound-absorbing materials. They tend to be situated horizontally, allowing the full effect of gravitational deposition. Temperature gradients in silencers tend to be higher than for normal exhaust pipework as the surface area is higher, causing higher than normal thermophoretic deposition [42].

Engine type can influence the reliability of PN measurements as diesel engines are less susceptible to anomalous data than gasoline engines. Modern gasoline engine PN measurements are more susceptible to artefacts that are caused by ‘spikes’ in the data compared to diesel engines due to the smaller particle size distribution. A typical diesel particle size distribution will have an ultrafine (D_p > 2.5µm) peak situated in the accumulation mode that is absent in gasoline PN measurements. Sporadic peaks in PN data from gasoline engines can overwhelm engine-out exhaust particulate matter by of 3 – 4 orders of magnitude [76]. These artefacts can be caused when performing a transient-increase in operating condition since the hotter exhaust temperature may cause a higher PN as particulate matter is re-entrained [79], affecting particulate emissions measurements.

Changing the fuel composition will influence particle number and size distribution as the chemical components available throughout the reaction will

be different. Fuel composition from the pump can differ, such as annually in the UK to account for differences in ambient air temperature, causing PN emissions to vary significantly [80].

Wei *et al.* [52] observed a reduction of 60% in PN when the transfer line residence time (TLRT), whereby the sample is taken from the exhaust stream and measured, was increased from 0.1 to 2.1 seconds. PN reduced as mechanisms such as agglomeration and impaction occurred more often, reducing the number of individual particles.

An increase in the volume concentration was observed, which was likely caused by increased time available for nucleation that generated more particulate matter. The net increase from 0.1 to 2.1 seconds was 15%, Figure 2.8 [52]. Accumulation mode particles are the bulk of the volume and these mostly-solid agglomerates would not have been greatly influenced by TLRT once formed. Desorption of volatile components whilst in transit may have been the cause of reduced particulate volume.

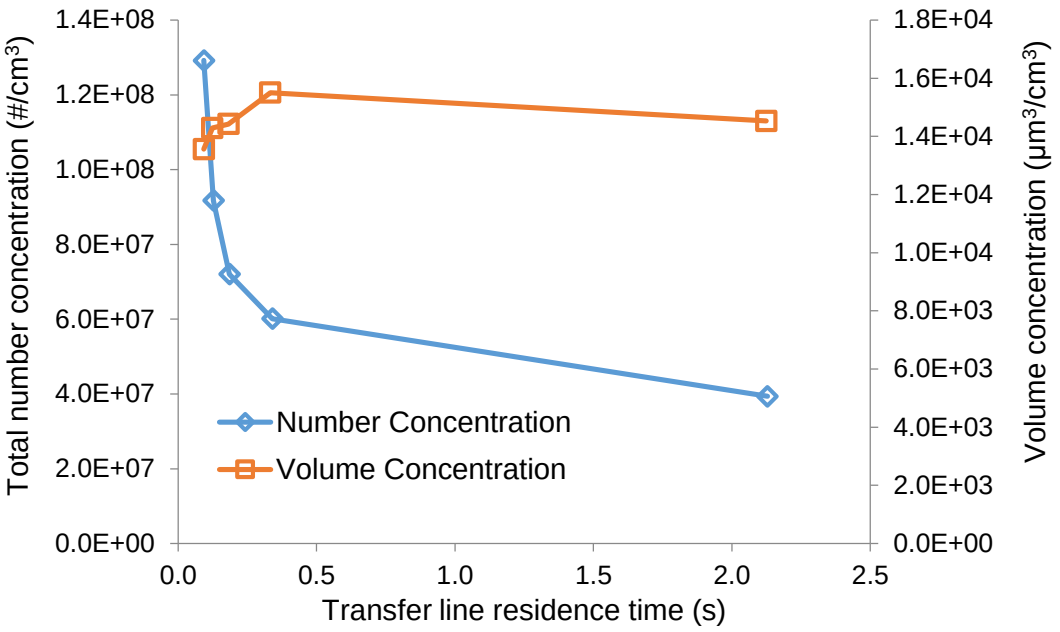

Figure 2.8 Influence of transfer line residence time on particulate number and particle volume concentration from a medium-duty diesel engine, samples taken 0.1 m downstream of the turbocharger (adapted from [52])

The order in which tests are carried out was identified by a number of sources to significantly influence PN [60], [74], [79]. The majority of effects are attributed to the storage-release mechanisms that also affect hydrocarbon emissions [52]. These mechanisms release material during high power operation causing PN measurements to increase by three to four orders of magnitude, completely overwhelming normal levels [76].

The order that test points are carried out can be compared to preconditioning as each test point will condition the system for the subsequent set point. A more evident preconditioning effect was observed by Rojas [79]. The inter-test operational history of the engine significantly affected steady-state mass-based particulate measurements. Two steady-state test cycles (R49 and ESC) were used and the transient operations in between modes were influential to the measurements made whilst at steady-state.

Another report by Abdul-Khalek *et al.* [81] found a CoV of 120% in steady-state PN measurements due to insufficient settling times between test points. These influences are attributed to the deposition and subsequent re-entrainment of particulate matter from the exhaust system, Figure 2.29. Effects of pre-conditioning have also been found to alter PN measurements the following day [60].

Conditions in the exhaust affect the speed of various PN reduction mechanisms. The method by which particulate number should be measured, as recommended by the PMP [60], stipulates that the raw exhaust gas is prepared for measurement by dilution. A schematic showing the concept of all dilution tunnels is shown in Figure 2.9 [42]. This helps prevent false-positive readings caused by volatile and semi-volatile species in the exhaust, which are not classified as solid carbonaceous matter and thus should be excluded.

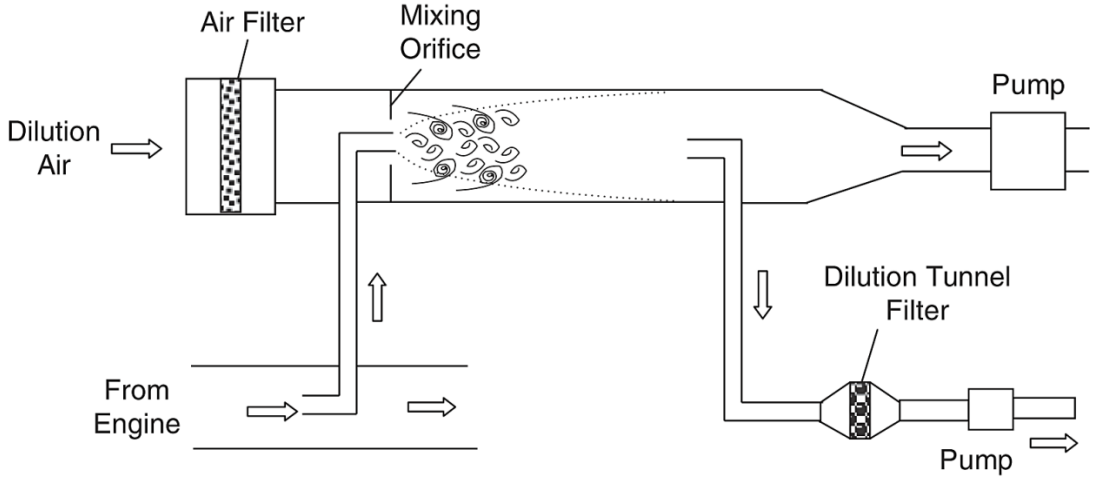

Figure 2.9 Dilution tunnel schematic [42]

The air used for the dilution process can influence PN if it is not sufficiently controlled as the dilution temperature and ratio can alter nucleation, with lower temperatures and higher dilution ratios promoting nucleation [12]. It was

observed by Shi *et al.* [82] that the number and size distribution of particles varied when the dilution air was provided at different states of dryness, Figure 2.10 [82]. Increased humidity caused higher PN and significantly increased nucleation mode particles. This is due to the higher rate of binary nucleation which is found with lower temperatures and higher levels of humidity during the dilution and cooling of hot exhaust [78].

Sulphate and nitrate components were also measured and a difference observed between the two states of dilution air. None were detected on particles which had a diameter of between 73 – 116 nm when the dilution air was dry. Humid air caused significant quantities of both to be present on particles at this smaller size, suggesting these components could travel farther into the respiratory tract.

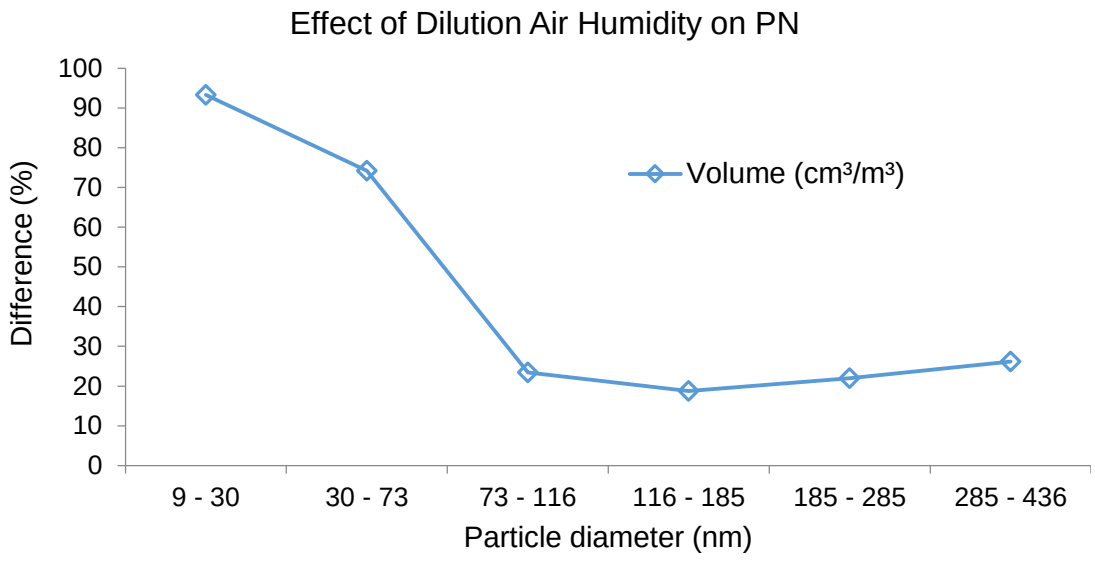

Figure 2.10 Changes to particle size distribution between dry (filtered) and humid (ambient) dilution air (adapted from [82])

Wei *et al.* [52] discovered that changing dilution temperature from 25°C to 15°C increased nucleation-mode particles approximately by a factor of 10. The cooler temperature is thought to increase nucleation-mode particles by increasing the gas-to-particle transition rate.

2.7.5 PN measurement

Particles are inherently difficult to measure as the diameters of those of interest are smaller than the wavelength of visible light. The measuring solutions available use a variety of methods to infer particle number since they cannot be counted individually. It is now standard for all emissions laboratories to have a dilution tunnel, such as that in Figure 2.9 [42], regardless of measurement principle. The instrument is then supplied with a homogenised sample.

Once the sample has been diluted it is fed into the respective measuring instrument. The particles in the sample are regarded as ‘particulates’ by legislation when they are in the diluted exhaust at ≤ 52°C. Conventionally, measurement is carried out by recording the change in mass of a filter [83], [84]. However this cannot distinguish individual particles and the smaller and less heavy particles, which cause more harm to health, would not get a fair representation. Alternative methods have since been developed that enable the counting of individual particulates and these are outlined in Table 2.2.

Table 2.2 Methods to measure particulate number

Measurement Method	Principles of Operation
Condensation nuclei (*particle*) counter (CNC or C*P*C)	Super-saturated gas adheres to particles allowing them to be optically counted
Scanning mobility particle sizer (SMPS)	Sorts particles according to their electrical mobility's using an increasing or decreasing electrostatic field
Laser induced incandescence (LII)	Briefly heating the particles and measuring the ensuing incandescence
Electrical low-pressure impactor (ELPI)	Inertial differences are used to sort particle sizes A number of impaction surfaces then capture the various groups

A benchmark comparison by Cavina *et al*. [85] of commercially available PN measurement systems found a very high correlation between measurement instruments [85]. The data were collected during a range of steady-state and transient chassis dynamometer tests. The first 80 seconds of a cold-start transient test cycle are shown, Figure 2.11 [85], highlighting how the initial PN peak was captured more accurately by the fast-response particle counter (DMS500).

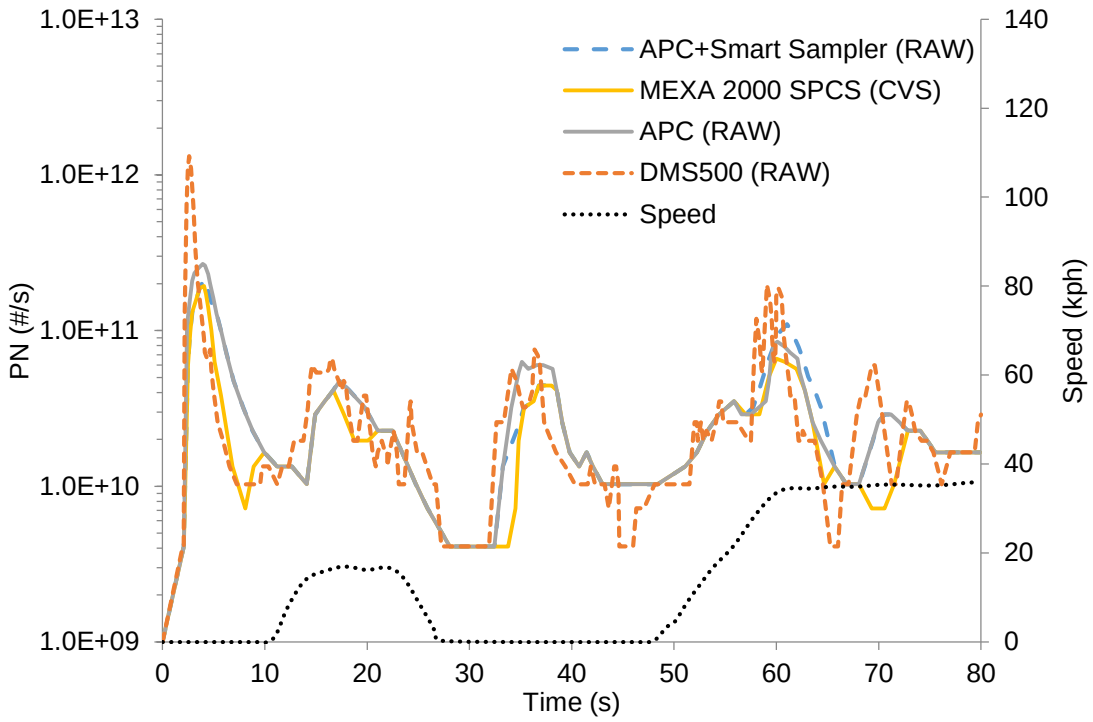

Figure 2.11 Instrument responses during start of NEDC cycle (adapted from [85])

The type of instrument used to measure particles for this thesis was a condensation particle counter (specifically an AVL Particle Counter (APC)). It allows a good transient response (~1 second) although the measurement principle does not distinguish particle size. The range of particulates detectable by the unit used range from approximately 23nm up to greater than 100nm. The counting efficiency varies significantly with particle size, Figure 2.12 [86]. In general, a repeatability of 5% for all particle measurement systems and a reproducibility of 10% is required for a modern engine calibration task [87].

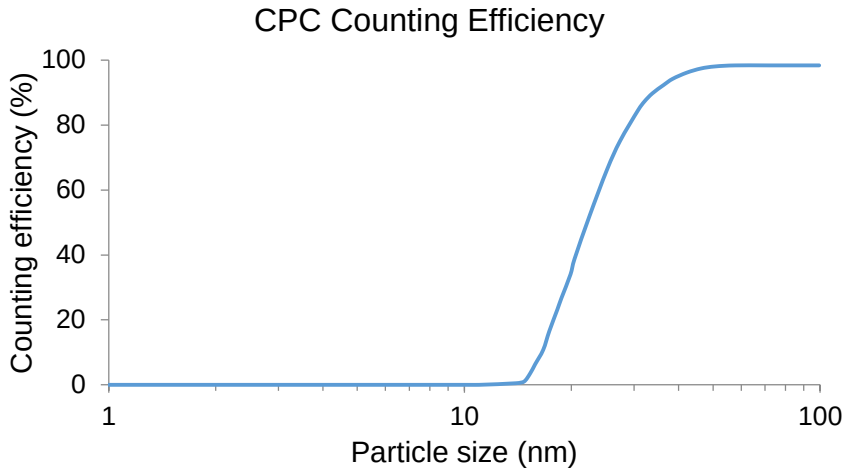

Figure 2.12 APC counting efficiency (adapted from [86])

The method that a condensation particle counter operates is as follows:

i. Exhaust gas is sampled and diluted with filtered compressed air using the C*hopper Diluter*
ii. A *heated body* warms the diluted exhaust gas in the evaporation tube to vaporise the volatile emission components
iii. The gases are diluted a second time via a porous tube diluter before being fed into the condensation particle counter (PNC / CPC) M*easurement Unit*
iv. Gaseous-state butanol is condensed on to the remaining solid particles to enlarge them
v. The particles are counted based on the scattered light pulses generated when the particles pass through a laser beam
vi. As per PMP specifications, counting efficiency of particles larger than 23nm is 50% ± 12%

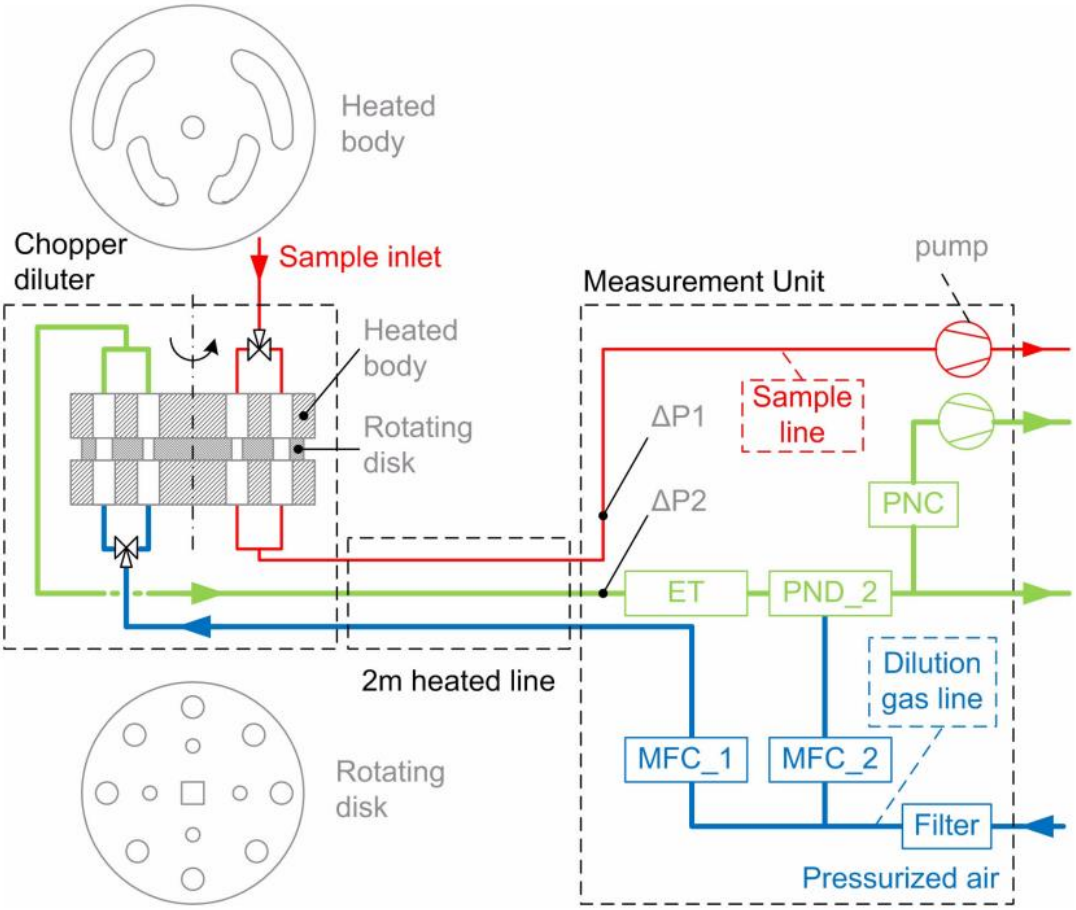

Figure 2.13 APC operating principle [86]

2.8 Steady-state engine testing for calibration

Calibrating an engine requires data to be measured from the engine during tests. Engine tests used for collecting this type of data can vary in style but are either steady-state or transient. Steady-state tests keep the engine and all control parameters constant, or steady, whilst recording data at each test point. Each test point may last for one or two minutes. Transient tests continuously change at least one control parameter throughout the test, in effect creating a test point for each data sample. Steady-state tests give more repeatable emission measurements [88]–[90] and will be the focus of discussion.

Data from engine tests are used to generate computer models of the physical system. Some commonly used techniques in the automotive industry include Gaussian process regression [91], General Linear [92] and Neural Network modelling architectures [93]. There are trade-offs for each method such as a faster initial data capture or more flexible model fitting. These models can then be used to optimise the performance of the engine away from the test bed, or “offline” [93], [94].

2.8.1 Identifying steady-state

Reliable steady-state data can only be collected when the UUT is running under representative operating conditions. In engine testing, an operating condition is usually described in terms of an engine mode and a dynamometer mode, such as speed-torque. The engine (or throttle) may be manipulated in three different ways [44]:

i. To maintain a constant throttle opening (position mode)
ii. To maintain a constant speed (speed mode)
iii. To maintain a constant torque (torque mode)

The dynamometer may be manipulated in four different ways:

i. To maintain a constant control setting (position mode)
ii. To maintain a constant speed (speed mode)
iii. To maintain a constant torque (torque mode)
iv. To reproduce a particular torque-speed characteristic (power law mode)

Once the operating condition has been set the thermal state of the engine can settle, after which steady-state measurements may be obtained. The typical duration of this settling period depends on the experience of the operator and

the experimental work being carried out. Martyr [44] suggests conditions are steady-state when the change in force sensed at an AC dynamometer air gap > 100ms. However Eastwood *et al.* [88] defined ‘typical’ steady-state in their work as when the rate of change in engine speed (at fixed load) is no more than 9 rpm/second.

The thermal inertia of an exhaust gas recirculation (EGR) cooler was observed to have significant effects on transient intake charge conditions [89]. It may be necessary to monitor additional variables, such as the temperature of the EGR cooler, to reliably identify steady-state operation.

Research carried out by Black [95] aimed to expedite steady-state engine calibration. The author found the temperature of oil in the sump was a reliable variable to indicate that the engine was operating under stable conditions. The method used was to wait 20 seconds following a 15-second period when the oil temperature changed less than 1°C. Engine coolant was also used to ensure the engine was stable. It was necessary for engine coolant temperature to remain within 2°C of the set point prior to observing sump oil temperature.

Vojtisek-Lom *et al.* [40] found temperatures in the exhaust have a strong influence on emissions of particulate mass (PM), hydrocarbons (HC) and carbon monoxide (CO). This suggests that if exhaust temperatures are continuing to vary then PM emissions are likely to be unstable. Higher temperatures, measured post-turbocharger, appear to reduce the emissions of PM, Figure 2.14. Vojtisek-Lom *et al.* [40] observed a similar trend for HC and CO emissions, although the performance of diesel and rapeseed oil fuels

are more similar. The authors suggest exhaust gas temperature could be explored as an inexpensive indicator of the quality of the combustion for the purpose of engine control. Many of the data presented uses exhaust gas temperature on the x-axis. The temperature of exhaust may not be a reliable metric as the real value can be poorly represented due to fluctuations caused by the response time and turbulence [96]. Inconsistent temperatures are likely to have a detrimental effect on the data and testing will no longer be 'steady-state'.

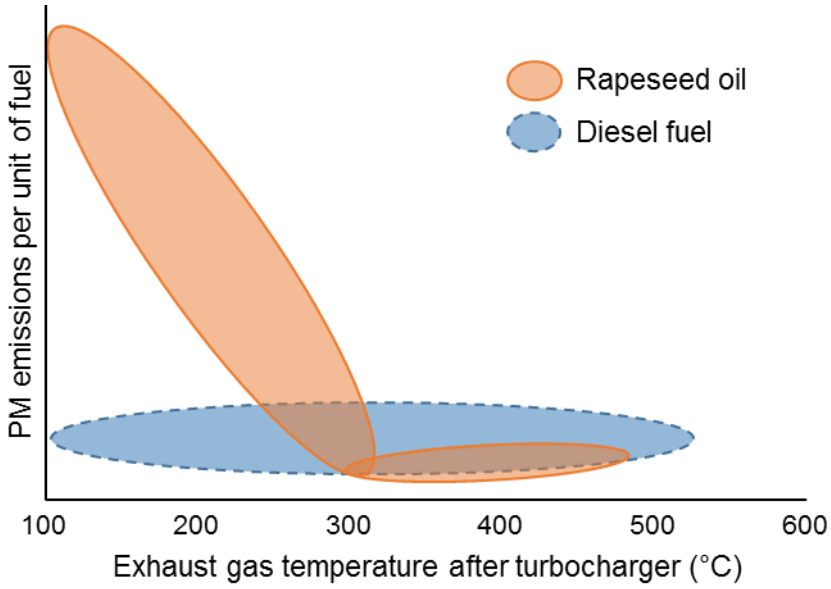

Figure 2.14 Effect of exhaust gas temperature on particulate mass emissions (adapted from [40])

A common method to identify stable operating conditions is by monitoring temperatures [40], [95]. Research from Vojtisek-Lom *et al.* [40] suggested exhaust temperature could be used as an inexpensive indicator of the quality of combustion. Thermocouples can be used to measure temperature and are cheap, readily available and robust. They can be retrofitted without the use of specialist tools or knowledge so almost all facilities can enhance their

measuring capabilities. They also do not require calibrating once installed unlike other types of sensors such as pressure transducers [97] or emissions benches [98].

Tharp and Cheng [99] reviewed hydrocarbon emissions from a homogeneous direct-injection gasoline/gasohol engine and determined in-cylinder temperature as a prime factor in predicting exhaust emissions. In particular, they state hydrocarbon emissions are susceptible to change with piston and cylinder wall temperatures. These two temperatures in particular have a big effect as the mass of residuals, which are hydrocarbon components remaining from previous cycles, contained in the crevices is reduced at higher temperatures. This is due to the Ideal Gas Law, which explains how temperature will cause a rise in pressure and volume. Also Henry's Law states at higher temperatures less fuel will saturate into the oil layer which is present on the internal surfaces, further reducing residuals.

Henry's Law:

> "*At a constant temperature, the amount of a given gas that dissolves in a given type and volume of liquid is directly proportional to the partial pressure of that gas in equilibrium with that liquid*."

Discovering which temperature is the most relevant can prevent the re-testing of unstable test points or waiting excessive durations for the temperature to settle.

2.9 Engine mapping and calibration

Modern engine development is increasingly relying on data-driven techniques as there are a greater number of inputs and responses to characterise. Data-driven techniques have a number of benefits over traditional “one-at-a-time” techniques as computer processing is exploited to quickly find the optimal solution using advanced statistical methods. The use of DoE for engine mapping is discussed further in Section 2.10.

An engine’s calibration aims to provide optimal performance across the whole operating range. Calibration is the process by which the operational characteristics of an engine is changed through manipulation of all its control mechanisms. The calibration targets a geographical-vehicle-driver combination to provide the best performance while remaining within legislative emission limits. To optimise engine performance the calibration sets all control actuator values to generate efficient combustion through optimised timing of events. Actuator positions are derived from the calibration phase of development.

Each new vehicle must conform to emissions legislation and there are numerous legislated outputs in the current European directive, Euro 6. This was effective from 1st September 2014 for the approval of new vehicles and 1st January 2015 for the registration and sale of new vehicles. Diesel passenger vehicles must reduce NOx emissions by over 55% and combined HC and NOx by 26% compared to Euro 5. Gasoline passenger vehicles are expected to conform to PN limits for the first time, with a total of $6x10^{11}$ particles/km [100]. A reduction of almost 27% in CO_2 emissions is set for 2020

for all new passenger cars [101]. If the new limits are adopted early there are also tax incentives available from member states.

Once the devices for controlling emissions are fitted on the production line they must last for 160,000 km [2]. A poor engine calibration can cause poor control over the A/F ratio that will hinder the lifetime of after-treatment systems. Poor A/F control may also generate carbon build-ups on the internal surfaces of the engine. Carbon build-ups are likely to reduce the performance of the engine by preventing valves from sealing effectively and causing injector performance to reduce. Build-ups on the internal surfaces can randomly detach, causing erroneous PN measurements [79].

2.9.1 Calibration resolution

Appropriate actuator values will be set by the ECU during normal operation of the engine. The signal path for some engine actuators will be a combination of electronic and mechanical whereas others are fully electronic. For every actuator the precise rotational location of the engine needs to be known. It has been observed that instantaneous speed changes appreciably with combustion [102], which may in turn cause miscalculation of engine position.

The values set, which are defined during calibration, aim to optimise engine performance for the operating conditions determined by engine sensors. Commonly controlled engine actuators and difficulties present in timing are shown in Table 2.3.

Table 2.3 Actuator timing variations

Actuator	Sources of variance
Valve timing	Linkage wobble
	Stepper-motor imprecision
	Stepper-motor response time
Injection timing	Injector rise-time (needle inertia)
	Fuel viscosity [103]
Spark timing	Dwell time [104]
	Spark gap angle (affects flame kernel development [49])
Fuel rail pressure	Fuel density and viscosity [105]
	Fuel-rail resonance (common rail injection systems only)

An ECU will send signals based on timing that is measured from the crank shaft. A position sensor that works using inductance is usually mounted on the flywheel. This can provide a resolution of between 1 to 0.5 degrees depending on the number of teeth on the flywheel.

For precise measurement of crankshaft position an optical encoder is necessary. This can provide upwards of 0.3 degrees resolution. However placing the encoder at the non-flywheel end of the crankshaft may cause errors due to the torsional effects in the crankshaft itself [102].

2.10 Model based experiment design

The Design of Experiment (DoE) method is an approach to select the fewest number of test points in order to derive enough information about behaviour of

a response over a range of input values [43]. The concept of DoE was originally introduced to agriculture by Sir Ronald A. Fischer in the 1920's [106]. Statistical principles such as randomisation, replication and blocking were used to design agricultural experiments. His work was the foundation for further research and development in DoE.

The application of DoE in the automotive industry has been common practise for little more than a decade [107]. Initial experiments were designed for the optimisation of a catalyst system [108] and camshaft timings [109], [110].

The popularity of DoE in the automotive industry can be attributed to the development of response surface methodology by Box and Wilson [111], which sparked a new era in statistical experiment design. Response surface methodology allows complex physical interactions to be simulated and visualised using polynomials.

There are two strategies of DoE, single level (one-shot) and sequential (adaptive). As the name implies, one-shot DoE collects all data in one attempt. Single level DoE experiments can be planned using a classical, optimal or space-filling designs.

Classical designs use a model hypothesis to define a set of test points that minimise the effect of random errors in physical experiments [107]. This branch of DoE adopts either full factorial or fractional factorial test point planning, Figure 2.15. Full factorial treats all combinations of variables as equally important [112]. Fractional factorial design treats only a subset of

combinations between variables as important such that higher orders of interactions are neglected [113], [114].

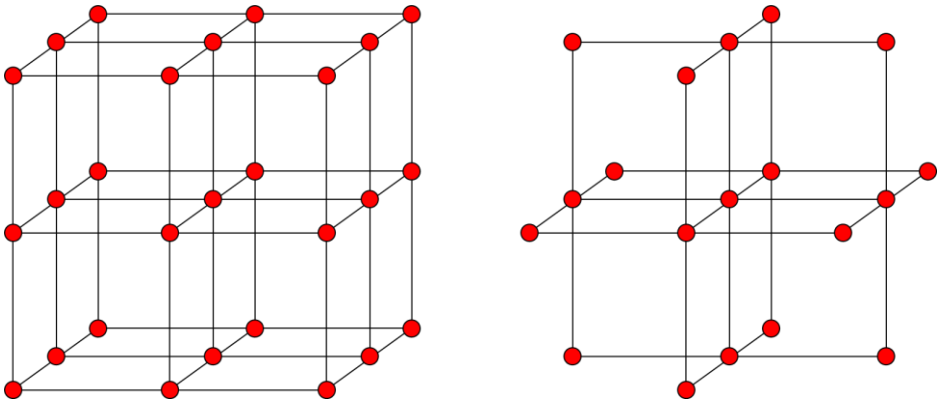

Figure 2.15 Full factorial (left) and fractional factorial experiment designs

The test points planned using a classical design will increase exponentially with each additional variable. Classical DoE designs are also not flexible, meaning any points that are not feasible will compromise the quality of the model. In summation, classical designs might not provide an efficient DoE technique for complex multi-dimensional nonlinear systems such as engine applications [115].

Optimal DoE designs adopt a pre-specified model type which is assessed with respect to a mathematical criterion [116], [117]. This allows a more optimised test plan that requires less experimental runs, Figure 2.16. This also allows for a constrained design space, whereas classical designs must be carried out within a symmetric boundary [118].

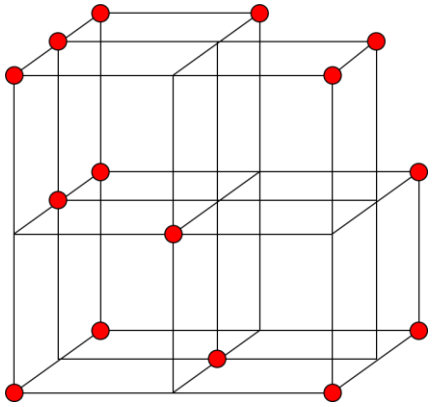

Figure 2.16 Optimal design for 3 variables

As with classical designs there is a degradation in design quality when infeasible points are dropped [119]. A substantial amount of *a priori* knowledge is also required, both with regards to model type and the number of test points [120]. A large amount of pretesting is therefore required for unknown engineering problems to provide the information required to plan the DoE [118].

Space-filling designs aim to distribute experimental test points uniformly through the design space to evenly map the response [9]. The strategy was adopted from the computer science field and first used for planning computer experiments [8].

Space-filling designs plan the experiment regardless of model type or system behaviour and are frequently used as an experimental design option for steady-state engine mapping when the system behaviour is unknown [9]–[11].

Efficiency of space-filling DoE technique is dependent on ability of DoE to have a good space-filling experimental design, i.e. test points are evenly distributed.

This is achieved by using a non-collapsing design [12], whereby each sample point has a unique value along any of the axes.

Space-filling designs are more flexible than classical and optimal designs. Infeasible points can be removed without degrading the experimental design integrity and extensive pretesting is not demanded.

It is necessary to use an iterative experimental design due to the following points [121]:

i. Infeasible test points due to design constraints or range limits of the parameters can be replaced to maintain model integrity.
ii. Poor model quality due to excessive measurement variation, outliers, or choice of model type can be corrected.
iii. Exploration of a non-observed design region initially assumed irrelevant.

2.10.1 DoE example

This section shows the generic processes that were used in this study to collect and process test data. Some typical control inputs and measured responses for a modern GDI engine are shown in Figure 2.17 [91]. Speed-Torque in this case will define the steady-state operating condition but this may be a combination of the control parameters listed in Section 2.2.

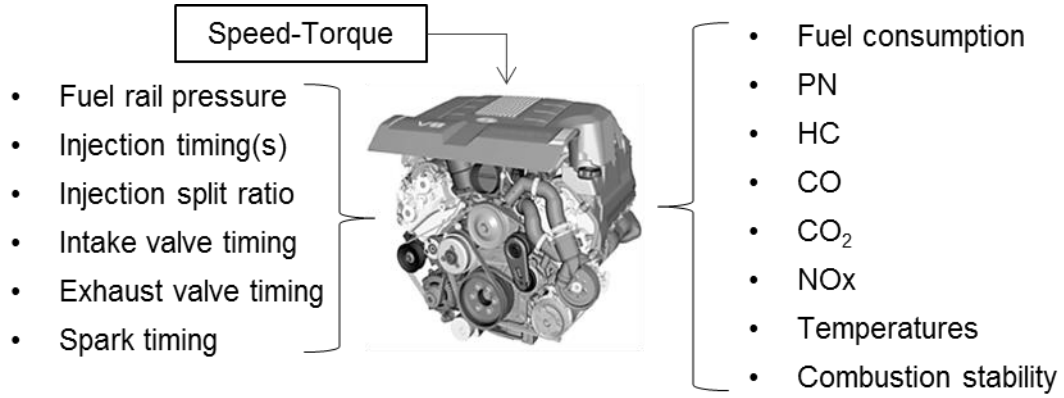

Figure 2.17 GDI engine control parameters and responses [91]

The flow chart in Figure 2.18 shows the stages used in a typical steady-state engine mapping and calibration DoE. The first task is to identify the engine parameters and responses that will be measured and controlled. The safe operating boundaries of the UUT at the different speeds and loads, constrained by factors such as knock and temperatures, will also be found during a screening process [122].

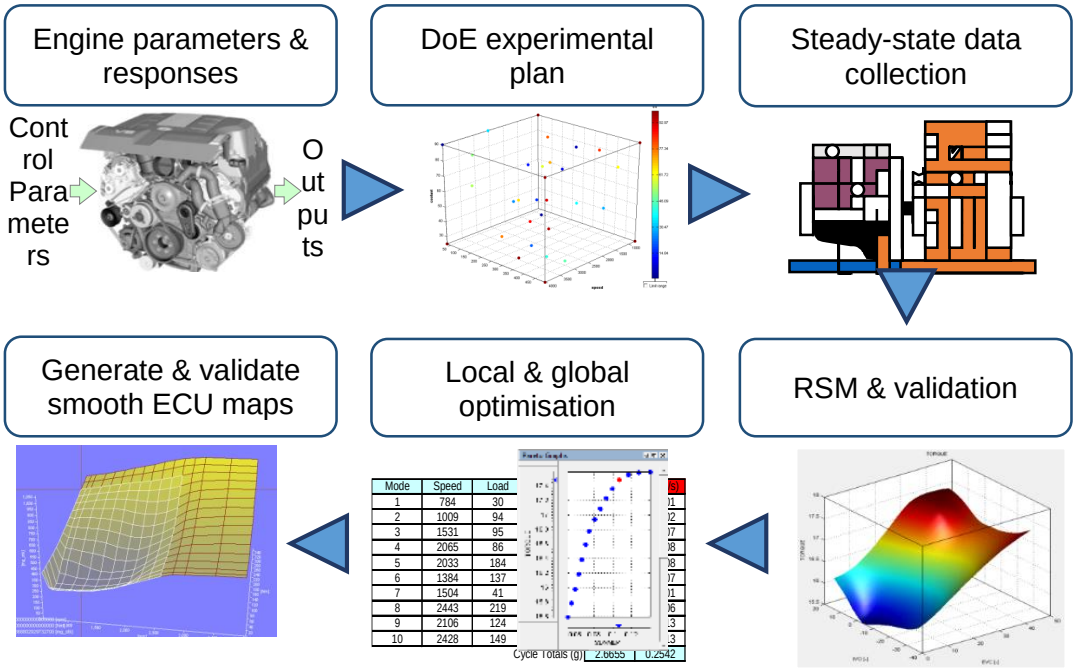

Figure 2.18 Model based calibration process

Next the test points are generated using space-filling algorithms such as Latin-Hypercube Sampling [38]. Data will then be collected at each of the test points and computers used to generate engine RSMs. This is the model building (MB) phase. The models are validated using additional test points in the model validation (MV) phase. Further testing may be required if the model fit is inadequate. This MB-MV sequence will iterate until the model fit is satisfactory.

Once the data are deemed suitable the models are used to generate a calibration based on the calibration targets. This may be one or a number of goals depending on the application. The optimised calibration is smoothed to improve driveability and prevent rapid actuator movements before uploading to the ECU. A final validation is performed on the engine with the new calibration.

The process outlined in Figure 2.18 above is a generic process that may be changed depending on the experience and ability of a facility. Dwyer *et al*. [91] combine the screening phase with the mapping and model building phase to speed up the process for a sequential steady-state engine mapping. The authors also use flexible MB-MV sequences to enhance the effectiveness of the engine data collection process.

Hametner *et al*. [123] used model based DoE to reduce the uncertainty of estimated model parameters by the generation of proper excitation signals. The authors found the model, which predicted engine exhaust temperature, performed better when optimised excitation signals were used as opposed to pseudo-random binary (PRB) signals. This indicates that using prior

knowledge of system behaviour to plan the test points will improve model parameterisation.

It can be concluded that modern calibration tasks must account for a wide array of variables and so the testing phases are critical periods as multiple interactions must be characterised. It is the task of the test-bed engineer to ensure that the data being collected are representative of the conditions outlined by the test plan to reduce the number of MB-MV iterations. Increasing the representativeness of data should help to improve the efficiency of the calibration process.

2.11 Data quality

One role of a test engineer is to ensure that sources of measurement error are kept to a minimum during testing and data quality is maintained. A number of factors can reduce the quality of information from the test preparation through test execution and finally in the post-processing of data.

Some typical sources and examples of poor data quality present in many organisations were identified by Beattie *et al*. [124]. Many of the examples are caused by a misunderstanding of the task that may be down to miscommunication or poor planning in general. Once a problem is recognised it can be remedied but resources will be wasted. Pre-empting the failure will speed up testing and reduce costs with potential additional benefits in the quality of the final calibration.

Beattie *et al.* [124] also suggested some general corrective measures. Three common solutions were standardisation, qualification and automation.

Standardisation can improve process efficiency as there is less need to cater for individual set ups. Qualification can improve the parameterisation of testing to prevent excess data from being recorded and avoid required data being skipped. Automation will primarily reduce human error and speed up each aspect of the testing.

Reducing test time whilst maintaining data quality can be achieved with adequate effort made to standardisation, qualification and automation. Insufficient effort paid to these three may also cause a reduction in data quality. Erroneous or anomalous data may also go unnoticed when automation is used if quality control checks are not employed.

2.11.1 System and measurement variability

Variations are inherent in measured data due to measurement imprecision. To effectively manage variation there needs to be knowledge of what the process should be doing, what can go wrong and what the process is doing. Sources of variation can then be identified at each stage of the process to provide an approximation of the precision expected at the data sink [124].

The magnitude of variations in data is dependent on the stability of the factors that influence the component being measured. The measurement repeatability of particulate emissions, for example, is low compared to fuel consumption as there are more influential factors [59]. Particulate emissions from a vehicle were recorded at a number of testing sites and the fluctuations in data are evident, Figure 2.19 [60]. In this case the vehicle, test procedure and type of

measuring device were kept constant but a poor level of intra-lab and inter-lab repeatability was observed.

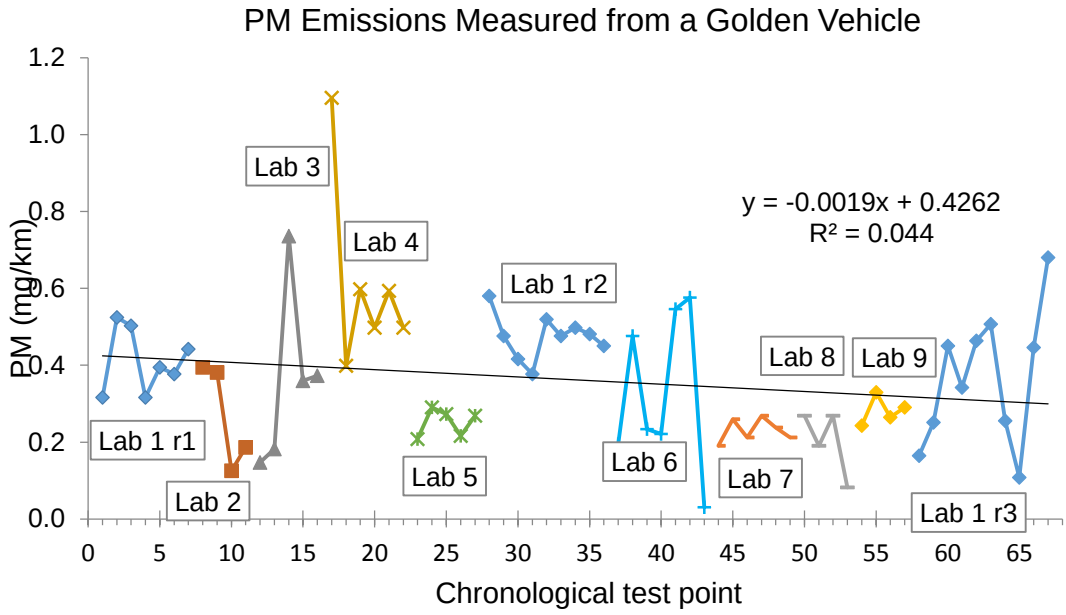

Figure 2.19 Long-term drift in PM emissions from a Golden Vehicle (adapted from [60])

Variability is present on a cyclic basis and describing the dynamics that cause this phenomena is the focus of a number of studies [4], [125]–[127]. Due to the reduced time available for mixture preparation there is larger cycle-to-cycle variability (CCV) observed in direct injection engines compared to port fuelled [125]. Differences in combustion between cycles are thought to be affected by four main factors: gas motion, A/F ratio, mixture homogeneity and residuals [128]. The largest changes are attributed to variations of mixture close to the spark plug at the time of ignition. Reductions in the differences in conditions from cycle-to-cycle will help improve control of the combustion, reducing both emissions and fuel consumption.

Adomeit *et al.* [125] observed the effects of injection on spray penetration and shape using particle image velocimetry (PIV), Figure 2.20 [125]. The interaction of turbulence and fuel injection leads to substantial increase in CCV of in-cylinder flow. Spray penetration and mixture formation would be affected by this, in turn causing variations in emissions, combustion stability and efficiency.

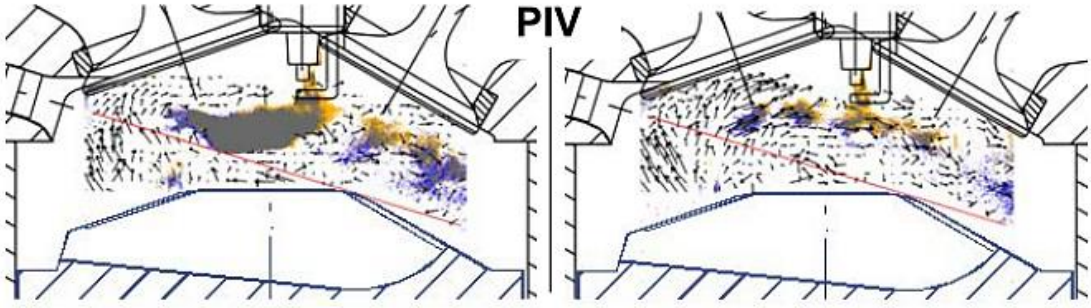

Figure 2.20 Cyclic fluctuations between two cycles at 10 CA after EOI [125]

A combustion bomb was used to test a variety of spark plugs at different equivalence ratios by Lee and Boehler [49]. Schlieren imaging, which is a method to visualise density variations in transparent media, was used to view the reaction from a viewing port, Figure 2.21 [49]. For a standard spark plug at an equivalence ratio (φ) of 0.65 the measurement variation in early flame growth period was up to 50% at 15 ms. Uncertainty dropped to 10% when a richer mix of φ = 0.85 was used. The mixture strength at the spark gap was found to be more influential than turbulence as a factor that affects flame kernel development propagation.

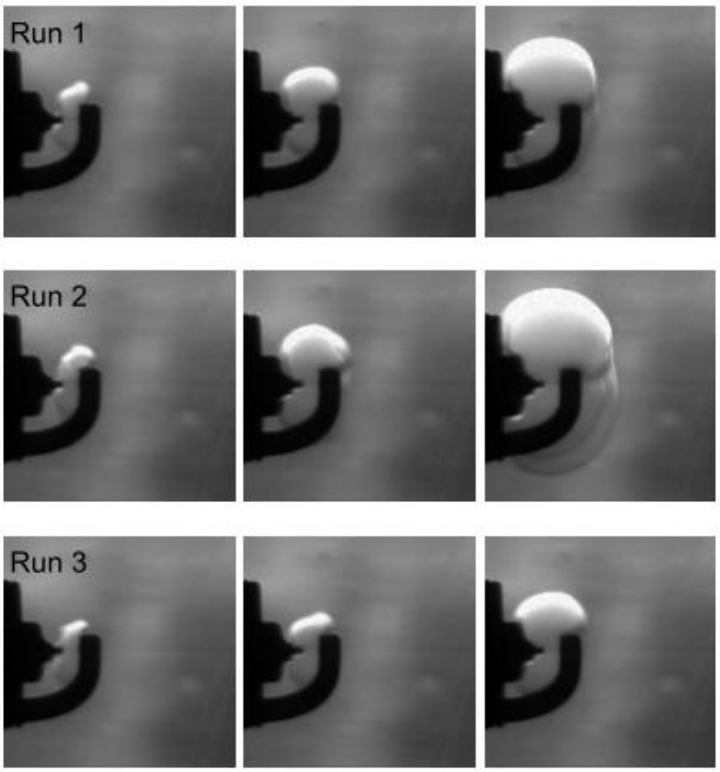

Figure 2.21 Kernel development variation between three repeated tests at t = 5, 10 and 15 ms after ignition [49]

Relating the differences in flow to emissions is usually carried out using computer simulations that are then validated with experimental data. Etheridge *et al.* used data from a 4-cylinder GDI engine to develop an engine simulation [129]. The Stochastic Reactor Model engine code was chosen and CO, HC, NOx and PN emissions were predicted. The model incorporates volume change, mixing, heat transfer, direct injection dynamics and flame propagation. The test engine was expected to have high cycle-to-cycle fluctuations in peak pressure as it was a direct injection variant.

Comparisons of the experimental and simulated data, Figure 2.22 [129], show good correlation between all emissions when operating at low load with high fuel stratification. Differences were observed in HC emissions with early SOI

as the model does not account for wall impingement that caused opposing trends in the data and simulation. Wall impingement is when fuel makes contact with internal surfaces, resulting in lower mixture preparation.

Very large differences (> 6400%) were observed in PN emissions for the two earliest injection timings. This may be caused by there being a greater time for errors in calculated mixture preparation to occur. A poor correlation in NOx emissions was also observed at the earliest injection timing.

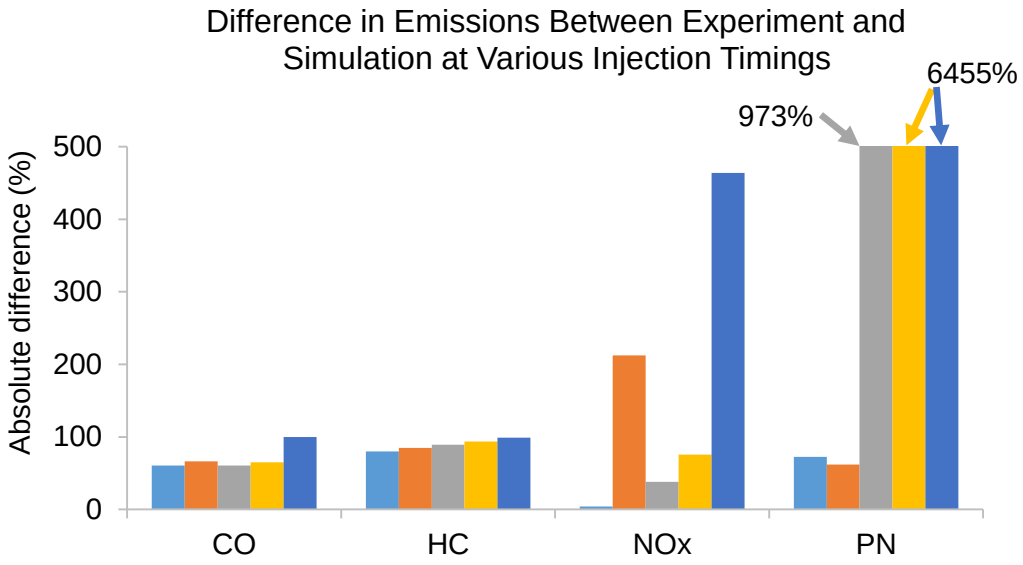

Figure 2.22 Differences in CO, HC, NOx and PN emissions at injection timings (from left to right: 50, 60, 70, 75 and 80 CA bTDC) between experimental data and a simulation (adapted from [129])

Other experimental differences that are difficult to model are inlet boundary conditions and residuals. Data based models for both these phenomena have shown them to both be substantial factors when attempting to reduce CCV [125], [130], [131].

Adomeit *et al.* [125] found that slightly fluctuating inlet boundary conditions may only cause small variations in the port flow but cause large differences in

the final flow within the cylinder. Simulations of the flow, Figure 2.23, show that CCV develops early in the induction stroke and are initiated in the region upstream of the intake valve. The image shows increasing differences in the speed of the mixture as the piston moves from near top dead centre (top-left image) to near bottom dead centre (bottom-right image). Small (< 2 m/s) flow variations in the intake manifold can be seen to cause up to 10 m/s variations in the whole cylinder by the time the induction stroke has finished.

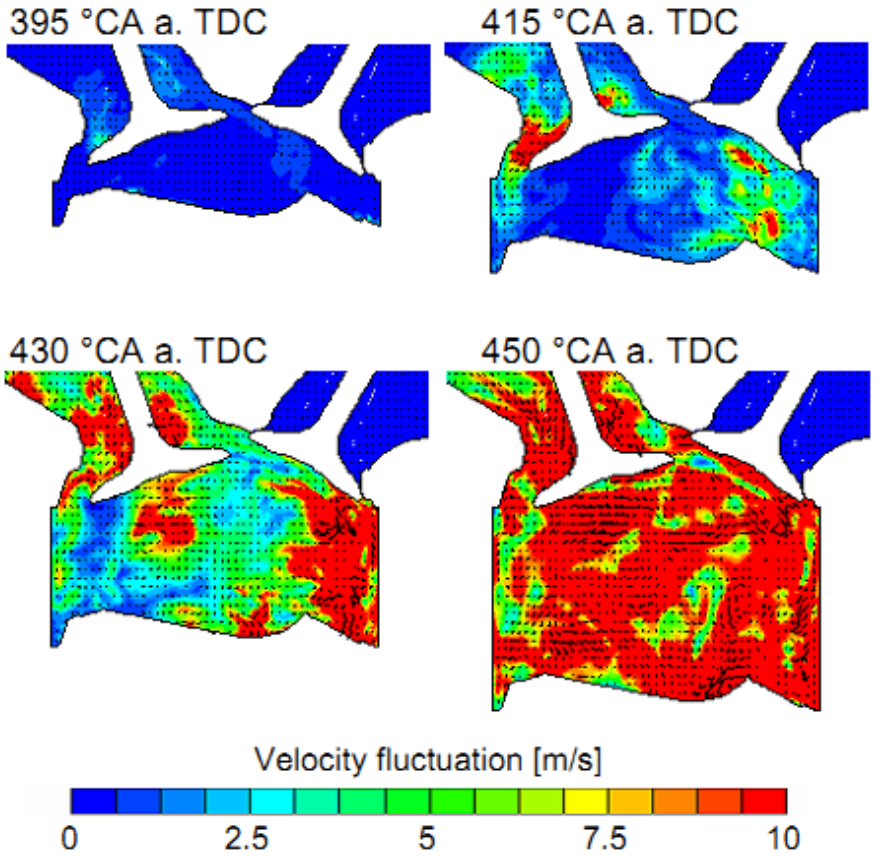

Figure 2.23 Modelled cyclic variations in velocity as the intake stroke progresses [125]

2.11.2 Repeatability

Repeatability is an ever present concern as legislated emissions targets reduce [100]. Test data quality targets are also under scrutiny as more engine responses are being modelled to fulfil the calibration targets. Improving confidence in the test data should mean less testing is required.

Data repeatability is described by international standards although the application of repeatability data is not described in the absence of reproducibility data. British Standard 5497-1:1987 Precision of Test Methods 1 [132] states repeatability as:

"*The closeness of agreement between mutually independent test results obtained under repeatability conditions*".

Repeatability conditions are defined in BS ISO 21748:2010(E) as:

"Observation conditions where independent test/measurement results are obtained with the same method on identical test/measurement items in the same test or measuring facility by the same operator using the same equipment within short intervals of time."

In summation, repeatability conditions are:

i. The same measurement procedure or test procedure
ii. The same operator
iii. The same measuring or test equipment used under the same conditions
iv. The same location
v. Repetition over a short period of time

Quantifying repeatability depends on the test being carried out. If a test point is repeated, such as a baseline test that is carried out each day, then they are successive readings of the same quantity and the coefficient of variation (CoV) can be calculated. This provides a direct indication of the scatter and since the data are normalised comparisons can be made between measured variables.

A repeatability index (RI) is described by Sougawa *et al*. [133] using Equation 2.9 where a larger RI represents a higher repeatability:

$$RI = \sum_{n=1}^{N} Score(n)/N \qquad \textbf{Equation 2.9}$$

where N is the summation of data point within a test and $Score(n)$ is described by Equation 2.10

$$Score(n) = \left|\left(1 - \frac{Data(n) \times 100}{Average(n) \times BasicErrorFactor}\right)\right| \times 100 \qquad \textbf{Equation 2.10}$$

where n is the data number in the test, , $Data(n)$ is the actual data at data number n, $Average(n)$ is the average of actual data at the value n for all tests and $BasicErrorFactor$ is the assumptive error value (%) at score zero.

In the study by Sougawa *et al*. [133], $BasicErrorFactor$ was set at 5%. Thus a score of 0 represents 5% error from the average and a score of 100 indicates that the data has the same value as the average.

The equations outlined above are designed to indicate the repeatability of a system using repeat test points. A DoE will avoid repeating the same test point the space filling algorithms used prevent two test points from occurring close together. As such the quality of data must be calculated from each test point. This can be achieved using fundamental statistical tools such as standard deviation.

Data recorded from steady-state test points should show no deviation and a representative polynomial should be a flat line that represents the mean. If there is deviation over the test point this will show as a high standard deviation and a fitted polynomial would have some gradient. Finding the gradient of the test point may also provide some additional information regarding the stability of the test point. It can be assumed that data with a relatively high deviation over time is not repeatable since the conditions are still stabilising. This deviation, or gradient, will likely depend on the prior test point or operating condition. As discussed in this section the sequence of steady-state test points can significantly influence the repeatability of particulate emissions measurements [60], [74], [79]. This is also demonstrated in Figure 3.15 [40] on page 74.

A test was carried out but the Technical Union for the Automobile, Motorcycle and Cycle Industries (UTAC) to determine the repeatability of emissions measurements between seven OEM chassis dynamometer facilities over a five month period [134]. The results shown, Figure 2.24 [134], demonstrate the difficulty in achieving reliable particulate measurements compared to the other

emissions. The high uncertainty was put down by the authors to influences from the vehicle, equipment and environment.

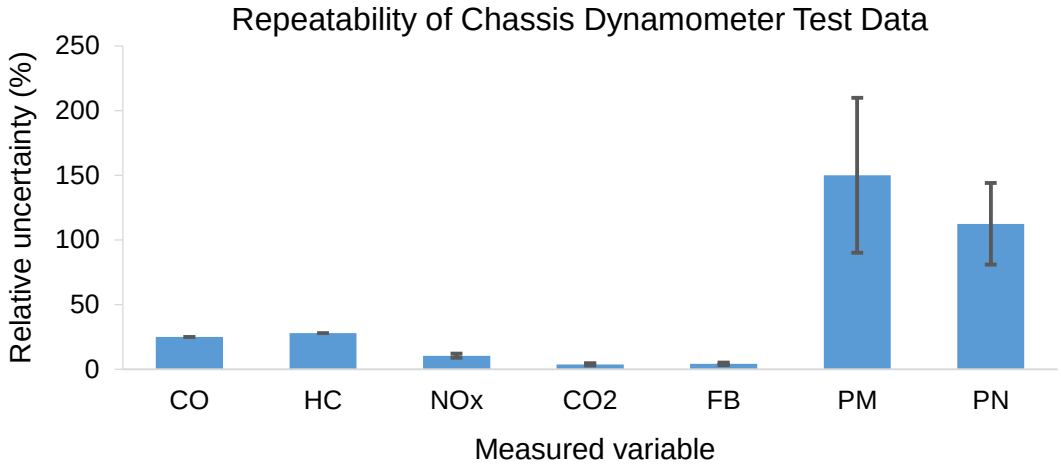

Figure 2.24 Repeatability of exhaust emissions and fuel consumption with error bars for ranges (adapted from [134])

The particulate measurements indicate that PN measurements are less varied than PM. Another report, this time concentrating solely on PN and PM measurement techniques, observed higher variance from particulate number techniques compared to mass for GDI vehicles [60]. A ‘golden vehicle’, which is the same car used by the participating facilities, was used for the study and it was observed that emissions were highly dependent on vehicle preconditioning.

Space-filling experiment designs are used to optimise engine calibrations when the performance of the system is not necessarily unknown [9]–[11]. It is paramount that the data are collected in concisely controlled test conditions. If the operating conditions deviate from the set conditions then the measurements will not be representative. When engine response surface models are parameterised using poor quality data, such as when

measurements are made in poorly controlled conditions, the optimisation will be carried out on a modelled system which is unrepresentative of the physical system.

Andrews *et al.* [135] observed CO and NO emissions, measured from a gasoline vehicle at various locations during a drive cycle, varied at different temperatures, Figure 2.25 [135]. The responses also increased or decreased at varying rates along the drive cycle. This would suggest that the response surface map would have a different characteristics, i.e. minima and maxima, depending on engine temperature.

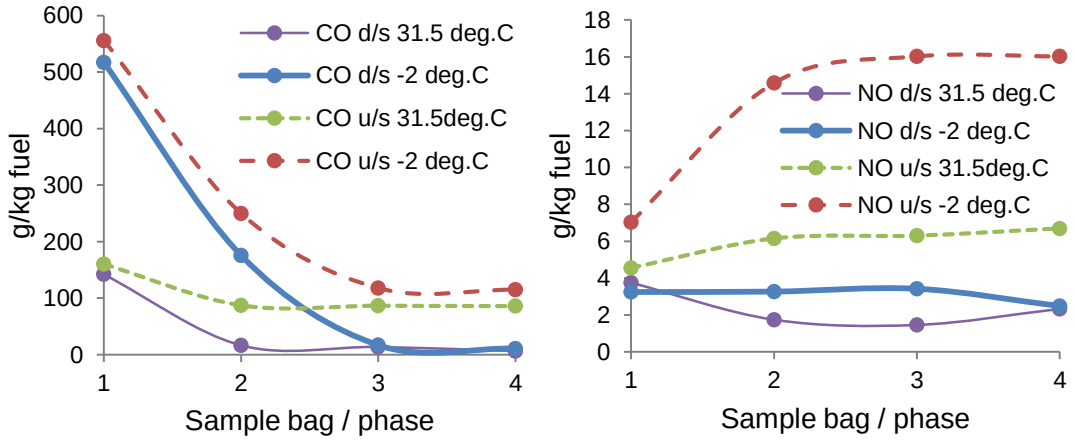

Figure 2.25 CO (left) and NO (right) emissions measured upstream and downstream (u/s and d/s) of the catalyst during various sections of drive cycle from a gasoline vehicle with catalyst face temperatures at 31.5°C and -2°C (adapted from [135])

Temperatures and pressures of engine fluids are all directly proportional [136] and so differing temperatures would also cause the engine performance to vary [1]. The particle size distribution measured from a GDI engine was distinctly different at all the operating temperatures as measured by a mass spectrometer, Figure 2.26 [73].

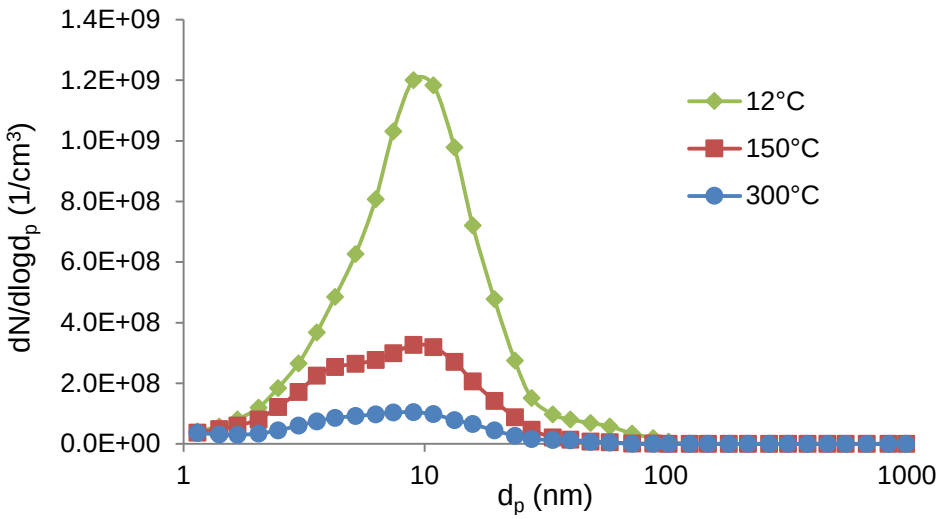

Figure 2.26 PN size distribution measured by a mass spectrometer from a single cylinder GDI engine at various coolant temperatures (adapted from [73])

Additional sources of variance will cause the system performance to deviate from the test conditions [73], [135]. The response surface model quality will be hindered, since more parameters than are measured are influencing conditions, potentially requiring additional test iterations to achieve the target model quality.

Variations in performance caused by changes in conditions such as temperature [96], preconditioning [40], humidity [63] and barometric pressure [49], should all be measured to explain potential changes in the response surface model.

2.12 Preconditioning

Steady-state calibration data is collected by changing actuator settings in between test points whilst maintaining the operating condition (speed-load, throttle-load etc.). An important assumption made during this process is that

conditions at each test point are stable. To mitigate transients the test points may be several minutes long and the mean value used for analysis.

When changing operating conditions the system must be allowed to settle before test data are recorded. Rojas [79] observed that very subtle differences in the conditions of the system were sufficient to produce significant changes in the processes that governed emissions. Many studies have found exhaust emissions are influenced by the prior operating conditions [39]–[41], [60], [77], [79], [137]–[139]. There is often no measurable changes in the thermal state of the system and the variations are thought to be caused by the accumulation and re-entrainment of matter on internal surfaces [83], [140].

Vojtisek-Lom *et al*. [40] observed HC, CO and PM emissions from a CI engine are affected by the operational history for tens of minutes. The results differed vastly depending on the fuel type but in general higher PM emissions levels were observed after low-load operation. The conditions that were used are shown in Table 2.4 below.

Table 2.4 Load conditions for Figure 2.27

Condition	Speed (rpm)	Load (Nm)
1	Idle	-
2	Lower[1]	Lower
3	Higher	Higher
4	1240	100
5	1480	45
6	1480	113

Figure 2.27 shows the influence of the different loads on the subsequent test conditions.

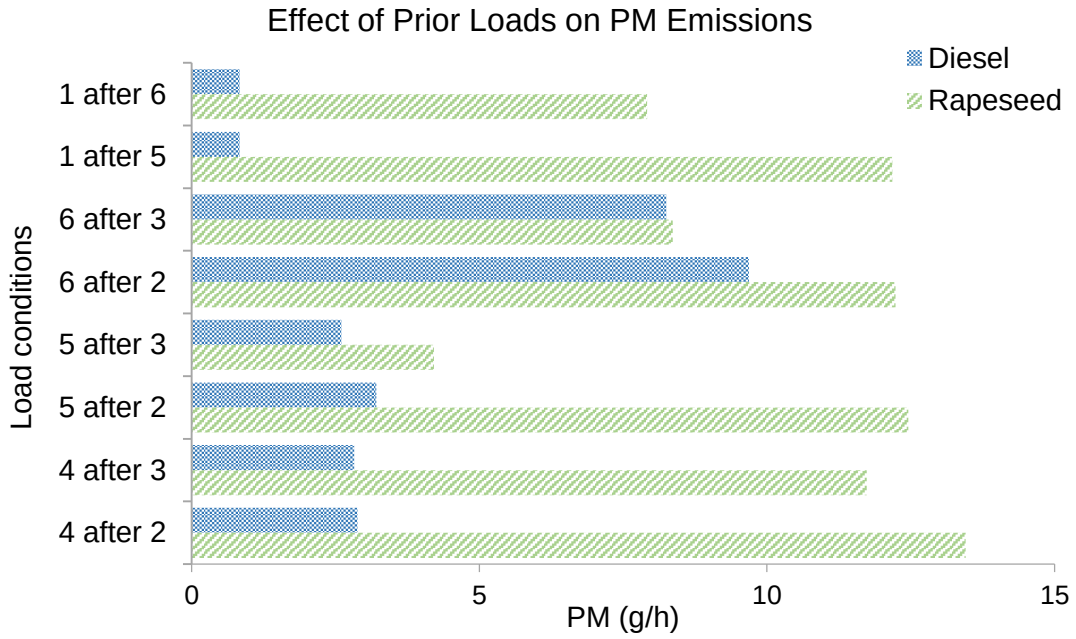

Figure 2.27 Effect of prior operating conditions on PM emissions (adapted from [40])

[1] Not specified in the work, ‘‘Lower’’ and ‘‘Higher’’ are simply explained as a lesser or greater value than the previous condition

Giechaskiel *et al.* [39] found PN measurements from light duty diesel vehicles depended on the speed of the preceding operating condition. An eight-fold increase in PN was observed when approaching a 100 kph test point from 90 kph compared to 110 kph. This was attributed to the storage and release of sulphates in the exhaust which are more abundant at higher temperatures due to the greater sulphur-to-sulphate conversion rate. Low-sulphur fuel has been promoted in the UK since 2000 [141] although storage-release processes exist for hydrocarbon components too [83].

Andersson *et al.* [137] observed large differences in particle size distribution at nominally equivalent idle conditions during steady-state testing of light duty diesel engines. The variations were dependent on the prior operating conditions. The largest and most numerous particles were observed following the highest load and speed. The authors found particle size distributions are more stable in the accumulation mode (150 nm) region but long durations are required to reach stable nucleation mode (10 nm) particle measurements. This suggests the smaller particles are influenced by changes in conditions for longer.

A joint research project aiming to determine the repeatability of particle measurement techniques proposed by the Particle Measurement Program (PMP) was carried out by nine test laboratories in the EU, Korea and Japan [60]. Various preconditioning routines were used to observe the effect on PN emissions measured over the New European Drive Cycle (NEDC), Table 2.5. The Extra Urban Driving Cycle (EUDC) is a 400 second drive-cycle segment that represents a more aggressive high-speed driving mode [142].

Table 2.5 Types of vehicle preconditioning routines tested

First	Second	Soak (h)
120kph; 20 mins	3 x EUDC	>6
120kph; 10 mins	1 x EUDC	~6
None	2 x EUDC	~6
None	None	>6
None	None	None

In general, PN emissions measured during an NEDC were lower when the severity of the preconditioning decreased, Figure 2.28. The authors clarify that the majority of the effects were observed in the first 3 minutes of testing following the preconditioning. The soak period following the preconditioning is thought to affect the amount of particles that settle within the vehicle's particulate filter interstices, which leads to higher solid emissions than for shorter soak periods. This should have little influence when a particulate filter is not used although the catalyst has shown to have an influence [83], [143].

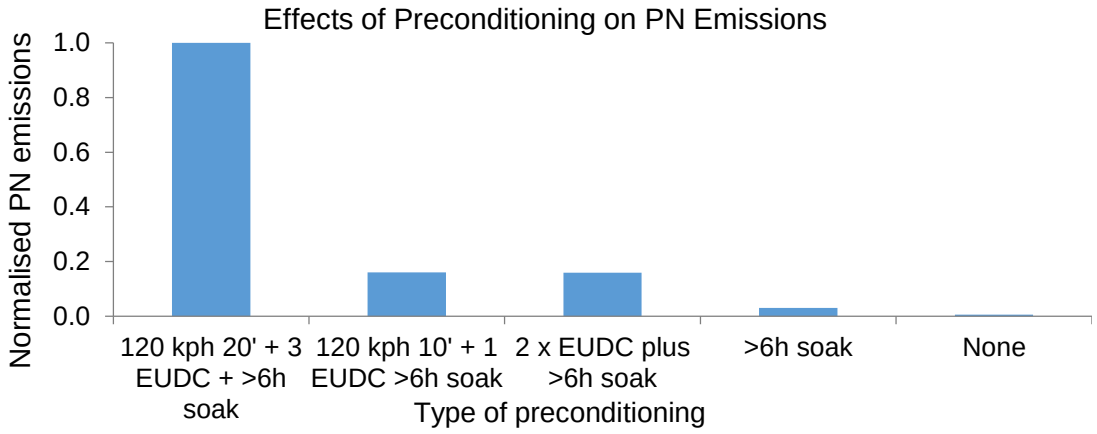

Figure 2.28 Effects of vehicle preconditioning on PN emissions, results normalised to EUDC results with 'full' (120 kph 20' + 3 EUDC + >6h soak) preconditioning (adapted from [60])

The Particle Measurement Program was mandated by UN-ECE GRPE (Working Party on Pollution and Energy) to develop a repeatable technique for measuring PN [41]. The study used a substantial preconditioning consisting of a 45 minute routine with two operating modes. The aim was to raise the temperature of the exhaust to purge the exhaust and transfer system of materials that accumulate at the lower power operating conditions.

Yamada *et al*. [138] evaluated the PMP-recommended number counting method, which uses a two-stage dilution system with hot and cold air to remove volatile particles, and identified preconditioning as a requirement to improve PN measurement repeatability. A full-load preconditioning was found to be effective at generating reliable PN measurements by Ivanisin *et al*. [139]. Rojas [79] also found high speed operation for 10 minutes produced an exhaust-system cleaning condition.

The use of preconditioning 'in-line' with measuring phases of a test were shown to drastically reduce variation in PN and D_P by Yokoi *et al.* [77]. The

authors tested a direct injection 2.5 litre diesel engine at a range of steady-state test points that were designed to form or remove deposits prior to measuring data. The results showed that preconditioning for one hour can reverse the build-up of residuals that occurs during low-load low-speed operation. Figure 2.29 shows the change in size distribution at steady-state compared to the initial measurement after running for one hour at idle then again after the preconditioning. The particle size distribution was measured at the same test point indicating that an approximate increase of 90% can be seen from the nucleation-mode particles after an idle duration of one hour.

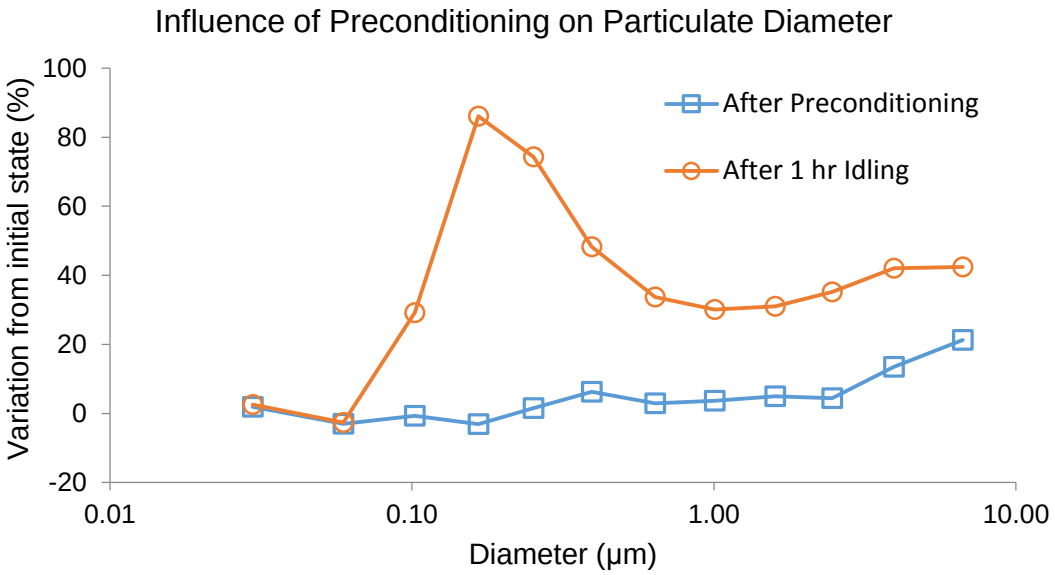

Figure 2.29 Influence of exhaust system condition on D_P at 1200 rpm 45 Nm (adapted from [77])

In summation, evidence from literature [39]–[41], [60], [77], [79], [137]–[139] suggests preconditioning can have a dramatic effect on the levels of exhaust emissions and, specifically, particulate emissions. Nucleation mode particulates are mostly affected [77], these are the smallest category of measured particles. There is not complete agreement in terms of what effects

preconditioning has on subsequent levels [77], [137], which may be caused by differences in instrumentation and methodology[134].

2.12.1 Removing the effects of preconditioning

It is impractical to completely remove preconditioning from an engine test as each test point will cause a certain degree of preconditioning on the system. However preconditioning can cause significant differences between tailpipe and engine-out emissions measurements [133]. The aim of preconditioning should be to present conditions that are representable by removing the stochastic influence of artefacts on measurements such as storage and release of particulate matter [144].

An intra-laboratory experiment observed a CoV of up to 71% in tailpipe PN emissions [60]. This poor repeatability was directly attributed to the effects of preconditioning. This situation should be avoided as data may not be representative of the operating conditions.

The test environment for a drive-cycle emissions test is controlled such that the conditions are fair and reproducible for each OEM [145]. Fuel consumption improvements of up to 8.7% can be attained by using fully charged batteries and 2.6% with properly inflated tyres [146]. Preconditioning can also be used to ensure exhaust emissions measurements are not higher than engine-out levels [139], [147], which is particularly influential on particle number and mass emissions [79]. OEM's can exploit these techniques to ensure the vehicle doesn't produce uncharacteristically poor fuel consumption and emissions measurements.

Preconditioning for optimum conditions (i.e. minimum emissions) is not representative of real-world driving. However preconditioning an engine can improve the repeatability of measurements [60] allowing the optimisation to be carried out on data that are representative of the physical system. Performance and driveability of the car will not be hindered by emissions-altering phenomena such as particulate build-up and release the but this will generate unrepresentative PN and PM emissions [83], [144].

Reducing anomalous measurements is a practical approach to avoiding having to repeat experiments. Repeating test points can generate a normal distribution and improve confidence of the measurements, however the test points used in a typical DoE are not repeated.

2.13 Summary

Optimising a modern engine calibration requires more test data than ever before as there are additional complexities from stricter legislative and consumer demands [79], [100], [101]. Maximum usability of data can be attained by ensuring that the data are high quality, both in terms of accuracy and precision. Steady-state testing is preferred over transient testing in modern EMC scenarios as it provides more repeatable data [88]–[90]. Emissions measurements are sensitive to changes in operating conditions and keeping the engine parameters stable reduces measurement deviation [79], [125].

When the engine parameters are changed, such as in between test points or operating conditions, there must be a stabilisation period otherwise emissions

measurements may be erroneous [39], [40], [52], [60], [74], [79], [137]. Increased robustness could be added with a method of identifying when the system has stabilised. Besides differences in engine operating parameters temperatures are the most influential factor on emissions levels. Consideration must be given to monitoring the relevant temperatures if repeatable emissions measurements are to be obtained [40], [89], [95].

There is evidence that the prior operating condition will affect the levels of CO, HC, PM and PN emissions after temperatures have stabilised [39], [40], [137]. This is because of preconditioning that occurs to the system, which can alter the exhaust chemistry due to different components remaining on the internal surfaces that are then re-entrained. Preconditioning can also be exploited to 'cleanse' system to ensure representative emissions measurements [60], [77], [79], [138], [139].

The field of engine mapping and calibration makes use of model based experiment design to meet the challenges presented during optimisation of a modern engine. This methodological improvement in engine development is continuing to adapt in order to ensure future targets can be met [36], [91], [123].

Increasing data quality by reducing erroneous measurements allows computer models to more accurately represent the physical system. Automation is a method to reduce errors as it can remove systematic human errors. These errors can also be reduced with improved planning and communication within

a company [124]. However PM and PN emissions data repeatability remains a concern for OEM's despite the progress in EMC methodology [134] [60].

Chapter 3

Mathematical Theory

This chapter describes the methods chosen to process data.

3.1 Standard deviation and coefficient of variation

Standard deviation (σ) is widely used in statistics to indicate the degree of dispersion. It takes into account the deviation of every value from the mean and it is found using the following equation

$$\sigma = \sqrt{\frac{\sum(x - \bar{x})^2}{n}}$$ **Equation 3.1 [148]**

where $\bar{x}$ is the mean of a set of n values. The standard deviation will vary relative to the mean, which causes comparisons between different data sets not straightforward. When the scatter of two data sets require comparison, such as PN emissions and CO_2 emissions, then the coefficient of variation (CoV) can be used. This can be calculated by dividing the standard deviation by the sample mean,

$$CoV = \frac{\sigma}{\bar{x}}$$ **Equation 3.2**

This allows the scatter of data from multiple sources to be compared.

3.2 Correlation coefficients

A correlation coefficient was used to measure the bivariate distributions. Several techniques to calculate the correlation statistic were considered. The three correlation methods considered were Pearson's product-moment correlation coefficient, Kendall rank correlation coefficient and Spearman's rank correlation coefficient.

1.1.1 Pearson's product-moment method

Pearson's correlation (*r*) provides a standard measure of how similar two samples are in a linear fashion. The statistic can be calculated using

$$r = \frac{\sum d_x d_y}{\sqrt{\left(\sum {d_x}^2 \sum {d_y}^2\right)}}$$

Equation 3.3 [149]

Pearson's correlation reflects the degree of linear relationship between two variables and is presented as a value between -1 and +1 for a perfectly negative or perfectly positive relationship, respectively. The product moment correlation coefficient is more accurate than Kendall's and Spearman's rank as some information is lost in the ranking, but Pearson's statistic assumes normally distributed values, however, which cannot be guaranteed.

1.1.2 Kendall's rank correlation coefficient

This was considered as it provides a ranked correlation between two measured quantities. Given that the pair of values (x_i, y_i) have been given the ranks (*q, s)* it can be calculated using

$$r_k = 1\frac{4Q}{n(n-1)}$$ **Equation 3.4 [149]**

where Q is equal to the number of intersections between the ranked data. This is visualised in Figure 3.1 [149], where Q would equal 3:

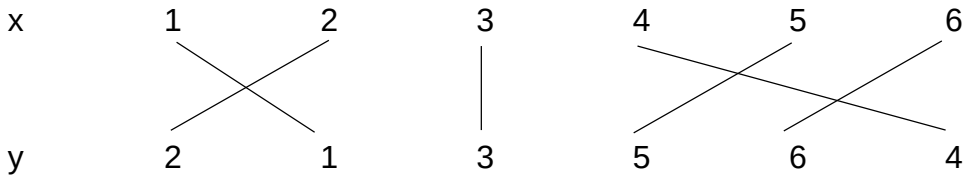

Figure 3.1 Joins between two corresponding ranks of data [149]

This is appropriate as the initial analysis of data was to find out whether there is a significant correlation between a change in actuator settings and the instability of and engine output. The process is slightly more complicated than the other two correlation statistics, which could possible add sources of error.

1.1.3 Spearman's rank correlation coefficient

Pearson's correlation is only able to measure linear relationships, whereas some engine responses may respond in a non-linear fashion. Valve timing, for example, may produce the minimum level of NOx at the middle of its range, generating a 'U'-shaped correlation. This relationship will be overlooked using Pearson's correlation. A method by which data in this form may be recognised is by using Spearman's rank correlation coefficient (Spearman's rho).

Spearman's rho is capable of identifying a correlation exists with two variables that vary in a non-linear fashion whilst managing to identify linear relationships

to a similar level as Pearson's. Given that the pair of values (x_i, y_i) have been given the ranks (q, s), then Spearman's rho (ρ) is calculated using

$$\rho = 1 - \frac{6\sum D^2}{n(n^2-1)}$$ **Equation 3.5 [149]**

where $D = q - s$. Spearman's rho also has the advantage of being extremely simple compared to Pearson's and Kendall's rank statistics. For measurement data which may not be exact, such as including outliers, this method should generate a more robust statistic.

3.3 Significance testing

Due to the potentially stochastic nature of the measurements being made it was necessary to perform an integrity check on the correlations being drawn. This is also good practise as some correlations cannot be predicted. This was performed using a null hypothesis test, where '1' indicates a rejection of the null hypothesis and '0' indicates a failure to reject the null hypothesis. Values in between indicate varying levels of certainty, e.g. a value of 0.05 indicates a failure to reject the null hypothesis with a certainty of 95%.

Because the sample being analysed are relatively small (< 30) the Student-*t* statistic is used in place of normal variate Z [149]. This method was developed by W. S. Gosset in 1908, who wrote under the pen-name of 'Student'. A two-sample *t*-test was used to calculate the hypothesis result, given by

$$t = \frac{\bar{x} - \bar{y}}{\sqrt{\frac{{s_x}^2}{n} + \frac{{s_y}^2}{m}}}$$ **Equation 3.6**

where $\bar{x}$ and $\bar{y}$ are the sample means, s_x and s_y are the standard deviations and n and m are the sample sizes. The case herein assumes that the data samples are from populations with different variances.

Chapter 4

Developing a Robust Steady-State Engine Test Methodology

4.1 Introduction

Test data that have a low precision and accuracy will reduce the efficiency of an engine calibration. This will inevitably result in a sub-optimal solution, which may result in slower product development if the target is not achieved.

The aim of this chapter is to create a systematic process to measure high quality, representative and repeatable steady-state data from an internal combustion engine.

4.2 Equipment and facility

A photographic description of the facility used to collect data for this thesis is provided in Appendix A2. Two gasoline engines, a V8 and an inline-4, were used in the experiments. Details of the engines specifications and test instrumentation are provided in Appendix A3 and Appendix 0 respectively. A schematic of the V8 test rig is shown in Figure 4.1, that of the inline-4 in Figure 4.2.

Two PC's were used to run the test software and record data. A synchronisation system was developed which allowed data from both PC's to be time-aligned in post-processing. A more detailed description of how data were channelled is presented in Appendix A6; the software interfaces for the test cell PC’s are also shown.

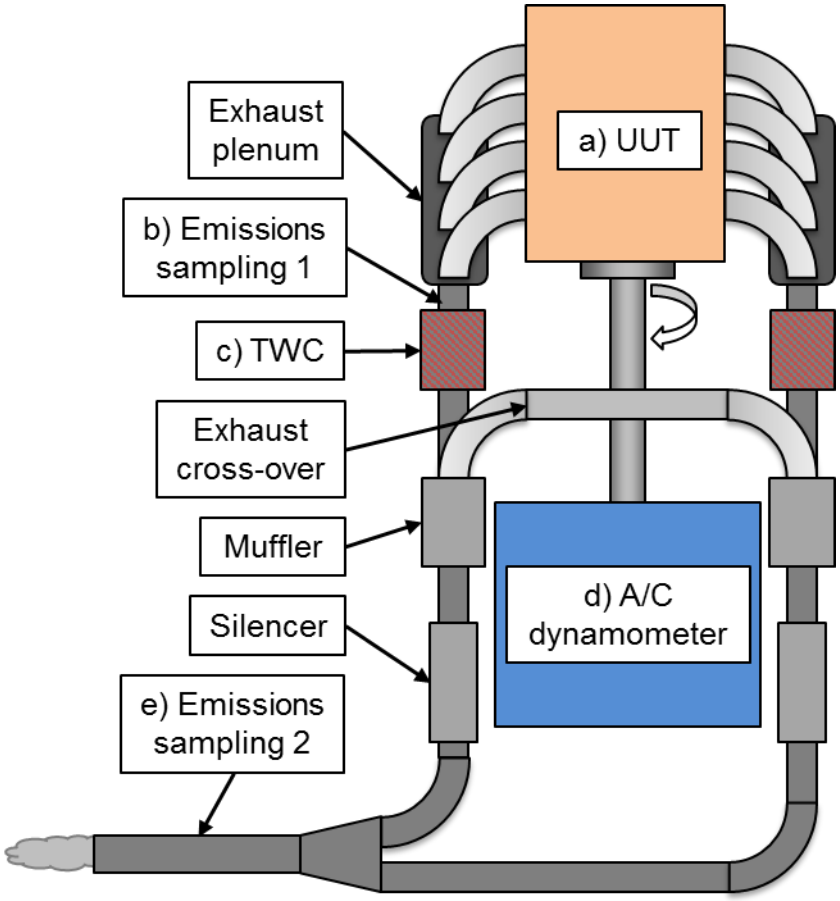

Figure 4.1 Schematic of the system with the JLR AJ133 power unit. Instrumentation installed: piezoelectric 8 in-cylinder pressure transducers, engine oil pressure and temperature (temp. measured at sump and gallery), gas temperatures (intake manifold, intake and exhaust ports) (a), gaseous emissions sampled at 1 Hz using HORIBA gaseous emissions analyser (b), three-way catalyst (two for the AJ133 V8, one for the EcoBoost I-4) (c), four-quadrant Eddy-current transient dynamometer (d) and particulate emissions sampling point 3.2m downstream of the exhaust manifold post-TWC and mufflers/silencers (e)

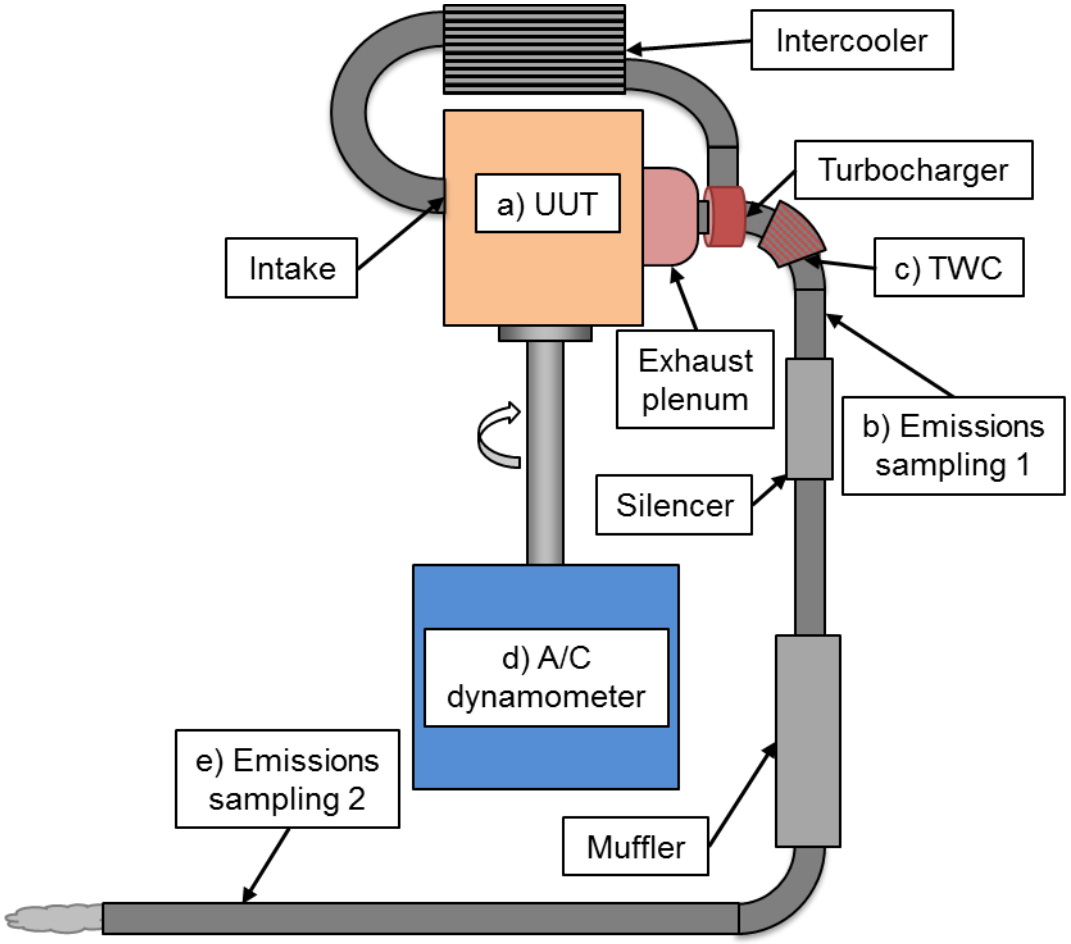

Figure 4.2 Schematic of the system with Ford EcoBoost power unit. Instrumentation installed: piezoelectric in-cylinder pressure transducer (cylinder 3), engine oil pressure and temperature, gas temperatures (compressor oulet, engine intake) (a), gaseous emissions sampled at 1 Hz using HORIBA gaseous emissions analyser (b), three-way catalyst (c), four-quadrant Eddy-current transient dynamometer (d) and particulate emissions sampling point 3.2m downstream of the exhaust manifold post-TWC and mufflers/silencers (e)

4.3 Experimental method

A number of steady-state experiments were carried out using two gasoline internal combustion (IC) engines. Initially a 5 litre naturally aspirated V8 was tested and then this was swapped out for a 1.6 litre turbocharged inline-4. Power was absorbed from both engines using the same fully transient A/C dynamometer. Engine coolant temperature was conditioned using an external

cooler to ± 0.5°C. Fuel was supplied at a fixed pressure and temperature. The test bed control software used was AVL PUMA Open 1.3.2 and all data were sampled at 1 Hz.

Four experiments were undertaken using the V8. In the first experiment the response of engine fluids were observed when various step-changes in engine speed and load were applied. The test was repeated five times across four days to verify the repeatability of the engine fluid temperature responses. Temperatures of engine coolant leaving the engine, oil temperature from the engine sump and engine gallery were measured.

The second experiment, *Identification of steady-state for repeatable emissions*, compared data from various engine responses when different steady-state indicators were used at a repeated operating condition.

The third experiment, *Comparing steady-state indicators for high quality engine measurements*, recorded engine responses at a number of steady-state engine mapping test points. The quality of data were compared when the recording of data was triggered by different temperatures stabilising. The test points were run once using coolant temperature and a second time using engine exhaust plenum skin temperature.

The fourth experiment, *Preconditioning for repeatable baseline emissions measurements*, focused on how the last operating condition of the day can influence test data on the following day. A number of steady-state speeds and loads were chosen to generate a range of conditions in the exhaust, ranging

from slow to fast gas velocity and low to high gas temperature. A standard test condition was used to observe the effects on data first thing the next day.

Data are then presented from an experiment that used the 1.6 litre inline-4, *Fast establishment of optimal steady-state indicator.* The conditions were controlled using the same hardware as with the V8 engine although charge air temperature was controlled using an external intercooler. This experiment aimed to find which variable was most reliable for indicating when the system was operating at steady-state.

4.4 Operating conditions

Several speed-load sites are repeatedly used for the experiments in this thesis. These operating conditions were chosen as they represent several key residence points in the operating range of the engine when driven on the European drive cycle. The work within this document was very closely linked to research by Kianifar [38], which focussed on improving the DoE strategy using these points. To make efficient use of the testing the operating conditions were shared. Engine simulations were carried out by the sponsoring company with three variations gearbox to determine the operating ranges, Figure 4.3.

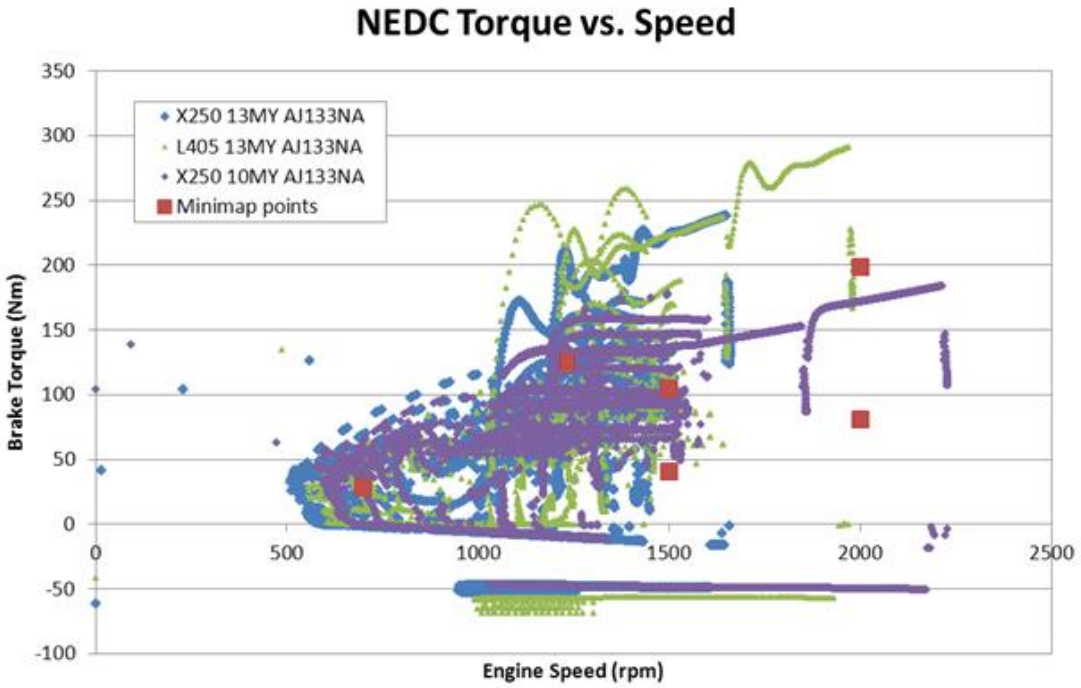

Figure 4.3 AJ133 GDI engine residency points during a NEDC test, for 3 different gearbox simulations (provided by Jaguar Land Rover)

Data from the simulations were used to determine the operating conditions (minimap points), which are listed in Table 4.1. After several tests the data from the lowest operating condition was deemed too unstable and this operating condition was removed from further tests. Operating condition 3 was added to the project list midway through the research project as this speed-load site better matched a gearbox that had improved performance.

Table 4.1 AJ133 GDI engine operating conditions

Operating condition	Engine speed (rpm)	Engine load (Nm)
1	700	28
2	1500	41
3	1250	125
4	1500	105
5	2000	81
6	2000	199

4.4.1 Test point selection

Test points at each of the operating conditions were chosen using a boundary search DoE procedure that involved a screening stage and an engine mapping stage.

Little knowledge existed about the GDI engine calibration on PN emissions for the V8 and the screening stage was planned accordingly. The valid design space for the calibrations at each of the steady-state speed-load operating points was defined. Automatic test strategies (e.g. AVL CAMEO) are able to quickly identify the design space for each parameter using exploration limits. This is combined in a self-adapting DoE to define the limits of the calibration parameters [150], [151]. However the information used in these initial steps is not used in further stages of the model building experiments.

The strategy adopted in this research was to use a space filling Optimal Latin Hypercube (OLH) DoE of a smaller size (e.g. 40-60 test points), in order to

support an effective design space exploration for potential areas of calibration trade-off. The OLH design uses the steps outlined in Figure 4.4 [152].

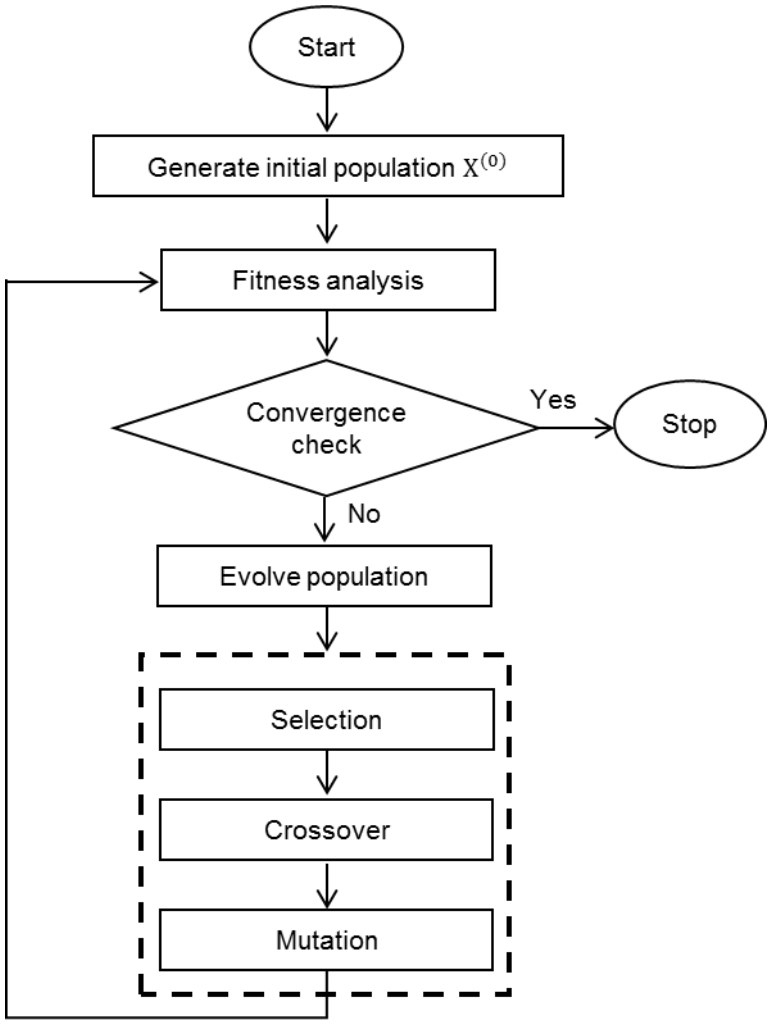

Figure 4.4 Flowchart of permutation genetic algorithm (PermGA) developed by Kianifar [152]

Data from the screening stage were processed in three steps to enable robust test point selection. The first step analysed the combustion stability to identify unstable test points. Combustion stability constraints were in terms of cyclic variability that depended on the engine power: SD(NMEP) less than 0.1 bar < 3bar NMEP < CoV(IMEP) less than 3%. The exhaust gas temperature also had to remain below 800°C in order to protect the catalytic converter substrate.

The second step was to fit engine response surface models to the data. Whilst insufficiently accurate for prediction purposes this allows interactions between calibration variables and responses to be studied and valid ranges of actuators to be determined.

The third step was to observe the consistency of physical interactions. Using analysis of models and trends at a given speed-load point both statistically and through engineering judgement the performance against the actuator settings were discussed to ensure the responses were logical. The influence of fuel rail pressure on fuel consumption and PN is shown in Figure 4.5 and Figure 4.6.

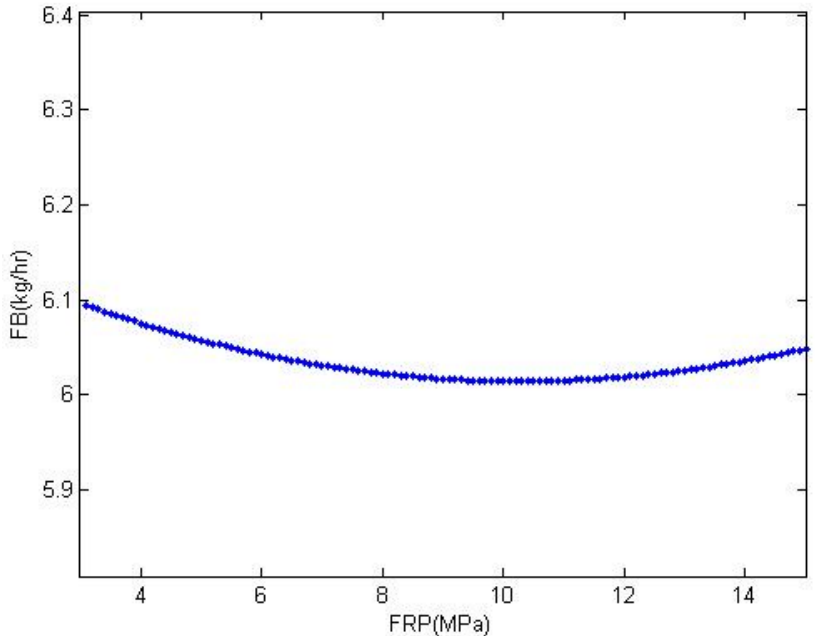

Figure 4.5 Influence of fuel rail pressure (FRP) on fuel consumption (FB). Increasing the pressure improved combustion efficiency via better mixture preparation up to a point, until the fuel began impinging onto the internal surfaces

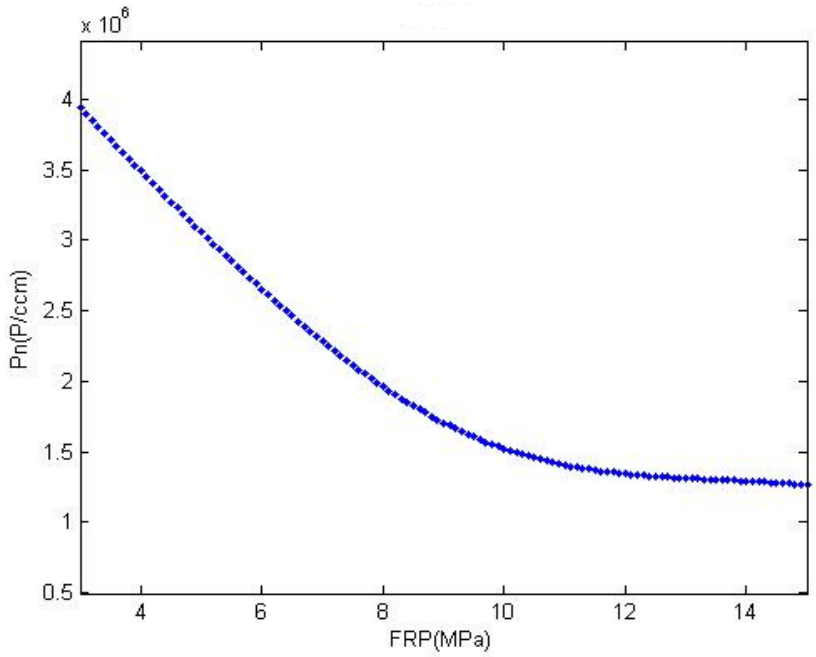

Figure 4.6 Influence of fuel rail pressure (FRP) on particulate number (Pn). Increasing fuel pressure dramatically improved mixture preparation with increased atomisation of fuel. Levelling off at a similar point to Figure 4.5 where fuel began interacting with the internal surfaces and reducing mixture preparation.

The engine mapping stage used the boundaries defined in the screening stage to plan and run detailed DoE's to fit accurate engine response surface models. The main model building DoE was based on a 50 test points OLH DoE. Of the initial 50 test points a subset of 40 was selected to be used for the experiments in this research. These excluded the 10 least stable points in terms of combustion stability to ensure high measurement repeatability. To adapt these test points for the EcoBoost engine the test points were normalised for the actuator limits that were defined during the boundary search of the EcoBoost engine. This ensured a similar distribution of test points as the V8 across the operating envelope.

4.5 Identification of steady-state following step-changes

A change in operating conditions will alter the demand on the test cell systems. The flow rate of coolant and fuel will vary proportionally to power produced by the engine. The dynamometer will also have to change the rate power is absorbed. The time that the test cell takes to settle following a change in operating conditions will vary depending on the response characteristics of the control systems and the magnitude of the change in operating conditions. It is only once system temperatures have settled that the cycle-to-cycle combustion variation will reduce to a minimum.

Several step-changes were performed on the unit under test (UUT) and temperature data from the engine fluids (engine coolant out, sump oil and gallery oil) were recorded. The steady-state conditions, shown in Table 4.2, range from high to low. The tests were repeated a five times; the first two tests occurred approximately four hours apart and the others were on separate days. The data were averaged across the tests and a curve fitted.

Table 4.2 Operating conditions used for the step-changes

Condition	Speed (rpm)	Load (Nm)	Power (kW)
1	2000	199	41.68
2	2000	81	16.97
3	1500	105	16.49
4	1500	41	6.44

The above test points were chosen because the engine conditions corresponded with operating conditions that represented the NEDC drive cycle

whilst remaining bound by the power limitations of the facility, Figure 4.7. The speeds and loads represent steady-state speed points on the European drive cycle that Jaguar Land Rover had requested were optimised.

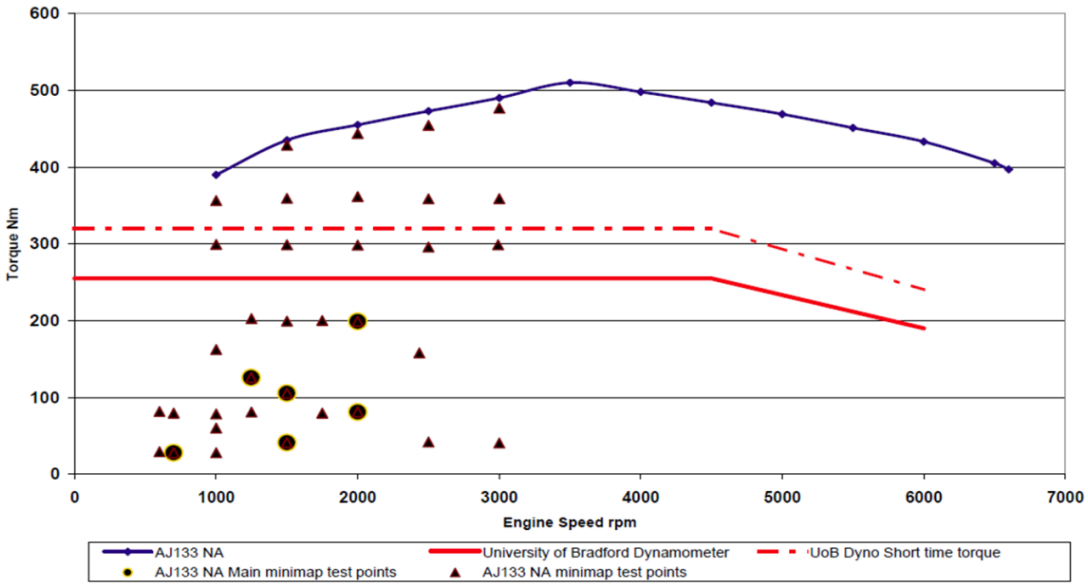

Figure 4.7 Speed and load operating conditions for the AJ133 GDI engine (provided by Jaguar Land Rover)

4.5.1 Results

The results presented in this section are from five repeat tests, the average value was taken and a simple polynomial fitted to smooth the steps created by the measurement resolution; plots of the raw data from each test are in Appendix A7. The polynomial order was chosen based on the lowest residuals, which are plotted below each figure. The data were collected during five tests on four separate days, the first two tests occurring on the first day.

The plot in Figure 4.8 shows coolant out temperature data following a step-change from Condition 1 to Condition 2. The reduction in demand placed on the external cooler causes the engine out coolant temperature to drop by 3°C.

The temperature increases again after approximately 70 seconds. Approximately 500 seconds passes before coolant out temperature stabilises sufficiently, i.e. remains close to the set point.

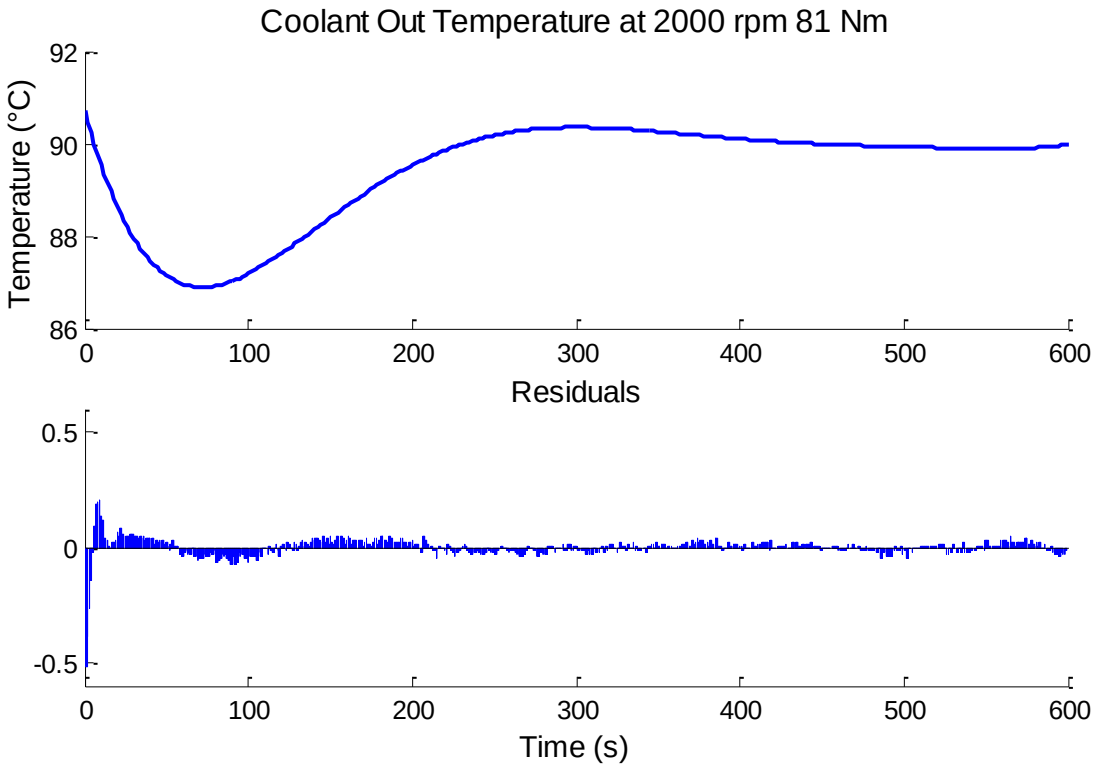

Figure 4.8 Engine coolant out temperature response following a step-change from 2000 rpm 199 Nm to 2000 rpm 81 Nm

Sump oil temperature data for the first step, Figure 4.10, initially reduces following the step-change. The settling temperature was significantly lower than the starting temperature. Oil temperature is regulated by an oil-water heat exchanger that is situated within the engine block and so changes in engine coolant temperature will generate a proportional response in engine oil temperature.

Since the power of the second steady-state condition was lower the oil settled at a lower temperature. The point at which the temperature gradient stopped

was approximately 400 seconds. This is not dissimilar to the period the engine coolant temperature took to stabilise, Figure 4.8 above, although the temperature difference is less pronounced.

Some noise is present in the sump oil temperature measurements, which can be seen by the residuals. This can be observed in all traces from the original data, Figure 4.9, and is thought to be due to the placement of the thermocouple.

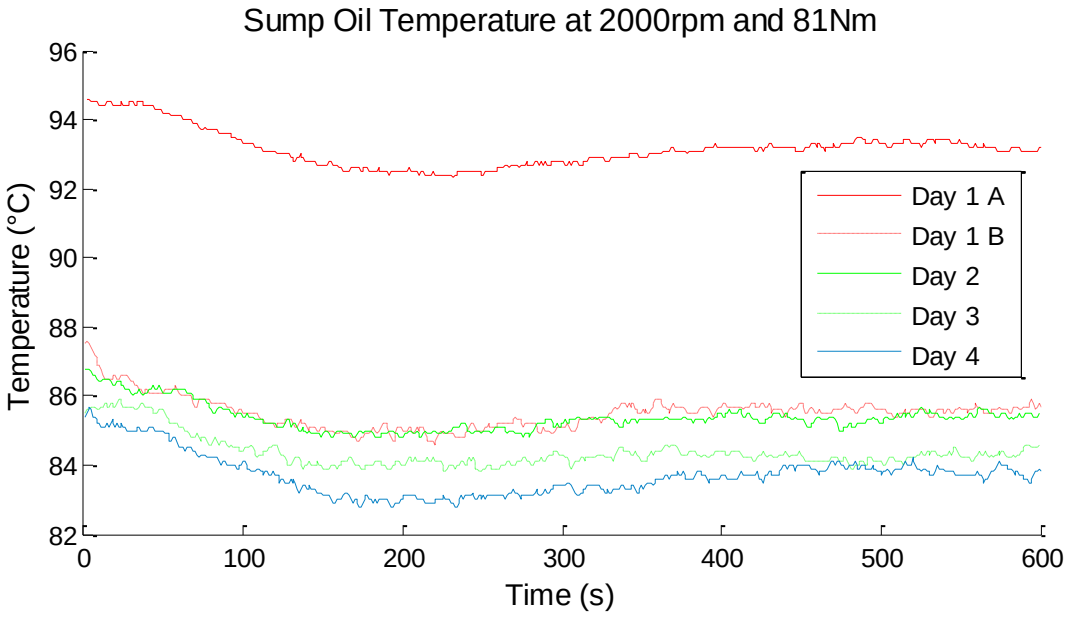

Figure 4.9 Engine sump oil temperature response following a step-change from 2000 rpm 199 Nm to 2000 rpm 81 Nm

Sump oil temperature on Day 1 A was significantly higher than the remainder of the tests. This may be due to the ECU actuating a valve to use a smaller oil circuit that is used during cold-starts to assist with engine warm-up. This erroneous data set also raises the temperature being discussed.

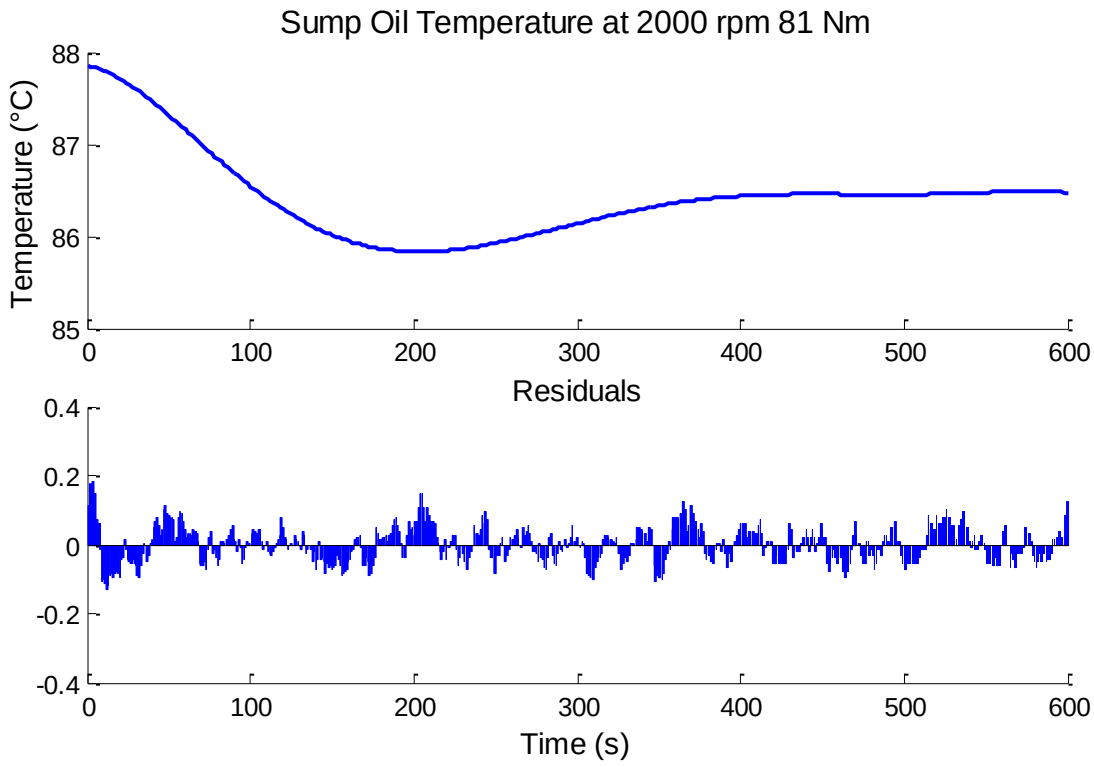

Figure 4.10 Engine sump oil temperature response following a step-change from 2000 rpm 199 Nm to 2000 rpm 81 Nm

The response of gallery oil temperature data following the first step change, Figure 4.11, was more rapid than sump oil response shown above. Gallery oil is in closer proximity to the cylinders and so will immediately experience lower radiative heat following a step change. The drop in gallery oil temperature lasted for approximately 100 seconds, which is in between the duration for engine coolant (70 seconds) and sump oil temperature (195 seconds).

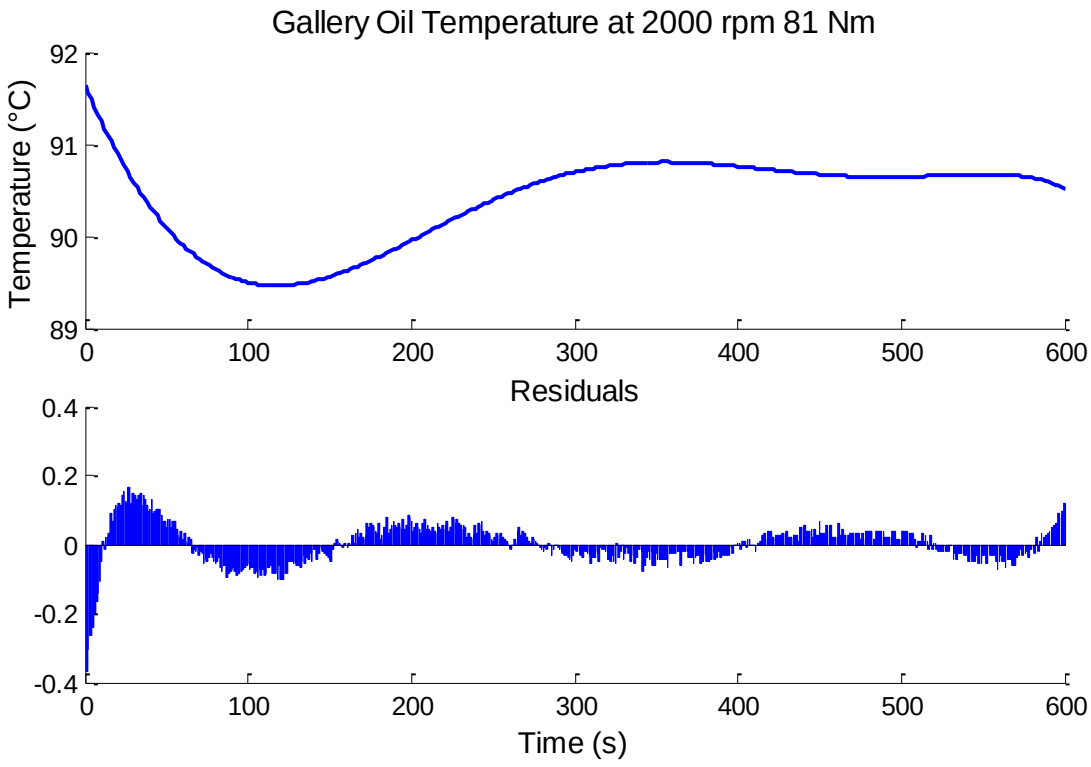

Figure 4.11 Engine gallery oil temperature response following a step-change from 2000 rpm 199 Nm to 2000 rpm 81 Nm

The temperature reduced at approximately 350 seconds due to the coolant temperature, seen in Figure 4.8 above. Gallery oil temperature appears stable after approximately 500 seconds. The drop in temperature immediately prior to the end of test is caused by the data from Day 3, Figure 4.12.

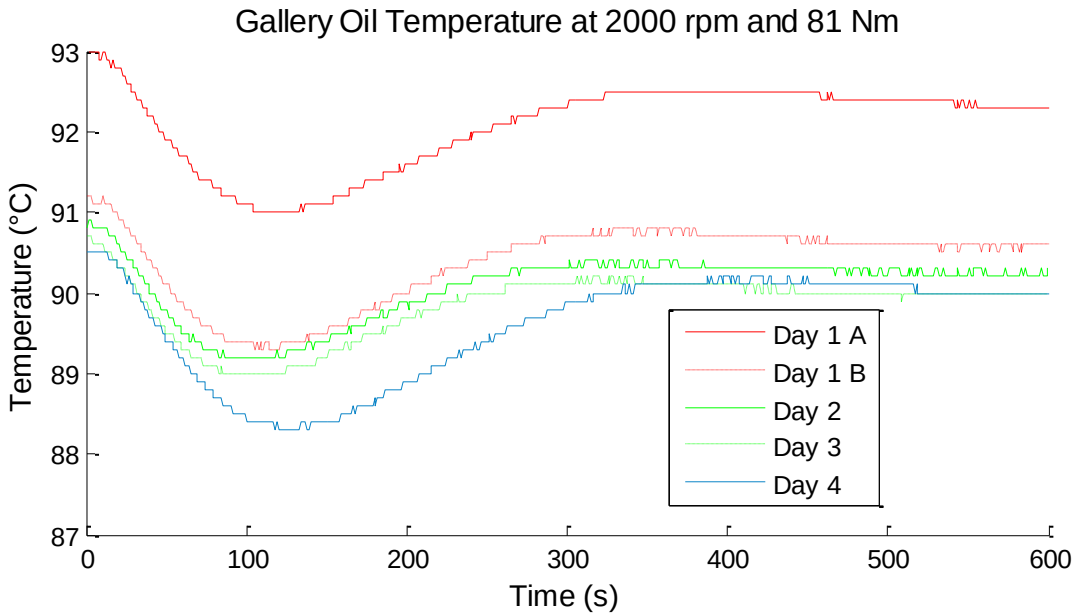

Figure 4.12 Engine gallery oil temperature response following a step-change from 2000 rpm 199 Nm to 2000 rpm 81 Nm

The second step-change was from 2000 rpm 81 Nm to 1500 rpm 105 Nm. Although the speed decreased by 500 rpm the power remained between 16 kW and 17 kW due to the increase in load. Parasitic losses were expected to reduce with the speed, increasing thermodynamic efficiency.

The step-change was not instantaneous due to the control system dynamics. This caused the torque to increase, hence initially there is an increase in coolant out temperature. This is not visible in the fitted polynomial although the residuals indicate a poor fit and the overshoot is visible in Figure 4.13. Figure 4.14 shows a similar trend as for the first step-change, with the external cooler initially having to over-work for the conditions to regulate the temperature. A control response from the cooler is observed after approximately 90 seconds.

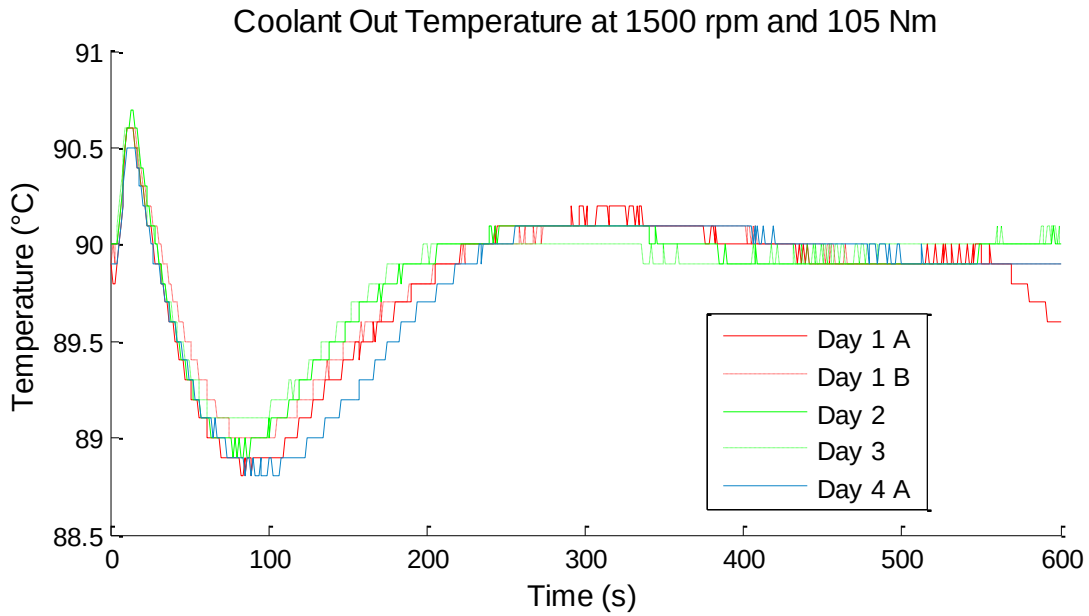

Figure 4.13 Engine coolant out temperature response following a step-change from 2000 rpm 81 Nm to 1500 rpm 105 Nm

Slight variations in the test data are seen by the residuals fluctuating, although the system returned to stable after approximately 300 seconds. A sudden decrease in the trace was due to Day 1 A data, Figure 4.13. This was likely caused by additional oil from the post warm-up circuit being accessed; this action may have caused a high sump oil temperature in Figure 4.9.

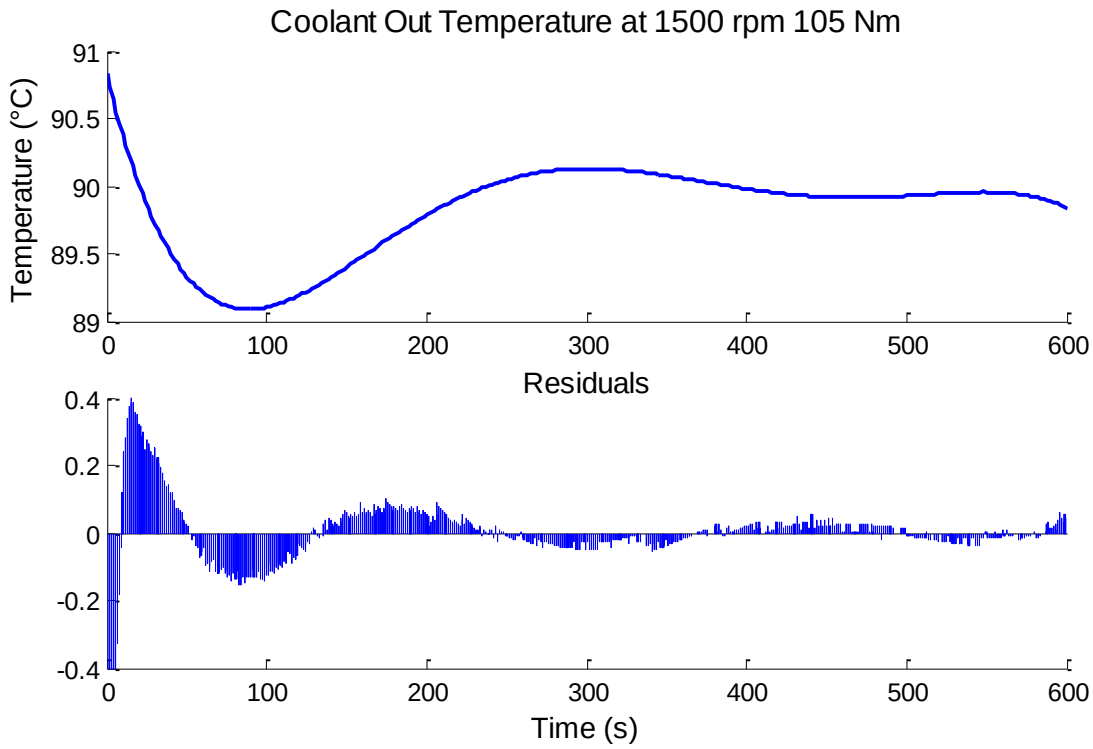

Figure 4.14 Engine coolant out temperature response following a step-change from 2000 rpm 81 Nm to 1500 rpm 105 Nm

The temperature of oil in the sump following the second step-change is shown, Figure 4.16. This is a first order response and as such would be easy to predict during a test however the data are noisy. This can be seen in the residuals and also Figure 4.15. Oil sump temperature stabilised after approximately 300 seconds.

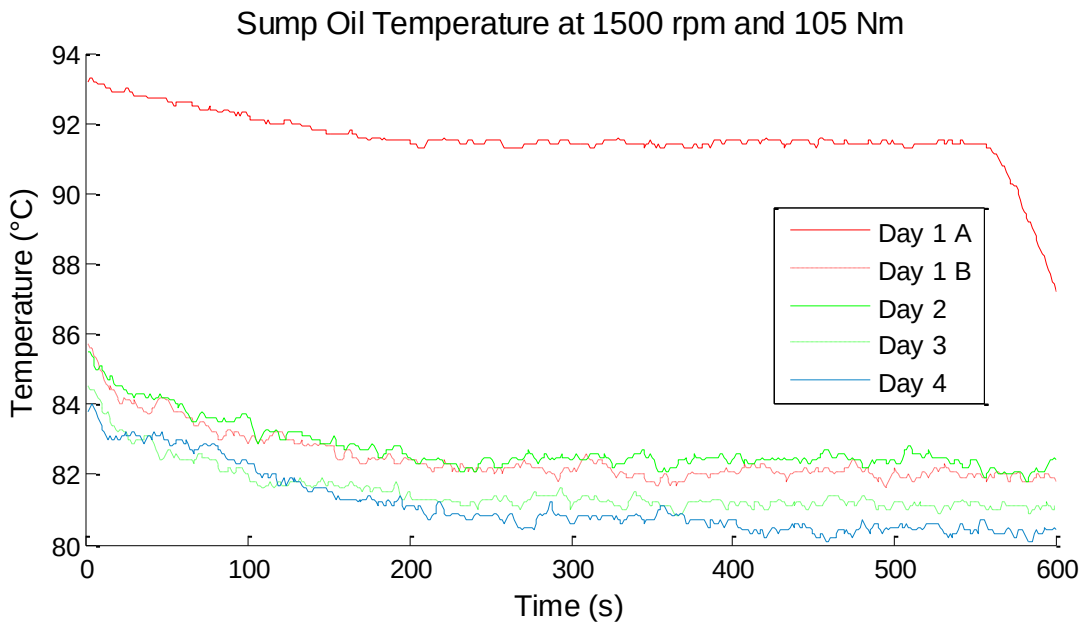

Figure 4.15 Engine sump oil temperature response following a step-change from 2000 rpm 81 Nm to 1500 rpm 105 Nm

In contrast to the engine coolant-out data, Figure 4.14, there was no initial increase in sump oil temperature. Oil temperature in the sump is affected by oil returning from a number of sources in the engine block, which creates a damping effect to temperature spikes observed in any one area.

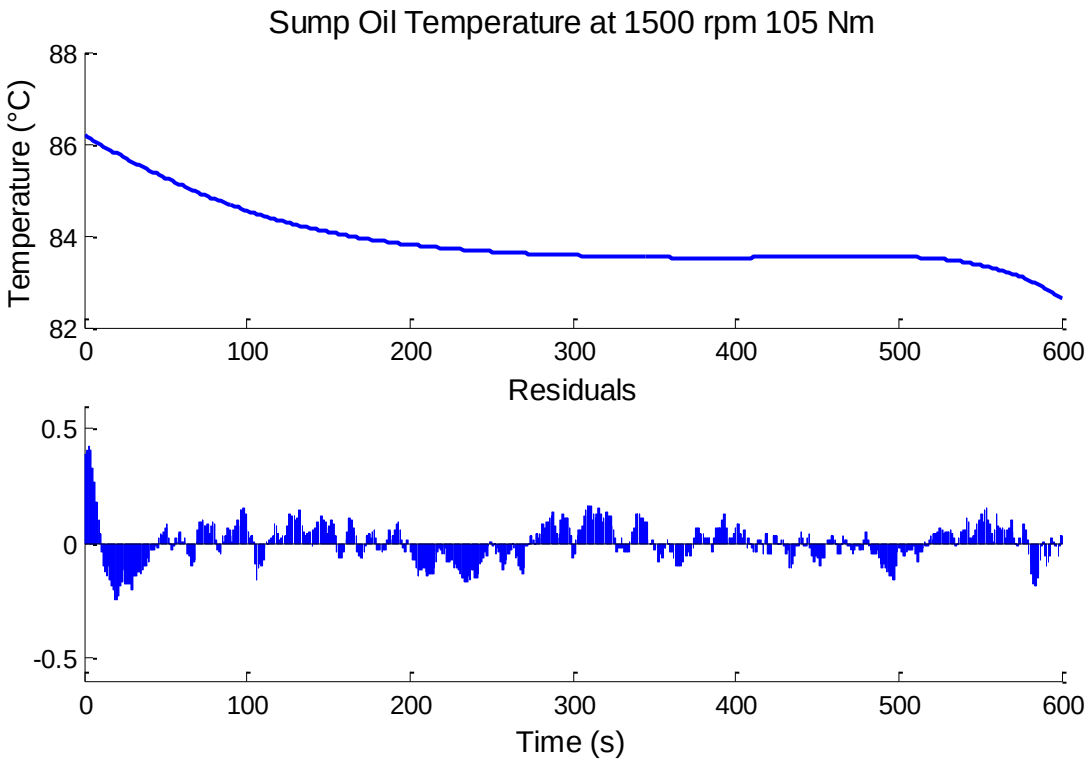

Figure 4.16 Engine sump oil temperature response following a step-change from 2000 rpm 81 Nm to 1500 rpm 105 Nm

Gallery oil temperature, Figure 4.18, reduced quicker than sump oil temperature following this step change. The trend was more similar to the coolant water which also increased slightly following the minimum until approximately the same point at 300 seconds.

A sharp reduction in temperature at about 550 seconds from Day 1 A, Figure 4.17, correlates with engine coolant and sump oil temperature data Figure 4.14 and Figure 4.16. This was likely due to the ECU reverting an internal valve to that of the other tests, i.e. increasing the volume of circulating oil.

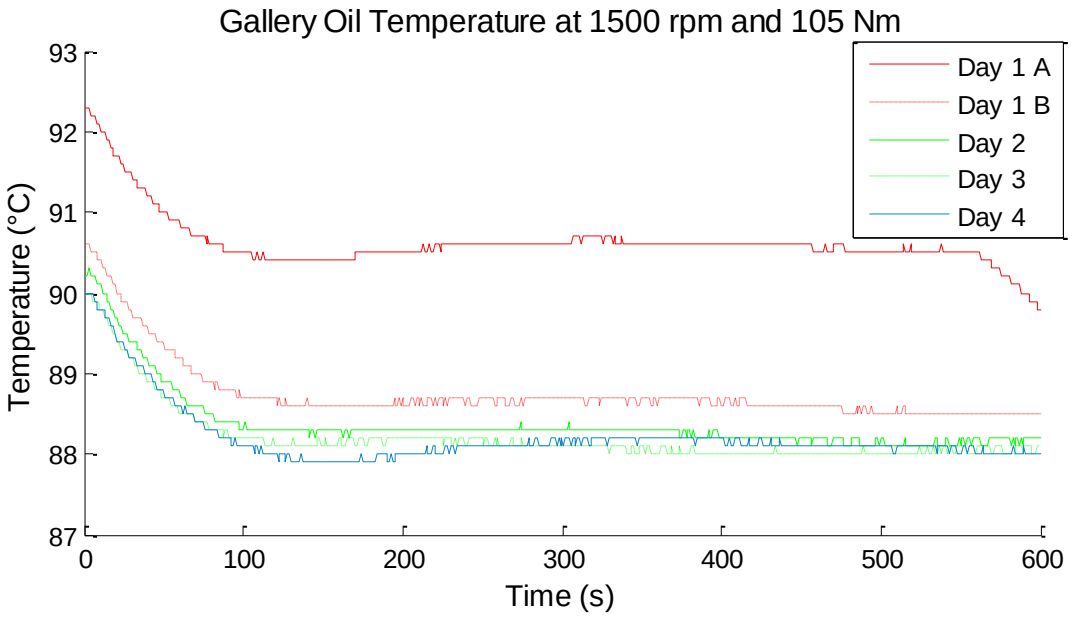

Figure 4.17 Engine gallery oil temperature response following a step-change from 2000 rpm 81 Nm to 1500 rpm 105 Nm

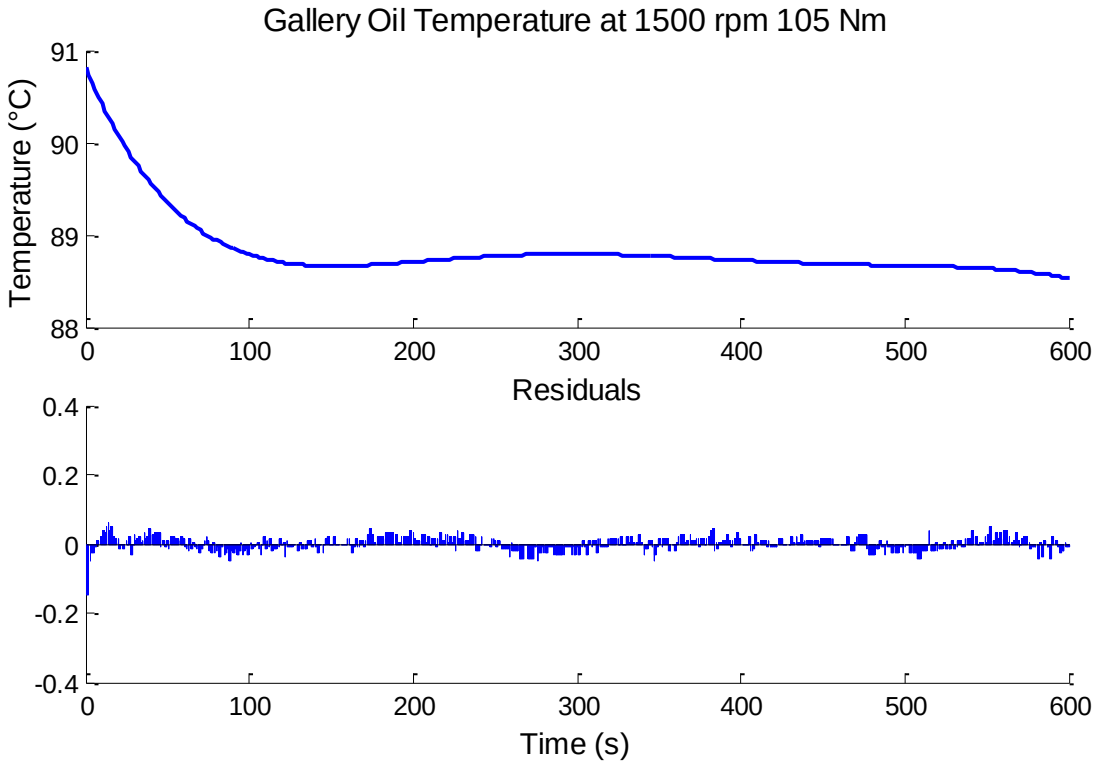

Figure 4.18 Engine gallery oil temperature response following a step-change from 2000 rpm 81 Nm to 1500 rpm 105 Nm

There was no initial increase in the temperature of gallery oil, Figure 4.17, which would have been caused by the dynamometer control increasing

applied load before reducing speed. This suggests the oil temperature is influenced by moving parts in the engine, whereas coolant out temperature is primarily affected by combustion conditions.

The time at which each temperature dropped on the Day 1 A data is compared, Figure 4.19. Sump oil was the first temperature to drop, suggesting that the difference in temperature compared to the other tests was due to the engine control as opposed to differences in test conditions.

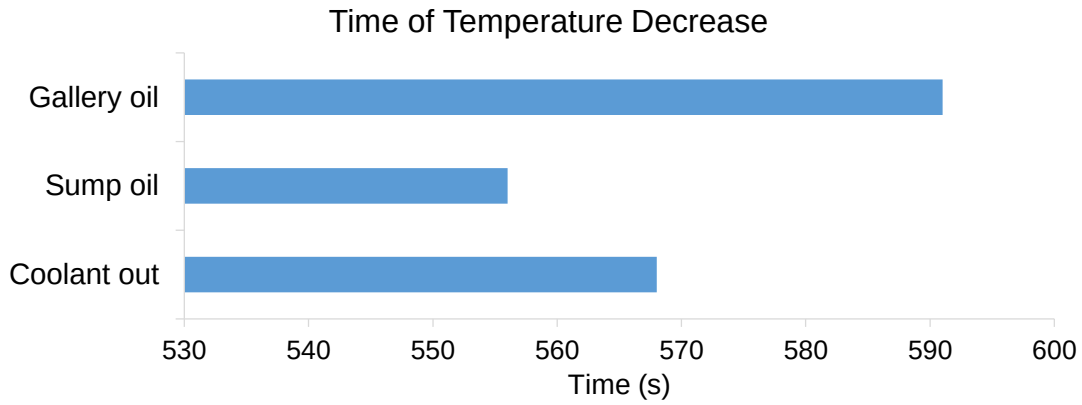

Figure 4.19 Time of temperature drop during steady-state operation

Coolant out temperature data for the step from 1500 rpm 105 Nm to 1500 rpm 41 Nm is shown in Figure 4.20. A similar response was observed at this step change as with the first, Figure 4.8, as both conditions maintain engine speed but reduce load. The coolant out temperature returned to the set point quicker as the external cooler was under less load.

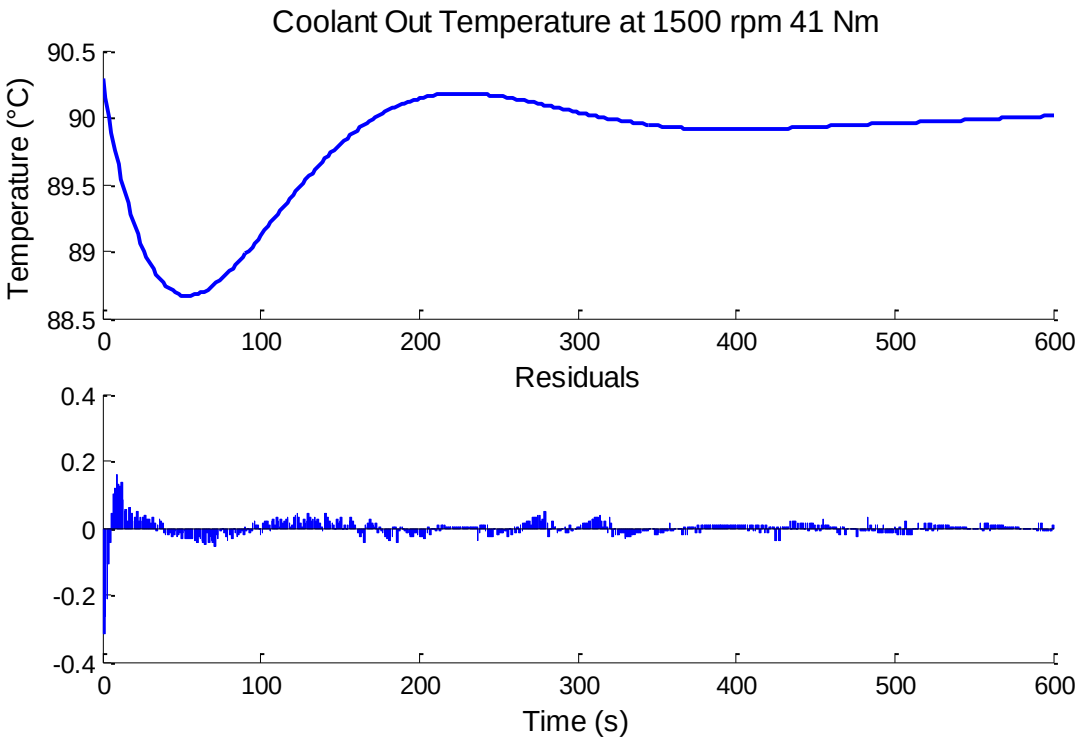

Figure 4.20 Engine coolant out temperature response following a step-change from 1500 rpm 105 Nm to 1500 rpm 41 Nm

The temperature data from sump oil shows stability after approximately 200 seconds, Figure 4.22. The data are very noisy and it is less clear for some of the traces shown in Figure 4.21 where the temperature settles. The trace from Day 1 A in Figure 4.21, which initially starts off high, also settles within a similar time span.

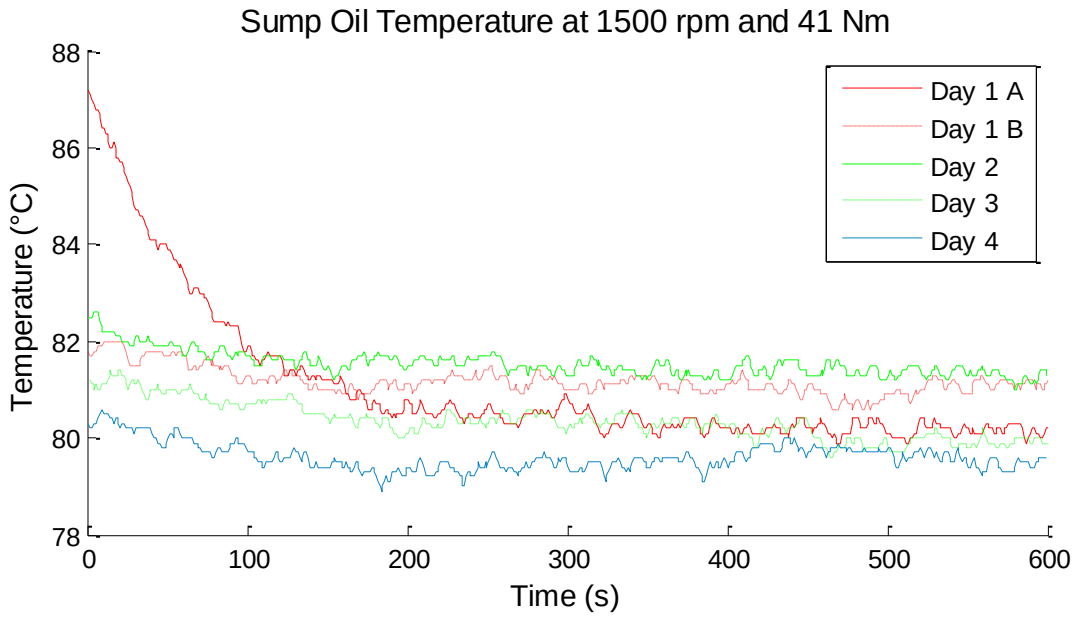

Figure 4.21 Engine sump oil temperature response following a step-change from 1500 rpm 105 Nm to 1500 rpm 41 Nm

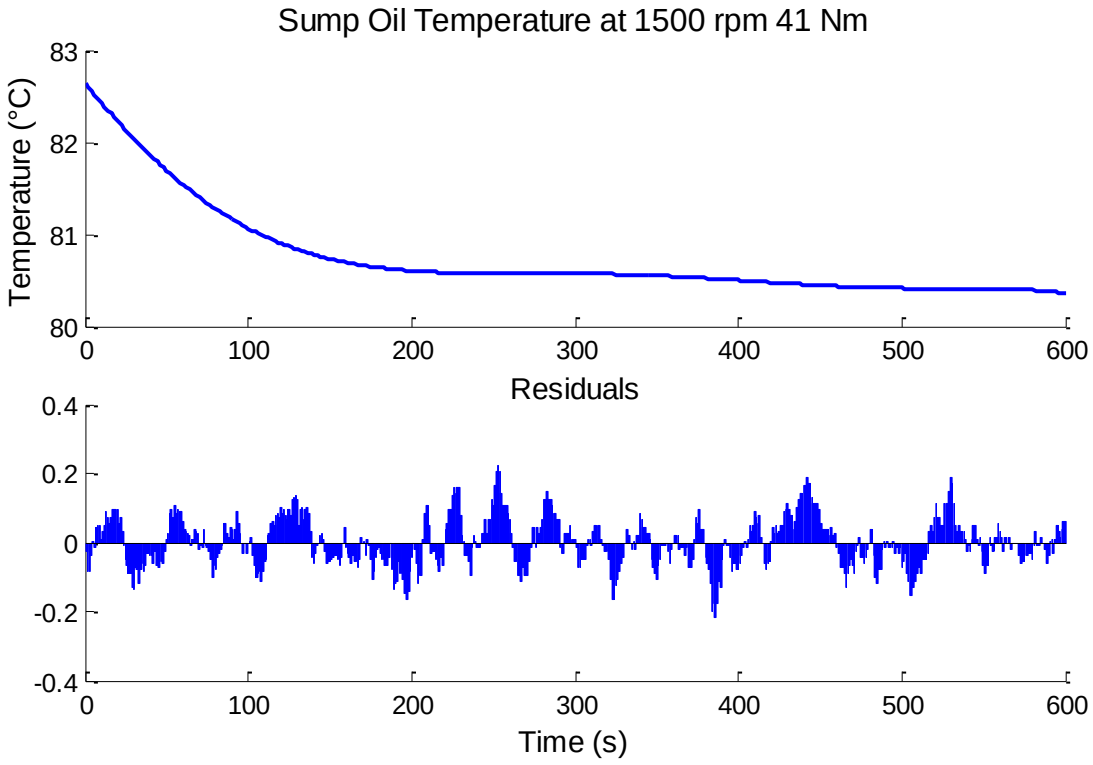

Figure 4.22 Engine sump oil temperature response following a step-change from 1500 rpm 105 Nm to 1500 rpm 41 Nm

Following the final step-change gallery oil temperature, Figure 4.24, varied in proportion with the coolant out temperature, Figure 4.20. There was a similar increase in temperature that peaked at approximately 220 seconds before the temperature settled by 450 seconds.

As can be seen with the previous Day 1 A temperature traces, Figure 4.23, the initial temperature was high. All traces were stable at approximately 350 seconds.

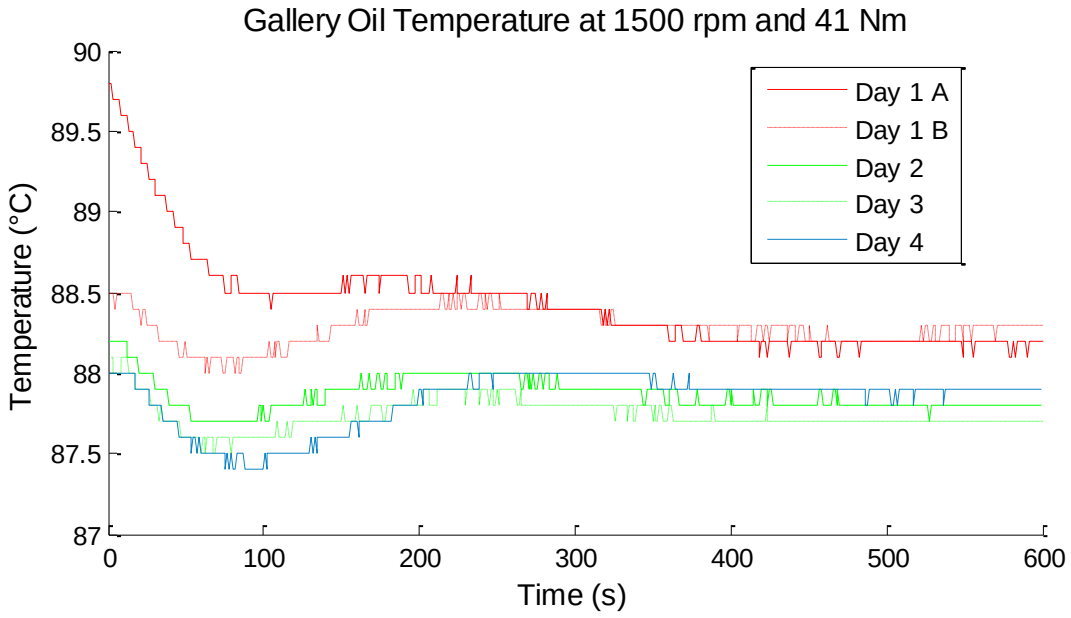

Figure 4.23 Engine gallery oil temperature response following a step-change from 1500 rpm 105 Nm to 1500 rpm 41 Nm

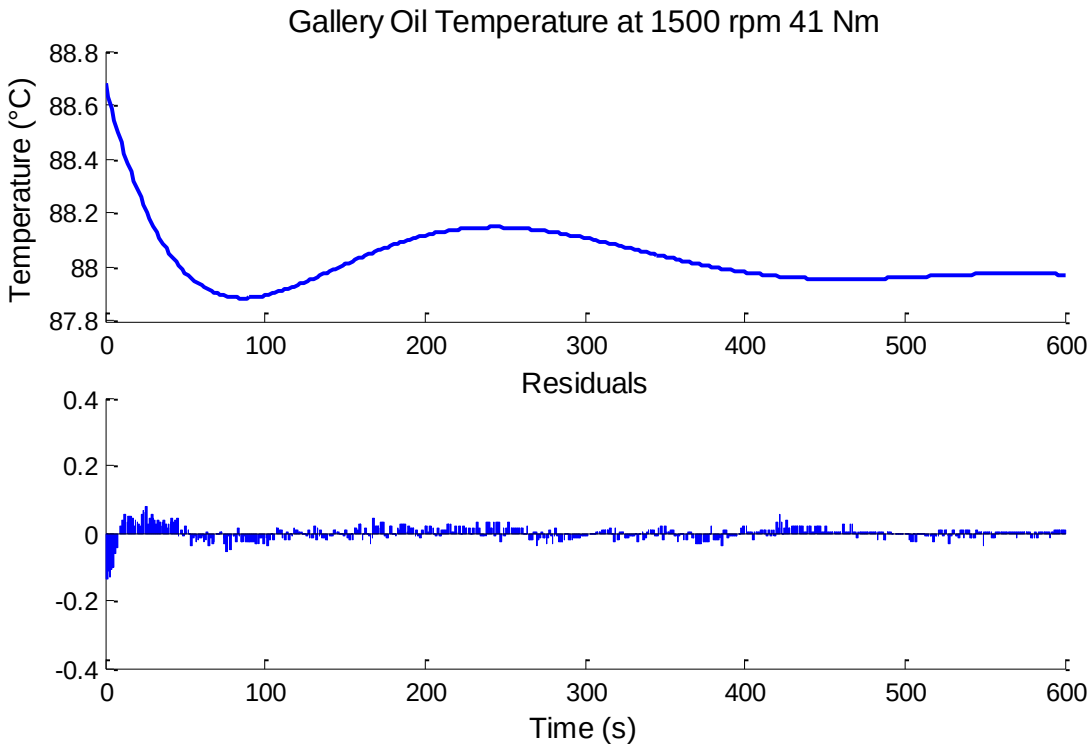

Figure 4.24 Engine gallery oil temperature response following a step-change from 1500 rpm 105 Nm to 1500 rpm 41 Nm

4.5.2 Discussion

A number of step-changes in speed and load were applied to a 5 litre naturally aspirated gasoline V8 engine. Temperature data from engine coolant out, sump oil and gallery oil were presented.

Sump oil temperature data provided smooth transitions following the step-changes without having experienced the overshoots or undershoots that the coolant water had. However the temperature data from the sump oil was significantly noisier than that in the engine gallery. This may be due to the turbulent nature of oil in the sump, which is held in a bowl-shaped reservoir and will be receiving oil from multiple areas of the engine that will have different operating temperatures. The fact that the sump oil temperature is influenced

by a wide range of engine components is a desirable feature as it could more accurately provide an indication of the state of the whole engine.

Since the coolant temperature is externally regulated it will always return to the same value. However temperature data from the engine coolant often fluctuated after returning past the settling value. This also effects the temperature of the engine oil and is due to the PID controller of the external cooler.

The engine sump oil is a good indicator of when the engine is operating at steady-state, and as the engine will be influenced by the performance of the external cooler then the engine coolant temperature should correlate with the condition of the UUT.

4.6 Identification of steady-state for repeatable emissions measurement

An engine mapping and calibration process relies on good quality emissions data. The use of baseline tests is commonly used in the industry to address day-to-day test variability. This section compares the repeatability of baseline emissions data when different indicators of steady-state were used.

Analysis of the data collected during Section 4.5 suggested engine sump oil temperature and engine coolant out temperature can be reliable indicators of engine condition. A third variable, exhaust plenum skin temperature, was also tested based on the literature reviewed in Section 2.8.1. Tests were carried out to detect which parameter is best suited to determine when the UUT is operating at steady-state.

The test procedure was as follows:

i. Start engine
ii. Wait until idle speed falls below 1000 rpm (catalyst light-off complete)
iii. Set baseline conditions (Table 4.3)
iv. Wait for the chosen steady-state indicator
v. Record data for 60 seconds
vi. End test

Gaseous emissions were sampled from the engine directly using a HORIBA MEXA 9100. The sample points were situated pre-catalyst from both banks to allow measurement from all cylinders simultaneously. Particulate emissions were sampled approximately 3.2 m downstream of the catalysts and analysed using an AVL condensation particle counter (CPC). Fuel consumption was measured using a Coriolis sensor housed in an AVL 735S fuel mass flow meter.

Data were logged for 60 seconds at 1 Hz once the chosen steady-state indicator was stable ±1°C for 60 seconds. The repeat conditions used for the baseline test are shown in Table 4.3.

Table 4.3 Baseline test conditions

Variable	Value	Unit
Speed	2000	rpm
Torque	81	Nm
Fuel temperature	20	°C
Engine coolant temperature	90	°C
Inlet valve opening	50	aTDC
Exhaust valve closing	31	aTDC
Engine fuel supply pressure	3	bar
Fuel rail pressure	110	bar
Spark timing	42	bTDC
Injection timing	300	bTDC

4.6.1 Particulate number results

Particulate number (PN) emissions results are shown in Figure 4.25. The boxplot indicates that there is less measurement variation when exhaust plenum skin temperature is used to indicate steady-state. PN emissions measurement variation is greater when coolant and oil are used.

The values for each data set are provided in Appendix A8, Table 0.3.

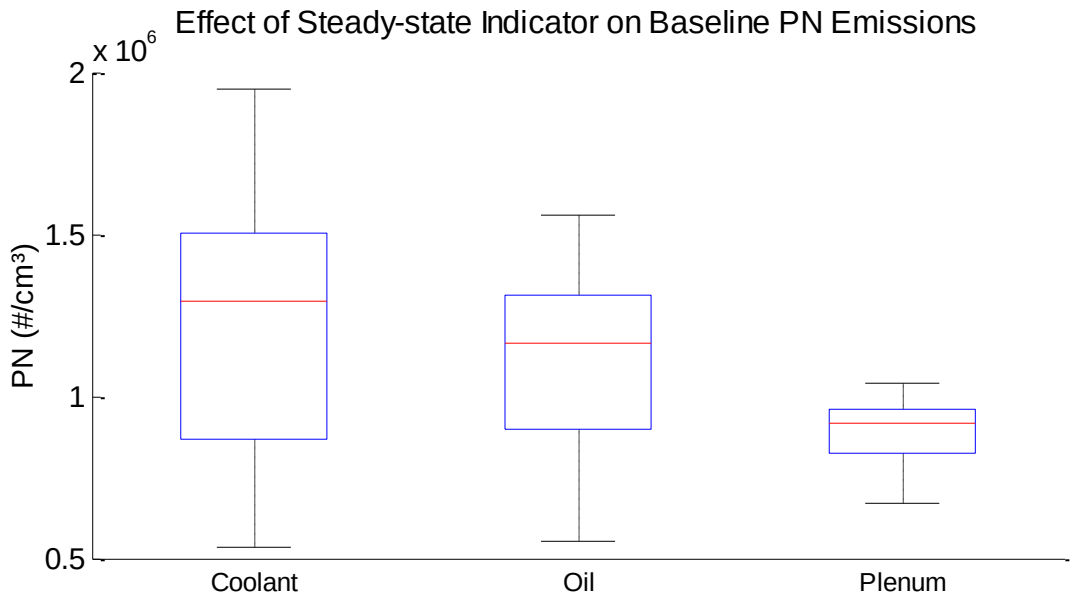

Figure 4.25 Baseline PN emissions measurements using different steady-state indicators

Reviewing the individual test points reveals that PN emissions underwent a gradual drift during the testing period, Figure 4.26. The coolant-out baseline tests were carried out over approximately one month and so it is plausible the weather had an effect on the data [82]. The particle counter was maintained regularly and the values would not have fallen again if this was due to instrument drift.

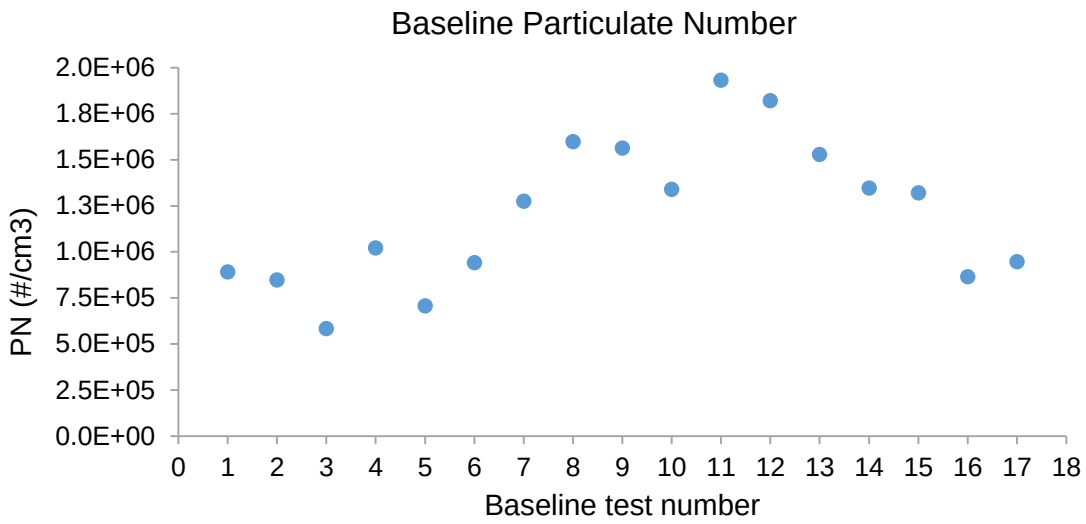

Figure 4.26 Baseline PN emissions using engine coolant as steady-state indicator

Further analysis of the PN data when using engine coolant reveals that standard deviation was higher for larger readings of PN, Figure 4.27. This could be due to a number of factors:

i. Larger magnitude readings will inherently tend to have a larger standard deviation since the sample mean is greater. However noise in the data is expected to be similar as the baseline test conditions are kept identical
ii. The larger values of PN were captured when PN was still increasing. This would suggest the engine was still not stable when data were collected, indicating that engine coolant was not a good indicator of the engine operating condition

The data suggests a functional relationship between magnitude and error which is a detrimental factor in the assumptions made by classical general linear methods used in response surface modelling [93]. As a result it is necessary to apply some other remedy to the problem, e.g. transformations or weighted least squares, before using the data for analysis. These additional processing steps can introduce errors to the data.

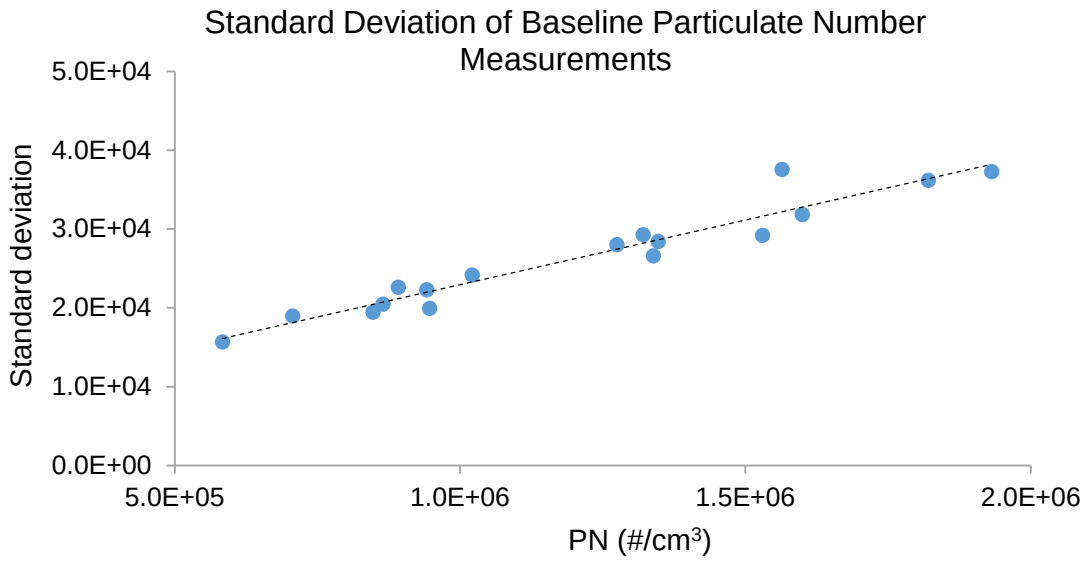

Figure 4.27 Baseline PN against the standard deviation of each test point

4.6.2 Fuel consumption and gaseous emissions results

The median values of fuel consumption measurements were similar across the steady-state indicators, Appendix A8. The spread of measurements was closes when using exhaust plenum skin temperature, Figure 4.28.

Sump oil temperature gave more repeatable fuel consumption measurements than engine coolant temperature by better indicating steady-state operation. This is likely because oil temperature is affected by more engine components and so can provide a better representation of the engine's thermal condition.

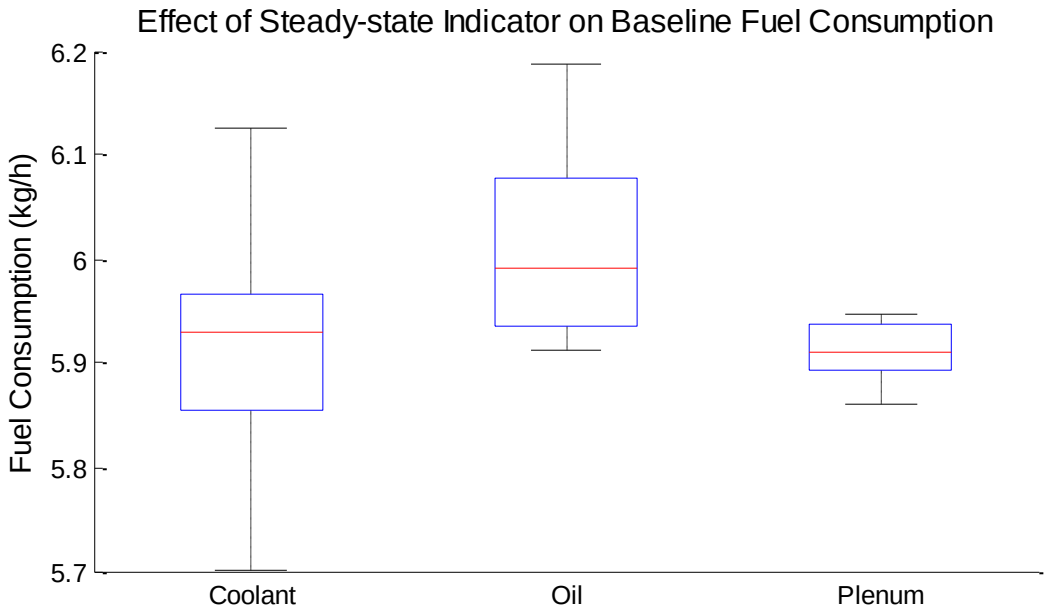

Figure 4.28 Baseline fuel consumption measurements using different steady-state indicators

Carbon monoxide (CO) emissions measurements were most repeatable when using exhaust plenum skin temperature to identify steady-state operation, as indicated by Figure 4.29.

In general carbon monoxide emission recorded at baseline showed a good degree of repeatability, shown by coefficient of variations (CoV's) of approximately 0.1 or less for all three steady-state indicators. The values are provided in Table 0.5 in Appendix A8. Carbon monoxide emission measurements from direct injection naturally aspirated gasoline vehicles can be less stable than port-fuelled engines because less time is available for mixture preparation. This can result in fuel-rich regions during combustion, causing less CO to oxidise into CO_2 as shown in Figure 2.5 on page 25.

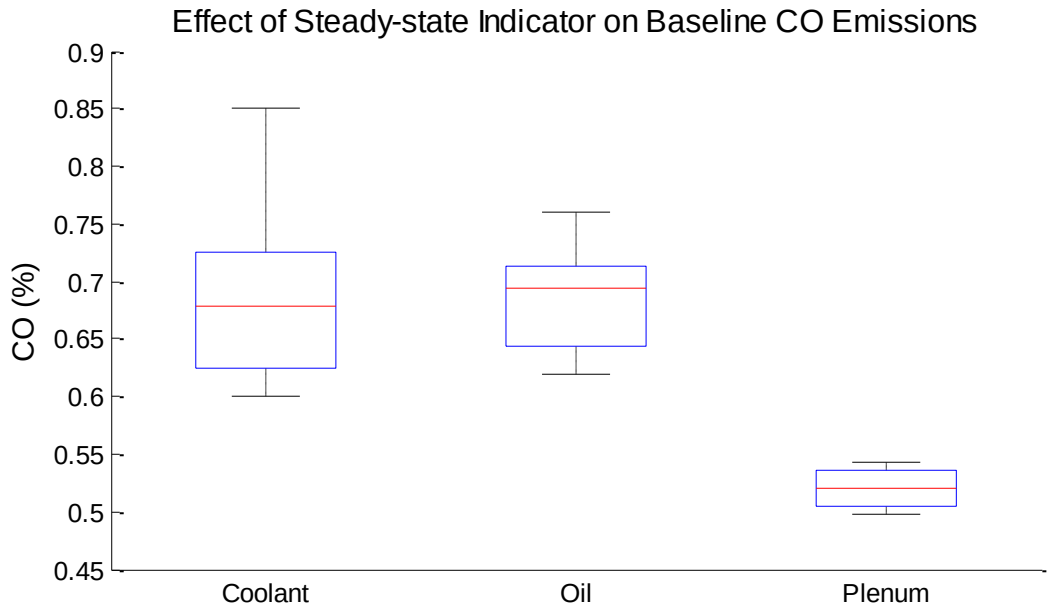

Figure 4.29 Baseline CO emissions measurements using different steady-state indicators

The ranges for carbon dioxide at baseline were similar when using the coolant-out and exhaust plenum for indicators of steady-state, Figure 4.30. In general the data were of high quality, indicated by a CoV < 0.01 as shown in Table 0.6 in Appendix A8.

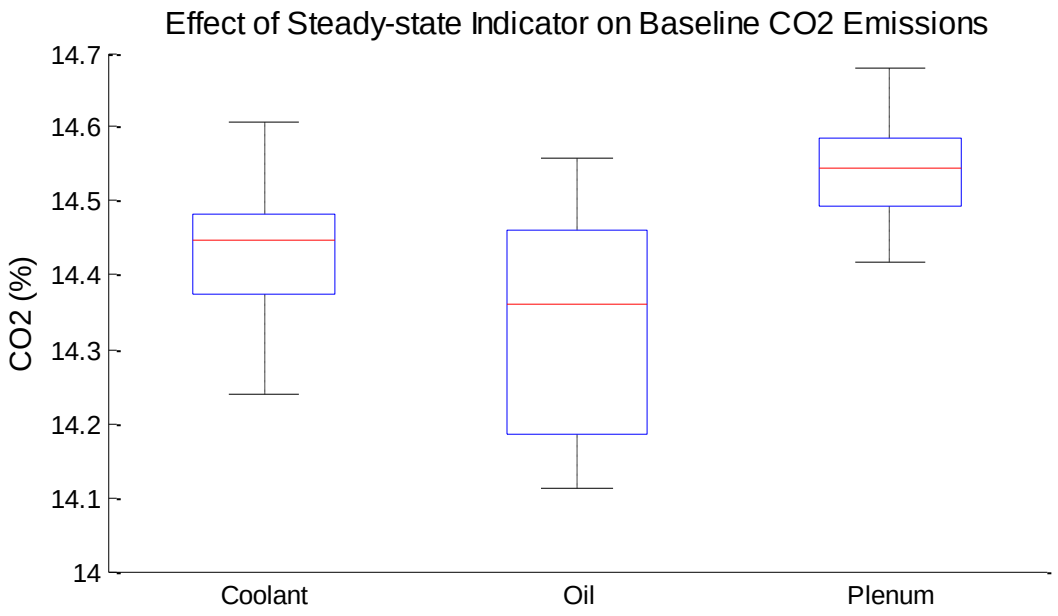

Figure 4.30 Baseline CO_2 emissions measurements using different steady-state indicators

The hydrocarbon emissions data appear similarly distributed when coolant-out and plenum skin steady-state indicators were used, Figure 4.31. Engine sump oil had a slightly larger spread but the median is similar to when coolant was the steady-state metric.

In general the data showed a very high level of repeatability, indicated by the CoV's bordering or less than 0.05. The results for this stage can be found in Table 0.7 Appendix A8.

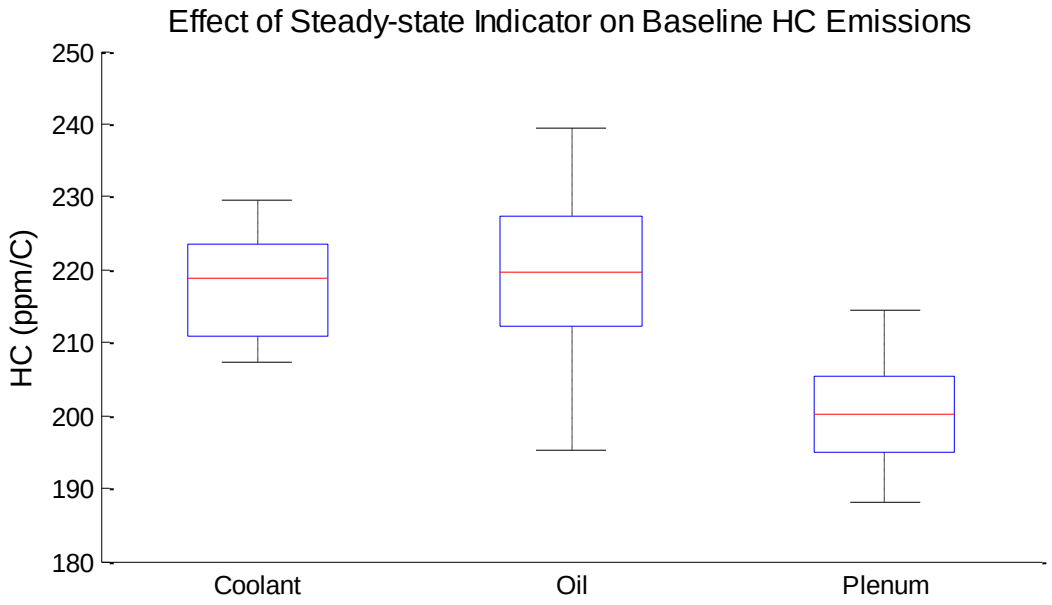

Figure 4.31 Baseline HC emissions measurements using different steady-state indicators

A boxplot of baseline oxides of nitrogen emissions, Figure 4.32, indicates a more repeatable state can be achieved when using coolant-out or oil sump temperature rather than plenum skin temperature. The median when using exhaust plenum skin temperature is lower, but the large second quarter suggests there were a wider range of lower values. The data from the upper quartile was more closely grouped.

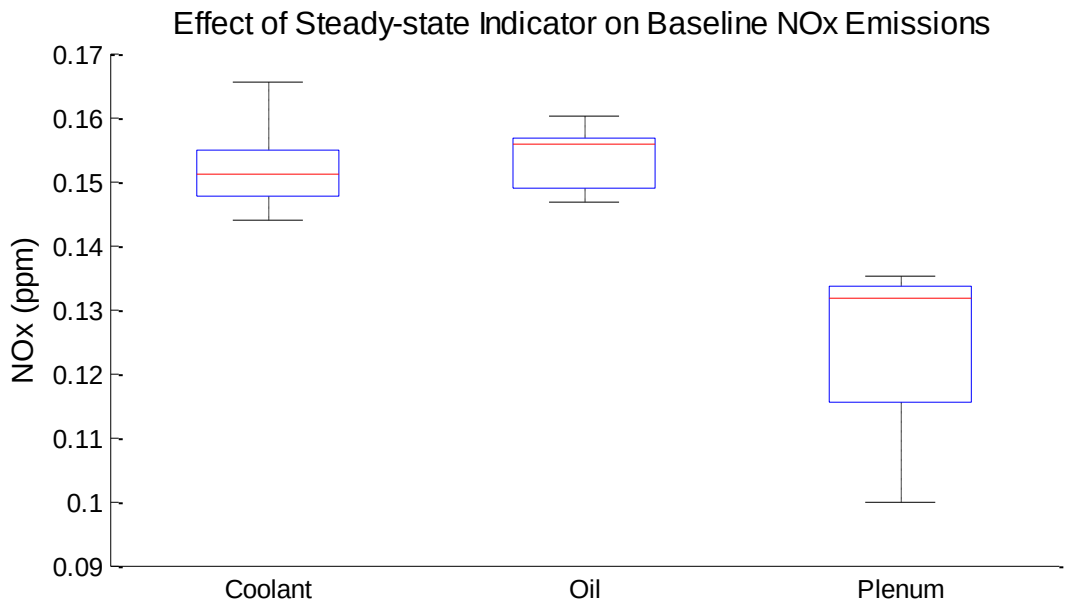

Figure 4.32 Baseline NOx emissions measurements using different steady-state indicators

In general the data were more repeatable when using exhaust plenum skin temperature to indicate a stable baseline operating condition. This was not true for NOx emissions, where coolant and oil temperatures performed better.

4.7 Comparing steady-state indicators for high quality engine measurements

Engine data were measured from forty test points when two different engine temperatures were used to indicate a steady-state condition. Differences in data quality are discussed. The temperatures chosen were engine coolant and exhaust plenum skin. Engine coolant is a commonly monitored temperature and can be used to judge when the engine conditions have stabilised following a change in speed and/or load. Exhaust plenum skin temperature was identified in chapter 4.6 as providing the most repeatable conditions to measure exhaust emissions.

The forty steady-state test points spanned a range of engine operating conditions that are described in Table 4.4. Each test point was comprised of a unique set of actuator settings (IVO, EVC, FRP, SOI) and spark timing was set at each test point to achieve 50% mass fraction burned (MFB) at 8 aTDC.

Table 4.4 Operating conditions of repeated test points

Node	Test points	Speed (rpm)	Load (Nm)	Power (kW)
1	36 - 40	700	28	2.05
2	31 - 35	1500	41	6.44
3	26 - 30	1500	105	16.49
4	1 - 20	2000	81	16.97
5	21 - 25	2000	199	41.68

4.7.1 Results

The differences in measured data between the two steady-state indicators at each test condition were calculated and are shown in Figure 4.33, these results will now be discussed. The data for each test point are plotted in Appendix 0.

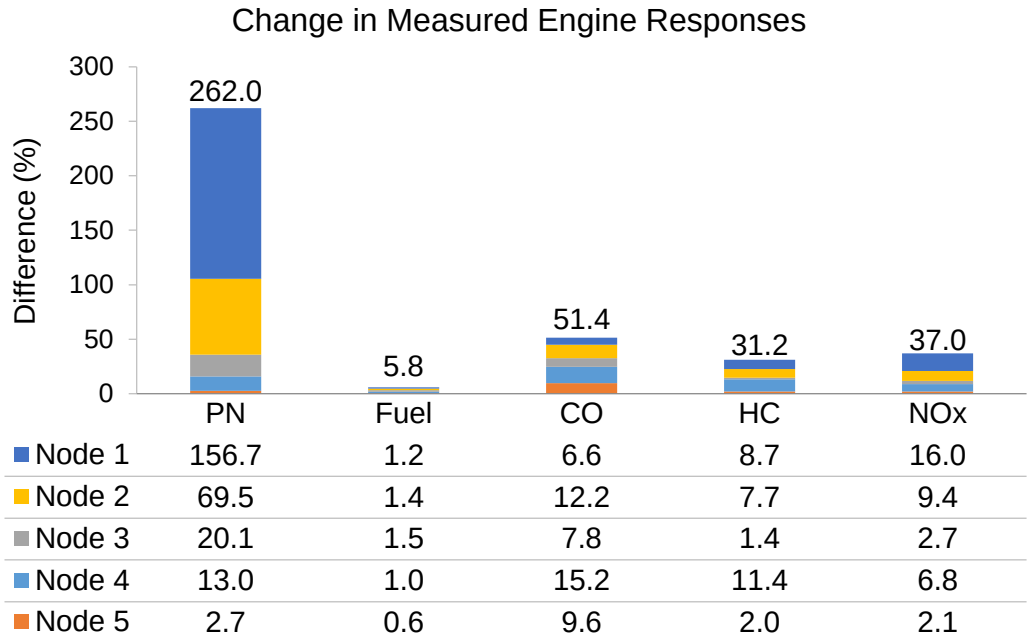

Figure 4.33 Average change in measured engine response between coolant and plenum steady-state indicator. Node 1 = lowest speed/load, Node 5 = highest

Particulate number emissions were the most significantly affected with a total difference between tests of 262%, of which over 150% was from the lowest speed and load operating point. The change of over 150% at 700 rpm 28 Nm suggests that the data collected at this point may be of very low quality. At lower speeds and loads there is a higher rate of deposition onto the internal surfaces of the engine and exhaust. Higher rates of deposition were observed by Bika *et al.* [153] at lower temperatures, which reduced the number of nucleation mode particulates. These deposits can then be disturbed and re-entrained to be measured as engine-out emissions. As the speed and load increases the variation in PN emissions reduces. The smallest difference was 2.7% at the highest operating condition. The lower sensitivity at this high operating condition is likely due to the engine-out PN emissions being less

sensitive to small variations caused by the random re-entrainment of particulate matter from the internal surfaces.

The least affected by the change in steady-state indicator was fuel consumption. The largest difference was 1.5% at 1500 rpm 105 Nm. The amount of fuel required by the engine during an operating condition changes little once the block has reached normal operating temperatures. Fuel consumption may vary when pumping losses change but this may only occur when the engine oil is significantly more viscous, such as immediately following key-on, or when large changes in the actuator settings are made, such as different valve timings.

Carbon monoxide emissions changed by a sizeable amount at all of the operating conditions but the least affected was the lowest speed and load. CO emissions are one of the primary reactions during combustion and the chemistry freezes at lower temperatures, [4], therefore it is likely that engine-out CO emissions are most affected by the conditions immediately following ignition. The most affected operating condition of 2000 rpm 81 Nm is a relatively high-speed, low-load point; this is also the case for the second most affected of 1500 rpm 41 Nm. Under conditions where there is throttled operation there is a lower mass of air and fuel present in the cylinder upon ignition, potentially reducing the initial flame speed and causing more combustion variability. Higher powered operating conditions will use more fuel and air per cycle, generally improving combustion stability by improving the density of fuel and air upon ignition.

Similarly, hydrocarbon emissions are mostly affected in terms of the absolute difference in measured value at 2000 rpm 81 Nm. The least influenced operating conditions are 1500 rpm 105 Nm and 2000 rpm 199 Nm, which are relatively high-load conditions for the engine speed. As with carbon monoxide emissions the combustion stability is expected to be better at these higher loads. Hydrocarbon oxidation can be influenced by conditions throughout combustion and if there is oxygen and temperatures are sufficiently high within the catalyst then oxidation will continue [1].

NOx emissions changed the greatest amount at the lowest operating condition. The least affected was at the highest power condition of 2000 rpm 199 Nm, where combustion stability is expected to be higher. A difference of 9.4% was experienced at 1500 rpm 41 Nm, which is a relatively low powered operating condition compared to 1500 rpm 105 Nm where the difference was a 2.7%. NOx emissions are higher when there is a diffusion flame which will be more prominent at lower powered operating conditions.

To compare the magnitude of differences across different operating conditions the measured response per kW power produced was calculated. As in Figure 4.33 the differences between the two steady-state indicators are shown, Figure 4.34.

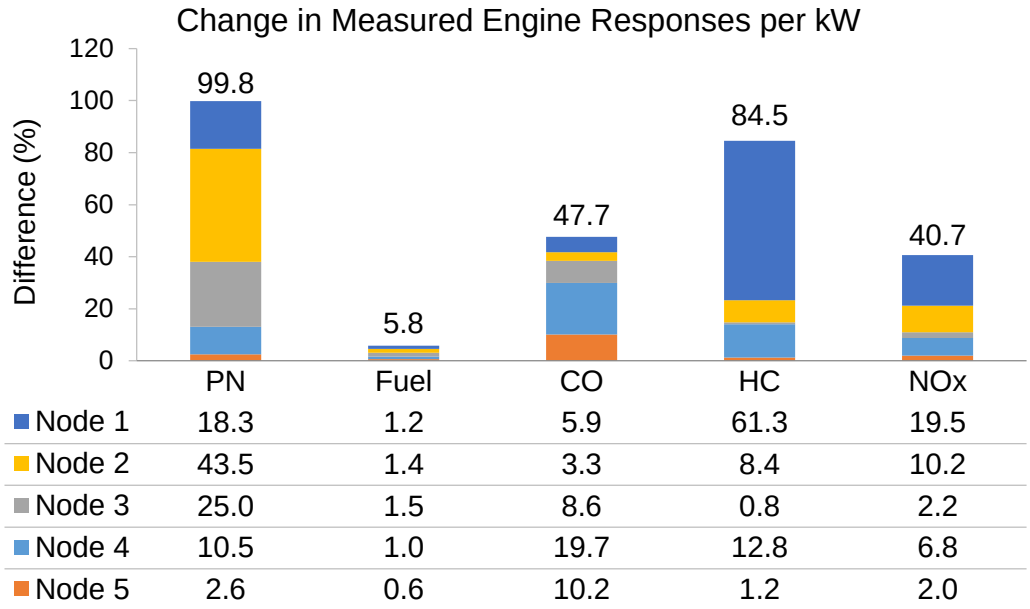

	PN	Fuel	CO	HC	NOx
Node 1	18.3	1.2	5.9	61.3	19.5
Node 2	43.5	1.4	3.3	8.4	10.2
Node 3	25.0	1.5	8.6	0.8	2.2
Node 4	10.5	1.0	19.7	12.8	6.8
Node 5	2.6	0.6	10.2	1.2	2.0

Figure 4.34 Percent change in measured engine response per kW between coolant and plenum steady-state indicator. Node 1 = lowest speed/load, Node 5 = highest

This distribution is similar to that shown in Figure 4.33 although hydrocarbons are a more prominent in terms of summed difference with a value 84.5%. This highlights that there is a greater difference in terms of power-related HC emissions than is first indicated by the absolute difference shown in Figure 4.33 above.

The distribution between operating conditions has also shifted since the results are normalised for the operating condition. It shows that HC emissions are more sensitive to changes in the steady-state indicator at lower loads, whereas at Node 3 there is almost no discernible change.

PN changed the greatest amount at Node 2, which is a relatively low-load and low-speed operating condition. This would generate low turbulence in-cylinder

as the gas velocities are low and there is a smaller mass of fuel being injected, which reduces the kinetic energy [154].

Figure 4.35 shows the temperature of exhaust gases measured immediately before the catalyst whilst operating at the different speed and load conditions. Higher exhaust gas temperatures will assist the oxidation of unburned hydrocarbons at higher load conditions, whereas the lower load conditions will have exhaust temperatures that are lower. Differences in HC emissions were lower at the same speeds with higher loads, Node 3 and 5 in Figure 4.33 and Figure 4.34.

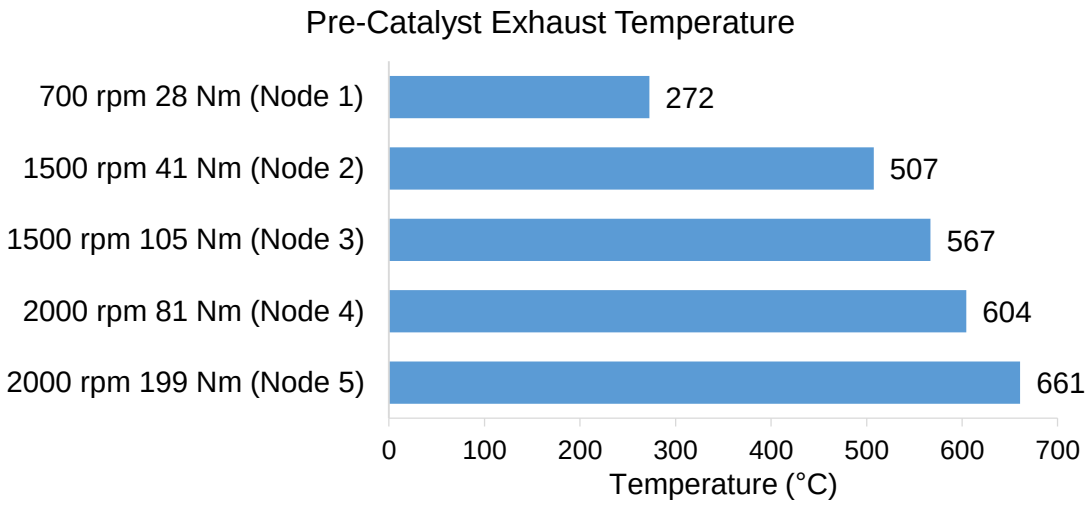

Figure 4.35 Mean pre-catalyst exhaust gas temperatures during engine mapping tests

The coefficient of variation (CoV) of engine responses from each of the test points was calculated to determine how much the response varied during the test points. The data in Figure 4.36 shows the average CoV for each steady-state indicator, where a smaller value indicates less variation over the test point. The test-averaged CoV was lower for all the engine responses when using exhaust plenum skin temperature as a steady-state indicator. This

indicates a greater stability during the test point. Measurements taken when the engine is closer to steady-state will be more representative and should help generate higher quality engine models.

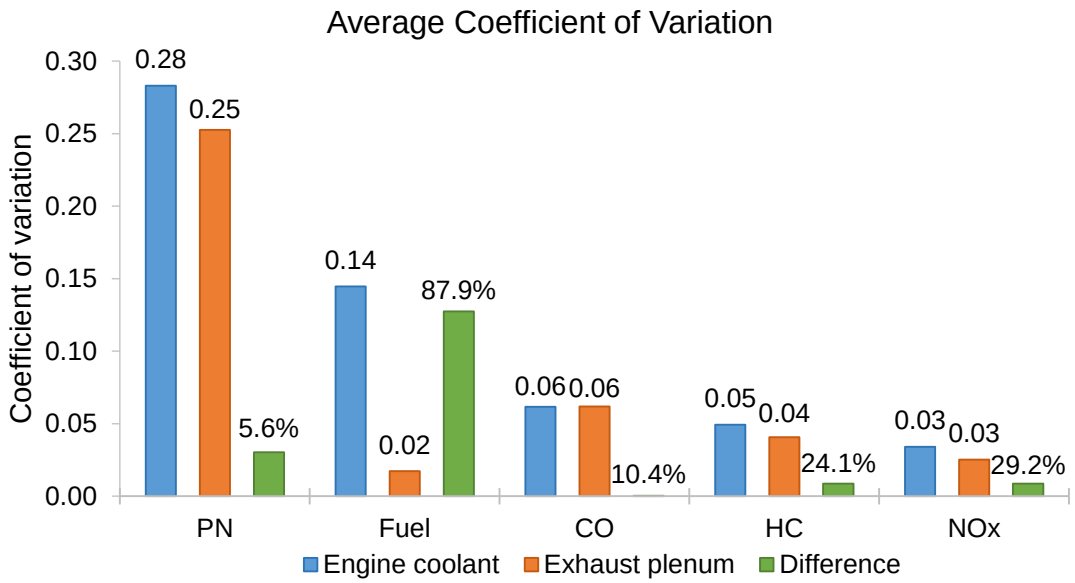

Figure 4.36 Coefficient of variations of data during recording of steady-state test points when using different steady-state indicators

PN data are the least stable for both steady-state indicators. The difference of 5.6% indicates that the exhaust plenum skin temperature can improve the quality of PN data across a highly varied range of steady-state engine test points. Exhaust plenum skin temperature provided the best data when used to collect baseline data, Figure 4.25 on page 118. However baseline test conditions are more repeatable since the pre-test conditions could be replicated more easily. The large difference in absolute values of the data recorded, Figure 4.33, is not reflected by a similarly sized change in CoV. The majority of the difference was observed at the lower operating condition and so the effect can be skewed by a relatively small difference in measured PN.

The largest change is for fuel consumption, the CoV of which reduces by almost 87.9% when using exhaust plenum skin temperature instead of coolant temperature. The magnitude of this change indicates that there was little to no variation in fuel consumption measurements when the test point data were recorded using exhaust plenum skin temperature. Baseline fuel consumption variation was similarly improved, Figure 4.28.

The test-averaged CoV of CO measurements was 10.4% lower when using exhaust plenum as a steady-state indicator. The overall level of CoV was good, as measurements of CO from naturally aspirated engines are inherently unstable [155].

The average CoV for hydrocarbon emissions was improved by 24.1% when using exhaust plenum skin temperature instead of engine coolant to identify steady-state. Engine coolant and exhaust plenum skin temperature performed similarly during the baseline test, Figure 4.31, although the medians were approximately 10% different.

NOx emissions measurements are significantly improved with exhaust plenum skin temperature as the steady-state indicator with a CoV of approximately 30% lower across the range of test points. NOx data quality was lower during the baseline study in chapter 4.6 compared to coolant temperature, shown in Figure 4.32. However there is a high degree of uncertainty when measuring NOx emissions in general, Figure 2.4.

4.7.2 Discussion

A number of test points were retested to observe the effects on data quality when a different indicator of steady-state was used. The test points covered several steady-state speeds and loads that represent the European emissions drive cycle. The test set points contained a range of actuator settings (IVO, EVC, SOI and FRP) and spark timing was set to achieve 50% MFB at 8 aTDC.

It was demonstrated that using a different steady-state indicator had a significant effect on some of the engine responses measured, Figure 4.33. The most affected was particulate number emissions as the measured values changed by over 150% on average when operating at the lowest speed and load.

The coefficient of variations were found to be improved when exhaust plenum skin temperature was used as steady-state indicator, Figure 4.36. This suggests that the engine responses were more stable, increasing the repeatability of the test conditions.

Each engine test set point contained a combination of actuator settings designed to simulate a unique operating condition. There multiple non-linear interactions occurring and changing the steady-state indicator may cause one test point to be more optimum for an engine response compared to another. As an example this can be observed in test point 4, Figure 4.37, where PN emissions are lower when coolant was the steady-state indicator. Test point 5, however, shows the opposite case. As such there may have been some test points that were more representable when using engine coolant as a steady-

state indicator. The aim of this research is to improve the overall quality of data that are recorded during engine mapping testing. This enhance the engine response surface models that are generated using the test data.

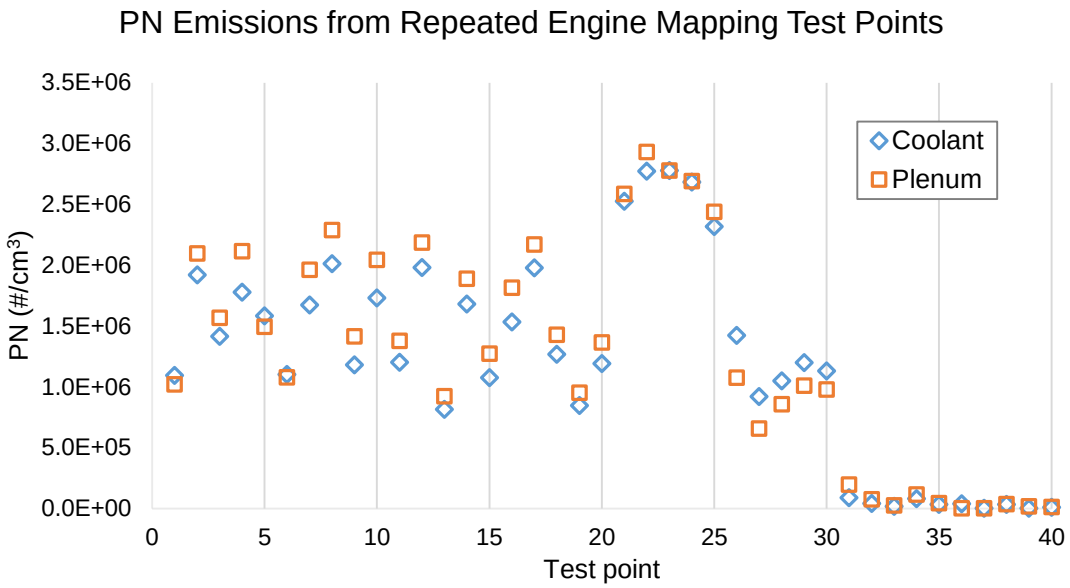

Figure 4.37 PN emissions measurements from a selection of test points repeated using different steady-state indicators

The use of a steady-state indicator that can more accurately reflect the condition of the engine has allowed improvements in the engine testing measurement repeatability. There are still un-explained sources of variability in some of the engine responses. Particulate matter emissions are the newest of exhaust species to become legislated and this will be the focus to improve the repeatability of baseline measurements.

The repeatability of particulate matter emissions measurements, regarded as the most variable exhaust emission [60], improved. Exhaust plenum skin temperature provided a better representation of the thermal condition of the engine, and thus the state of the formation mechanisms that are involved in particulate formation.

4.8 Preconditioning for repeatable baseline emissions measurements

To investigate how engine responses are affected by preconditioning a number of tests were carried out. A range of engine operating conditions were selected to create varied conditions in the exhaust, Table 4.5.

Table 4.5 Preconditioning test points

Test #	Preconditioning (rpm – Nm)	Power (kW)
1	Idle (~650 – 0)	0.06
2	700 – 28	2.05
3	3500 – 30	11.00
4	3500 – 60	21.99
5	2000 – 199	41.68

According to some literature the most effective method of removing build-ups in the engine and exhaust system is to operate at an operating point that generates high exhaust temperatures [77]. This should remove heavy hydrocarbon deposits from the internal surfaces by means of evaporation. Measurements should therefore be representative of the operating conditions with minimal influence from re-entrained material. An opposing theory is that high levels of particulates (by number and mass) will be seen at the higher speeds and loads, which may contaminate the internal surfaces [137].

The preconditioning test was run as the last test of the day and the engine would be shut down immediately following the run. The engine would be allowed to soak for 20 minutes at each preconditioning point. The baseline test would be carried out the next day using a controlled start-up routine. The

baseline operating condition is 2000 rpm 81 Nm (16.97 kW) which lies approximately mid-way in the range of power outputs.

4.8.1 Results

Results for the engine emissions are presented as a percent deviation from the normal baseline levels.

The results suggest that a higher value of measured PN will occur as a result of a low powered preconditioning, Figure 4.38. The effects of preconditioning is more pronounced at lower end of the power spectrum. The effects may be due to a large build-up of heavy hydrocarbon components on the internal surfaces of the exhaust system, [77]. These build ups can then be re-entrained during the baseline operating condition, increasing the amount of material available for nucleation into particulates.

Higher power preconditioning, i.e. hot and fast exhaust gases, lowers particulate number to below the value normally observed during baseline tests. During everyday testing of this engine the maximum speed and load was 2000 rpm 199 Nm. Often the engine would be tested at a much lower power condition for many hours without operating at a higher condition. This could cause some deposition on the internal surfaces during everyday usage, causing the normal baseline value to be skewed relative to these tests.

A line of best fit was applied to the data, Figure 4.38, and the coefficient of determination is shown. The equation of the fitted polynomial was solved to find where it crosses the x-axis, which should indicate the optimum preconditioning power to obtain a value of PN that is closes to the mean

baseline data. The lower solution for y = 0 suggests preconditioning at 15.4 kW that is not far from the baseline power of 16.97 kW.

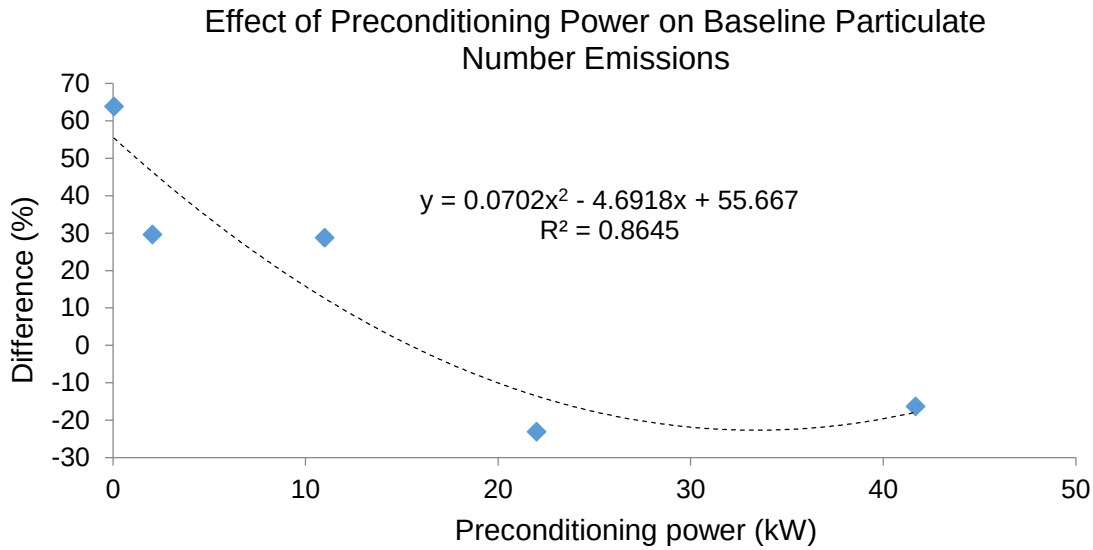

Figure 4.38 Effects of prior day preconditioning on baseline PN emissions

The effect of preconditioning on the previous day had little to no effect on the fuel consumption during baseline testing, Figure 4.39. The aim of preconditioning was to alter the state of the internal surfaces for improved emissions measurements. There was a similar lack of effect observed when different steady-state indicators were used, chapter 4.7.1, compared to emissions and specifically PN.

As the warm-up routine was kept the same before each baseline test the fuel consumption would be unlikely to vary. Changes in fuel consumption may be caused by larger changes in operating conditions, such as valve timing.

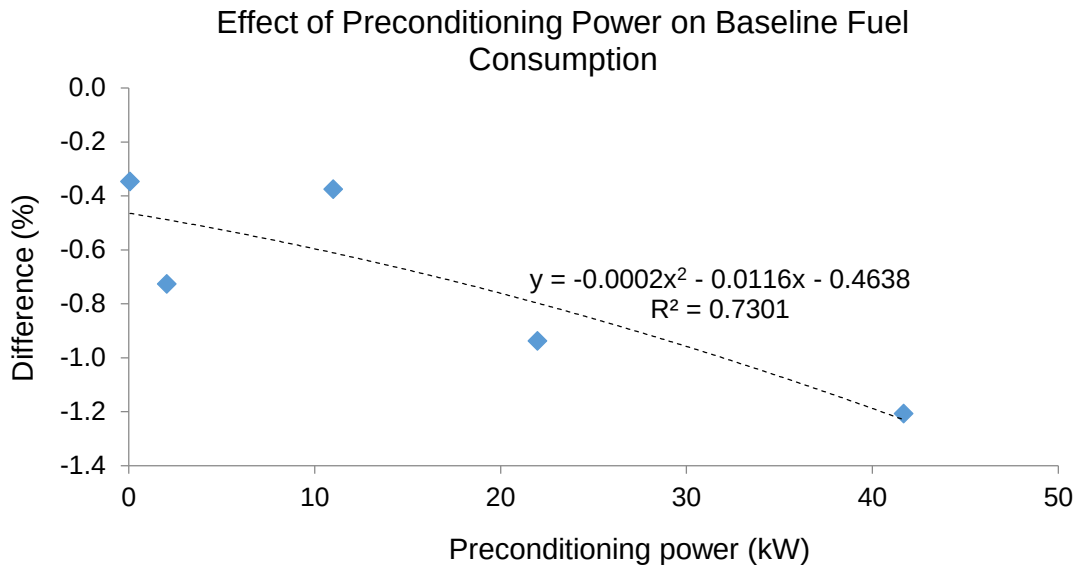

Figure 4.39 Effects of prior day preconditioning on baseline fuel consumption

CO emissions were influenced by a maximum of 5.1% by preconditioning, Figure 4.40. The largest influence was observed when lower power preconditioning routines were used. The highest rated preconditioning caused a deviation of less than 1%. The influence of preconditioning on CO emissions may be negligible when carried out at 6.1 kW although this requires further testing to validate.

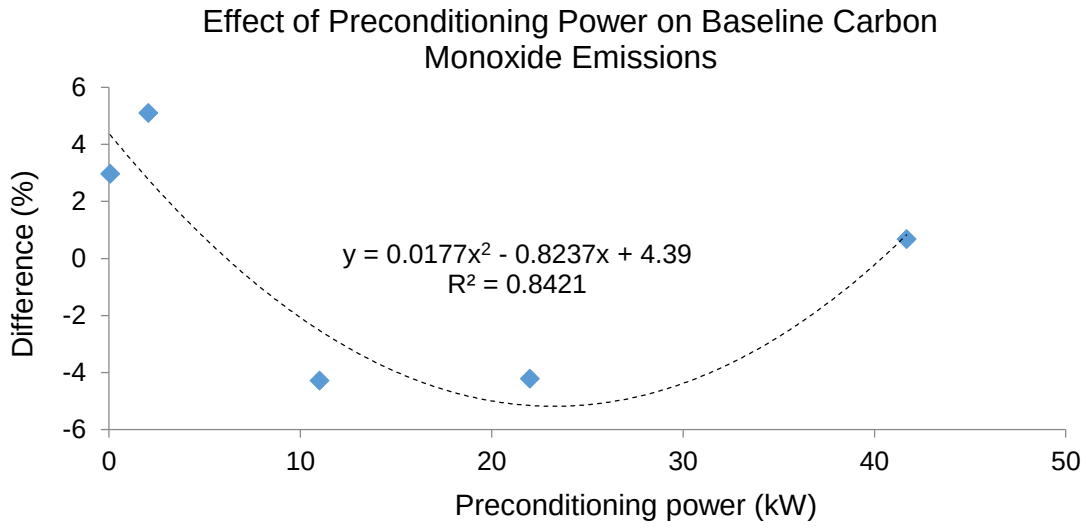

Figure 4.40 Effects of prior day preconditioning on baseline CO emissions

The influence of preconditioning on CO_2 emissions was very little at all the operating conditions, Figure 4.41. The trend is similar to that with CO emissions although the differences could be caused by measurement error.

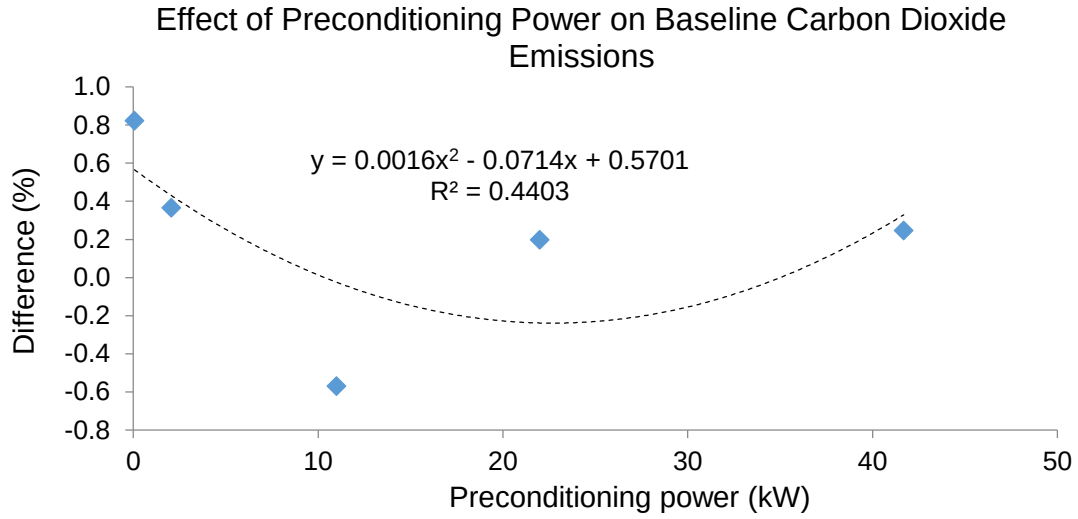

Figure 4.41 Effects of prior day preconditioning on baseline CO_2 emissions

There is no clear trend on hydrocarbon emissions, Figure 4.42, although all of the preconditioning tests cause HC emissions to fall below the baseline average.

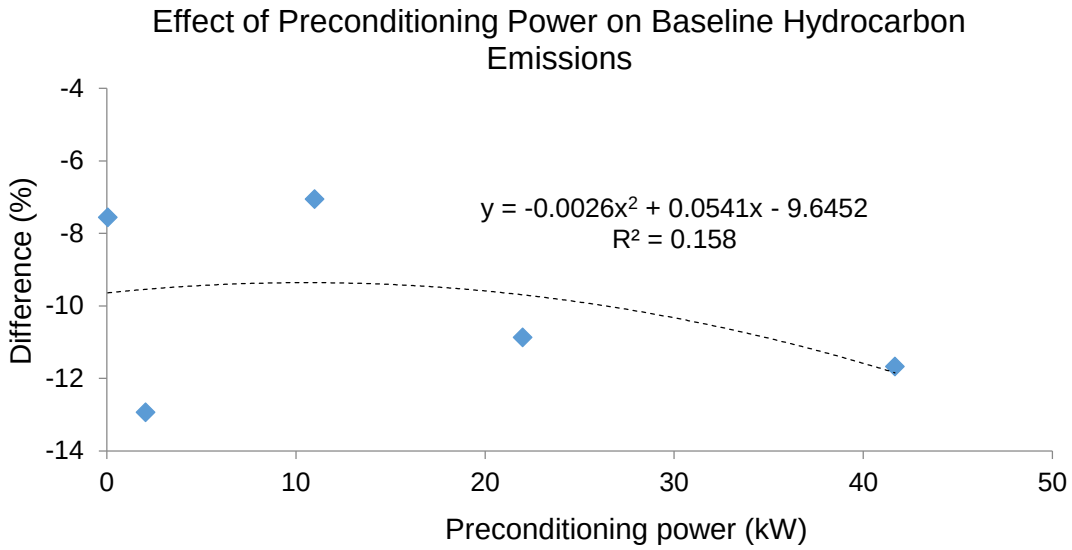

Figure 4.42 Effects of prior day preconditioning on baseline HC emissions

An inverse relationship to PN appears with NOx emissions when preconditioning under varying power loads, Figure 4.43.

The range of NOx data, which is generally lower than the baseline average, indicates that preconditioning of any type will reduce the levels measured during the subsequent baseline. It is plausible that operating at steady-state for 20 minutes, regardless of power throughput, conditions the combustion chamber surfaces such that they are homogeneous, resulting in better combustion and lower NOx.

The 11 kW and 22 kW preconditioning routines were carried out at a significantly higher engine speed than the largest preconditioning set point. This higher peak piston speed may cause an uneven preconditioning on the combustion chamber surfaces due to uneven tangential loading on the piston rings [156]. This would lower mixture preparation and combustion efficiency.

This may also be the case with the idle mode preconditioning as the combustion chamber design is unlikely to be optimised for operating at idle.

The derivative of the fitted line was solved to obtain the point closest to the curve, i.e. closest to a zero percent preconditioning offset position:

$$\frac{d}{dx}\left((-0.0263)x^2 + 0.9726x - 10.001\right) = 0 \qquad \textbf{Equation 4.1}$$

The solution for the closest to zero percent deviation is when x = 18.49 kW, which is not far from the baseline power (17 kW). Further studies should be carried out to verify these findings as the data is inconclusive for NOx emissions.

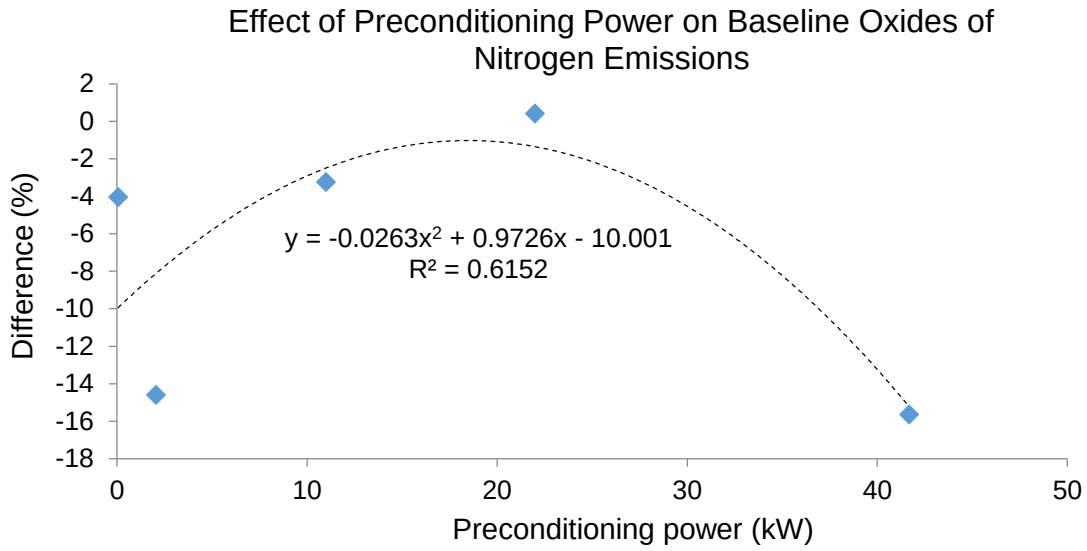

Figure 4.43 Effects of prior day preconditioning on baseline NOx emissions

4.8.2 Discussion

A repeat operating condition should provide repeatable measurements unless there are additional factors not taken into account. The baseline data observed in this chapter suggests that there is a significant influence caused by pre-

conditioning. The speed of the engine will largely control the exhaust gas velocity whereas the load affects the exhaust gas temperature. It is thought a combination of these two factors, heat and velocity, will dictate the influence of preconditioning. The interaction of the two is unclear but higher temperatures will generally aid desorption of heavy hydrocarbon components, the removal of which may not be effective with higher gas velocities alone.

Additionally there are the effects on the combustion chamber surfaces that need to be considered. It is unlikely that NOx emissions are greatly affected by the conditions in the sample lines as the chemistry of NOx formation is only affected by the peak temperatures and there is little evidence of temporary deposition, known as ‘hang-up’, which has been shown to influence both HC and PN emissions [77], [157]. What may be occurring is the conditioning of combustion chamber surfaces since a more consistent coating will improve mixture homogeneity.

The test method contained sources of variance that may have caused erroneous data. One such was that the warm-up routine on the following test day took place in varying ambient conditions. This would have affected the conditioning of the surfaces since the surface temperatures and loss/re-entrainment mechanism rates would have been different.

Another possible source of variance was that the time frame between preconditioning and the baseline test, which varied from one to seven days. A longer period may have allowed the more volatile components that were stored on the internal surfaces to desorb before the engine was restarted. The

heavier components remaining would therefore require more energy before re-entrainment into the exhaust stream. For the shorter durations there may have been residual heat energy remaining in the system. This will likely contribute to the warming up phase the following test, thus helping to purge the volatile species.

Possible methods to avoid these sources are rounded up in Table 4.6.

Table 4.6 Possible sources of error during preconditioning

Source of Variance	Remedy
Ambient conditions	It is not possible to eliminate this from the current test facility since the combustion air is not conditioned. Monitoring the ambient conditions should help to explain any erroneous responses.
Inconsistent inter-test duration	Retain strict test process and avoid testing when a weekend will prevent testing the following day. If there are problems in the facility that require a number of days to fix then restart preconditioning from the first day's test.

A number of issues have been identified when preconditioning occurs on a separate day to the test. It would be beneficial to incorporate the preconditioning into the test. Giechaskiel *et al.* [39] used an 'in-line' preconditioning event which vastly improved the quality of the data. It should therefore be possible to include a step within a regular engine mapping test scenario that can take place in between test points, effectively returning the system to a known condition as the effects may be as important to data quality as instrument calibration.

4.9 Fast establishment of optimal steady-state indicator

Sections 0 to 4.8 have discussed the processes involved in establishing a reliable steady-state indicator. The Ford EcoBoost engine was used to validate the findings from the Jaguar engine. This was achieved by finding optimum steady-state indicator using a step-change test. This should identify a steady-state indicator for use with a newly installed UUT.

A number of steady-state test points were chosen that cover the range of speeds and loads used in normal operation, Table 4.7. A wide open throttle (WOT) condition at top speed was not attainable with the facility so the range was adjusted to suit. At each test point the engine was allowed to stabilise until the engine responses changed less than 1% within 60 seconds. The test was repeated three times and the results were averaged.

Table 4.7 Steady-state test points used for step-changes

Test Point	Speed (rpm)	Throttle (%)
1	750	0
2	1500	25
3	1850	35
4	2150	50
5	2500	70
6	2150	50
7	1850	35
8	1500	25
9	750	0

4.9.1 Results

The steady-state step test outlined in Table 4.7 above was run three times. Spearman's rho was calculated for each pair of temperature – engine-response (CO, CO_2, HC and PN) and the median calculated. The data for the PN correlations, along with error bars showing the standard deviation from the three test runs, is presented in Figure 4.44.

The two most significant correlations are TC15 and TC18 with values of 0.838 and 0.832 respectively. TC15 was measuring exhaust plenum skin temperature and TC18 was measuring post-cat exhaust temperature. The standard deviations are also very close at 0.084 and 0.114, also respectively. As such both these temperatures should be used to identify steady-state to achieve the most repeatable data.

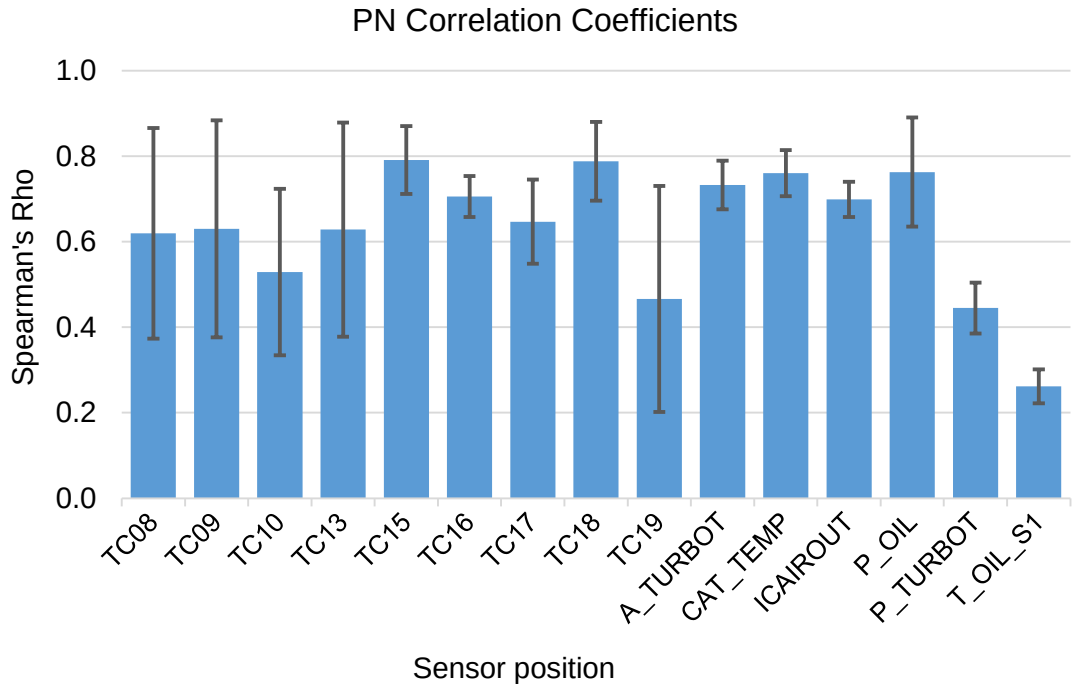

Figure 4.44 Steady-state correlation results with error bars spanning two standard deviations. Sensor is a thermocouple unless preceded by 'P…' which denotes a pressure

4.10 Summary

Five steady-state experiments to improve data quality by testing methodological changes were carried out. Four of the experiments were on a 5 litre naturally aspirated gasoline engine and one was carried out on a 1.6 litre turbocharged gasoline engine.

The first test used several steady-state step-changes to observe the effect of a different operating condition on the control of engine fluid temperature. Coolant out temperature was recorded, as was oil temperature in the sump and gallery. The following conclusions were drawn:

i. Changing the operating condition can affect the thermal state of the engine for at least 10 minutes

ii. The control systems are put under varying demands if the power law is maintained with constant power (kW) but speed and load are varied
iii. Coolant and oil temperature measurements are susceptible to localised temperature spikes that are not representative of the entire engine block
iv. Engine sump oil temperature measurements were more damped than gallery oil temperature measurements. However the sump oil temperature measurement noise was higher
v. Dry-coolers that are used for managing engine coolant can cause the engine temperature to fluctuate if improperly calibrated. This was observed in the greater than first-order response of the engine oil following the step-changes
vi. If a dry-cooler responds to a change but the change is caused by poor control of the engine by the test cell controller then it may increase the duration until settling. This poor control was observed during step-changes when the speed decreased but the load increased. The load increased first (faster response of the dynamometer) causing an initial spike in power that then dropped. Anomalies such as this are not observed in the sump oil temperature data since the response is damped

The second test compared exhaust emissions and fuel consumption data quality from a repeat test point when using different temperatures to indicate stable operation; engine sump oil, coolant out and exhaust plenum. The repeat test point was set via the test cell controller and ECU calibration software to ensure good repeatability of conditions. The following points were observed:

i. Particulate number emissions data was more repeatable when the exhaust plenum skin temperature was used for indicating steady-state conditions (data values in Appendix A8, Table 0.3)

ii. A drift was observed in PN emissions throughout the testing period that was attributed to ambient conditions since the measurements returned close to initial readings
iii. A functional relationship was observed between PN and standard deviation. This is detrimental to response surface modelling techniques such as classical general linear methods since an assumption made is that measurement error is uniform across the measurement space
iv. More repeatable fuel consumption measurements were generated when using exhaust plenum skin temperature to identify steady-state operation
v. CO emissions measurements were more repeatable when using exhaust plenum skin temperature to identify steady-state operation. CO emissions from GDI engines are inherently poor due to the short time allowed for mixture preparation
vi. Repeatability of CO_2 emissions measurements were all good (CoV < 0.01) although plenum skin provided measurements with closer spread
vii. HC emissions measurements at the repeat test point were optimal when coolant was used to indicate steady-state
viii. Repeatability of NOx emissions measurements was higher when oil sump temperature was used

The third test repeated a number of engine set points across five operating conditions using different steady-state indicators, exhaust plenum skin and engine coolant. Emissions measurement data quality was compared and the following observations were made:

i. PN varied significantly with a test-averaged difference of over 150% at the lowest operating condition. This may be caused by deposition on the internal surfaces. It is more likely that deposition occurs at lower speeds since the exhaust gas energy (velocity and

temperature) is lower. Measurement variation reduced as the power increased.

ii. PN changed the most when the measurements were normalised per kW. The most greatly affected operating condition was Node 2, Figure 4.34

iii. In contrast, CO emissions were affected the least at the lowest operating condition. Lower rpm allows more time for mixture preparation although there is less energy in the charge to induce turbulence. When calculated per kW the lowest change was observed at Node 2, Figure 4.34

iv. HC emissions were not greatly affected at by the change in operating condition. However normalising with respect to power showed that there is a high influence on the steady-state indicator at the lowest operating condition. An improvement in the quality of data was observed when the exhaust plenum was used as a steady-state indicator, Figure 4.36

v. The largest change was observed in fuel consumption with 87.9% lower variation (calculated using CoV). A CoV of 0.14 is relatively high (as compared to the gaseous emissions) but 0.02 is more expected. The value of 0.14 may be erroneous and further investigation required.

vi. The CoV of HC emissions improved by 24.1% when using exhaust plenum as a steady-state indicator

vii. PN showed the highest degree of variation across both tests with an improvement of 5.6% when using exhaust plenum as the steady-state indicator

viii. NOx emissions showed a good level of quality with both steady-state indicators, as did CO

The fourth experiment tested the influence of prior-day operating conditions on measurements made the following morning. A range of speeds and loads were chosen to generate various exhaust conditions from low to high velocities

and temperatures. Results are presented as percent deviation from the mean baseline values. The following was observed:

i. PN emissions were lower when a higher power preconditioning was used. This is attributed to the hotter and faster exhaust gases cleaning the internal surfaces of the exhaust system. There are less components able to be re-entrained and measured
ii. Higher PN emissions were observed following preconditioning at lower powers as there would be a greater level of deposition occurring on the internal surfaces that would then be re-entrained at the baseline condition (which is at a higher speed and load, therefore greater sheer forces) the following morning
iii. Fuel consumption varied little depending on the preconditioning.
iv. CO emissions increased when preconditioning occurred at higher or lower powers than the baseline condition
v. CO_2 emissions were not greatly affected by preconditioning
vi. HC emissions measurements were lower for all of the preconditioning states
vii. In general, preconditioning at the same condition as the baseline test point causes the smallest change compared to the mean baseline values. This may be due to conditions in the exhaust being repeated the following morning

The fifth experiment was carried out on a different engine: the Ford EcoBoost in chapter 4.9. It was designed to identify the optimal steady-state indicator using a single test. The following was concluded:

i. Changing the steady-state indicator has shown to greatly affect the measured emissions. It is paramount that the optimal variable be identified to ensure the data are of high quality
ii. Two thermocouples were identified as having the greatest correlation with PN emissions. These will then be used as a steady-state indicator for the second set of engine mapping tests

iii. Differences in the measured responses may not always be significant when using a different steady-state indicator. However the improved CoV of the data suggests the representability is greater and therefore the test duration can be reduced

iv. Preconditioning does affect the condition of the UUT in terms of emissions although the effects can be quickly undone by a high-emission operating point

v. A brief experiment can be used to quickly determine a reliable steady-state indicator

Chapter 5

Sequencing Steady-State Test Points for Minimal Variance in the Critical Engine Responses

5.1 Introduction

Section 3 of this thesis reviewed steady-state methodology for measuring emissions and some revised methodological steps were suggested. Preconditioning was apparent as one of the most influential factors in terms of reducing variation in emissions measurements. Ensuring the system has been properly prepared before collecting test data can improve data quality but the effects of preconditioning may last as little as 3 minutes [60]. To further improve data quality the methodology used during testing was examined.

Errors in test data are assumed to be normally distributed when applying a General Linear Modelling method to engine experimentation. Deviations from normally distributed error have been observed by Dvorak *et al.* [93] across the operating region. To test whether errors are normally distributed a sample of steady-state test data were analysed. If the sum of errors is close to zero then the distribution is Gaussian. A value other than zero suggests a bias that could cause problems when using DoE methodology.

5.2 Investigative analysis on steady-state data

Steady-state test measurements were made at five operating conditions, or ‘nodes’, Table 5.1. The data were collected in stable regions of the engine

operating envelope such that the data would not likely contain anomalous values. The engine used for these test points was the Jaguar V8.

Table 5.1 Operating conditions at each node

Node	Speed (rpm)	Load (Nm)	Power (kW)
1	700	28	2.05
2	1500	41	6.44
3	1500	105	16.49
4	2000	81	16.97
5	2000	199	41.68

At least 40 test points were run at each node using the following methodology:

i. Start engine and perform daily checks
ii. Proceed to desired node (speed and load)
iii. Allow exhaust plenum skin temperature to stabilise (< 1°C change in one minute)
iv. Collect test data for current speed and load

The variables that were changed are shown in Table 5.2 and each test point was comprised of a unique set of values. The values were pre-determined by a DoE method with the exception of spark advance, which was entered manually at each test point to align 50% MFB with 8 aTDC using in-cylinder pressure data.

Table 5.2 Actuator settings at each test point

Actuator	Abbreviation	Unit
Fuel rail pressure	FRP	MPa
Inlet valve opening	IVO	aTDC
Exhaust valve closing	EVC	aTDC
Spark advance	SA	bTDC
Start of injection	SOI	bTDC

The measured engine responses are shown in Table 5.3.

Table 5.3 Engine responses

Engine response	Abbreviation	Unit
Carbon monoxide	CO	%
Carbon dioxide	CO_2	%
Particulate number	PN	$\#/cm^3$
Oxides of nitrogen	NOx	ppm
Hydrocarbons	HC	ppm/C

5.2.1 Engine response mean error analysis

To quantify the magnitude that the engine responses were changing over a test point the percent difference between the first and last five values was calculated, Figure 5.1. The sum of the differences is then used for analysis.

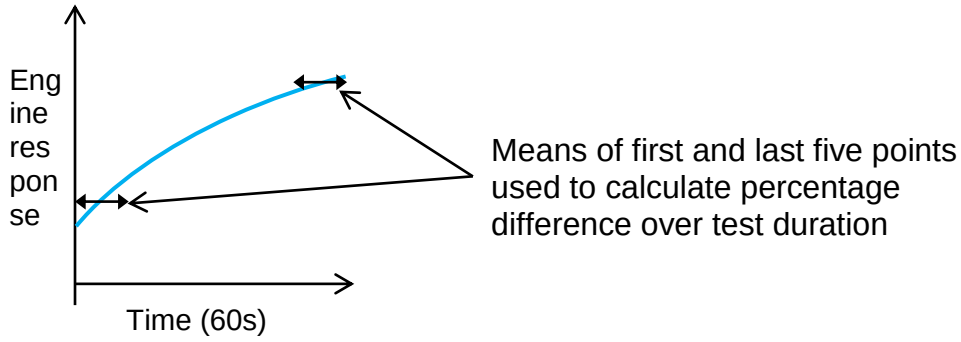

Figure 5.1 Percentage change used five points to reduce errors from noisy data

The percent differences, presented in Figure 5.2, show that various engine responses were changing a significant amount during testing at some of the nodes. PN emissions changed an average of -9.5% across test points at Node 1, indicating that the engine response was negatively biased on average. The variation of PN observed at the other nodes was lower and at Node 5 the mean variation was 0%. Using data that has a non-zero mean error will introduce errors in a DoE since the processes are not designed to account for them.

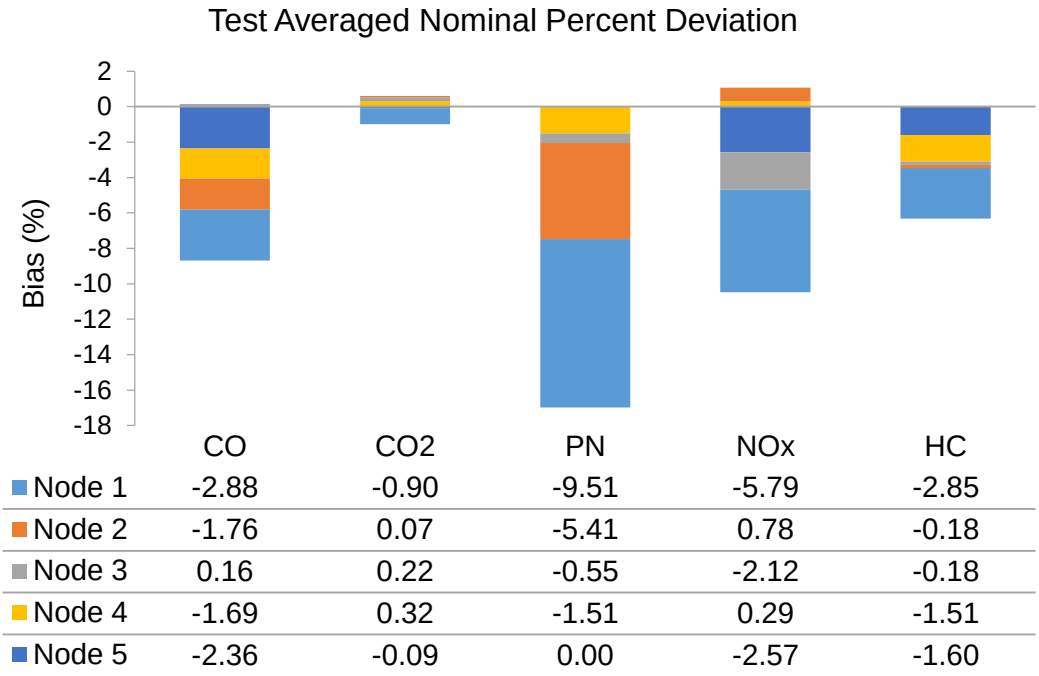

	CO	CO2	PN	NOx	HC
Node 1	-2.88	-0.90	-9.51	-5.79	-2.85
Node 2	-1.76	0.07	-5.41	0.78	-0.18
Node 3	0.16	0.22	-0.55	-2.12	-0.18
Node 4	-1.69	0.32	-1.51	0.29	-1.51
Node 5	-2.36	-0.09	0.00	-2.57	-1.60

Figure 5.2 Percent change calculated as per-test and averaged

The absolute changes in engine responses for each node are presented in Figure 5.3. The values show the average that each variable changed during testing at the five speed-load conditions.

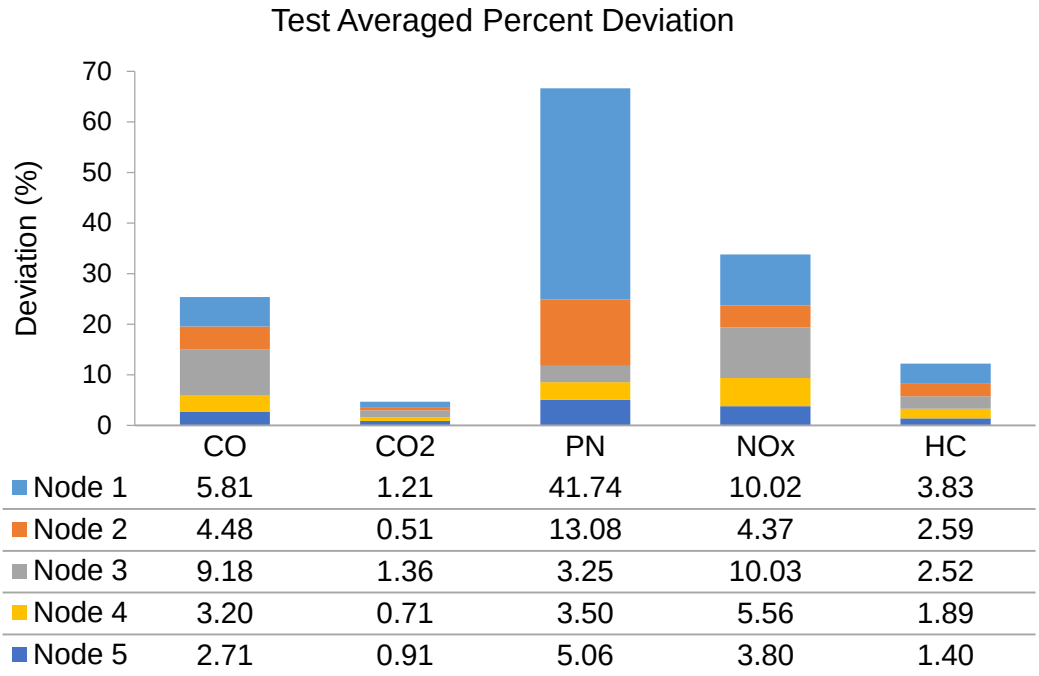

	CO	CO2	PN	NOx	HC
Node 1	5.81	1.21	41.74	10.02	3.83
Node 2	4.48	0.51	13.08	4.37	2.59
Node 3	9.18	1.36	3.25	10.03	2.52
Node 4	3.20	0.71	3.50	5.56	1.89
Node 5	2.71	0.91	5.06	3.80	1.40

Figure 5.3 Absolute mean percent change per node

PN emissions varied the most during testing. PN at Node 1 changed by 41.7% on average. At Node 5, where the nominal percent change in Figure 5.2 was zero, there is a deviation of over 5%.

NOx and CO emissions were also prone to variation during testing. CO_2 and HC emissions were less likely to change during measurement.

In effect the data in Figure 5.3 is the cumulative variation of the values used for Figure 5.2 and so all the values are inevitably higher. However it highlights that even though the mean variation may be close to zero there could be regions of the operating envelope that contain greater errors.

5.3 Correlation between actuator movement and the mid-term stability of engine responses

As the average error was found to be non-zero the cause of instability, assuming steady-state conditions, is from changing actuator values. The actuator values are a known control parameter that can be correlated with the variations in engine responses.

The analysis used the actuator settings from each test point to find the difference in value from one test point to the next. The previous actuator setting is deducted from the actuator setting at each test point, an example is shown in Table 5.4.

Table 5.4 Method to find actuator difference

Test point	Actuator value	Actuator delta
1	25	see[2]
2	10	-15
3	15	5

This change could then be correlated with the emissions data from the test point, which was captured at 1Hz for 60 seconds, to indicate whether the change in actuator value caused a deviation in the measured response. The deviation was calculated as the percent change in the measured response after the initial step-change, Table 5.5. The initial step-change was contained within a fixed duration of 10 seconds immediately following a change in

[2] The prior test point's actuator settings would be used to calculate this value. If there was no previous test point the baseline values would be used.

actuator setting. The data after this period until the response settled (< 1% change over one minute) was used to determine the deviation.

Table 5.5 Method to find measured response deviation

Test point	Initial response	Stable response	Percent change
1	1000	800	20.00
2	1200	1350	-12.50
3	1650	1500	6.25

The actuator delta and percent change for each test point are then placed into columns and a correlation analysis performed on each pairing. This determines if there is a correlation between the pairs at each node, using the values extracted at each test point as a data sample.

The correlation analysis was performed on actuator – engine-response pairings. The actuators were start of injection, fuel rail pressure, inlet valve opening, exhaust valve closing and spark advance. The engine responses were CO, CO_2, hydrocarbons, NOx and PN.

An independent two-tailed Student's-*t* statistic was used to clarify whether the data pairs are in fact dependent (the data occurred from the same population or not) as proven by rejecting the null hypothesis at a significance level of less than 10% (t < 0.1). The *t* value is calculated using

$$t = \frac{\bar{x} - \mu}{\sigma/\sqrt{(n-1)}}$$ **Equation 5.1**

where $\bar{x}$ is the sample mean, μ is the population mean and σ is the standard deviation.

5.3.1 Results

The correlations identified as significant are listed for each operating node in Table 5.6. The output tables for the t-scores and correlation coefficients are provided in Appendix A12. A correlation was determined to be significant if the Student's *t*-score was below 0.1 i.e. proved significant to a 90% confidence. A full description of the statistical analysis is provided in chapter 3.3.

Table 5.6 Correlations identified with significant t-scores

Node 1	Node 2	Node 3	Node 4	Node 5
FRP – CO	*FRP – PN*	SOI – CO_2	*FRP – PN*	IVO – CO_2
FRP – CO_2	*FRP – NOx*		*FRP – NOx*	**EVC – NOx**
IVO – CO_2	IVO – NOx		SA – HC	**EVC – HC**
IVO – HC	**EVC – CO**		SOI – NOx	SOI – CO_2
EVC – NOx	SA – HC		SOI – HC	
SA – CO_2				
SA – HC				

As shown by the correlations there are a number of causal relationships identified between engine actuators and the long-term instability observed in engine responses at all operating nodes.

Fuel rail pressure (FRP) is shown to have correlations with CO, CO_2, PN and NOx. Increasing FRP will improve mixture homogeneity by reducing the droplet size, which in turn increases combustion efficiency [1]. However the

fuel could also impinge onto the internal surfaces if the injection timing is such that the piston crown is near enough to top dead centre upon injection [69]. This will cause pooling of fuel, severely reducing the ability for the air and fuel to mix properly before ignition which causes soot emissions [158]. Fuel will mix with the lubrication and become a residual component within the oil film that may remain on the internal surfaces for several cycles [1]. This build up will affect subsequent cycles in terms of air-fuel ratio and emissions.

Inlet valve opening (IVO) has correlations with CO_2, HC and NOx. As inlet valve timing varies the cylinder is filled with charge air at varying rates. The velocity of air entering the cylinder will vary depending on the pressure in the cylinder. For later IVO timings the pressure difference will be greater, inducing tumble and swirl within the cylinder. This motion will vary the rate of mixing of air and fuel, which alters combustion duration and emissions [159].

Exhaust valve closing (EVC) has correlations with NOx, CO and HC. The effects of changing EVC is similar to IVO but it controls the timing of exhaust gases leaving the combustion chamber. Early timings will generate high exhaust gas temperatures as an incompletely oxidised charge leaves the combustion chamber and continues to burn [1].

Spark advance (SA) has correlations with CO_2 and HC emissions. The start of combustion is a critical factor and the rate of burn is highly sensitive to the air-fuel ratio at the spark plug location upon ignition [128].

Start of injection (SOI) has correlations with CO_2, NOx and HC. It is possible for fuel to enter the exhaust manifold immediately following injection if there is

overlap between SOI and EVC. This will create hot conditions in the exhaust that will inevitably alter the build-up of components on the internal surfaces [89]. These will be purged under the correct conditions causing emissions that are not representable [160].

Reducing the effects of changing actuators on the engine responses could improve data quality as the engine responses would be changing a lower amount during data acquisition. As pointed out by Beattie *et al.* [124] this would increase the confidence of the RSM's, in turn improving the quality of the engine calibration.

5.4 Ordering DoE test points

Forty DoE points from operating condition Node 4 (2000 rpm and 81 Nm) were tested in six different orders to observe the influence on the measured engine responses from the Jaguar V8. The test points are derived from an engine mapping exercise. The points are within a region that was defined by a boundary search such that the combustion stability was good over all the test points.

The test points were reordered using actuator values, with each actuator being used to create a set of points. This is described by using several example test points in the following tables. Table 5.7 shows five example test points as they would be generated from a DoE algorithm.

Table 5.7 Original order of DoE test points

Test point	IVO	EVC	FRP	SA	SOI
1	21.15	6.00	9.65	13.00	297.75
2	10.19	12.38	13.76	25.00	327.66
3	2.35	17.46	10.33	10.00	333.54
4	-2.43	38.06	10.20	11.00	289.41
5	35.67	11.33	8.27	8.00	320.30

The test points in Table 5.8 are the same combinations of actuator values as Table 5.7 but sorted with respect to IVO. Each actuator (IVO, EVC, FRP, SA and SOI) was used to order the test points and the test points were run six times in total, which includes the original (DoE) ordering.

Table 5.8 IVO-dependent DoE test points

Test point	IVO	EVC	FRP	SA	SOI
1	-2.43	38.06	10.20	11.00	289.41
2	2.35	17.46	10.33	10.00	333.54
3	10.19	12.38	13.76	25.00	327.66
4	21.15	6.00	9.65	13.00	297.75
5	35.67	11.33	8.27	8.00	320.30

The test data were collected under steady-state operating conditions using the steady-state methodology described in Appendix A10 except spark timing was recorded and repeated for the subsequent tests to retain operating conditions. The original test data were re-recorded to reduce the time between test runs and increase the repeatability of test conditions.

5.4.1 Results

The difference in measured engine responses changed significantly depending on the order of the test points. Some metrics to describe the variation are shown in Figure 5.4 below. These include the average (calculated over the forty test points), the minimum and maximum differences between measured values at each of the test points.

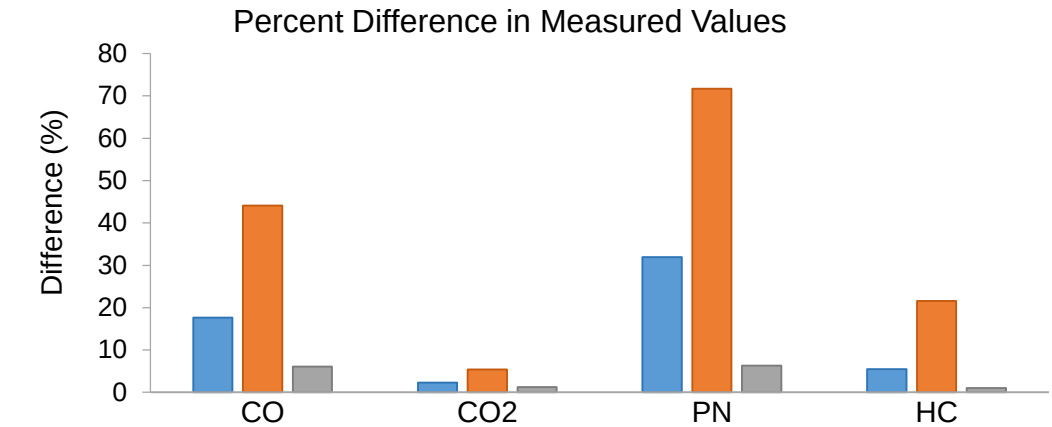

	CO	CO2	PN	HC
Average	17.7	2.3	31.9	5.4
Max	44.1	5.4	71.7	21.6
Min	6.1	1.2	6.3	1.0

Figure 5.4 Change in engine emissions between test point orders

The ranges show that the order which test points are carried out can have a significant effect on measured data. At this operating condition and with these particular test points particulate number emissions are less stable compared to the other exhaust emissions. The largest difference in values at a test point was also PN with a range of 71.7%.

The formation mechanisms involved with particulates are more strongly influenced by changes in operating conditions compared to other exhaust emissions. Differences between DoE test points will be purposefully large in

an attempt to minimise noise by causing a significant measurable change in the system. The sample line is situated 3.2 meters downstream of the exhaust manifold and there is a high chance of deposition and re-entrainment mechanisms to occur within the exhaust system. These mechanisms can uncontrollably alter the observed particulate levels as stabilisation periods can be longer than test points.

Carbon monoxide emissions are heavily influenced by test point ordering as indicated by the minimum change of 6.1%. The volume of CO in the exhaust gases can be altered by unburned hydrocarbons that are adsorbed by deposits on the combustion chamber surfaces. These deposits are then re-entrained mainly during the exhaust phase of the cycle, sporadically altering the air-fuel ratio and causing the burn profile to change. A richer mixture will reduce peak temperatures and the oxygen available, both reducing the oxidation of CO to CO_2.

The hydrocarbon mean range of 5.5% and may be caused by hydrocarbon hang-up in the sample line or the build-up of residuals in the lubricating oil on the engine's internal surfaces, both phenomena being well documented [1]. Build-up will occur more readily when the combustion is incomplete and organic matter is present for extended durations over the cycle. Changes in catalyst temperature can also affect the conversion efficiency of unburned hydrocarbons [51].

CO_2 emissions are the most repeatable with an average range of 2.3%.

The t-scores were calculated for each of the test point runs, Figure 5.5, showing that the engine responses do not have an equal degree of correlation when the test points are ordered by the different engine actuators. This is a confirmation that ordering test points using different methods will change the degree of dependence of the engine responses on the movements of the engine actuators.

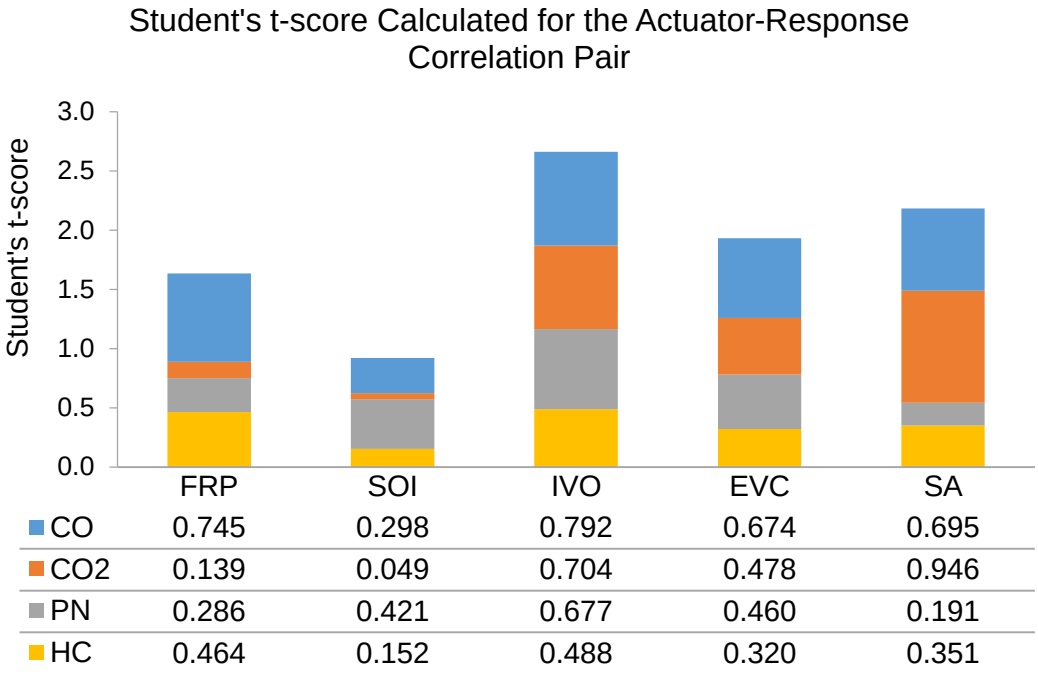

	FRP	SOI	IVO	EVC	SA
CO	0.745	0.298	0.792	0.674	0.695
CO2	0.139	0.049	0.704	0.478	0.946
PN	0.286	0.421	0.677	0.460	0.191
HC	0.464	0.152	0.488	0.320	0.351

Figure 5.5 Cumulative t-score for actuator-response correlations when test points were ordered by the respective engine actuator

When the test points are ordered by the actuator values the t-scores vary. It is desirable to have larger t-scores as this indicates that there is less correlation between the engine actuators and exhaust emission stability.

Figure 5.6 is a cumulative bar-plot that shows the t-scores for CO exhaust emissions during each of the DoE tests. CO emissions are identified as having

a correlation with EVC when the test points are ordered by SA based on a certainty of 90%.

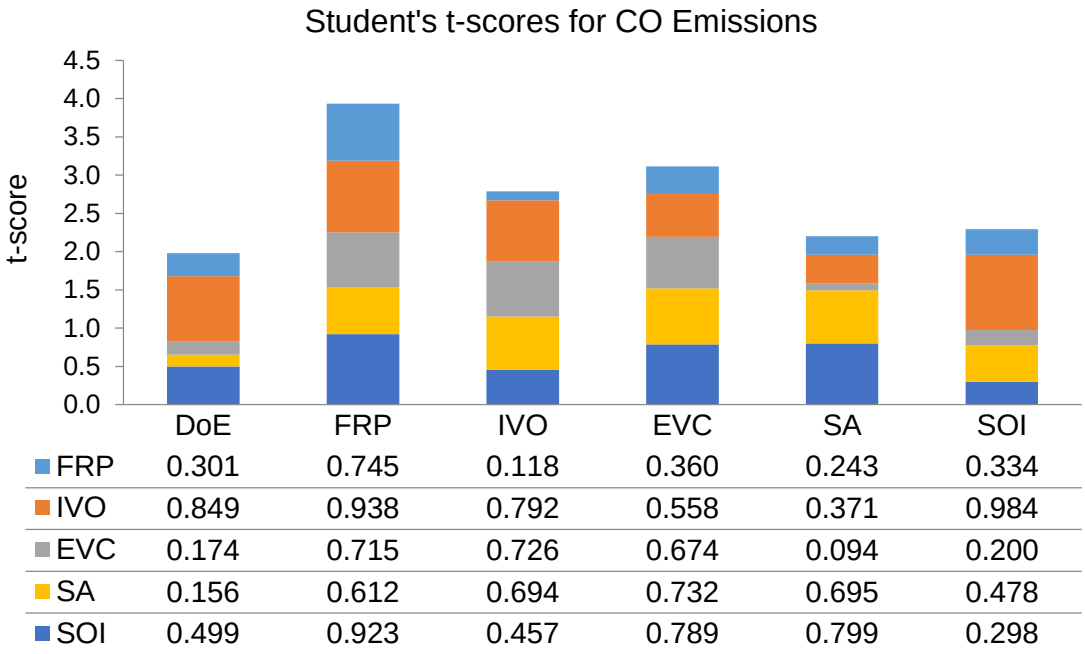

	DoE	FRP	IVO	EVC	SA	SOI
FRP	0.301	0.745	0.118	0.360	0.243	0.334
IVO	0.849	0.938	0.792	0.558	0.371	0.984
EVC	0.174	0.715	0.726	0.674	0.094	0.200
SA	0.156	0.612	0.694	0.732	0.695	0.478
SOI	0.499	0.923	0.457	0.789	0.799	0.298

Figure 5.6 Cumulative Student's t-scores of correlations between CO and engine actuators during engine mapping tests

When run in the original order there was a significant correlation between CO_2 and IVO. CO_2 emissions are identified as having a correlation with SOI when ordered by EVC and SOI, Figure 5.7.

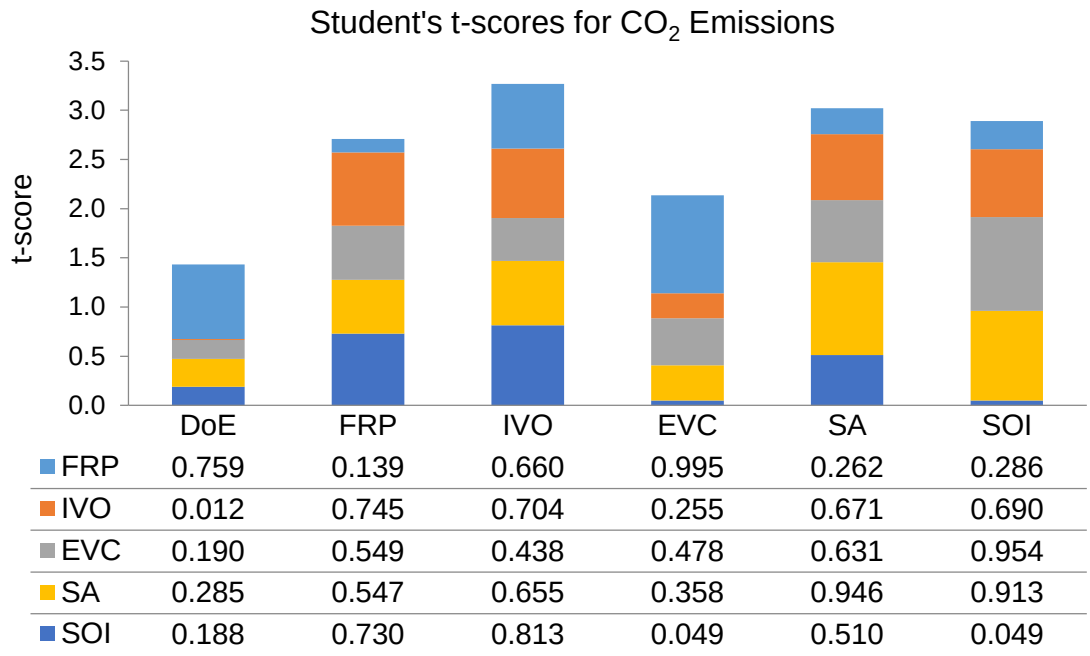

	DoE	FRP	IVO	EVC	SA	SOI
FRP	0.759	0.139	0.660	0.995	0.262	0.286
IVO	0.012	0.745	0.704	0.255	0.671	0.690
EVC	0.190	0.549	0.438	0.478	0.631	0.954
SA	0.285	0.547	0.655	0.358	0.946	0.913
SOI	0.188	0.730	0.813	0.049	0.510	0.049

Figure 5.7 Cumulative Student's t-scores of correlations between CO_2 and engine actuators during engine mapping tests

PN emissions instability was correlated with SOI and FRP when the test points were ordered as the DoE algorithm stipulated, Figure 5.8. There was also a correlation with SA when ordered by FRP; FRP when ordered by IVO; FRP when ordered by SA and FRP when ordered by SOI.

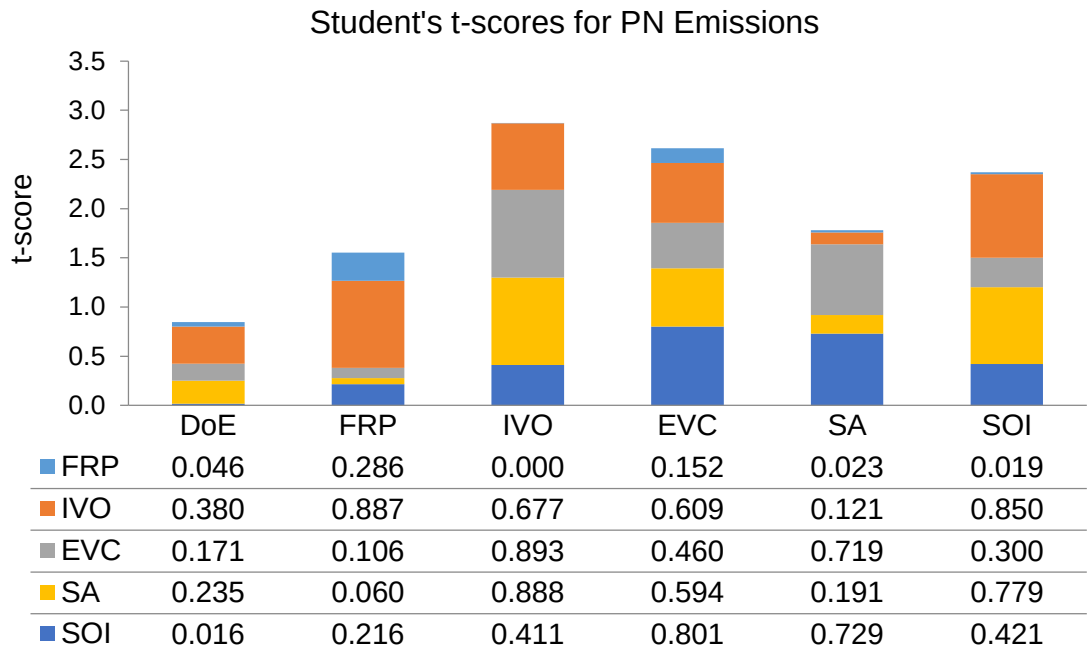

	DoE	FRP	IVO	EVC	SA	SOI
FRP	0.046	0.286	0.000	0.152	0.023	0.019
IVO	0.380	0.887	0.677	0.609	0.121	0.850
EVC	0.171	0.106	0.893	0.460	0.719	0.300
SA	0.235	0.060	0.888	0.594	0.191	0.779
SOI	0.016	0.216	0.411	0.801	0.729	0.421

Figure 5.8 Cumulative Student's t-scores of correlations between PN and engine actuators during engine mapping tests

The instability of HC emissions during testing was correlated with SOI and SA when the test points were run using the original order, Figure 5.9. Correlations were also identified between SA and EVC when ordered by FRP; SA and EVC when ordered by IVO; FRP when ordered by EVC and SA, EVC and FRP when ordered by SOI.

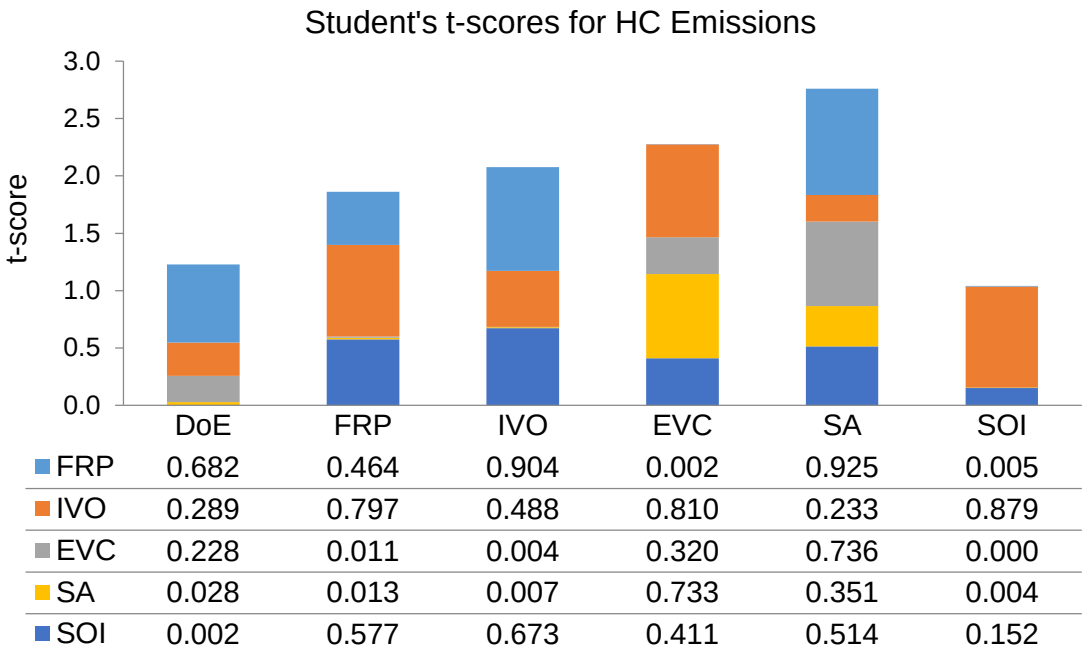

	DoE	FRP	IVO	EVC	SA	SOI
FRP	0.682	0.464	0.904	0.002	0.925	0.005
IVO	0.289	0.797	0.488	0.810	0.233	0.879
EVC	0.228	0.011	0.004	0.320	0.736	0.000
SA	0.028	0.013	0.007	0.733	0.351	0.004
SOI	0.002	0.577	0.673	0.411	0.514	0.152

Figure 5.9 Cumulative Student's t-scores of correlations between HC and engine actuators during engine mapping tests

The correlation analysis from the different orderings of test points suggests it may be possible to reduce the effects of actuators by re-ordering the test points. However there may be more test-to-test correlations caused by ordering the test points in a manner such as using one of the engine inputs.

It may be possible to mitigate test-to-test carry over effects by intelligently sequencing the test points such that the effects of changing actuator settings on the mid- to long-term stability of engine responses is minimised.

5.5 Sequencing DoE test points with step inputs

Data from the DoE test points in Section 5.4 indicate test point order can have a significant influence on measured exhaust emissions. If the test points were sequenced to inflict minimal test-to-test carry-over then the data should be more representable and of higher quality. This following section will introduce

an approach to order a selection of DoE test points intelligently, or sequenced, using minimal *a priori* knowledge.

A number of design objectives were considered when developing the test point sequencer. These are presented in the following list:

i. Engine conditions vary throughout the day
ii. Deposits on the injectors and valve heads, wear of bearings, state of engine oil, responsiveness of external cooler (also dependent on the external water circuit temperature)
iii. Engine simulations can be generated but are impractical
iv. A lot of data (60+ test points at each speed/load) are required before any useful information can be extracted
v. A target should be to collect all data for one engine operating condition (speed and load) without stopping
vi. The difficulty in repeating a test set point increases with time
vii. The order of test points will alter the results
viii. It was shown in Section 5.4 that the order a set of engine mapping points significantly alters the data
ix. Cannot rely on complex engine models for simulated response as these still require a large amount of time to generate data
x. Want to be able to model/predict/represent a complex system in the simplest terms possible
xi. Beneficial to carry out sequencing test prior to testing at each engine operating condition
xii. Engine conditions (engine, exhaust system, test cell air temperature, ambient conditions, etc.) are prone to vary continuously. Although it is impractical to review the state of the system for every test set point due to the time penalty this would incur it may be possible to perform a sequencing test prior to each speed-load operating condition on-line
xiii. Method to sequence test points should be short

The factors listed above restrict the options available for ordering a set of test points. If a full engine simulation was available prior to testing then this could be used to determine the optimum sequence for test points to be ordered since the performance could be predicted. However the data required for a model with suitable precision is likely to take many hours or days to collect and thus is unrealistic for the current target. The sequencing method should depend on a small data set, acquired from a small number of points that can be repeated without requiring a large effort from the testing facility.

The aim was to develop a method of sequencing test points for improving data quality from one or more chosen measured responses. A test was used to order the test points that did not produce a large time or cost penalty. The test should be capable of characterising the response of any number of engine responses in relation to the actuator movements; for this study exhaust emissions are specified (CO, CO_2, HC and PN) but fuel consumption data are also included in the analysis.

5.5.1 Test point sequencing

The test points should be sequenced so that the settling time for a given response is minimised. This will improve data quality by increasing the representativeness of data as the deviation of the response is reduced. The type of test points used contain actuator settings (IVO, EVC, FRP and SOI) that are changed as close together as possible. Data are then recorded for a fixed duration (usually around 60 seconds) before the next actuator settings are entered. It follows that these step-changes should be ordered so that the

effect on stability of the response is minimised once the initial performance effect of the actuator is realised.

To characterise the stabilisation times quickly there should be a minimum number of test points. These should be able to provide sufficient detail about the stability of emissions to then sequence a set of test points for improved data quality through reduced test-to-test carry-over effects.

Useful DoE models depend on a good boundary search, otherwise known as hull determination, and this test is always carried out before a set of test points. A hull determination finds the safe operating envelope that the engine can operate within before some variable exceeds a pre-defined limit. The limits may be temperatures, pressures, combustion stability or other physical constraints. This is generally performed by incrementing the value of one actuator until a limit is violated, then decrementing the same actuator until a limit is reached. If the maximum of minimum range of the actuator is met before a limit is violated then the maximum or minimum is set as the limit.

A test that has a similar structure to the boundary search could be used to characterise the emissions response. This would have a number of benefits:

i. Standard test
    a. Well-rehearsed for most engine developers
    b. Carried out for every new engine
    c. Not much planning or preparation required
ii. Simple, steady-state test
    a. No complex engine controller required
    b. Data to be collected are from instrumentation previously installed
iii. Relatively short duration test

a. Low impact on testing

iv. Easily repeatable throughout the day
    a. As a benchmark to track instrument/facility drift

v. To recalibrate the sequencing algorithm
    a. The first test can be a combination of boundary search and sequencing test

A schematic of a generic boundary search is shown in Figure 5.10. This diagram shows the actuator value, which starts at the default value, being stepped up until the engine response (e.g. coolant temperature) reaches or exceeds a set limit. The condition is allowed to stabilise then the actuator returns to the base value. The conditions are once again allowed to stabilise then the process is repeated but with the actuator value decrementing.

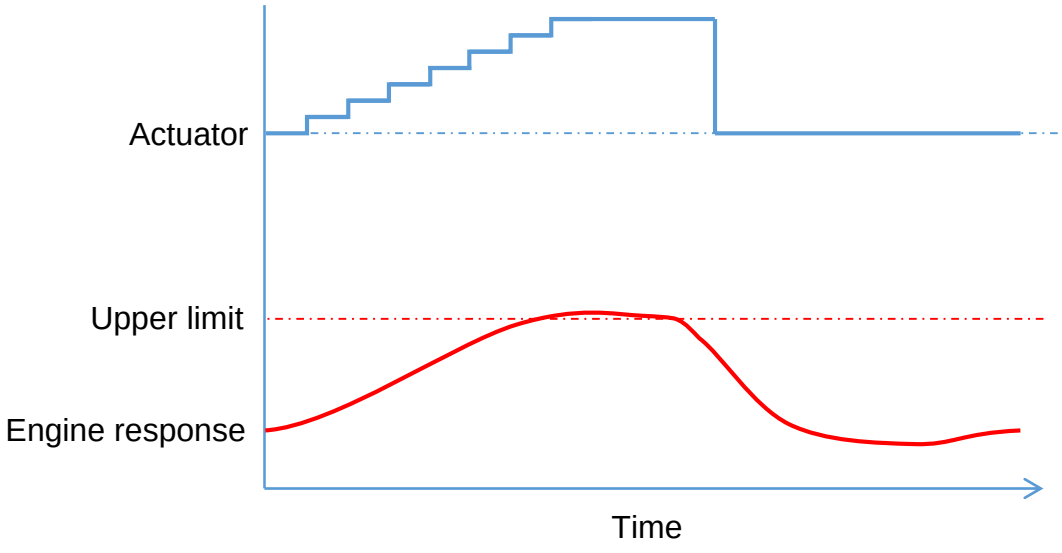

Figure 5.10 One step of a typical boundary search for an engine actuator

The boundary search is carried out for every actuator that will be moved during the engine calibration tests and limits may be set on a number of engine variables such as oil pressure and temperature, exhaust gas temperature, combustion stability and so-on. This process can be a labour-intensive

exercise but there are software packages (e.g. AVL CAMEO) that are able to run this process autonomously.

Once the limits are obtained from the initial boundary search it is possible to use these as step-inputs with the knowledge that the system will be running close to but not over the safe operating limits. A test such as that depicted in Figure 5.11 could then be carried out for the purposes of optimising the order that a set of test points are carried out.

Following each step-change in actuator value the exhaust emissions would be recorded. At the stage where the observed value has stabilised to within a satisfactory limit (e.g. 5% over one minute) then the next step-change would be made. Emissions would be recorded and monitored until they have stabilised. This process would continue for each of the actuators in the same fashion as for the boundary search and the corresponding data would provide information on how long each exhaust emission took to stabilise following a step-change in the engine actuator.

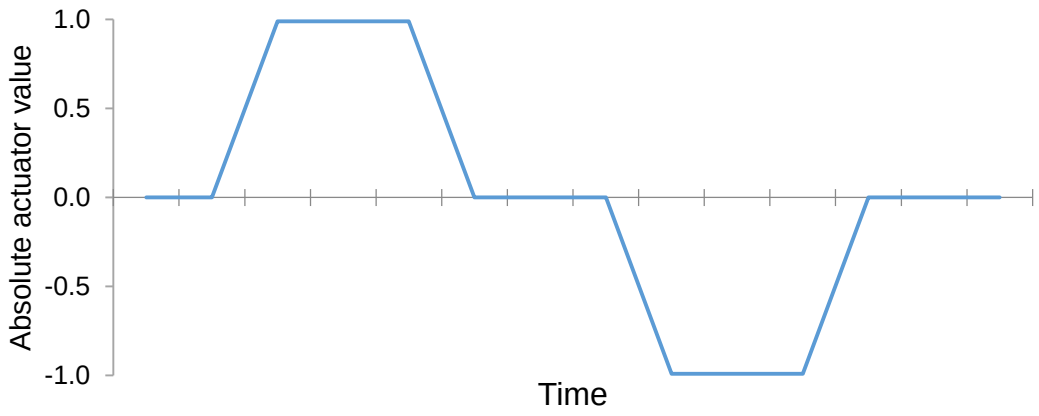

Figure 5.11 Example of a test used for characterising stabilisation times

An engine is a non-linear system and so the stabilisation time required at different regions of the operating envelope will vary. As such a more complex system identification (SID) will be used with intermediate steps, Figure 5.12.

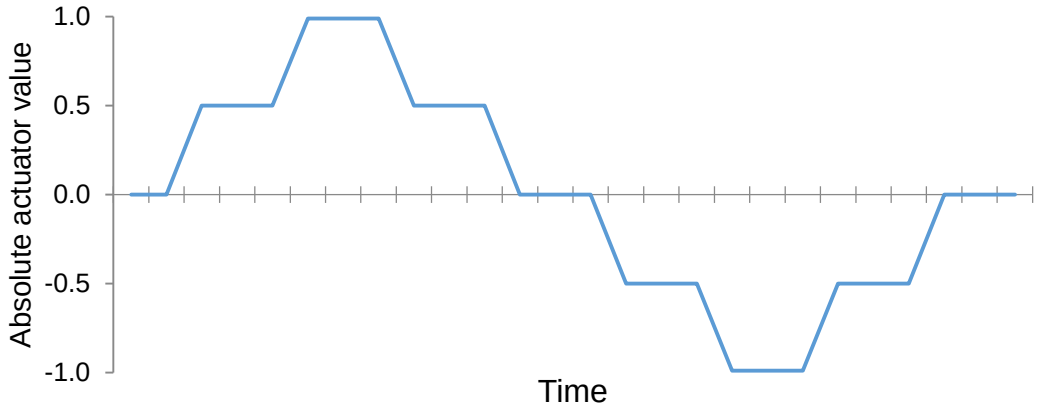

Figure 5.12 More complex SID with additional steps

5.5.2 Data acquisition and processing stages

To observe the effects on the data integrity when the same set of DoE test points are run in alternate orders the data were analysed using the following steps:

i. Collect data for 60 seconds at 40 steady-state DoE test points with IVO, EVC, SOI and FRP settings using the test method in Appendix A14, repeat 3 times:

a. Initial run in order dictated by DoE algorithm (pseudo-random)
b. Second run in sequence found from the boundary search SID, Figure 5.11
c. Third run in sequence found from the intermediate-step SID, Figure 5.12

ii. Extract raw data from each test point
    a. Calculate coefficient of variation and gradient (deviation) of data for each test point to use as data quality metrics

All test points were collected on the same day in one run to prevent anomalous data; this may be caused by changes in atmospheric conditions, instrument calibration or operator error.

5.6 Results

Forty test points were used to collect data. The test points were chosen as part of an engine mapping exercise and are the same as those in chapter 5.4. The sequence of the test points was changed to observe the effects of test point ordering on the results. The original order (DoE 1) was determined by a DoE in which the test points are ordered to give high movement between test points. Results from two more orders of test points (DoE 2 and DoE 3) are presented. The order of these additional test point runs was determined the results of the system identification tests outlined in Figure 5.11 and Figure 5.12. The results of the system identification tests were then used to optimise the test point order with respect to particulate number emissions. A detailed example of the test point ordering method is provided in chapter 6.

Results are presented with respect to DoE 1. Changes in PN emissions compared to the original ordering are shown in Figure 5.13. This shows how

PN can be significantly different even when the test conditions are assumedly the same.

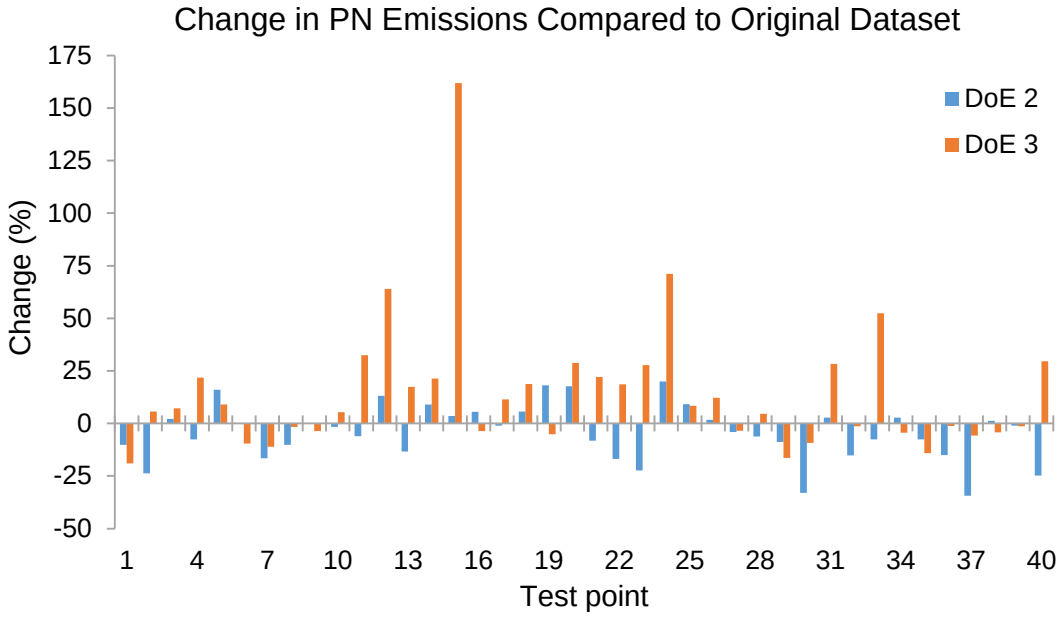

Figure 5.13 Influence on PN emissions when test points were ordered differently

The mean values of each engine response changed depending on the order of test points. Figure 5.14 shows the difference in response as a factor of DoE 1. The most significant difference observed was with PN when DoE 3 was run. It appears as though most of the engine responses would not have changed much on average.

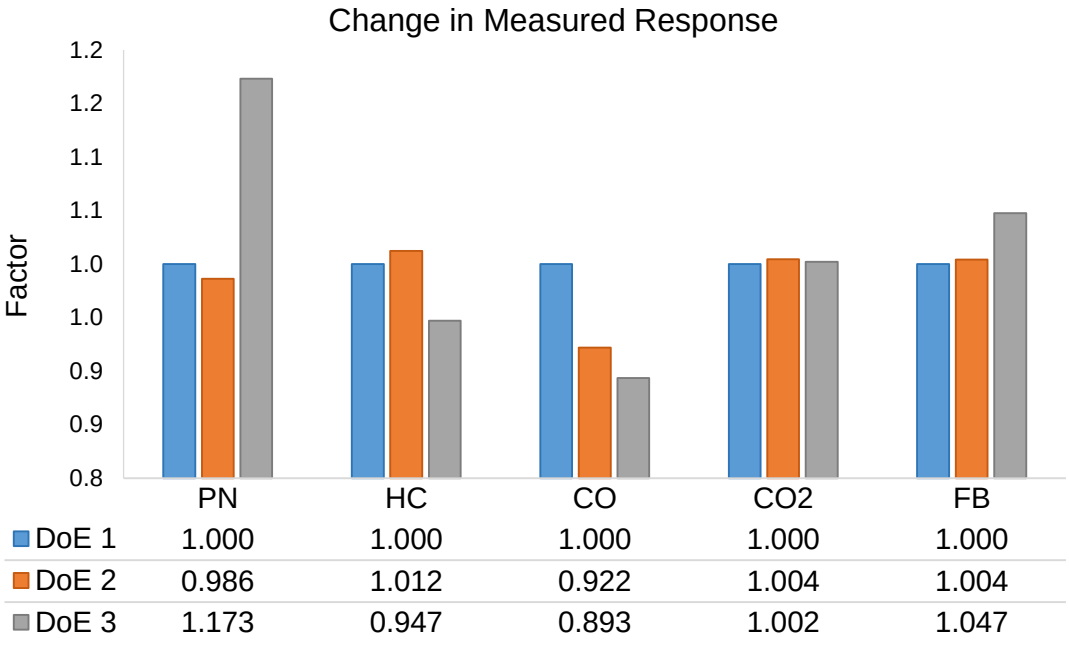

Figure 5.14 Difference in mean value between tests duration

The coefficient of variation was calculated for the samples recorded during each test point. The average CoV for the original test, DoE 1, is presented in Figure 5.15. This is calculated from the standard deviation of data divided by the mean value, which provides a metric of variation that is normalised to allow comparisons between parameters with different ranges.

Measuring data using the original ordering of test points provides a baseline as to how varied the data tend to be. PN emissions are the least stable, which corroborates with literature findings [42], [77].

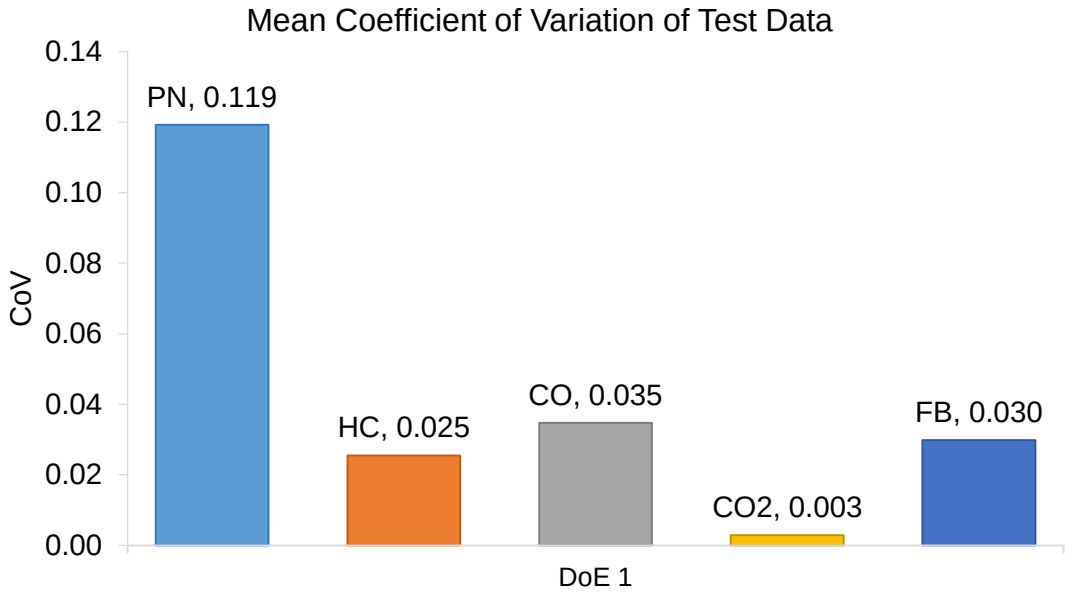

Figure 5.15 Coefficient of variation of data collected during original DoE test

The percent change compared to the original DoE is presented in Figure 5.16. When the test points were ordered using the simple SID, i.e. DoE 2, the average CoV of PN reduced by 19.4%. The average CoV increased by 14.1% when the more complex SID was used, DoE 3. The change in average CoV could indicate that PN emissions were more or less noisy, or that the rate of change had altered.

Changing the order of the test points had an effect on the other emissions and fuel consumption. The most affected was HC emissions with a 57.4% increase in CoV for DoE 3. However the initial CoV was relatively small, Figure 5.15, and so it may not be detrimental to the results.

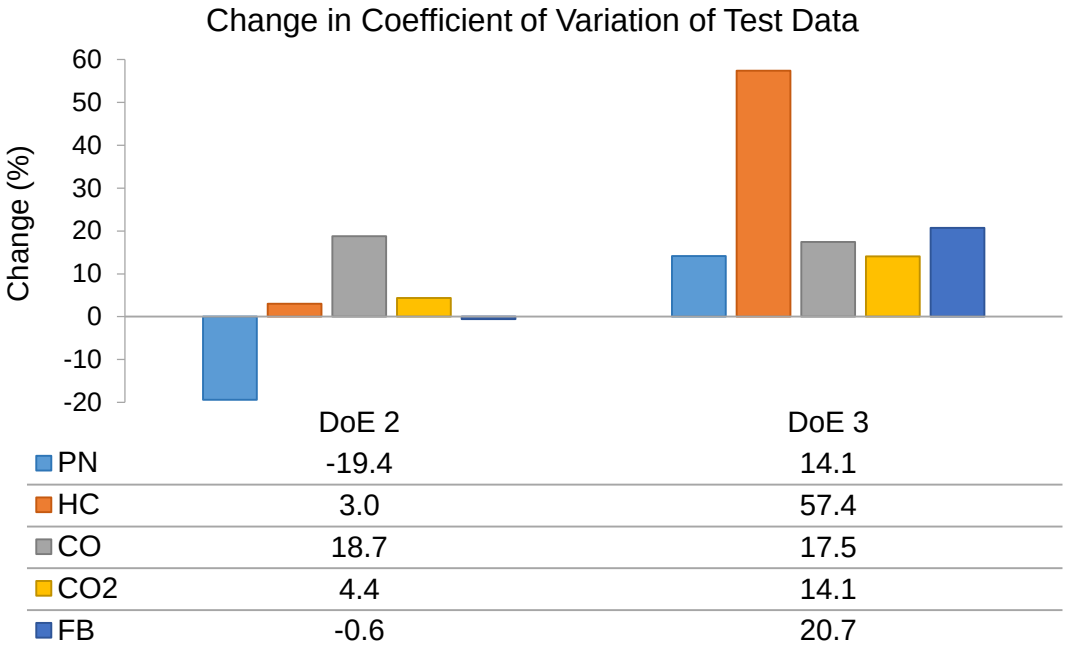

Figure 5.16 Percent difference in CoV over forty test points compared to original DoE

The main aim of sequencing test points was to reduce the test-to-test carry-over effects. An indication of test-to-test carry-over is a gradient in the data which suggests the response is not yet stable. A linear polynomial was fitted to the test point data and the average gradient for each response during each DoE was calculated. The results for the original DoE are presented in Figure 5.17. The trend is similar for the CoV in Figure 5.15 since both metrics will increase in direct proportion as the data deviates from the mean.

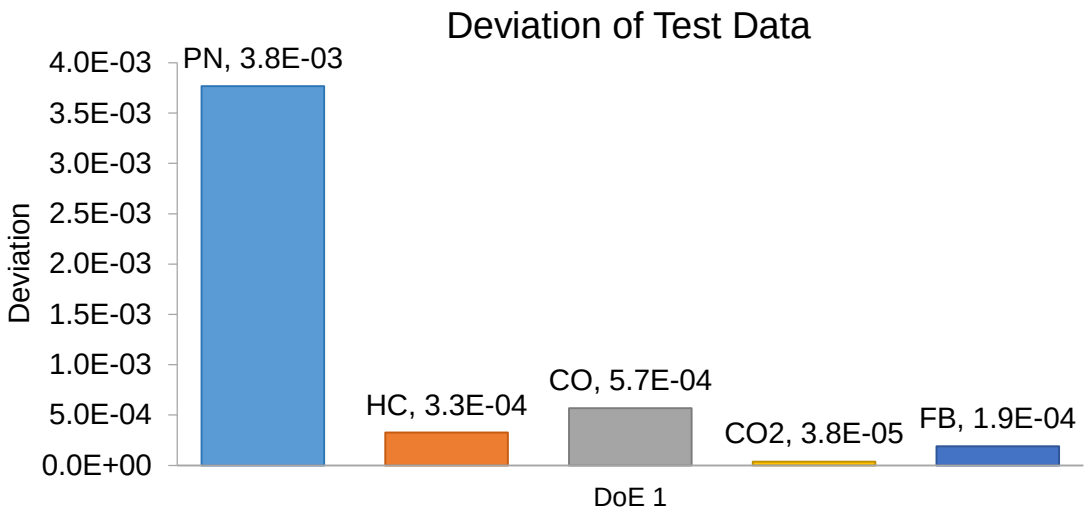

Figure 5.17 Average deviation in test data for the original DoE (values normalised using dataset mean)

In order to present the results for the different ranges side-by-side the values were normalised and are shown in Figure 5.18.

A reduction of 31.9% in PN deviation was observed when the test points were ordered according to the basic SID. The more complex SID reduced the deviation by 0.7%.

The deviation of the other responses were affected by running in different orders. HC emissions were more stable during DoE 2 testing with an average reduction of 10.9%. However an increase of 55.1% was observed during DoE 3.

An increase in deviation was observed for all of the other responses.

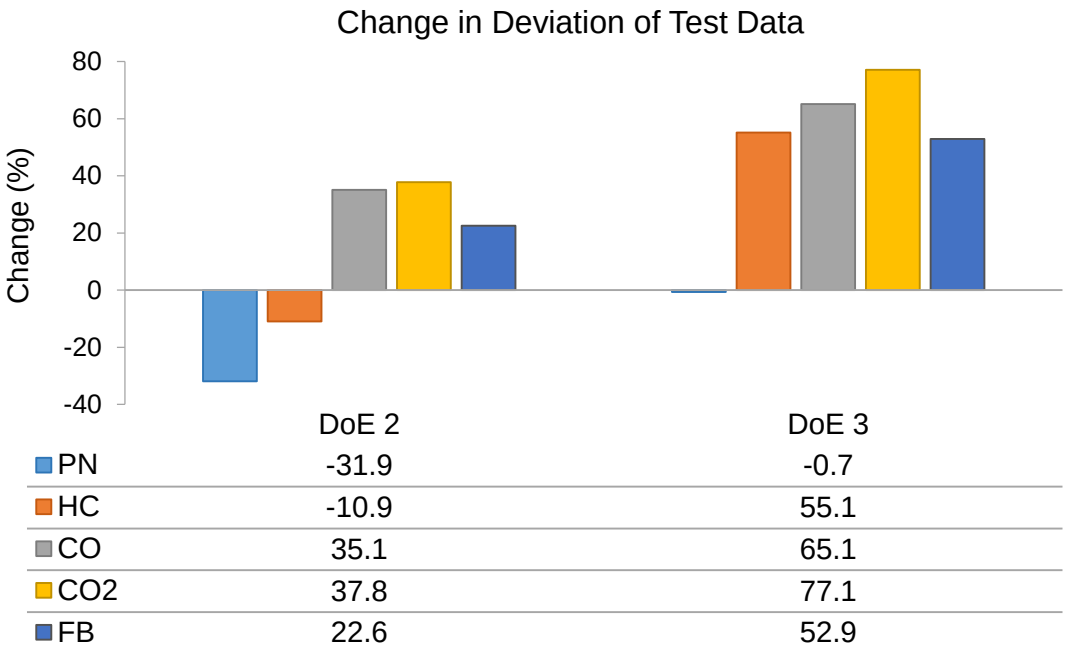

Figure 5.18 Average deviation of data from 40 DoE test points normalised using mean value of data set. Labels indicate improvement in deviation compared to DoE 1

5.7 Summary

This chapter used the methodological improvements discovered from the experiments in Section 3 to repeat a set of engine test points. The improved methodology should allow comparisons between methodologies without interference from poor data quality.

A number of investigations were performed on a set of DoE data in sections 5.2 and 5.4 that revealed significant errors in the data exist which are detrimental to an EMC. The first analysis was performed on a set of DoE test points to find whether the distribution of error is Gaussian. Figure 5.2 shows most variables were decreasing during the test points.

i. PN had the most significant bias with approximately -9.5% at Node 1, i.e. on average PN decreased by 9.5% over the Node 1 test

points. There was an average bias of 0% at Node 5, which was the highest power operating condition.

ii. CO_2 emission measurements were biased by less than 1% at each node.

iii. NOx emissions were more greatly influenced at Node 1 with a mean deviation of -5.79%.

A second analysis revealed that the data varied significantly during measurement as shown in Figure 5.3.

i. PN measurements varied by approximately 41% at Node 1. A significant deviation was observed for Node 2 at 13%.

ii. CO emissions varied by approximately 10% at Node 1 and 6% at Nodes 1 and 2.

iii. NOx emissions varied by approximately 10% at Nodes 1 and 3.

A third analysis was performed to correlate the changes in actuator values with the subsequent deviations in measured data. A number of significant correlations were identified in the data and are shown in Table 5.6.

i. This suggests that changing the engine actuators has an effect on the stability of engine responses that influences measurements.

Forty steady-state test points were ordered by each actuator and retested. Analysis was performed on data of the measured responses. The percent difference was calculated for each test point. The average, maximum and minimum differences in values are presented in Figure 5.4.

i. PN emissions were up to 71.7% different when the test points were ordered in a different manner. This difference was observed when the measured value for the SA-ordered test was significantly lower than the other test orders.

ii. CO emissions were also influenced by the ordering of test points. The maximum difference was 44.1%. This was observed at a test point that was substantially lower than the other orders.
iii. CO_2 emissions were not influenced greatly with a maximum difference of 5.4% and an average deviation of 2.3%. However the measured values for the IVO-ordered DoE were consistently higher than for the other test orders; this may indicate an instrument calibration error.
iv. A maximum deviation of 21.6% was observed for HC emissions however this was at a test point that generated high HC emissions.
v. An analysis on the correlations between engine actuators and measured responses indicated the Student's t-score varied when the test points were ordered in different ways, Figure 5.5.
vi. Further analysis on a response-by-response basis was carried out. The results indicate that ordering the test points in different manners can achieve varying levels of correlation between the engine actuators and measured responses. This suggests it may be possible to reduce the instability of the engine responses by sequencing the test points in a way to manage the test-to-test carry-over.

A possible approach to sequence test points was presented. The approach relied on minimal *a priori* knowledge. The benefits of this are two-fold: Less effort required by the facility and improved quality of findings since the time between preliminary testing and data acquisition is minimal. Intelligently sequencing test points relying on data measured from a system at a different time may generate data that are not representative of the system at the current state. The time between collecting the initial sequencing data, the subsequent analysis and the final testing should be minimised.

A system identification test was used to determine which correlations were most significant for a chosen response. The test points could then be sequenced such that the engine actuator was changed minimally between test points in order to reduce the test-to-test carry-over effects.

Two relatively simple system identification routines were used, schematics of which are shown in Figure 5.11 and Figure 5.12. The test points were then sequenced using the system identification data to improve PN data quality. Comparisons between the quality of data collected using the original test point order and the two sequenced orders were then presented.

i. The shorter system ID generated improved data quality from PN emissions in terms of 19.4% improved CoV and 31.4% improved deviation, Figure 5.16 and Figure 5.18 respectively.
ii. The deviation observed in HC emissions measurements was also improved when testing using the sequence dictated by the shorter system ID. PN and HC emissions are formed from similar processes, i.e. poor mixture preparation. HC hang-up also operates on similar principles as deposition of particulate matter.
iii. The more complex system ID may not generate responses that are substantially large for the processing steps used. The fewer steps generate more a more severe response in the system that may produce more reliable correlations to order the test points.

Chapter 6

Test Point Sequencing Software Tool

A software tool was developed to allow the findings in this methodology to be readily applied in future experiments. The tool provides an additional benefit of reducing human error that can occur throughout the numerous processing stages.

The software code was written in MATLAB and the interface using the Open GUI Layout Editor (GUIDE). The code was adapted from the processing steps used within this thesis.

6.1 Function

The tool was designed for use in an EMC process but could potentially be applied in any situation where steady-state data are being recorded from a nonlinear system. The functions of the software are as follows:

i. Calculates correlation coefficients then forms a correlation metric between the chosen engine responses and the control actuators
ii. The test file should include data that were recorded during the step-change system ID test
iii. Sequence a series of test points to minimise test-to-test carry over effects that were identified during the correlation analysis
iv. These should be at one steady-state operating condition

6.2 Tool use notes

This section describes the steps used for ordering test points with a worked example. Measurements of particulate number emissions are used to

demonstrate the process. The coding for this process is available at the URL in reference [161] and the relevant sections are referred to in this section.

i. Carry out boundary search as described in Section 5.5.1

ii. Note the start and end of each section in the data (“Step” and “Settle” times). These must then be inputted to the relevant cells on the MATLAB GUI, 1a and 1b in Figure 6.1.

iii. The order with which each of the control actuators are moved during the system ID is critical as this will affect the correlation results. The order used in this example is shown in row *2* of Table 6.1 – IVO; EVC; SA; FRP; SOI. The graphical user interface only shows three control actuators (IVO, EVC, SOI and FRP) but the process remains the same.

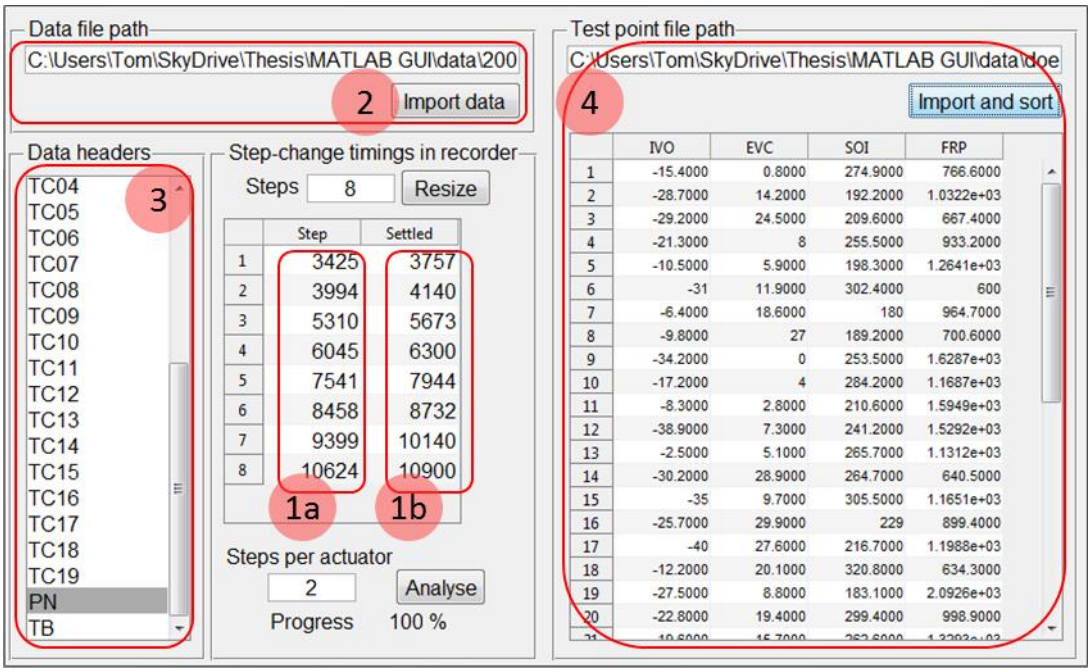

Figure 6.1 Test point sequencer graphical user interface

iv. Import the test data from comma separated test file (2). The relevant section of MATLAB code for this can be found under *Import test data* in the html file at the following reference [161] and the processing which takes place is described here:

v. The column headers will then be listed, Figure 6.1 (3). From these the user can select which responses the test points should be

ordered to minimise the response time of. PN is shown to be selected.

vi. The data are then analysed for the gradient of data and the settling time. The “Step” and “Settled” values are used to book-end the periods of data that are analysed. The gradient is found using a fitted linear polynomial, example results are shown in cells *B3* to *F6* in Table 6.1. An exponential equation is fitted and solved for when the gradient equals zero, at which point the data are settled; example results are shown in cells *B13* to *F16* in Table 6.1. The coding for this is shown in the section headed *Analyse data for gradients and settling periods* [161].

vii. The absolute values for each column of data for the gradient section of Table 6.1 are summed (row *7*) and normalised (corrected) with the median of each across the test (row *9*). This allows multiple engine responses to be used with equal weight regardless of measurement range.

viii. The sum of each column of the exponential solutions, row *17* Table 6.1, is multiplied by the corrected sums of the linear gradients. This generates a metric (row *18* Table 6.1) which is then normalised between zero and the maximum value (row *19* Table 6.1).

ix. The metrics which are shown here indicate that FRP was the most strongly influential engine parameter with regards to PN, whereas IVO was the least influential.

Table 6.1 Example table to illustrate calculation of sorting metrics for particulate number results

	A	*B*	*C*	*D*	*E*	*F*
1	Linear Gradient					
2		IVO	EVC	SA	FRP	SOI
3	1	-348.27	-130.60	-366.81	-464.75	87.96
4	2	79.62	72.66	-258.65	48.40	205.17
5	3	-136.44	-9.42	-112.35	3895.48	1497.71
6	4	48.66	-388.53	-4.98	-606.44	-342.19
7	Sum	-356.44	-455.89	-742.79	2872.69	1448.65
8	Magnitude	612.98	601.21	742.79	5015.08	2133.02
9	Corrected	3.70E-04	3.63E-04	4.48E-04	3.03E-03	1.29E-03
10						
11	Exponential Solutions					
12		IVO	EVC	SA	FRP	SOI
13	1	135.13	235.49	210.10	359.18	60.01
14	2	177.16	215.63	512.25	641.71	392.22
15	3	55.34	81.02	241.48	125.64	70.75
16	4	255.34	389.30	68.42	84.88	45.70
17	Sum (s)	622.98	921.44	1032.24	1211.42	568.67
18	Metric	0.23	0.33	0.46	3.66	0.73
19	Normalised Metric	0.06	0.09	0.13	1.00	0.20

x. The DoE test point .csv file is then imported and sorted, Figure 6.1 (4). The steps for this process are explained using eight test points in Table 6.2 to Table 6.5. The coding for this is under the section titled *Import and sort DoE Test Points* in the html file at the reference [161]

xi. Firstly the data are imported using a similar process as for the test data file. The test points are stored in an array which resembles Table 6.2.

xii. Each column of test points is normalised between the minimum and maximum actuator setting, generating columns which range from zero to one, Table 6.3.

xiii. Each value is then multiplied by the relevant normalised metric, which was calculated above. The rows of each products are summed. This step is shown in Table 6.4.

xiv. The ‘summed’ column is then used to sort the test points, from minimum sum value to maximum. The original actuator values are returned and the new array, along with the original test point number, is shown in Table 6.5.

Table 6.2 Example test points

Test #	IVO	EVC	SA	FRP	SOI
1	10.2	12.4	36.8	13.8	327.7
2	2.3	17.5	42.0	10.3	333.5
3	-2.4	38.1	66.8	10.2	289.4
4	35.7	11.3	34.5	8.3	320.3
5	12.4	-3.9	33.8	9.0	307.1
6	11.2	42.9	58.5	11.8	312.9
7	-6.9	2.0	37.5	10.5	302.6
8	-1.2	20.4	45.0	9.8	261.5

Table 6.3 Test point values normalised between zero and one

Test #	IVO	EVC	SA	FRP	SOI
1	0.40	0.35	0.09	1.00	0.92
2	0.22	0.46	0.25	0.38	1.00
3	0.11	0.90	1.00	0.35	0.39
4	1.00	0.32	0.02	0.00	0.82
5	0.45	0.00	0.00	0.13	0.63
6	0.43	1.00	0.75	0.65	0.71
7	0.00	0.13	0.11	0.40	0.57
8	0.14	0.52	0.34	0.28	0.00

Table 6.4 Product of normalised test points and Normalised Metric from

Test #	IVO	EVC	SA	FRP	SOI	Sum
1	0.025	0.032	0.011	1.000	0.183	1.252
2	0.014	0.042	0.032	0.375	0.200	0.662
3	0.007	0.082	0.126	0.352	0.077	0.643
4	0.063	0.030	0.003	0.000	0.163	0.258
5	0.028	0.000	0.000	0.126	0.126	0.280
6	0.027	0.091	0.095	0.650	0.143	1.005
7	0.000	0.011	0.014	0.401	0.114	0.541
8	0.009	0.047	0.043	0.275	0.000	0.374

Table 6.5 Sorted test points

Sum	Original Test #	IVO	EVC	SA	FRP	SOI
0.258	4	35.7	11.3	34.5	8.3	320.3
0.280	5	12.4	-3.9	33.8	9.0	307.1
0.374	8	-1.2	20.4	45.0	9.8	261.5
0.541	7	-6.9	2.0	37.5	10.5	302.6
0.643	3	-2.4	38.1	66.8	10.2	289.4
0.662	2	2.3	17.5	42.0	10.3	333.5
1.005	6	11.2	42.9	58.5	11.8	312.9
1.252	1	10.2	12.4	36.8	13.8	327.7

6.3 Tool use comments

The step-change system ID test should be similar to those described in Section 5.5.1. The algorithms are most effective when the step-changes induce a large change in the responses. To ensure this the actuators should be fixed at the mid-point of their operational range until being controlled.

Chapter 7

Conclusions

Developments in automotive engine design allow ever-increasing performance targets to be met. Testing and analytical methods should be updated in unison with engine development to fully exploit the available performance.

Modern statistical techniques and improved equipment capabilities provide opportunity to make better use of current hardware. EMC is employed as a holistic approach to tackle calibration tasks using methods relevant to current engine technology.

Advanced modelling techniques are applied to properly represent the nonlinearities of engine performance. Vast amounts of test data are used to ensure the models adequately represent the physical system before optimisation is carried out offline. Experiments are designed using various model based statistical methods, all which fall under the label design of experiments (DoE). This type of experimental planning aims to reduce the number of test points required by maximising the usefulness of data.

Several oversights were identified in the planning and testing phase of steady-state DoE experiments: improper engine preparation, preconditioning and test point ordering. These all attribute to reductions in data quality which may lead to additional test data being required.

Improper engine preparation, i.e. poor steady-state identification, can cause significant measurement variation. Action can be taken by using thermocouples, which are readily available and an ideal instrument for this challenge. They can be used to monitor the temperatures that are most relevant to the measured variables.

Preconditioning was identified by a number of studies as a method to improve PN measurement data quality. It can be used to cleanse the system of unwanted residual components. The effects can be short-lived but this can prevent anomalous measurements caused by the random re-entrainment of matter.

Steady-state test point ordering is not discussed in literature but test-to-test carry over is known to influence measurements when changing operating conditions, i.e. preconditioning. Particulate emissions are highly susceptible to instabilities during steady-state operation and increasing the repeatability of these measurements will assist engine calibration.

A sequence of experiments were carried out to determine how to measure high quality steady-state data. Initially the stability of an engine following a change in speed and load was observed by measuring engine fluid temperatures. Results from these experiments are presented in Section 4.5. The monitored parameters were affected for up to 10 minutes following the disturbances. Larger operating condition changes are expected to result in increased settling times.

The engine fluid temperatures did not respond in the same fashion. Oil temperature was measured from the sump and gallery whilst coolant was measured from the engine outlet. The characteristic overshoot associated with control systems was observed in the coolant temperature and engine gallery oil temperature.

Compared to engine sump oil the engine gallery oil temperature more closely matched that of engine coolant. The engine oil temperature was regulated via an internal heat exchanger between the oil and coolant. Engine sump oil temperature measurements were more damped but there was more noise. This is thought to be due to the turbulent nature of the oil pan as oil is returning from numerous engine components that are operating under different temperatures.

Monitoring temperatures that are in control by external sources, such as engine coolant, will always depend on the response characteristics of the PID controller. It is essential that the PID controller is suitably setup although there is still chance of a longer settling time being caused by a premature response to a temperature spike. This was observed due to the test bed controller increasing engine load before reducing engine speed. This caused the coolant temperature to increase slightly before it dropped.

The following test results are from Section 4.6. Different engine temperatures were used to indicate steady-state operation at a repeat test point in these tests. Engine responses that are typically used in an EMC were recorded and the repeatability discussed. The most stable engine fluid temperatures

discussed previously, engine sump oil and engine coolant, plus exhaust plenum skin were used to indicate when the engine had achieved steady-state operation at a baseline operating condition. This test was carried out in the morning prior to any other running. All engine operating conditions were maintained between tests including the actuator values, which were set using ECU calibration software.

It was evident that exhaust plenum skin temperature was the most appropriate variable to use to identify steady-state. PN emissions, fuel consumption, CO and CO_2 emissions were all more repeatable.

NOx emissions measurements were more repeatable when oil sump temperature was used to identify steady-state. HC emissions measurements were more repeatable when coolant was used as the steady-state indicator.

A sequence of test points that spanned five operating conditions were repeated in Section 4.7. The test points used either exhaust plenum skin temperature or engine coolant temperature as steady-state indicators when changing speed and load. PN measurements were the most varied between steady-state indicators. An average difference of 150% was observed between the values of PN emissions at Node 1, the lowest operating condition. This dropped to 69.5% at Node 2, 20.1% at Node 3, 13.0% at Node 4 and 2.7% at Node 5. The variation in PN measurements during the test points was improved by 5.6% when using exhaust plenum as the steady-state indicator at 0.47 from 0.50.

Fuel consumption changed by less than 1.6% between indicators across all operating conditions. The CoV was significantly improved from 0.26 to 0.03 when using exhaust plenum as the steady-state indicator.

CO emissions measurements were most influenced at Nodes 2 and 4 with mean differences of 12.2% and 15.2% respectively. The CoV was similar for the indicators at 0.11 for engine coolant and 0.10 for exhaust plenum.

HC emissions changed by 11.4% at Node 4 dependent on the steady-state indicator. A 24.1% improvement in the CoV, from 0.09 to 0.07, was also observed when exhaust plenum was used, although both these values indicate good data quality.

NOx emissions changed by 16.0% at Node 1 depending on steady-state indicator. A 9.4% change was observed at the Node 2 test points, 2.7% at Node 3, 6.8% at Node 4 and 2.1% at Node 5. The CoV was good during both tests at 0.06 and 0.04 for coolant and plenum respectively.

The fourth test presented in Section 4.8 observed the influence on baseline emissions measurements when different types of preconditioning occurred the prior day. The preconditioning operating conditions spanned a range of speeds and loads designed to put the exhaust system under varying degrees of temperature and flow rate.

Higher powered preconditioning events caused lower PN, CO and HC emissions measurements. Fuel consumption and CO_2 emissions were not significantly affected by preconditioning. It is thought the higher temperature

exhaust gas reduces the mass of residual build up on the internal surfaces. These are more prominent in the exhaust system as there is a greater surface area and as the PN sample point is farther downstream than the other gaseous emissions this would influence PN emissions more distinctly. The sample line to the emissions analyser is a fairly long (>5m) PTFE tube which is susceptible to hydrocarbon hang-up, which is a similar process, although the temperatures are much lower compared to in the exhaust stream.

Section 4.9 presented results from the fifth test, which aimed to quickly identify the optimal steady-state indicator. An experiment was designed that contained a number of steady-state speeds and load operating conditions to cover the safe operating region of the engine. The operating conditions were approached using step-changes and engine responses were measured. Correlations between the engine-mounted sensors and responses indicated which engine sensor was best suited to obtain repeatable response measurements. Two thermocouples were identified as having the highest correlation to the chosen engine response (PN). These were then used as steady-state indicators for the experimentation in Section 5.5.

An improved method of preparing an engine for measuring emissions during steady-state testing was presented in Section 3. An investigation on the order tests points are carried out was then performed.

Analysis on a set of DoE data in Section 5.2 revealed the data were decreasing during most of the test points. This causes the bias to be negative, which is against an assumption made by Gaussian-based engine models.

PN emissions were dropping by almost 10% on average during steady-state testing at low power conditions. This means that models from PN data would predict values that are higher than the physical system. The deviation of PN measurements at Node 1 was approximately 40%. This may translate to a similar error when modelling or it could cause the model to be a poor representation of the physical trends. Node 2 PN measurements were falling by over 5% and the average deviation was 13%.

The majority of CO, NOx and HC emissions measurements were negatively biased. CO and NOx emissions deviated by approximately 10% at Node 3. NOx emissions also deviated by 10% at Node 1.

The findings suggest that the engine responses are not stable during measurements. The deviations observed were during the sixty second testing duration and it is plausible that a greater change would have been observed had the test points lasted longer.

Correlations between the deviations observed and the movements of actuator settings were calculated in Section 5.3. Using Student's t-test it was proven that there are a substantial number of correlations.

Forty test points from Node 4 were repeated in various orders and the differences in measurements were presented in Section 5.4. The orders were based on the actuator values such that the actuator would be at its lowest value in test point one and highest at test point forty. The test points were repeated once per actuator plus one more time in the original order.

The measured engine responses changed significantly depending on the order. An average difference of over 30% between test points was observed in PN emissions. The mean differences in CO emissions was 17.7%, CO_2 was 2.3% and HC was 5.4%.

The correlation coefficients also varied depending on the order of test points, which may be caused by preconditioning.

The optimum sequence of test points was not determined by ordering the test points by any one of the actuators. A correlation test was used in Section 5.5 and the results used to sequence the test points.

Two relatively basic correlation tests were compared. They were devised with step-changes to cause a large difference in the system responses that could be measured with high confidence. A correlation analysis was carried out on the two sets of data. This determined which actuator values influenced the engine responses most. Using this information the test points were ordered based on the lowest predicted measurement variation in PN.

Out of both tests the larger step changes produced the better results. They were compared by calculating the deviation of PN data over the test points, which was over 30% improved compared to the original ordering of test points. The deviation of PN measurements improved by less than 1% when sequenced using the more complex step-change correlation experiment.

The findings of this thesis were compiled in a software program. The use of the software, including how it operates, is explained using a worked example

in Section 6. The program sequences test points based on data acquired from a step-change system identification test. This reduces possible human error, which may be significant as there are multiple stages in the processing prior to sequencing the test points. It also allows the findings to be applied to any nonlinear system as test-to-test carry over can be found in any system with complex responses.

7.1 Further Work

The data collected for the final comparison used test points which were one minute long. Although this may be a typical length for a test point it could generate some anomalies since the data are relatively noisy. Re-collecting the data using longer test points could offer some stronger results.

The data were collected at one operating condition. It may offer some more information to run the test points at additional operating conditions.

The DoE test point sequence were optimised for one engine response, which was PN data. It is possible to sequence the test points for optimal data from multiple responses although this may hinder the integrity of each as a compromise will have to be made.

The test point sequencing software could distinguish between increasing and decreasing values during step-change system ID for test point sequencing. This should improve the test order as an additional dynamic is incorporated.

7.1.1 Combined steady-state identifier and test point sequencing

A short test routine was devised that indicates the optimal engine parameter to be used for indicating steady-state operation (Section 4.9). Another routine was devised that was used for sequencing a sample of steady-state test points (Section 5.5.1). For the case of an EMC these two tests could be combined. Such a test may use stepped steady-state power conditions up to WOT at the rated speed, Figure 7.1.

The steady-state operating conditions be the same as those that will be used for the engine mapping tests as it is not possible to model the system response at a different speed-load combination than that at which data are measured.

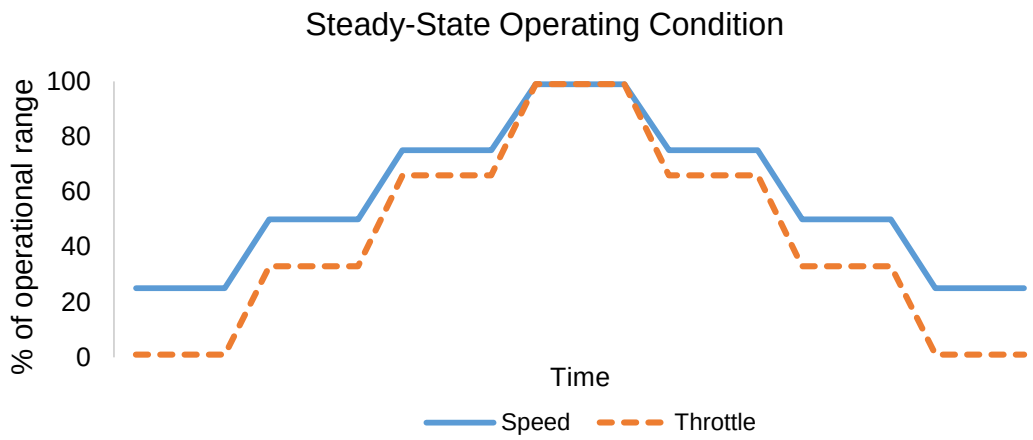

Figure 7.1 Speed and throttle operating conditions

Each of the flat sections in the figure above represent an arbitrary duration whereby the key monitored parameters are allowed to stabilise. Once the parameters of interest have stabilised the test routine outlined in Figure 7.2 can be carried out.

The routine would commence with all actuator values at the mid-point of their ranges (0.5 on the scale). One actuator would undergo a step-change to the maximum and the system allowed to settle. Once returned to a steady-state operating condition the first actuator would be moved back to the start value and the system allowed to settle once more. The same process would occur with the first actuator moving to the lowest value, the system settling, then returning to the start point. The same process would repeat for each actuator as illustrated in the figure below.

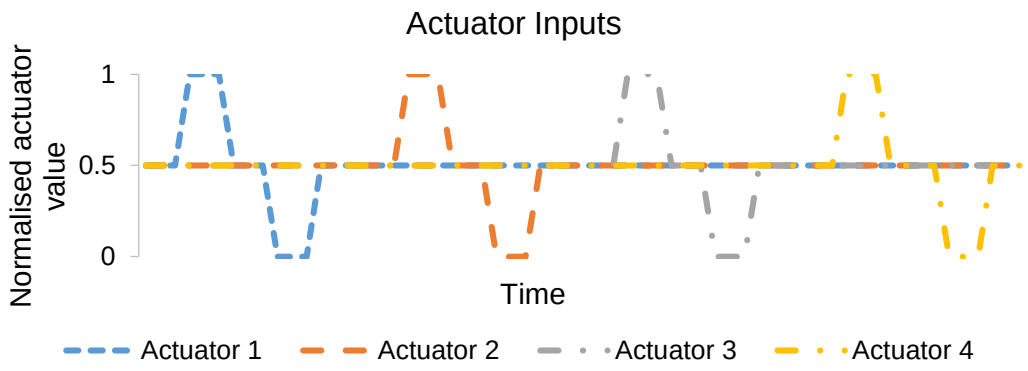

Figure 7.2 Example of how control inputs can be modulated during system ID

The system responses may undergo a change that reflects the step-change in actuator value, such as shown in Figure 7.3. The measured responses of greatest importance, such as those being used to generate mathematical models of the system, should be allowed to stabilise before a further disturbance to the system is made. This is to allow proper analysis of the data and prevent any test-to-test carry over from occurring and skewing the results, which is the phenomena that is attempted to be avoided by this process.

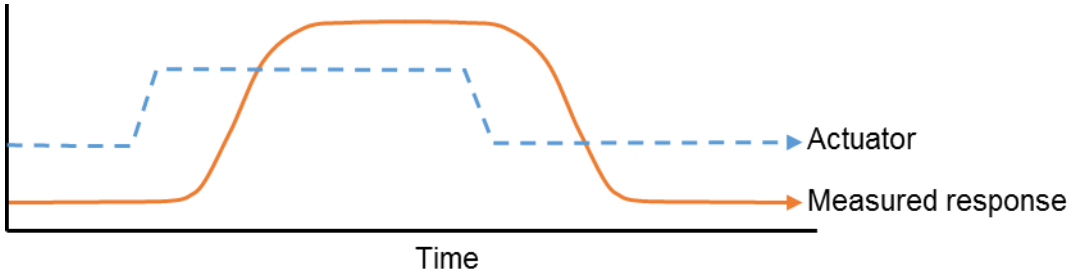

Figure 7.3 Example engine response following a step up and down

Following the tests and measurement of data outlined in Figure 7.1 to Figure 7.3 it would be possible to sequence test points in the optimal fashion for minimised test-to-test carry over. The appropriate steady-state indicator for the operating conditions can also be identified from each step-change in operating condition. These two factors have been shown to increase repeatability of data, improving data quality and confidence in the conclusions drawn.

References

[1] J. B. Heywood, *Internal Combustion Engine Fundamentals*. McGraw-Hill, 1988.

[2] Europa, “Summaries of EU Legislation,” 2012. [Online]. Available: http://europa.eu/legislation_summaries/environment/air_pollution/l28186_en.htm.

[3] AVL, “AVL Expo.” 2014.

[4] P. Price, R. Stone, T. Collier, and M. Davies, “Particulate Matter and Hydrocarbon Emissions Measurements : Comparing First and Second Generation DISI with PFI in Single Cylinder Optical Engines,” no. 724, 2006.

[5] D. Mehta, T. Alger, M. Hall, R. Matthews, and H. Ng, “Particulate Characterization of a DISI Research Engine using a Nephelometer and In-Cylinder Visualization,” *Exp. SI Engine Combust. Perform.*, no. 724, 2001.

[6] A. Teraji, T. Tsuda, T. Noda, M. Kubo, and T. Itoh, “Development of a Novel Flame Propagation Model (UCFM : Universal Coherent Flamelet Model) for SI Engines and Its Application to Knocking Prediction,” vol. 2005, no. 724, 2005.

[7] D. Martin, P. Pischke, and R. Kneer, “Investigation of the influence of multiple gasoline direct injections on macroscopic spray quantities at different boundary conditions by means of visualization techniques,” *Int. J. Engine Res.*, vol. 11, no. 6, pp. 439–454, Dec. 2010.

[8] J. Sacks, W. J. Welch, T. J. Mitchell, and H. P. Wynn, “Design and Analysis of Computer Experiments,” *Stat. Sci.*, vol. 4, no. 4, pp. 409–423, Nov. 1989.

[9] S. J. Bates, J. Sienz, and D. S. Langley, “Formulation of the Audze–Eglais Uniform Latin Hypercube design of experiments,” *Adv. Eng. Softw.*, vol. 34, no. 8, pp. 493–506, 2003.

[10] M. Liefvendahl and R. Stocki, “A study on algorithms for optimization of Latin hypercubes,” *J. Stat. Plan. Inference*, vol. 136, no. 9, pp. 3231–3247, 2006.

[11] T. Z. Vassili Toropov Uwe, Uwe Schramm, Atul Sahai, Royston D. Jones, “Design Optimization and Stochastic Analysis based on the Moving Least Squares Method,” 2005.

[12] E. R. van Dam, B. Husslage, D. den Hertog, and H. Melissen, “Maximin Latin Hypercube Designs in Two Dimensions,” *Oper. Res.*, vol. 55, no. 1, pp. 158–169, Feb. 2007.

[13] Air Resources Board, “Key Events in the History of Air Quality in California,” 2014. [Online]. Available: http://www.arb.ca.gov/html/brochure/history.htm. [Accessed: 09-Jul-2014].

[14] ECOpoint Inc., “Cars and Light-Duty Truck Emissions - US,” 2007. [Online]. Available: https://www.dieselnet.com/standards/us/ld.php.

[15] Delphi, “Worldwide Emissions Standards Passenger Cars and Light Duty Vehicles,” 2012.

[16] European Comission, “Reducing CO2 emissions from passenger cars,” 2014. [Online]. Available: http://ec.europa.eu/clima/policies/transport/vehicles/cars/index_en.htm.

[17] A. J. Martyr and M. A. Plint, *Engine Testing: Theory and Practice*, 3rd ed. 2007.

[18] ECOpoint Inc., “Cars and Light Trucks Emission Standards - China,” 2014. [Online]. Available: https://www.dieselnet.com/standards/cn/ld.php.

[19] Cummins, “On-Highway Emissions,” pp. 2012–2013, 2016.

[20] Delphi, “Worldwide Emissions Standards,” pp. 39–51, 2014.

[21] G. Hagen and U. Vaidya, “An approach for nonlinear model extraction from time-series data,” *2008 Am. Control Conf.*, vol. 0, no. 5, pp. 3875–3880, Jun. 2008.

[22] L. Ljung, “Approaches to Identification of Nonlinear Systems.”

[23] M. I. Soumelidis, R. K. Stobart, and R. A. Jackson, “A Nonlinear Dynamic Model for Three-Way Catalyst Control and Diagnosis,” *SAE Tech.*, no. 724, 2004.

[24] G. E. P. Box, “Science and Statistics,” *Am. Stat. Assoc.*, vol. 71, no. 356, pp. 791–799, 1976.

[25] T. Godward, H. Schilling, and S. Schaum, “Use of Dynamic Testing and Modeling in the Engine Calibration Process,” pp. 211–230.

[26] M. A. Dr. Mostrafa, “System Response,” 2010.

[27] C. Atkinson and G. Mott, “Dynamic Model-Based Calibration Optimization: An Introduction and Application to Diesel Engines,” 2005.

[28] Y. He and C. Lin, “Development and Validation of a Mean Value Engine Model for Integrated Engine and Control System Simulation,” *SAE Int.*, 2007.

[29] J. A. Cook and B. K. Powell, “Modeling of an internal combustion engine for control analysis,” *Control Syst. Mag. IEEE*, vol. 8, no. 4, pp. 20–26, 1988.

[30] P. Yoon, S. Park, and M. Sunwoo, “A Nonlinear Dynamic Model of SI Engines for Designing Controller,” 2000.

[31] P. Bowles and J. Batteh, “A Transient, Multi-Cylinder Engine Model Using Modelica,” *SAE Tech.*, 2003.

[32] W. Baumann, T. Dreher, K. Röpke, and S. Stelzer, “DoE for Series Production Calibration,” in *7th Conference on Design of Experiments (DoE) in Engine Development*, 2013, pp. 125–135.

[33] G. R. Vossoughi and S. Rezazadeh, “Optimization of the Calibration for an Internal Combustion Engine Management System Using Multi-Objective Genetic Algorithms,” *Evol. Comput. 2005. 2005 IEEE Congr.*, vol. 2, p. 8, 2005.

[34] AVL LIST GmbH, “AVL BOOST,” 2015. [Online]. Available: https://www.avl.com/boost.

[35] Gamma Technologies, “GT SUITE,” 2014. [Online]. Available: https://www.gtisoft.com/. [Accessed: 01-Jan-2015].

[36] J. Friebe, C. Schwarz, and T. Dao, “Model-based Design of Hybrid Electrical Vehicle Devices using Automated Optimization Strategies,” in *7th Conference on Design of Experiments (DoE) in Engine Development*, 2013, pp. 231–246.

[37] D. Münning, J. Piewek, A. Wagner, C. Felsch, M. Zillmer, C. Gühmann, and P. Eilts, “Application of a Hybrid Optimization Method in the Diesel Hybrid Drive Train Development Process,” in *7th Conference on Design of Experiments (DoE) in Engine Development*, 2013, pp. 269–288.

[38] M. R. Kianifar, F. Campean, and D. Richardson, “Sequential DoE Framework for Steady State Model Based Calibration,” *SAE Int. J. Engines*, vol. 6. SAE International, pp. 843–855, 2013.

[39] B. Giechaskiel, L. Ntziachristos, Z. Samaras, R. Casati, V. Scheer, and R. Vogt, “Effect of Speed and Speed-Transition on the Formation of Nucleation Mode Particles from a Light Duty Diesel Vehicle.” SAE International, 2007.

[40] M. Vojtisek-Lom, M. Pechout, J. Blažek, L. Moc, and T. Hlavenka, “Effects of Current and Prior Operating Conditions on Particulate Matter Emissions from a Diesel Engine Operated on Heated Rapeseed Oil.” SAE International, 2009.

[41] B. Giechaskiel, M. Carriero, G. Martini, and J. Andersson, “Heavy Duty Particle Measurement Programme (PMP): Exploratory Work for the

Definition of the Test Protocol," *SAE Int. J. Engines*, vol. 2, no. 1, pp. 1528–1546, 2009.

[42] P. Eastwood, *Particulate Emissions from Vehicles*. SAE International and John Wiley & Sons, Ltd., 2008.

[43] D. Gorissen, K. Crombecq, W. Hendrickx, and T. Dhaene, "Adaptive Distributed Metamodeling," in *High Performance Computing for Computational Science - VECPAR 2006*, Springer Berlin Heidelberg, 2007, pp. 579–588.

[44] A. J. Martyr and M. A. Plint, *Engine Testing: The Design, Building, Modification and Use of Powertrain Test Facilities*, 4th ed. Elsevier Ltd., 2012.

[45] D. Broome, "Induction Ram Part one: The inertia and wave effects of ram, and a summary of published work," *Automob. Eng.*, p. 4, 1969.

[46] D. Broome, "Induction Ram Part two: Inertial aspects of induction ram," *Automob. Eng.*, p. 5, 1969.

[47] D. Broome, "Induction Ram Part three: Wave phenomena and the design of ram intake systems," *Automob. Eng.*, p. 4, 1969.

[48] A. Chevalier, M. Müller, and E. Hendricks, "On the Validity of Mean Value Engine Models During Transient Operation," *SAE Tech.*, 2000.

[49] Y. G. Lee and J. T. Boehler, "Flame Kernel Development and its Effects on Engine Performance with Various Spark Plug Electrode Configurations," *SAE Tech.*, 2005.

[50] EPA, "Ambient Concentrations of Carbon Monoxide," 2010. [Online]. Available: http://cfpub.epa.gov/eroe/index.cfm?fuseaction=detail.viewInd&lv=list.listbyalpha&r=231329&subtop=341.

[51] Cambustion, "Gasoline Direct Injection (GDI) HC Emissions," 2011. [Online]. Available: http://www.cambustion.com/sites/default/files/instruments/HFR500/HFR07v01 GDI HC emissions.pdf.

[52] Q. Wei, D. B. Kittelson, and W. F. Watts, "Single-Stage Dilution Tunnel Performance," *SAE Tech.*, 2001.

[53] W. Piock, G. Hoffman, A. Berndorfer, P. Salemi, and B. Fusshoeller, "Strategies Towards Meeting Future Particulate Matter Emission Requirements in Homogeneous Gasoline Direct Injection Engines ," *SAE Int.*, no. September, 2011.

[54] B. R. Mili, A. Boréave, W. Y. Hernandez, M. N. Tsampas, N. Charbonnel, B. D. Anna, C. B. Lyon, and A. Einstein, "Ultrafine particulate matter emissions from a gasoline direct injection engine," vol. 1494, no. 2009, p. 5256, 2012.

[55] A. C. James, W. Stahlhofen, G. Rudolf, M. J. Egan, W. Nixon, P. Gehr, and J. K. Briant, “The Respiratory Tract Deposition Model Proposed by the ICRP Task Group,” *Radiat. Prot. Dosimetry*, vol. 38, no. 1–3, pp. 159–165, 1991.

[56] D. W. Dockery, C. A. Pope, X. Xu, J. D. Spengler, J. H. Ware, M. E. Fay, B. G. Ferris, and F. E. Speizer, “An Association between Air Pollution and Mortality in Six U.S. Cities,” *N. Engl. J. Med.*, vol. 329, no. 24, pp. 1753–1759, 1993.

[57] W. H. O. W. Group, “Health Aspects of Air Pollution with Particulate Matter , Ozone and Nitrogen Dioxide,” 2003.

[58] N. Matthias, C. Farron, D. Foster, M. Andrie, R. Krieger, P. Najt, K. Narayanaswamy, A. Solomon, and A. Zelenyuk, “Particulate Matter Sampling and Volatile Organic Compound Removal for Characterization of Spark Ignited Direct Injection Engine Emissions,” *SAE Int. J. Fuels Lubr.*, vol. 5. SAE International, pp. 399–409, 2011.

[59] D. B. Kittelson, “Measurement of Exhaust Particulate Matter,” pp. 1–36, 1999.

[60] J. Andersson, B. Giechaskiel, R. Muñoz-Bueno, R. Sandbach, and P. Dilara, “Particle Measurement Programme (PMP) Light-duty Inter-laboratory Correlation Exercise (ILCE_LD) Final Report,” Institute for Environment and Sustainability, 2007.

[61] F. Köpple, P. Jochmann, A. Kufferath, and M. Bargende, “Investigation of the Parameters Influencing the Spray-Wall Interaction in a GDI Engine - Prerequisite for the Prediction of Particulate Emissions by Numerical Simulation,” pp. 911–925, 2014.

[62] M. J. Kleeman, S. G. Riddle, M. A. Robert, and C. A. Jakober, “Lubricating oil and fuel contributions to particulate matter emissions from light-duty gasoline and heavy-duty diesel vehicles.,” *Environ. Sci. Technol.*, vol. 42, no. 1, pp. 235–42, Jan. 2008.

[63] J. Yanowitz, M. S. Graboski, L. B. A. Ryan, T. L. Alleman, and R. L. McCormick, “Chassis Dynamometer Study of Emissions from 21 In-Use Heavy-Duty Diesel Vehicles,” *Environ. Sci. Technol.*, vol. 33, no. 2, pp. 209–216, Jan. 1998.

[64] D. B. Kittelson, “Engines and nanoparticles: a review,” *J. Aerosol Sci.*, vol. 29, no. 5–6, pp. 575–588, 1998.

[65] K. Aikawa, T. Sakurai, and J. J. Jetter, “Development of a Predictive Model for Gasoline Vehicle Particulate Matter Emissions,” *SAE Tech.*, 2010.

[66] H. Wang and M. Frenklach, “A detailed kinetic modeling study of aromatics formation, growth and oxidation in laminar premixed ethylene and acetylene flames,” *Combust. Flame*, 1997.

[67] B. R. Graskow, D. B. Kittelson, M. R. Ahmadi, and J. E. Morris, “Exhaust Particulate Emissions from Two Port Fuel Injected Spark Ignition Engines,” *SAE Tech.*, 1999.

[68] L. Chen and D. of E. Science, “Measurement of Particulate Emissions from Gasoline Direct Injection Engines PRS Transfer Report,” Saint Cross College, 2008.

[69] F. Zhao, M. C. Lai, and D. L. Harrington, “Automotive spark-ignited direct-injection gasoline engines,” *Prog. Energy Combust. Sci.*, vol. 25, no. 5, pp. 437–562, 1999.

[70] M. M. Maricq, D. H. Podsiadlik, and R. E. Chase, “Gasoline Vehicle Particle Size Distributions: Comparison of Steady State, FTP, and US06 Measurements,” *Environ. Sci. Technol.*, vol. 33, no. 12, pp. 2007–2015, Jun. 1999.

[71] Y.-Q. Pei, J. Qin, and S.-Z. Pan, “Experimental study on the particulate matter emission characteristics for a direct-injection gasoline engine,” *Proc. Inst. Mech. Eng. Part D J. Automob. Eng.*, Jan. 2014.

[72] K. Choi, J. Kim, C.-L. Myung, M. Lee, S. Kwon, Y. Lee, and S. Park, “Effect of the mixture preparation on the nanoparticle characteristics of gasoline direct-injection vehicles,” *Proc. Inst. Mech. Eng. Part D J. Automob. Eng.*, vol. 226, no. 11, pp. 1514–1524, May 2012.

[73] P. Price, R. Stone, D. OudeNijeweme, and C. Xiangdong, “Cold Start Particulate Emissions from a Second Generation DI Gasoline Engine,” *SAE Tech.*, 2007.

[74] J. Färnlund, C. Holman, and P. Kågeson, “Emissions of Ultrafine Particles from Different Types of Light Duty Vehicles,” Swedish National Road Administration, 2001.

[75] B. R. Graskow, D. B. Kittelson, M. R. Ahmadi, and J. E. Morris, “Exhaust Particulate Emissions from a Direct Injection Spark Ignition Engine,” *SAE Tech.*, no. 724, 1999.

[76] M. M. Maricq, R. E. Chase, D. H. Podsiadlik, and R. Vogt, “Vehicle Exhaust Particle Size Distributions: A Comparison of Tailpipe and Dilution Tunnel Measurements,” *SAE Tech.*, no. 724, 1999.

[77] T. Yokoi, M. Shinzawa, and Y. Matsumoto, “Measurement repeatability improvement for particle number size distributions from diesel engines,” *JSAE Rev.*, vol. 22, no. 4, pp. 545–551, 2001.

[78] I. Abdul-Khalek, D. Kittelson, and F. Brear, “The Influence of Dilution Conditions on Diesel Exhaust Particle Size Distribution Measurements,” *SAE Tech.*, no. 724, 1999.

[79] N. Y. Rojas, “Diesel Exhaust System Influences on Transient Particulate Emissions and Particle Size Distribution,” University of Leeds, 2001.

[80] L. Chen, R. Stone, and D. Richardson, “A study of mixture preparation and PM emissions using a direct injection engine fuelled with stoichiometric gasoline/ethanol blends,” *Fuel*, vol. 96, no. 0, pp. 120–130, 2012.

[81] I. S. Abdul-Khalek, D. B. Kittelson, B. R. Graskow, Q. Wei, and F. Brear, “Diesel Exhaust Particle Size: Measurement Issues and Trends ,” *SAE Tech.*, 1998.

[82] J. P. Shi and R. M. Harrison, “Investigation of Ultrafine Particle Formation during Diesel Exhaust Dilution,” *Environ. Sci. Technol.*, vol. 33, no. 21, pp. 3730–3736, 1999.

[83] G. E. Andrews, A. J. Clarke, N. Y. Rojas, D. Gregory, and T. Sale, “Particulate Mass Accumulation and Release in Practical Diesel Engine Exhaust Systems under Cold Start Conditions,” *SAE Tech.*, no. 724, 2000.

[84] M. J. Kleeman, J. J. Schauer, and G. R. Cass, “Size and Composition Distribution of Fine Particulate Matter Emitted from Motor Vehicles,” *Environ. Sci. Technol.*, vol. 34, no. 7, pp. 1132–1142, 2000.

[85] N. Cavina, L. Poggio, F. Bedogni, V. Rossi, and L. Stronati, “Benchmark Comparison of Commercially Available Systems for Particle Number Measurement.” SAE International, 2013.

[86] AVL, *AVL Particle Counter Product Guide*, no. January. 2010.

[87] O. Bechmann, S. Carli, W. Engeler, T. Garbe, G. Lach, L. Ryan, and K. Schindler, “Particulate emissions and their measurement in practice : Today and in the future.”

[88] P. G. Eastwood, K. Tufail, T. Winstanley, A. Darlington, S. Karagiorgis, Y. Hardalupas, and A. M. K. P. Taylor, “Estimation of deviations in NO and soot emissions between steady-state and EUDC transient operation of a common-rail diesel engine,” *SAE Int. J. Engines*, vol. 2. Consiglio Nazionale delle Ricerche, pp. 648–659, 2009.

[89] W. Glewen, D. Heuwetter, D. Foster, M. Andrie, and R. Krieger, “Analysis of Deviations from Steady State Performance During Transient Operation of a Light Duty Diesel Engine,” *SAE Int. J. Engines*, vol. 5. SAE International, pp. 909–922, 2012.

[90] G. J. Smallwood, D. R. Snelling, Ö. L. Gülder, D. Clavel, D. Gareau, R. A. Sawchuk, and L. Graham, “Transient Particulate Matter

Measurements from the Exhaust of a Direct Injection Spark Ignition Automobile." SAE International, 2001.

[91] T. P. Dwyer, M. R. Kianifar, W. J. Bradley, I. F. Campean, B. A. Mason, M. K. Ebrahimi, D. Richardson, and L. Beddow, "DoE Framework for GDI Engine Mapping and Calibration Optimisation for CO2 and Particulate Number Emissions," *IAV Conf. Berlin*, pp. 418–432, 2012.

[92] É. Ferrero-lesur, M. Castagné, and F. Nicolas, "Optimization of Multi-Cylinder Design by using DoE on Single-Cylinder Engine and Air-Loop Simulation," pp. 372–393.

[93] T. Dvorak, R. Rohrer, P. Lamb, R. Hoekstra, and R. Meyer, "Non-Constant Variance - Emission Modeling Methods for Offline Optimization and Calibration of Engine Management Systems," *SAE Int.*, no. 724, 2003.

[94] P. Klein, F. Kirschbaum, B. Hartmann, and Y. Bogachik, "Adaptive Test Planning for the Calibration of Combustion Engines – Application," in *27th Conference on Design of Experiments (DoE) in Engine Development*, 2003, pp. 17–30.

[95] J. R. Black, "Rapid calibration of diesel engines using a Judicious Engine Testing process," University of Bradford, 2012.

[96] K. Kar, S. Roberts, R. Stone, M. Oldfield, and B. French, "Instantaneous Exhaust Temperature Measurements Using Thermocouple Compensation Techniques," *SAE Tech.*, 2004.

[97] General Electric Company, "Druck calibration tools," 2015. [Online]. Available: http://www.ge-mcs.com/en/pressure-and-level.html. [Accessed: 01-Jan-2015].

[98] HORIBA, "HORIBA MEXA 9100 Manual." .

[99] R. S. Tharp and W. K. Cheng, "Hydrocarbon Emissions in a Homogeneous Direct-Injection Spark Engine: Gasoline and Gasohol," Massachusetts Institute of Technology, Massachusetts, 2008.

[100] ECOpoint Inc., "Cars and Light Trucks Emission Standards - EU," 2013. [Online]. Available: https://www.dieselnet.com/standards/eu/ld.php. [Accessed: 09-Jul-2014].

[101] Europa, "Reduction in CO2 emissions of new passenger cars," 2011. [Online]. Available: http://europa.eu/legislation_summaries/environment/air_pollution/mi0046_en.htm.

[102] J. Verdejo, "Analysis of Crankshaft Speed Fluctuations and Combustion Performance," 2008.

[103] J. Dernotte, C. Hespel, F. Foucher, S. Houillé, and C. Mounaïm-Rousselle, “Influence of physical fuel properties on the injection rate in a Diesel injector,” *Fuel*, vol. 96, no. 0, pp. 153–160, 2012.

[104] Bosch Motorsport, “Single Fire Coil C90i-pro.” [Online]. Available: http://www.bosch-motorsport.de/en-US/literature/en-US/Single_Fire_Coil_C90i-pro_Datasheet_51_en_5929897739.pdf.

[105] F. Boudy and P. Seers, “Impact of physical properties of biodiesel on the injection process in a common-rail direct injection system,” *Energy Convers. Manag.*, vol. 50, no. 12, pp. 2905–2912, 2009.

[106] F. Yates, “Sir Ronald Fisher and the Design of Experiments,” *Int. Biometric Soc.*, vol. 20, no. 2, pp. 307–321, 1964.

[107] M. A. Z. Khan, “Transient engine model for calibration using two-stage regression approach,” PhD Thesis, Loughborough University, 2011.

[108] J. Seabrook, *Statistics for engine optimization*. Professional Engineering Pub., 2000.

[109] W. Lach, R., Kiehn, R., Hans, C., Siebertz, K., Platzbacker, “DoE Application within the Analytical Valve Train Development,” in *Design of Experiments in Engine Development*, 2005, pp. 221–234.

[110] J. Seabrook, J. Collins, and S. Edwards, “Application of advanced Modelling Techniques to the Calibration of Gasoline Engines with Direct Injection and Variable Valve Timing,” in *Design of Experiments in Engine Development*, 2005, pp. 235–245.

[111] G. Box and K. Wilson, “On the Experimental Attainment of Optimum Conditions,” *J. R. Stat. Soc. Ser. B*, vol. 13, no. 1, pp. 1–45, 1951.

[112] D. C. Montgomery, E. A. Peck, G. G. Vining, and J. Vining, “Introduction to linear regression analysis,” 2001.

[113] D. M. Grove and T. P. Davis, *Engineering Quality & Experimental Design*. Essex, England: Longman Scientific & Technical, 1992.

[114] A. C. Atkinson, A. N. Donev, and R. Tobias, *Optimum experimental designs, with SAS*. Oxford University Press, 2007.

[115] J. Seabrook, B. ROGERS, G. FARROW, and J. PATTERSON, *International Conference on Statistics and Analytical Methods in Automotive Engineering*, vol. 22. John Wiley & Sons, 2002.

[116] F. Pukelsheim, *Optimal Design of Experiments (Google eBook)*. SIAM, 2006.

[117] V. Toropov, “Response surface methodology,” *Online Handout, University of Bradford*. .

[118] M. Guerrier and P. Cawsey, “The development of model based methodologies for gasoline IC engine calibration,” *SAE Trans.*, vol. 113, no. 3, pp. 981–1002, 2004.

[119] D. M. Grove, D. C. Woods, and S. M. Lewis, “Multifactor B-spline mixed models in designed experiments for the engine mapping problem,” *J. Qual. Technol.*, vol. 36, no. 4, pp. 380–391, May 2004.

[120] J. Seabrook, T. Salamon, S. Edwards, and I. Noell, “A comparison of Neural Networks, Stochastic Process Methods and Radial Basis Function for the Optimization of Engine Control Parameters,” in *Second Conference Design of Experiments in Engine Development*, 2003.

[121] K. Roepke, A. Emtage, and D. Sampson, “Proposal for a Generic Interface between Test Bench Automation System and DoE Modelling Application,” *Des. Exp. Engine Dev. IV - Expert. - Libr. Tedesco - Libr. Univ.*, no. 9783816929376, 2009.

[122] M. Kowalczyk and R. Isermann, “Process Online-Methods for the Integration of Measurements , Modeling and Map Optimization at Engine Test Benches,” *7th Conf. Des. Exp. Engine Dev.*, pp. 107–124, 2013.

[123] C. Hametner, M. Stadlbauer, M. Deregnaucourt, S. Jakubek, and T. Winsel, “Optimal experiment design based on local model networks and multilayer perceptron networks,” *Eng. Appl. Artif. Intell.*, vol. 26, no. 1, pp. 251–261, 2013.

[124] T. Beattie, R. P. Osborne, and W. Graupner, “Engine Test Data Quality Requirements for Model Based Calibration: A Testing and Development Efficiency Opportunity,” *SAE Tech.*, Apr. 2013.

[125] P. Adomeit, O. Lang, S. Pischinger, R. Aymanns, M. Graf, and G. Stapf, “Analysis of Cyclic Fluctuations of Charge Motion and Mixture Formation in a DISI Engine in Stratified Operation,” *SAE Tech.*, no. 724, 2007.

[126] J. K. Ball, R. R. Raine, and C. R. Stone, “Combustion analysis and cycle-by-cycle variations in spark ignition engine combustion Part 1: An evaluation of combustion analysis routines by reference to model data,” *Proc. Inst. Mech. Eng. Part D J. Automob. Eng.*, vol. 212, no. 5, pp. 381–399, May 1998.

[127] J. K. Ball, R. R. Raine, and C. R. Stone, “Combustion analysis and cycle-by-cycle variations in spark ignition engine combustion Part 2: A new parameter for completeness of combustion and its use in modelling cycle-by-cycle variations in combustion,” *Proc. Inst. Mech. Eng. Part D J. Automob. Eng.*, vol. 212, no. 6, pp. 507–523, Jun. 1998.

[128] M. Namazian, S. Hansen, E. Lyford-Pike, J. Sanchez-Barsse, J. Heywood, and J. Rife, “Schlieren Visualization of the Flow and Density Fields in the Cylinder of a Spark-Ignition Engine,” *SAE Tech.*, 1980.

[129] J. Etheridge, S. Mosbach, M. Kraft, H. Wu, and N. Collings, “Modelling soot formation in a DISI engine,” *Proc. Combust. Inst.*, vol. 33, no. 2, pp. 3159–3167, 2011.

[130] M. J. Kleeman, S. G. Riddle, M. A. Robert, and C. A. Jakober, “Lubricating Oil and Fuel Contributions To Particulate Matter Emissions from Light-Duty Gasoline and Heavy-Duty Diesel Vehicles,” *Environ. Sci. Technol.*, vol. 42, no. 1, pp. 235–242, 2007.

[131] P. Giansetti, G. Colin, P. Higelin, and Y. Chamaillard, “Residual Gas Fraction Measurement and Computation,” *Int. J. Engine Res.*, vol. 8, p. 18, 2007.

[132] *Precision of test methods — Part 1: Guide for the determination of repeatability and reproducibility for a standard test method by inter-laboratory tests*, no. September. 1993.

[133] Y. Sougawa, K. Koseki, H. Kawaguchi, J. Nishimura, K. Namiyama, Y. Yamagishi, and Y. Ogawa, “Improvement of Repeatability in Tailpipe Emission Measurement with Direct Injection Spark Ignition (DISI) Vehicles,” *Powertrain & Fluid Systems Conference & Exhibition*, vol. 2002–02–27. SAE International, San Diego, California USA, 2002.

[134] C. Vallaude, C. Berthou, D. Pingal, and S. Ficheux, “Particle Number Round Robin Test,” UTAC, 2009.

[135] G. E. Andrews, G. Zhu, H. Li, A. Simpson, J. A. Wylie, M. Bell, and J. Tate, “The Effect of Ambient Temperature on Cold Start Urban Traffic Emissions for a Real World SI Car,” *SAE Tech.*, no. 724, 2004.

[136] Clifford Matthews, *Engineers’ Data Book*, Third. Wiley, 2011.

[137] J. D. Andersson, B. G. A. Wedekind, D. Hall, R. Stradling, C. Barnes, and G. Wilson, “DETR/SMMT/CONCAWE Particle Research Programme: Sampling and Measurement Experiences.” SAE International, 2000.

[138] H. Yamada and Y. Goto, “Optimization of PM Measurements with a Number Counting Method,” *SAE Int. J. Engines*, vol. 1, pp. 1179–1185, 2008.

[139] M. Ivanisin and S. Hausberger, “Experimental Study on Particle Number Emissions of Modern Vehicle Engines.” SAE International, 2005.

[140] B. R. Graskow, D. B. Kittelson, I. S. Abdul-Khalek, M. R. Ahmadi, and J. E. Morris, “Characterization of Exhaust Particulate Emissions from a Spark Ignition Engine.” SAE International, 1998.

[141] BBC, “The facts about low sulphur fuel,” 2000. [Online]. Available: http://news.bbc.co.uk/1/hi/uk/1014912.stm.

[142] ECOpoint Inc, “ECE 15 + EUDC / NEDC.” [Online]. Available: https://www.dieselnet.com/standards/cycles/ece_eudc.php. [Accessed: 01-Jan-2015].

[143] H. Klein, E. Lox, T. Kreuzer, M. Kawanami, T. Ried, and K. Bächmann, “Diesel Particulate Emissions of Passenger Cars - New Insights into Structural Changes During the Process of Exhaust Aftertreatment Using Diesel Oxidation Catalysts.” SAE International, 1998.

[144] G. E. Andrews, J. Xu, and T. Sale, “Influence of Catalyst and Exhaust System on Particulate Deposition and Release from an IDI Diesel Passenger Car under Real World Driving,” *SAE Tech.*, 2002.

[145] ECOpoint Inc, “Emission Test Cycles,” 2015. [Online]. Available: https://www.dieselnet.com/standards/cycles/.

[146] C. J. Brace, R. Burke, and J. Moffa, “Increasing accuracy and repeatability of fuel consumption measurement in chassis dynamometer testing,” *Proc. Inst. Mech. Eng. Part D-Journal Automob. Eng.*, vol. 223, no. D9, pp. 1163–1177, 2009.

[147] B. Tesfa, R. Mishra, C. Zhang, F. Gu, and A. Ball, “NOx Prediction Based on Cylinder Pressure Measurement for Engine Emission Monitoring,” 2011.

[148] K. A. Stroud, *Engineering Mathematics*, Third. Macmillan Education Ltd, 1987.

[149] M. S. Ray, *Engineering Experimentation: Ideas, Techniques, and Presentation*. McGraw-Hill Book Company, 1988.

[150] H. Stuhler, T. Kruse, A. Stuber, K. Gschweitl, W. Piock, H. Pfluegl, and P. Lick, “Automated Model-Based GDI Engine Calibration Adaptive Online DOE Approach,” *SAE Pap.*, no. 2002–01–0708, pp. 2002–01–0708, 2002.

[151] H. J. Rajan, J. Kelly, H. Hoetzendorfer, N. Keuth, H. Pfluegl, T. Winsel, and S. Roeack, “Industrialization of base calibration methods for ECU-functions exemplary for air charge determination,” in *SAE Paper*, 2010, pp. 2010–01–0331.

[152] M. R. Kianifar, “Application of Multidisciplinary Design Optimisation Frameworks for Engine Mapping and Calibration,” 2015.

[153] A. S. Bika, A. Warey, D. Long, S. Balestrino, and P. Szymkowicz, “Characterization of Soot Deposition and Particle Nucleation in Exhaust Gas Recirculation Coolers,” *Aerosol Sci. Technol.*, vol. 46, no. 12, pp. 1328–1336, Dec. 2012.

[154] J. E. T. Rimmer, E. J. Long, C. P. Garner, G. K. Hargrave, D. Richardson, and S. Wallace, “The Influence of Single and Multiple Injection Strategies on In-Cylinder Flow and Combustion within a DISI Engine ,” *SAE Tech. Pap.*, 2009.

[155] N. M. Brown, “Characterisation of emissions and combustion stability of a port fuelled spark ignition engine,” University of Nottingham, 2009.

[156] A. Velji, K. Yeom, U. Wagner, U. Spicher, M. Rossbach, R. Suntz, and H. Bockhorn, “Investigations of the Formation and Oxidation of Soot Inside a Direct Injection Spark Ignition Engine Using Advanced Laser-Techniques.” SAE International, 2010.

[157] H. Fukushima, H. Uchihara, I. Asano, M. Adachi, S. Nakamura, M. Ikeda, and K. Ishida, “An Alternative Technique for Low Particulate Measurement.” SAE International, 2001.

[158] K. Klindt, “Reducing the particulate emission numbers in DI Gasoline Engines.”

[159] D. Lee and J. B. Heywood, “Effects of Charge Motion Control During Cold Start of SI Engines.” SAE International, 2006.

[160] W. Fan, Z. Lin, Y. Li, and Y. Li, “Effect of Temperature on NO Release during the Combustion of Coals with Different Ranks,” *Energy & Fuels*, vol. 24, no. 3, pp. 1573–1583, 2010.

[161] T. P. Dwyer, “Test point sequencing code written using MATLAB,” 2014. [Online]. Available: https://mega.co.nz/#!sZY2ULJJ!sYXoOHOhGghq70PsJaDmCEY004272PtNoa9s39aZdas.

Appendices

A1 Publications

T. P. Dwyer, M. R. Kianifar, W. J. Bradley, I. F. Campean, B. A. Mason, K. M. Ebrahimi, D. Richardson, and L. Beddow, “DoE Framework for GDI Engine Mapping and Calibration Optimisation for CO2 and Particulate Number Emissions,” IAV Conf. Berlin, pp. 418–432, 2012

T. P. Dwyer, W. Bradley, B. Mason and K. M. Ebrahimi, “Steady state determination for automotive engine dynamometer testing”, EMC Conference, Bradford University, August 2012

A2 Test environment and equipment

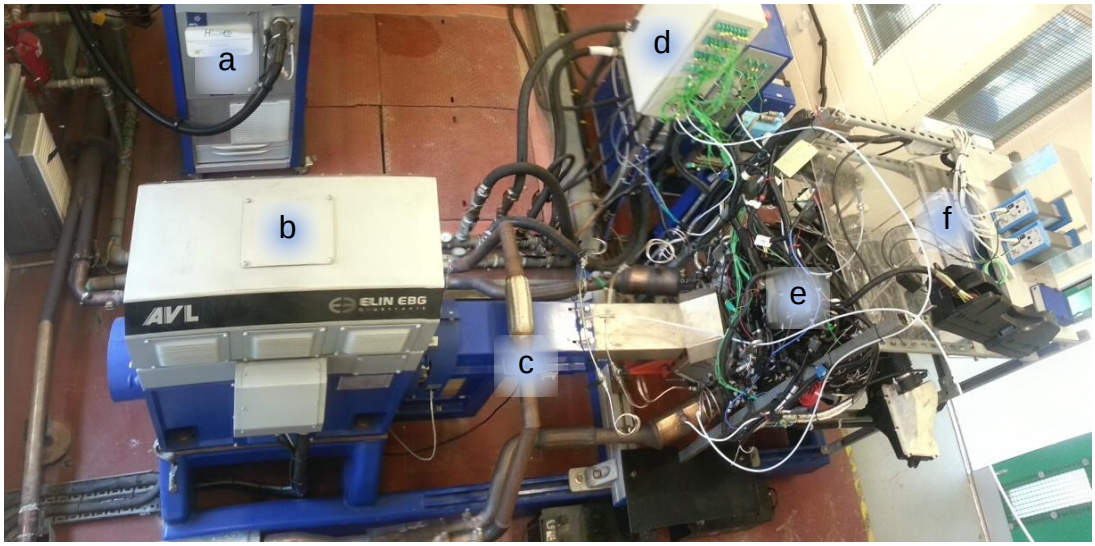

Figure 0.1 Birds-eye view of condensation particle counter (a), dynamometer (b), exhaust system with cross-over (c), thermocouple and sensor junction boxes (d), AJ133 V8 engine (e) and combustion analyser (f)

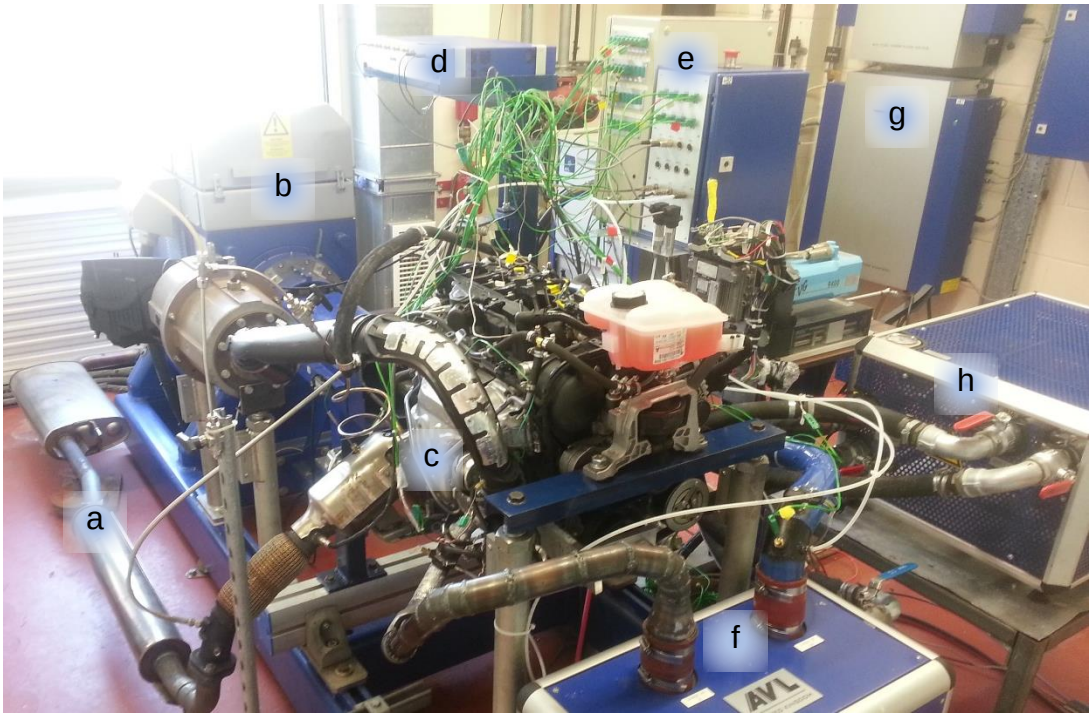

Figure 0.2 Photograph of Test Cell 1 at the University of Bradford with exhaust system (a), dynamometer (b), Ford EcoBoost I-4 engine (c), combustion analyser (d), thermocouple and sensor junction boxes (e), charge cooler (f), fuel conditioners (g) and engine coolant dry cooler (h)

The test cell used throughout this thesis is shown in Figure 0.3, the photo was taken from above the dynamometer.

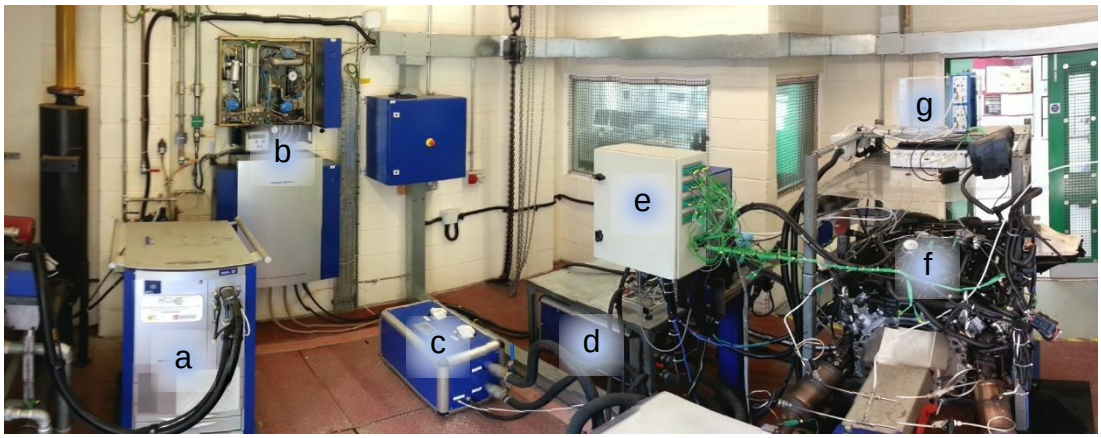

Figure 0.3 Panorama of Test Cell 1 at the University of Bradford with condensation particle counter (a), Coriolis fuel mass flow meter (top) and fuel temperature conditioner (bottom) (b), Charge cooler (used for EcoBoost engine) (c), engine coolant dry cooler (d), thermocouple and sensor signal boxes (e), UUT (AJ133 pictured) (f) and shelf-mounted combustion analyser and piezo-signal amplifiers (g)

A3 Engine specifications

Two direct injection spark-ignition engines were used for this study. The first was a 5 litre naturally aspirated V8 manufactured by Jaguar Land Rover (JLR). The model is a 2013 AJ133, a top-view cutaway of which is shown in Figure 0.4.

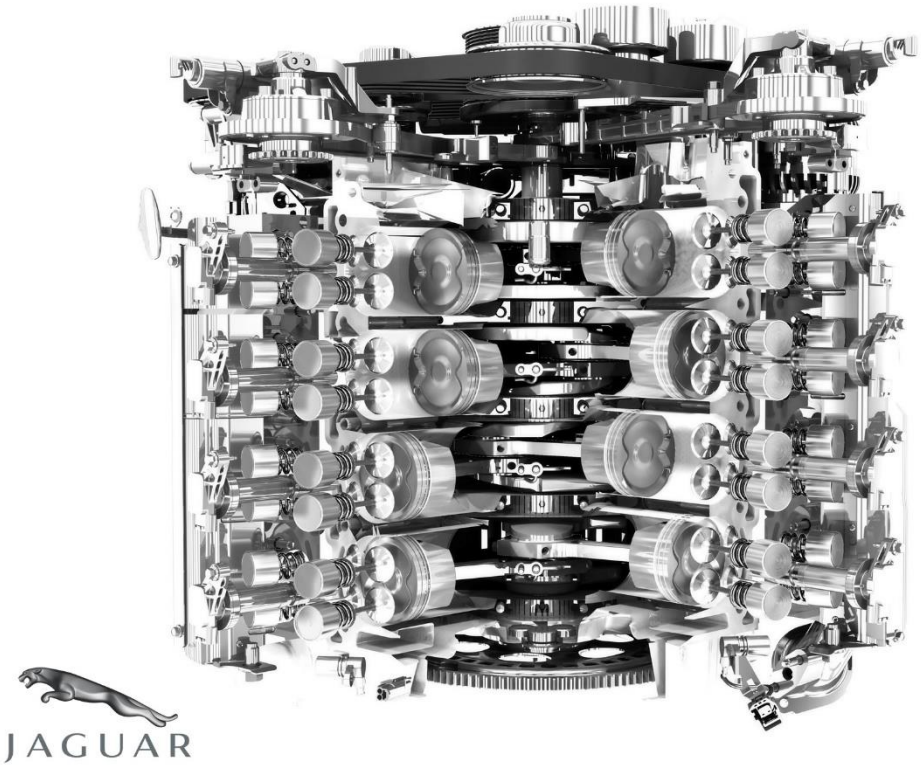

Figure 0.4 JLR AJ133 5 litre NA GDI V8

The second was a 1.6 litre turbocharged l-4 manufactured by Ford. The model is a 2011 GTDI EcoBoost, a cutaway of which is shown in Figure 0.5.

Figure 0.5 Ford Ecoboost 1.6 litre GTDI l-4

Photos of the engines installed into the test cell are in Appendix A2. The specifications of each engine is provided in Table 0.1.

Table 0.1 Engine datasheet

General	V8	l-4
Manufacturer	Jaguar Land Rover Ltd	Ford Motor Company
Model	AJ133	GTDI
Induction type	Naturally aspirated	Turbocharged
Capacity	5 litre	1.6 lire
Type	Gasoline direct injection (GDI)	Gasoline turbocharged direct injection
Cylinders	8	4

Injection		
Injection type	Spray-guided	Spray-guided
Injector position	Centre	
Injector holes	6	6
Combustion type	Homogeneous	Homogeneous
Valve Timing		
Valves per cylinder	4	4
Valve timing	Variable, cam torque actuated	Variable, twin independent
Inlet cam range	62 CA	
Exhaust cam range	50 CA	
Valve lift control	2 stage (5.5mm/10.5mm)	
Camshaft drive	2 x 8mm chains	
Intake Characteristics		
Inlet manifold tuning	2 stage (350mm/680mm); switch at 4700 rpm	N/A
Inlet manifold material	Plastic	Plastic
Throttle	83mm	
Construction		
Block	Aluminium	Aluminium
Cylinder Head	Aluminium	Aluminium
Piston Rod	Steel	Steel
Piston	Aluminium	

Compression Ratio	11.5	10.0
Bore	95.5 mm	79.0 mm
Stroke	93.0 mm	81.4 mm
Performance		
Maximum power	283 kW (385 hp)	112 kW (150 hp)
Maximum torque	515 Nm	240 Nm
Ancillaries		
Oil pump	G-rotor type	
Fuel pump	2 x 150bar (15MPa), single piston type	
Cooling type	Reverse flow (radiator → cylinder head → cylinder block)	
Other		
EGR	Internal	External

A4 Instrument parameters

The test cell hardware and software versions are shown in

Table 0.2.

Table 0.2 Test equipment datasheet

	Cell Controller
Manufacturer	AVL
Software	Puma Open v1.3.2
Temperature conditioning	Engine coolant; Intake air; Fuel
Fuel metering	AVL 735S mass flow meter (Coriolis effect)
Fuel conditioning	AVL 753C
Dynamometer	A/C transient
Dyno power rating	120 kW
	Gaseous Emissions
Manufacturer	Horiba
Type	MEXA-9100D (direct measurement) – single point
Emissions	CO; CO_2; NOx; THC; O2
CO/CO_2 detection method	Non-dispersive infrared (NDIR)
THC detection method	Flame ionization detector (FID)
O2 detection method	Magnetic
NOx detection method	Chemiluminescence Detector (CLD)
PC Communication	GPIB → RS232
	Particulate Emissions
Manufacturer	AVL
Type	AVL Condensation Particle Counter (CPC)

Sampling	Raw exhaust
Count efficiency	90% @ 41nm, 50% @ 23nm
Heated sample line	Yes
Pre-classifier cut-off	2.5µm
Evaporation tube temperature	350°C
Dilutions stages	2
PC communication	RS232
	ECU and Interface
ECU manufacturer	Bosch
Interface software	INCA V7.0
PC communication	Ethernet
ECU interface	Ethernet based using ETK interface (100Mbit/s)
	Indicating System
Manufacturer	AVL
Software	IndiCom
Hardware	IndiSmart (8 channel)
Inputs	Piezoelectric and analogue
PC Communication	Ethernet
	Additional Instrumentation
Manufacturer	National Instruments
Base system	NI cDAQ 9172 – Compact DAQ chassis
Modules	NI 9211 (x2) – Thermocouple input module (4 Ch)
	NI 9213 – Thermocouple input module (16 Ch)

	NI 9205 – Analog input voltage module (32 Ch) NI 9263 – Analog output voltage module (4 Ch)

A5 Instrument calibration

The HORIBA Gaseous emissions analyser was calibrated prior to testing each day. This included a SPAN and ZERO check. The main and secondary filters were also changed after approximately four hours running.

The particle counter was calibrated between every 2 – 4 weeks depending on the testing intensity. The Butanol was changed every 6 – 8 weeks.

Pressure transducers were calibrated upon delivery and the thermocouples were all calibrated prior to installation.

The dynamometer was calibrated when the engine was changed.

The fuel mass flow meter automatically performed a zero-flow and a calibration when powered on.

A6 Data collection

The data are collected from a number of sources before being combined into a single dataset. The infrastructure of the facility is outlined in Figure 0.6.

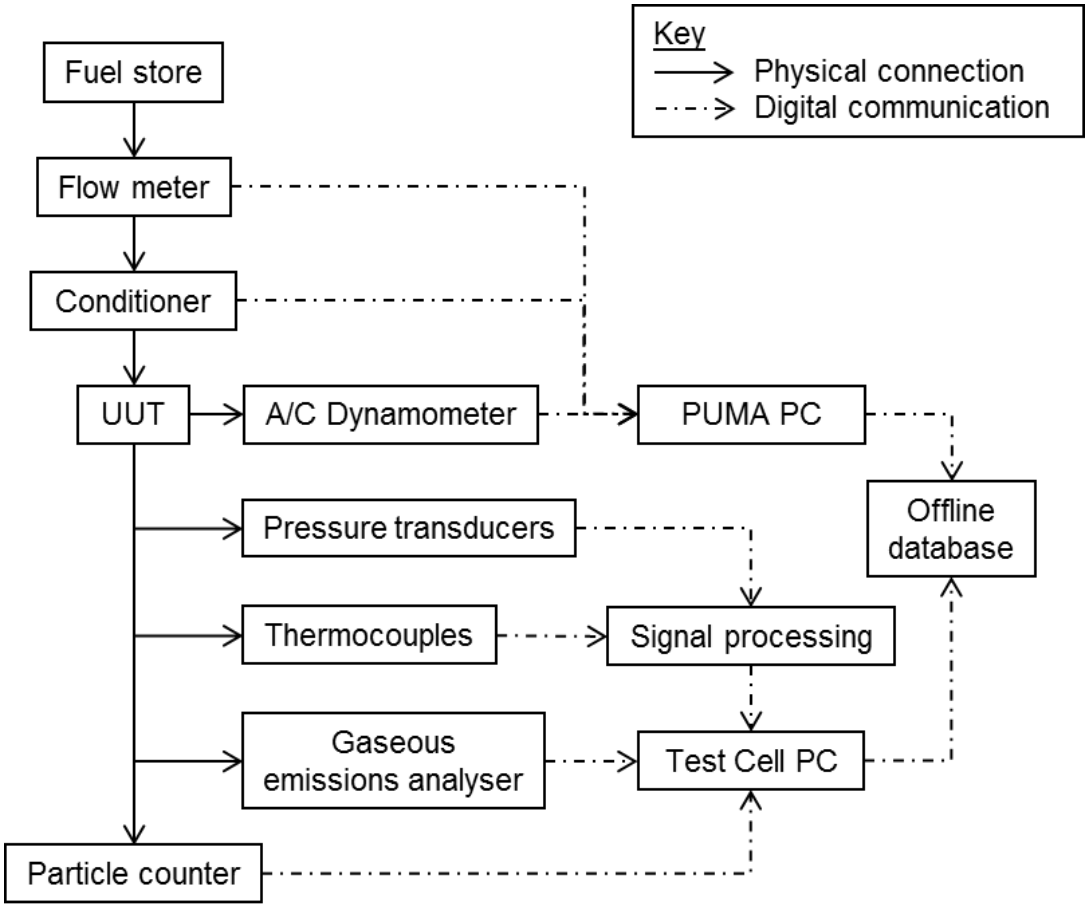

Figure 0.6 Schematic of the test cell hardware and connections

Fuel is fed under gravity from a day tank into the mass flow meter. This device pressurises fuel before feeding it into the conditioning device where the temperature is controlled. This fuel is then fed into a loop that circulates continuously to maintain the fuel temperature throughout the system. The engine will take the required fuel from a T-piece in the loop and the amount extracted from the system will be relayed by the flow meter to the PUMA PC. Information is also transmitted by the conditioner about the temperature of the fuel in the circuit.

An external cooler, not depicted in Figure 0.6, also has 2-way communications with the PUMA PC about the temperature of the engine coolant.

An A/C dynamometer is controlled by the test bed controller PC which runs PUMA Open 1.3.2.

Fast- (piezoelectric) and slow-response pressure transducers are used either in-cylinder or around the UUT and ancillaries, respectively.

To synchronise the data from multiple sources (HORIBA, APC, PUMA) an application was developed in LabVIEW, Figure 0.7.

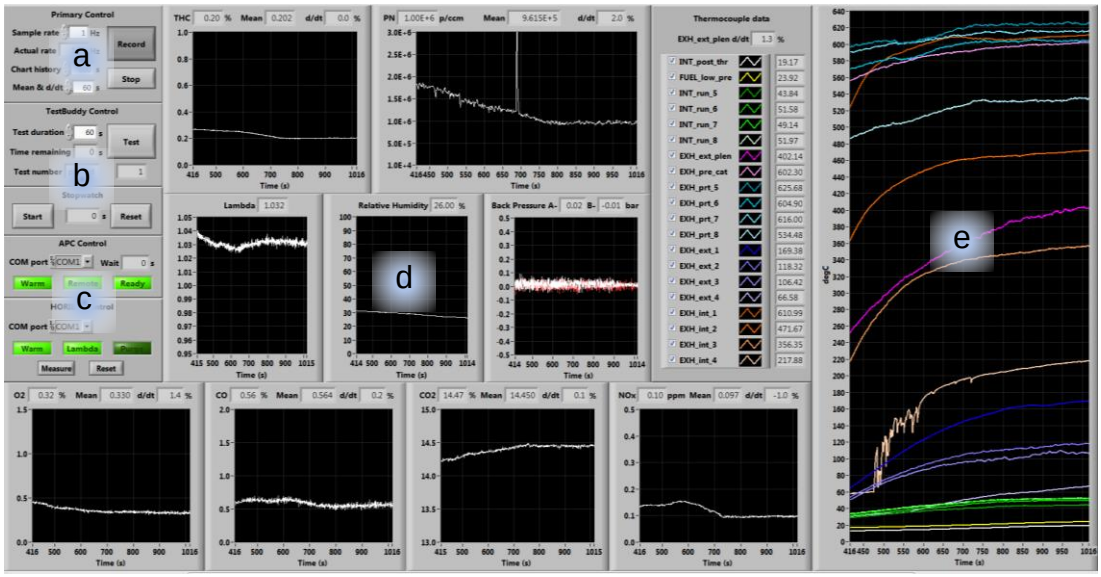

Figure 0.7 LabVIEW test application with control panel (a), system synchronisation (b) HORIBA and APC hardware control (c), emissions read-outs (d) and temperature readings (e)

The ECU interface (INCA) and in-cylinder pressure software (IndiCom) interfaces are shown in Figure 0.8.

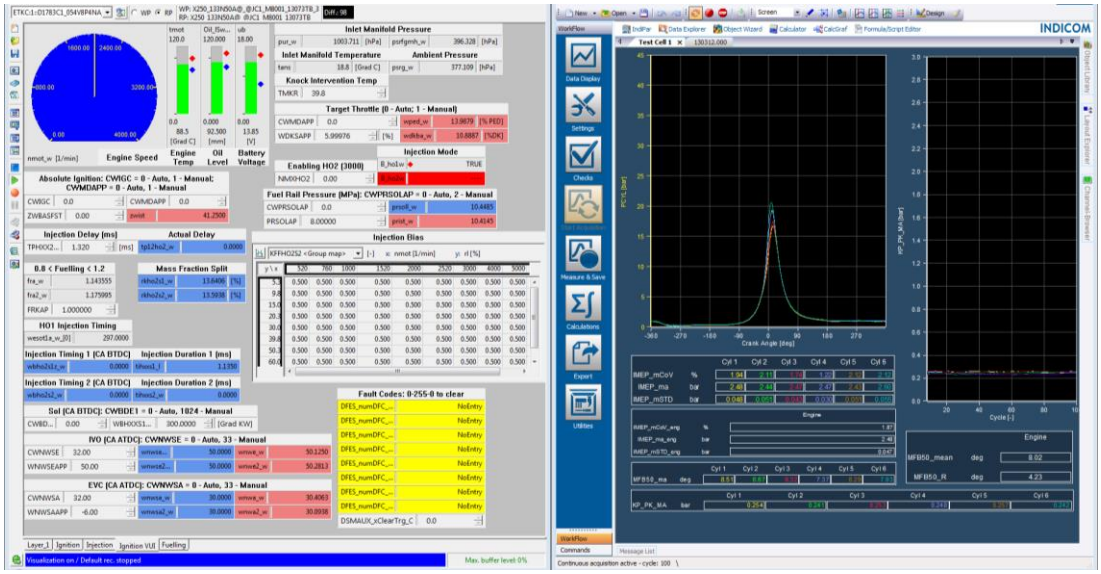

Figure 0.8 INCA (left) and IndiCom interfaces

Data from the PUMA PC and the secondary PC (that ran LabVIEW, INCA and IndiCom) were exported manually and processed automatically using a MATLAB function written specifically. The data could then be archiving in a database for ready access.

A7 Individual baseline data plots

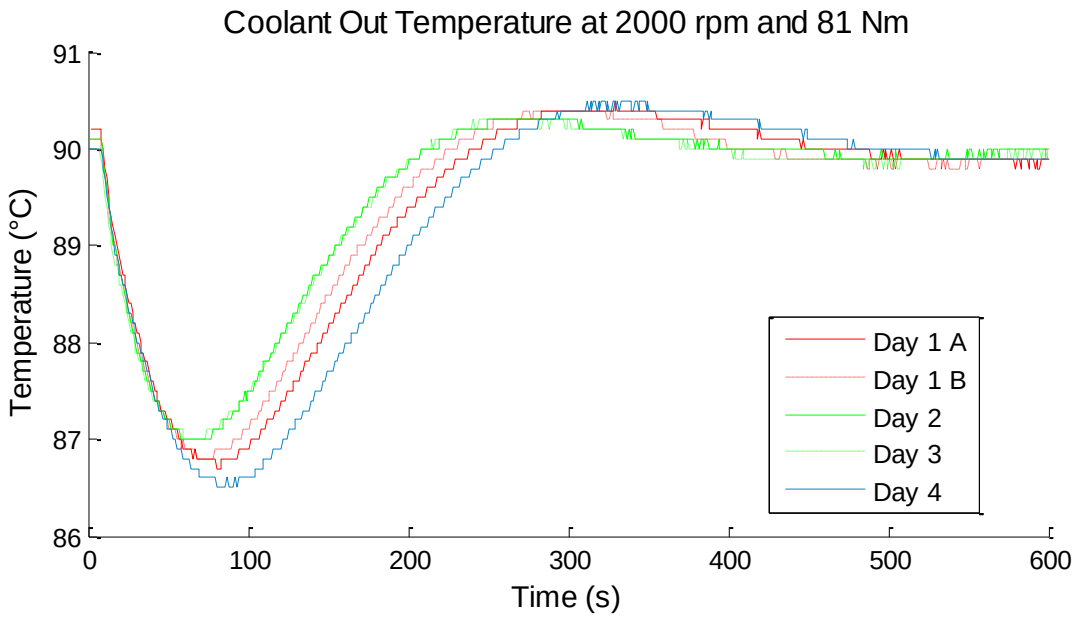

Figure 0.9 Engine coolant out temperature response following a step-change from 2000 rpm 199 Nm to 2000 rpm 81 Nm

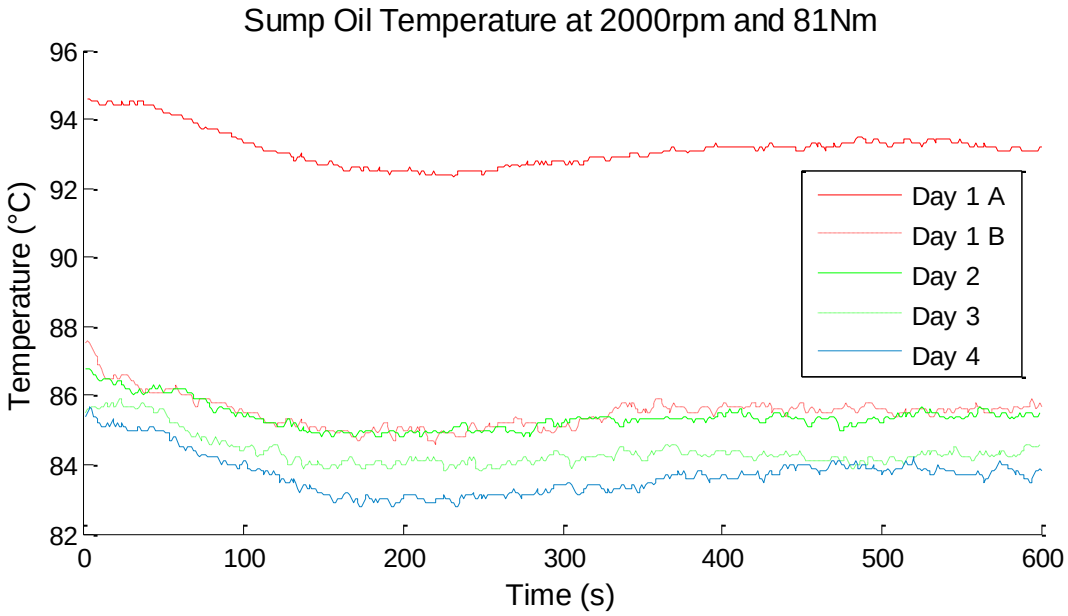

Figure 0.10 Engine sump oil temperature response following a step-change from 2000 rpm 199 Nm to 2000 rpm 81 Nm

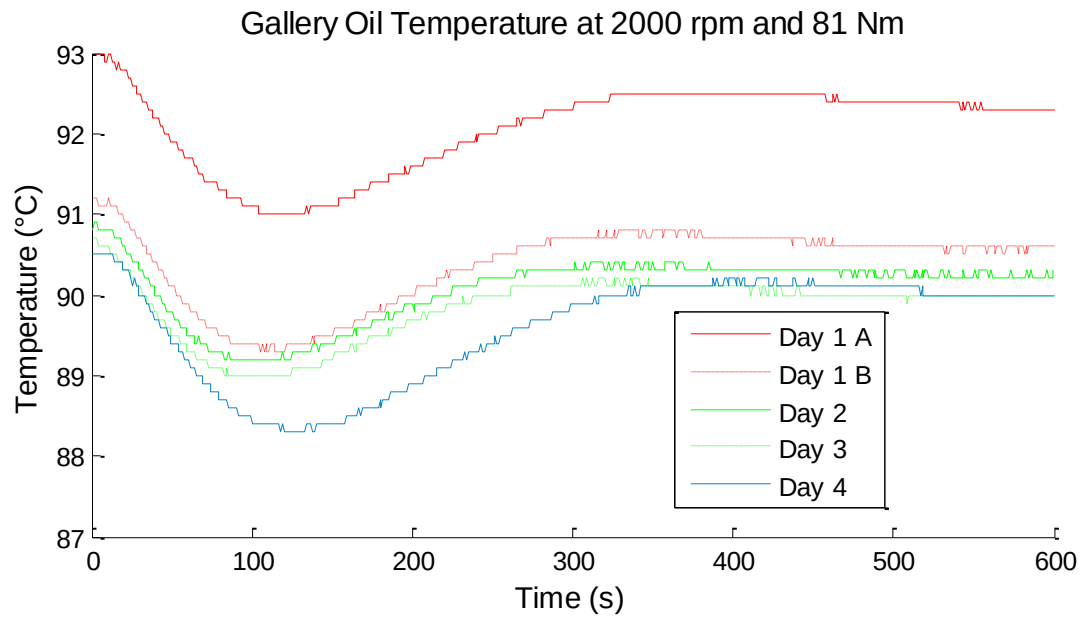

Figure 0.11 Engine gallery oil temperature response following a step-change from 2000 rpm 199 Nm to 2000 rpm 81 Nm

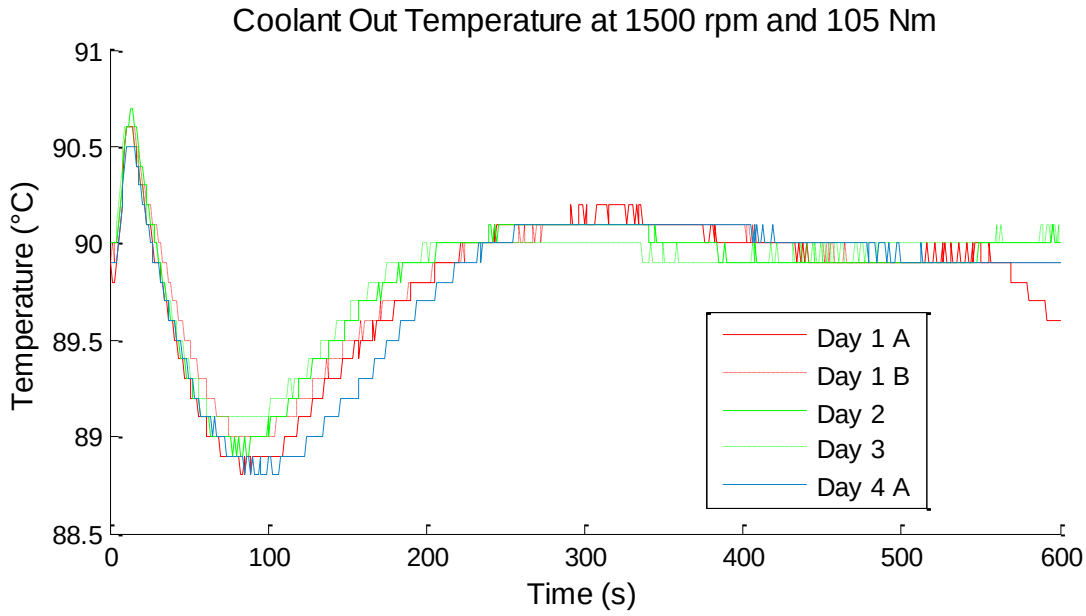

Figure 0.12 Engine coolant out temperature response following a step-change from 2000 rpm 81 Nm to 1500 rpm 105 Nm

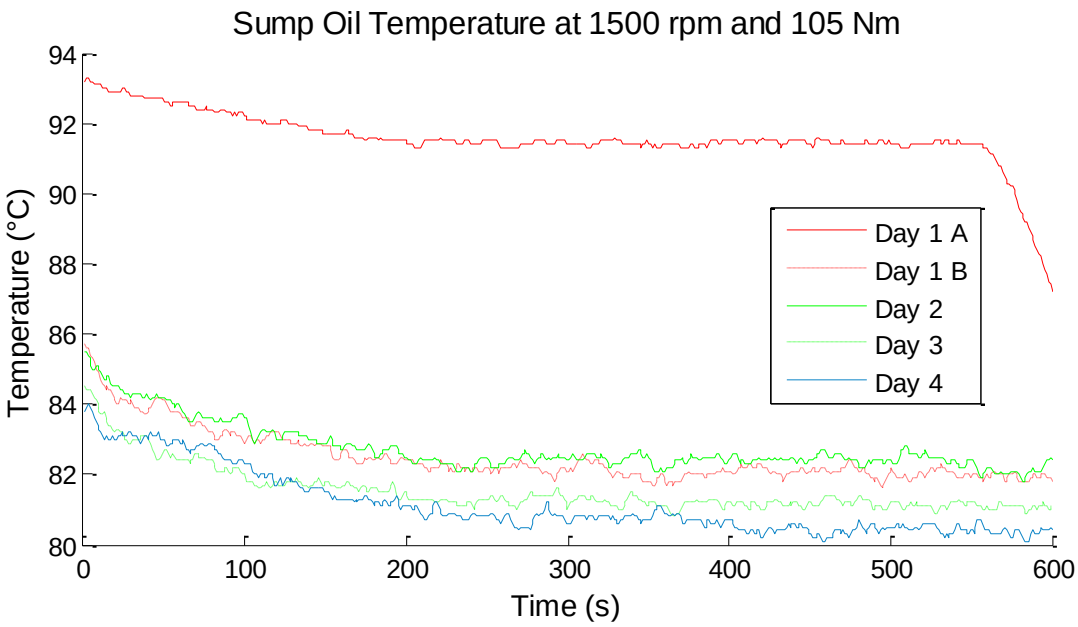

Figure 0.13 Engine sump oil temperature response following a step-change from 2000 rpm 81 Nm to 1500 rpm 105 Nm

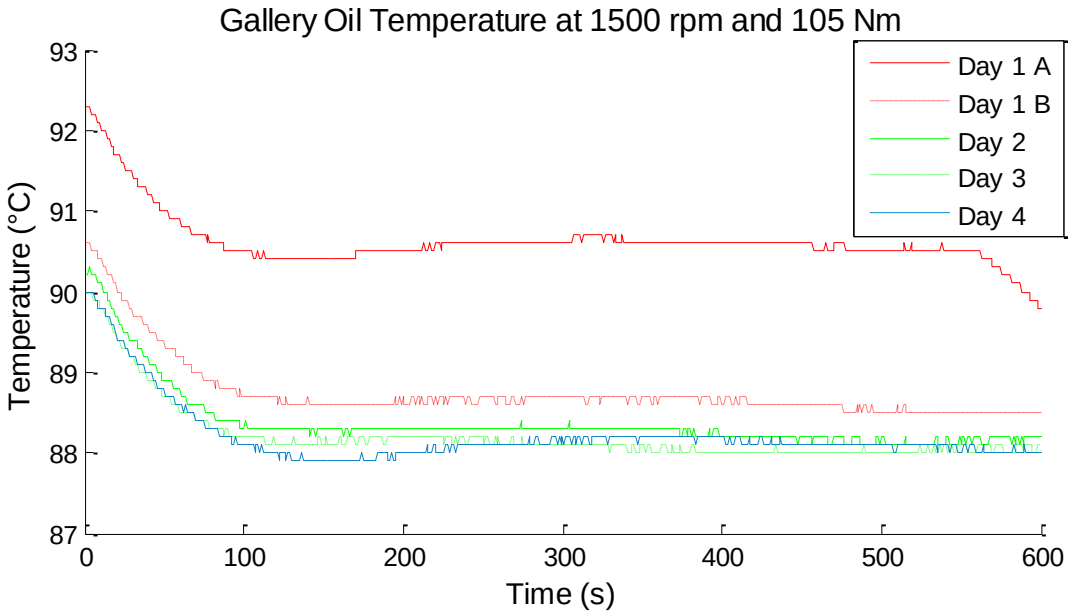

Figure 0.14 Engine gallery oil temperature response following a step-change from 2000 rpm 81 Nm to 1500 rpm 105 Nm

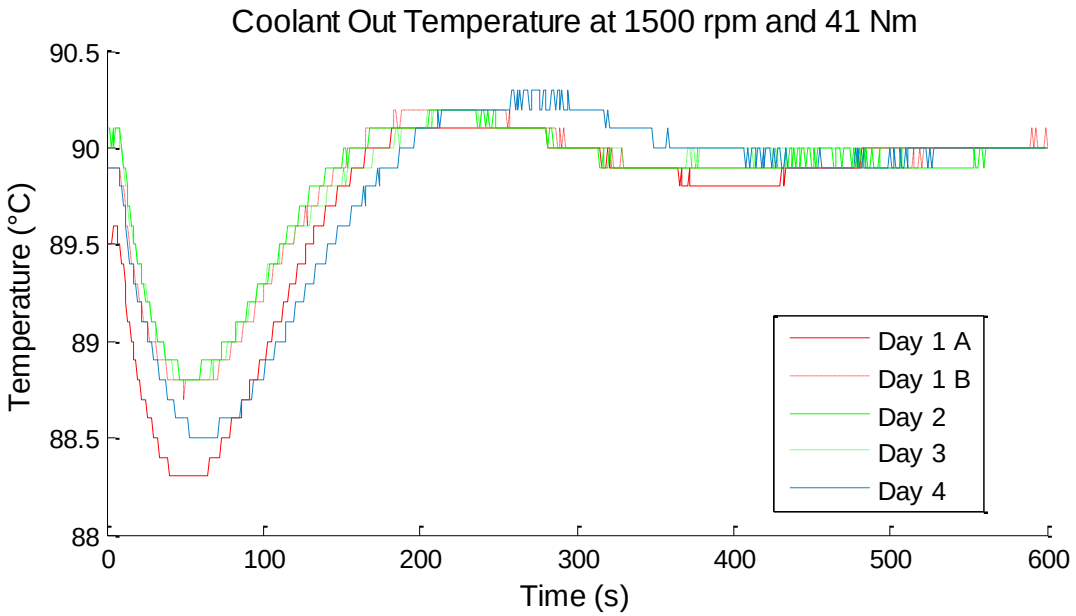

Figure 0.15 Engine coolant out temperature response following a step-change from 1500 rpm 105 Nm to 1500 rpm 41 Nm

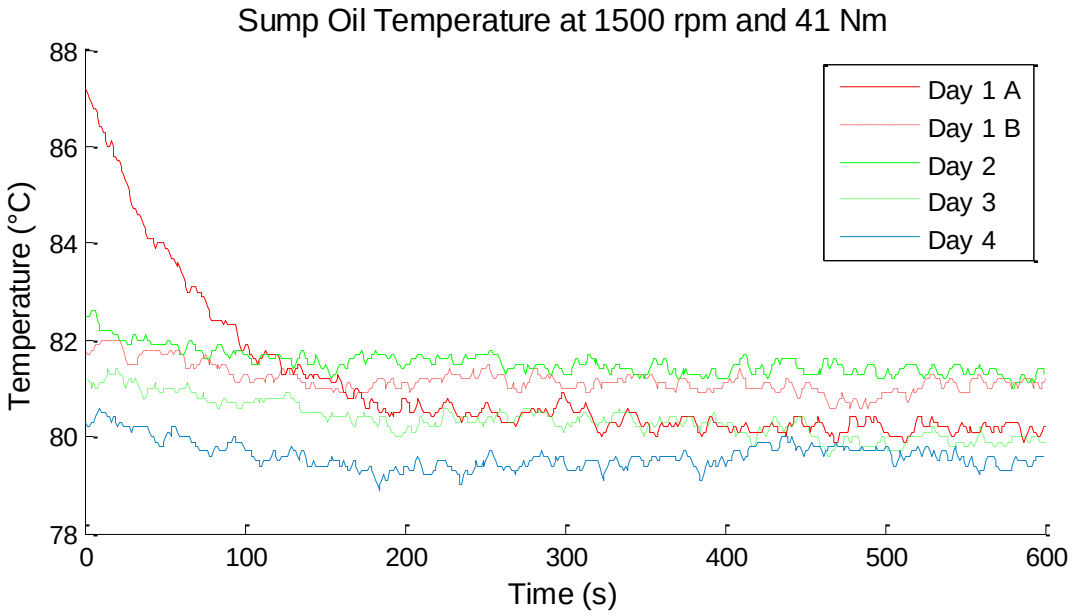

Figure 0.16 Engine sump oil temperature response following a step-change from 1500 rpm 105 Nm to 1500 rpm 41 Nm

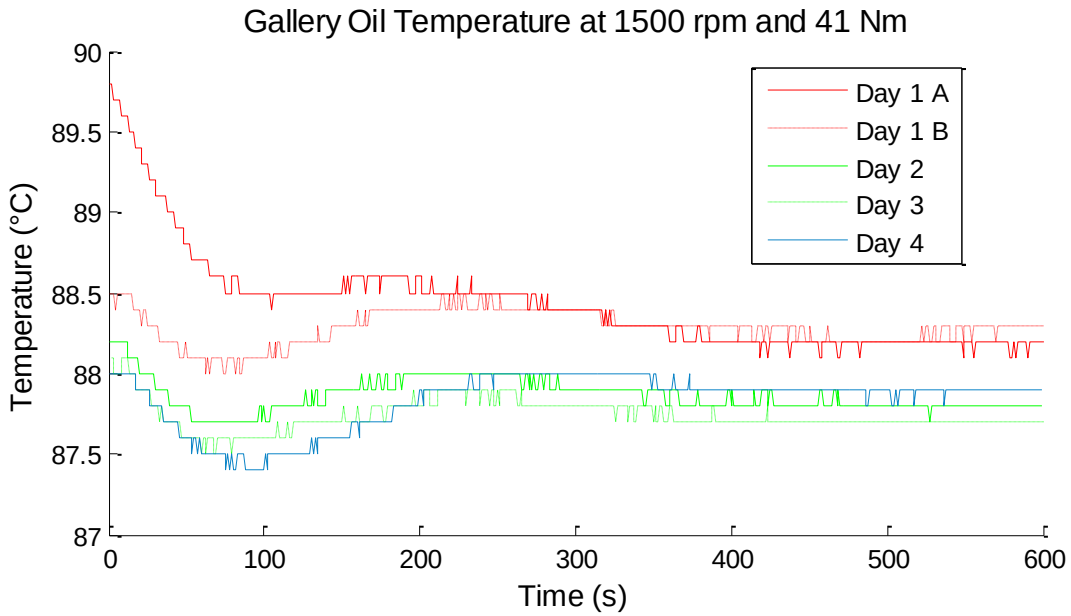

Figure 0.17 Engine gallery oil temperature response following a step-change from 1500 rpm 105 Nm to 1500 rpm 41 Nm

---

A8 Statistical comparisons of steady-state indicators

These are the mean, standard deviation and coefficient of variations of the baseline data that was recorded to compare the use of different steady-state indicators. During the process of generating boxplots there were a number of points deemed outliers and these were not included in the boxplots although the values were used for the figures.

Table 0.3 Baseline PN emissions

Indicator	Median (p/cm^3)	Mean (p/cm^3)	Std	CoV
Engine coolant-out	1.30E+06	1.21E+06	3.83E+05	0.301
Engine sump oil	1.17E+06	1.11E+06	3.06E+05	0.262
Exhaust plenum	9.21E+05	8.67E+05	1.43E+05	0.155

Table 0.4 Baseline fuel consumption

Indicator	Median (kg/h)	Mean (kg/h)	Std	CoV
Engine coolant-out	5.93	6.06	0.56	0.094
Engine sump oil	5.96	5.94	0.23	0.039
Exhaust plenum	5.91	5.77	0.34	0.058

Table 0.5 Baseline CO emissions

Indicator	Median (%)	Mean (%)	Std	CoV
Engine coolant-out	6.78E-01	6.86E-01	6.47E-02	0.095
Engine sump oil	6.93E-01	6.99E-01	8.17E-02	0.118
Exhaust plenum	5.20E-01	5.15E-01	2.89E-02	0.056

Table 0.6 Baseline CO_2 emissions

Indicator	Median (%)	Mean (%)	Std	CoV
Engine coolant-out	14.45	14.42	0.105	0.007
Engine sump oil	14.36	14.34	0.148	0.010
Exhaust plenum	14.54	14.51	0.150	0.010

Table 0.7 Baseline HC emissions

Indicator	Median (ppmC)	Mean (ppmC)	Std	CoV
Engine coolant-out	218.7	216.2	9.2	0.042
Engine sump oil	219.5	219.6	11.1	0.050
Exhaust plenum	200.1	200.2	28.9	0.056

Table 0.8 Baseline NOx emissions

Indicator	Median (ppm)	Mean (ppm)	Std	CoV
Engine coolant-out	1.52E-01	1.64E-01	3.39E-02	0.223
Engine sump oil	1.56E-01	1.54E-01	3.19E-02	0.205
Exhaust plenum	1.32E-01	1.25E-01	1.44E-02	0.109

A9 Comparing steady-state indicators for high quality engine measurements plots

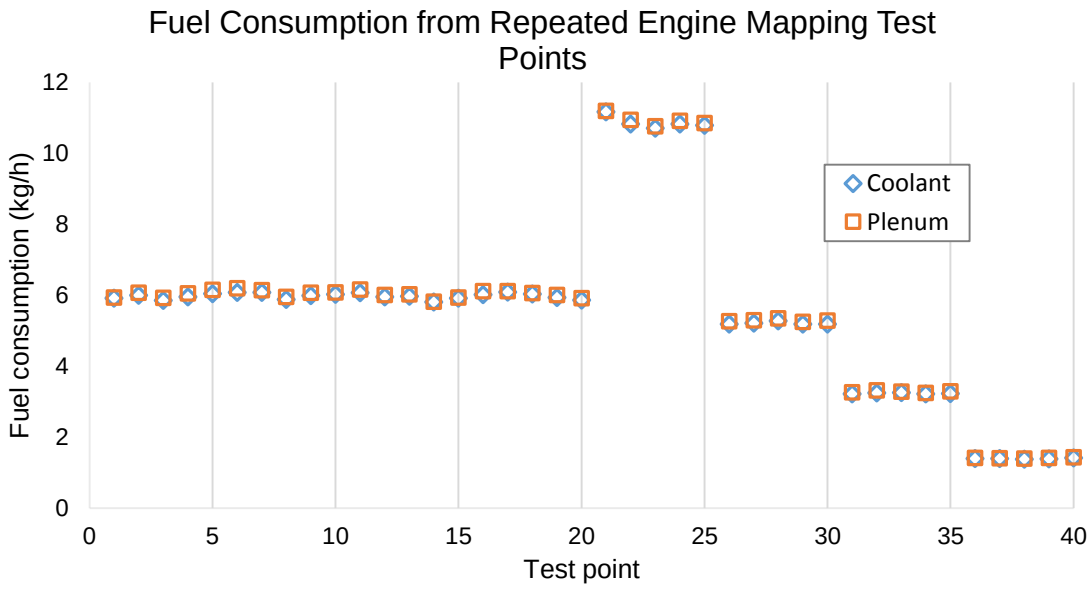

Figure 0.18 Fuel consumption measurements from a selection of test points repeataed using different steady-state indicators

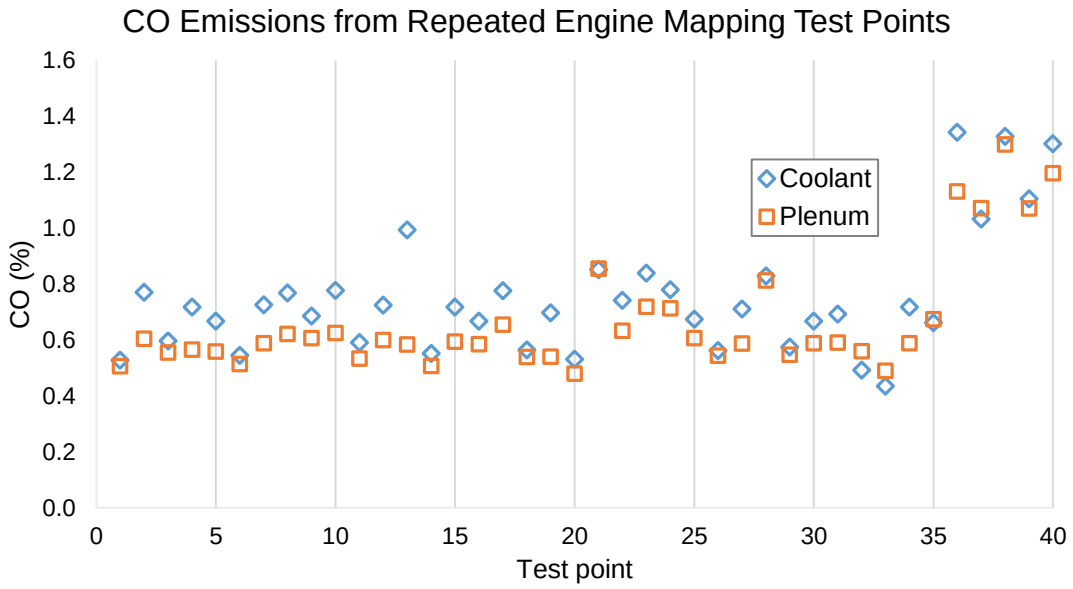

Figure 0.19 CO emissions measurements from a selection of test points repeataed using different steady-state indicators

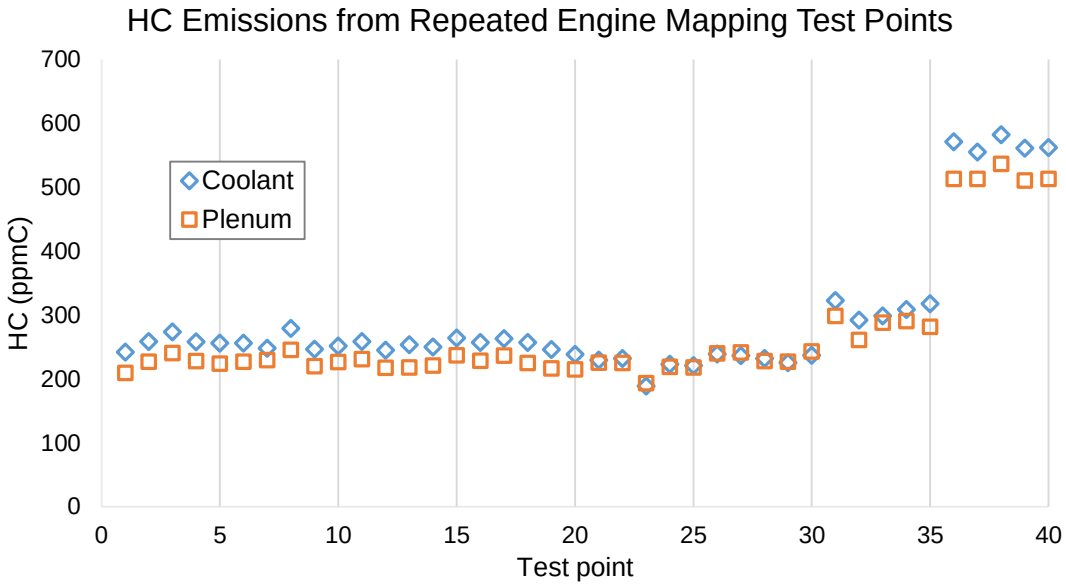

Figure 0.20 HC emissions measurements from a selection of test points repeataed using different steady-state indicators

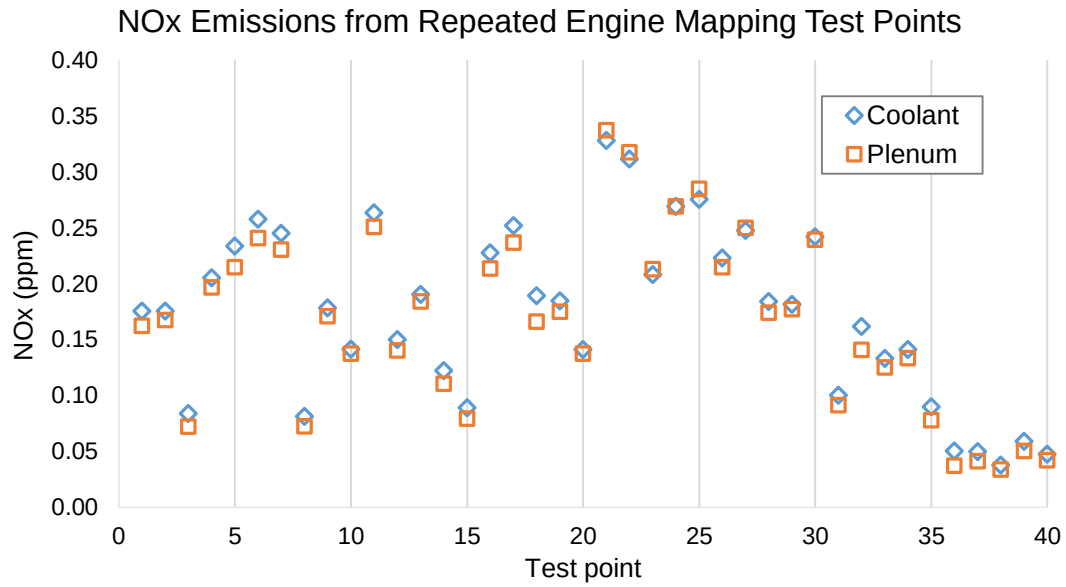

Figure 0.21 NOx emissions measurements from a selection of test points repeataed using different steady-state indicators

A10 Steady-state methodology

v. Start engine and perform daily checks
vi. Proceed to desired node (speed and load)
vii. Allow exhaust plenum skin temperature to stabilise
viii. Collect test data for current speed and load

A11 Steady-state baseline methodology

i. Turn on the engine
ii. Allow engine speed to drop below 800 rpm
    - Catalyst light-off complete
iii. Ramp the engine speed to 2000 rpm 81 Nm over a duration of 120 seconds
    - Automated ramp programmed into test-bed PC
iv. Allow exhaust plenum skin temperature to stabilise
    - Delta < 1% within 60 seconds

A12 Initial correlation results

Table 0.9 Node 1 t-scores

Actuator	CO	CO_2	PN	NOx	HC	Sum
FRP	0.013	0.095	0.130	0.913	0.488	1.639
IVO	0.212	0.025	0.476	0.549	0.051	1.312
EVC	0.284	0.366	0.198	0.065	0.665	1.577
SA	0.322	0.097	0.117	0.362	0.007	0.905
SOI	0.512	0.490	0.688	0.379	0.129	2.197
Sum	1.342	1.073	1.607	2.267	1.341	

Table 0.10 Node 1 Spearman's rho

Actuator	CO	CO_2	PN	NOx	HC	Sum (abs)
FRP	0.286	-0.194	-0.177	-0.013	-0.081	0.751
IVO	-0.146	0.259	0.084	0.070	0.227	0.785
EVC	-0.125	0.106	0.150	0.214	0.051	0.647
SA	-0.116	0.193	0.183	0.107	0.307	0.906
SOI	0.077	-0.081	0.047	0.103	-0.177	0.485
Sum (abs)	0.750	0.833	0.641	0.507	0.843	

Table 0.11 Node 2 t-scores

Actuator	CO	CO_2	PN	NOx	HC	Sum
FRP	0.431	0.214	0.046	0.104	0.578	1.374
IVO	0.278	0.401	0.448	0.091	0.270	1.488
EVC	0.101	0.481	0.768	0.385	0.142	1.878
SA	0.495	0.449	0.729	0.706	0.080	2.460
SOI	0.329	0.438	0.110	0.229	0.603	1.709
Sum	1.634	1.984	2.102	1.515	1.674	

Table 0.12 Node 2 Spearman's rho

Actuator	CO	CO_2	PN	NOx	HC	Sum (abs)
FRP	-0.092	0.145	-0.231	-0.189	0.065	0.723
IVO	-0.127	-0.098	-0.089	-0.197	-0.129	0.639
EVC	-0.191	-0.082	-0.035	0.102	-0.171	0.580
SA	-0.080	0.089	0.041	0.044	0.204	0.457
SOI	-0.114	-0.091	-0.186	-0.141	-0.061	0.592
Sum (abs)	0.604	0.505	0.581	0.672	0.629	

Table 0.13 Node 3 t-scores

Actuator	CO	CO_2	PN	NOx	HC	Sum
FRP	0.279	0.179	0.816	0.578	0.619	2.472
IVO	0.121	0.713	0.538	0.163	0.164	1.700
EVC	0.654	0.460	0.862	0.666	0.543	3.185
SA	0.642	0.159	0.512	0.932	0.933	3.177
SOI	0.268	0.090	0.894	0.735	0.650	2.637
Sum	1.965	1.601	3.622	3.073	2.909	

Table 0.14 Node 3 Spearman's rho

Actuator	CO	CO_2	PN	NOx	HC	Sum (abs)
FRP	0.127	0.157	-0.027	-0.065	0.058	0.434
IVO	0.180	0.043	0.072	0.163	0.162	0.621
EVC	-0.053	0.087	0.020	0.051	0.071	0.282
SA	0.055	0.164	0.077	0.010	0.010	0.316
SOI	0.130	0.197	0.016	-0.040	0.053	0.435
Sum (abs)	0.544	0.648	0.212	0.329	0.355	

Table 0.15 Node 4 t-scores

Actuator	CO	CO_2	PN	NOx	HC	Sum
FRP	0.905	0.457	0.026	0.010	0.199	1.599
IVO	0.574	0.467	0.486	0.398	0.661	2.586
EVC	0.799	0.137	0.829	0.792	0.056	2.612
SA	0.151	0.315	0.898	0.768	0.084	2.216
SOI	0.213	0.703	0.197	0.034	0.069	1.216
Sum	2.642	2.079	2.435	2.003	1.069	

Table 0.16 Node 4 Spearman's rho

Actuator	CO	CO_2	PN	NOx	HC	Sum (abs)
FRP	0.014	0.087	0.256	0.294	0.150	0.801
IVO	0.066	-0.085	0.082	0.099	0.051	0.383
EVC	-0.030	0.173	0.025	0.031	0.222	0.482
SA	0.167	0.118	0.015	0.035	0.201	0.536
SOI	0.145	0.045	0.151	0.245	0.211	0.797
Sum (abs)	0.423	0.508	0.529	0.703	0.836	

Table 0.17 Node 5 t-scores

Actuator	CO	CO_2	PN	NOx	HC	Sum
FRP	0.839	0.872	0.425	0.481	0.786	3.404
IVO	0.241	0.102	0.628	0.806	0.366	2.144
EVC	0.456	0.580	0.269	0.107	0.106	1.519
SA	0.213	0.732	0.405	0.273	0.723	2.346
SOI	0.863	0.040	0.829	0.483	0.734	2.950
Sum	2.613	2.326	2.557	2.150	2.715	

Table 0.18 Node 5 Spearman's rho

Actuator	CO	CO_2	PN	NOx	HC	Sum (abs)
FRP	0.024	0.019	-0.093	-0.083	0.032	0.251
IVO	0.137	0.190	0.057	0.029	-0.106	0.519
EVC	-0.087	0.065	0.129	0.188	0.188	0.657
SA	0.145	0.040	0.098	0.128	0.042	0.453
SOI	0.020	0.238	-0.025	-0.082	0.040	0.406
Sum (abs)	0.414	0.552	0.402	0.509	0.407	

A13 Ordered DoE correlation results

Table 0.19 Node 4 FRP ordered DoE Student's t-scores

Actuator	CO	CO_2	PN	HC	Sum
FRP	0.745	0.139	0.286	0.464	1.635
IVO	0.938	0.745	0.887	0.797	3.367
EVC	0.715	0.549	0.106	0.011	1.381
SA	0.612	0.547	0.060	0.013	1.232
SOI	0.923	0.730	0.216	0.577	2.445
Sum	3.933	2.710	1.554	1.862	

Table 0.20 Node 4 FRP ordered DoE Spearman's rho

Actuator	CO	CO_2	PN	HC	Sum (abs)
FRP	-0.043	0.195	0.141	-0.097	0.476
IVO	-0.010	0.043	-0.019	0.034	0.106
EVC	0.048	0.079	-0.213	0.330	0.671
SA	0.067	0.080	-0.246	0.323	0.717
SOI	0.013	-0.046	-0.164	0.074	0.296
Sum (abs)	0.182	0.443	0.783	0.858	

Table 0.21 Node 4 SOI ordered DoE Student's t-scores

Actuator	CO	CO_2	PN	HC	Sum
FRP	0.334	0.286	0.019	0.005	0.645
IVO	0.984	0.690	0.850	0.879	3.402
EVC	0.200	0.954	0.300	0.000	1.454
SA	0.478	0.913	0.779	0.004	2.174
SOI	0.298	0.049	0.421	0.152	0.920
Sum	2.295	2.891	2.370	1.040	

Table 0.22 Node 4 SOI ordered DoE Spearman's rho

Actuator	CO	CO_2	PN	HC	Sum (abs)
FRP	0.136	0.150	-0.325	-0.386	0.997
IVO	-0.003	0.057	0.027	0.022	0.108
EVC	0.180	0.008	0.146	0.486	0.821
SA	0.101	-0.016	0.040	0.396	0.552
SOI	-0.147	-0.275	-0.114	0.201	0.737
Sum (abs)	0.567	0.506	0.651	1.490	

Table 0.23 Node 4 IVO ordered DoE Student's t-scores

Actuator	CO	CO_2	PN	HC	Sum
FRP	0.118	0.660	0.000	0.904	1.683
IVO	0.792	0.704	0.677	0.488	2.661
EVC	0.726	0.438	0.893	0.004	2.061
SA	0.694	0.655	0.888	0.007	2.244
SOI	0.457	0.813	0.411	0.673	2.355
Sum	2.787	3.269	2.869	2.077	

Table 0.24 Node 4 IVO ordered DoE Spearman's rho

Actuator	CO	CO_2	PN	HC	Sum (abs)
FRP	0.207	-0.059	-0.467	-0.016	0.750
IVO	-0.035	-0.051	0.056	0.093	0.235
EVC	0.047	-0.104	0.018	0.371	0.540
SA	-0.053	-0.060	-0.019	0.348	0.480
SOI	0.099	-0.032	0.110	0.056	0.297
Sum (abs)	0.442	0.305	0.670	0.885	

Table 0.25 Node 4 EVC ordered DoE Student's t-scores

Actuator	CO	CO2	PN	HC	Sum
FRP	0.360	0.995	0.152	0.002	1.508
IVO	0.558	0.255	0.609	0.810	2.233
EVC	0.674	0.478	0.460	0.320	1.932
SA	0.732	0.358	0.594	0.733	2.418
SOI	0.789	0.049	0.801	0.411	2.051
Sum	3.113	2.135	2.616	2.276	

Table 0.26 Node 4 EVC ordered DoE Spearman's rho

Actuator	CO	CO_2	PN	HC	Sum (abs)
FRP	-0.124	-0.001	0.194	-0.413	0.733
IVO	-0.080	-0.154	0.070	0.033	0.336
EVC	0.057	0.097	0.101	-0.135	0.390
SA	0.047	0.125	-0.073	-0.047	0.291
SOI	0.037	-0.265	-0.034	0.112	0.447
Sum (abs)	0.345	0.641	0.471	0.740	

Table 0.27 Node 4 SA ordered DoE Student's t-scores

Actuator	CO	CO_2	PN	HC	Sum
FRP	0.243	0.262	0.023	0.925	1.453
IVO	0.371	0.671	0.121	0.233	1.396
EVC	0.094	0.631	0.719	0.736	2.180
SA	0.695	0.946	0.191	0.351	2.183
SOI	0.799	0.510	0.729	0.514	2.552
Sum	2.201	3.021	1.782	2.760	

Table 0.28 Node 4 SA ordered DoE Spearman's rho

Actuator	CO	CO_2	PN	HC	Sum (abs)
FRP	0.156	-0.149	-0.299	0.013	0.617
IVO	0.119	0.057	-0.206	-0.159	0.541
EVC	0.222	0.064	-0.048	0.045	0.379
SA	-0.053	-0.009	-0.174	0.125	0.361
SOI	0.034	0.088	0.046	0.087	0.256
Sum (abs)	0.584	0.368	0.774	0.429	

A14 Ford steady-state methodology

i. Start engine and perform daily checks
ii. Proceed to desired node (speed and throttle)
iii. Allow exhaust plenum skin temperature to stabilise
iv. Input actuator settings
v. Collect test data for sixty seconds
vi. Repeat steps iv and v for each test point